Kiel University
Christian-Albrechts-Universität zu Kiel
Universitätsverlag Kiel
Kiel University Publishing

NMDB@HOME 2020

Proceedings of the 1st virtual symposium on cosmic ray studies with neutron detectors July 13–17, 2020

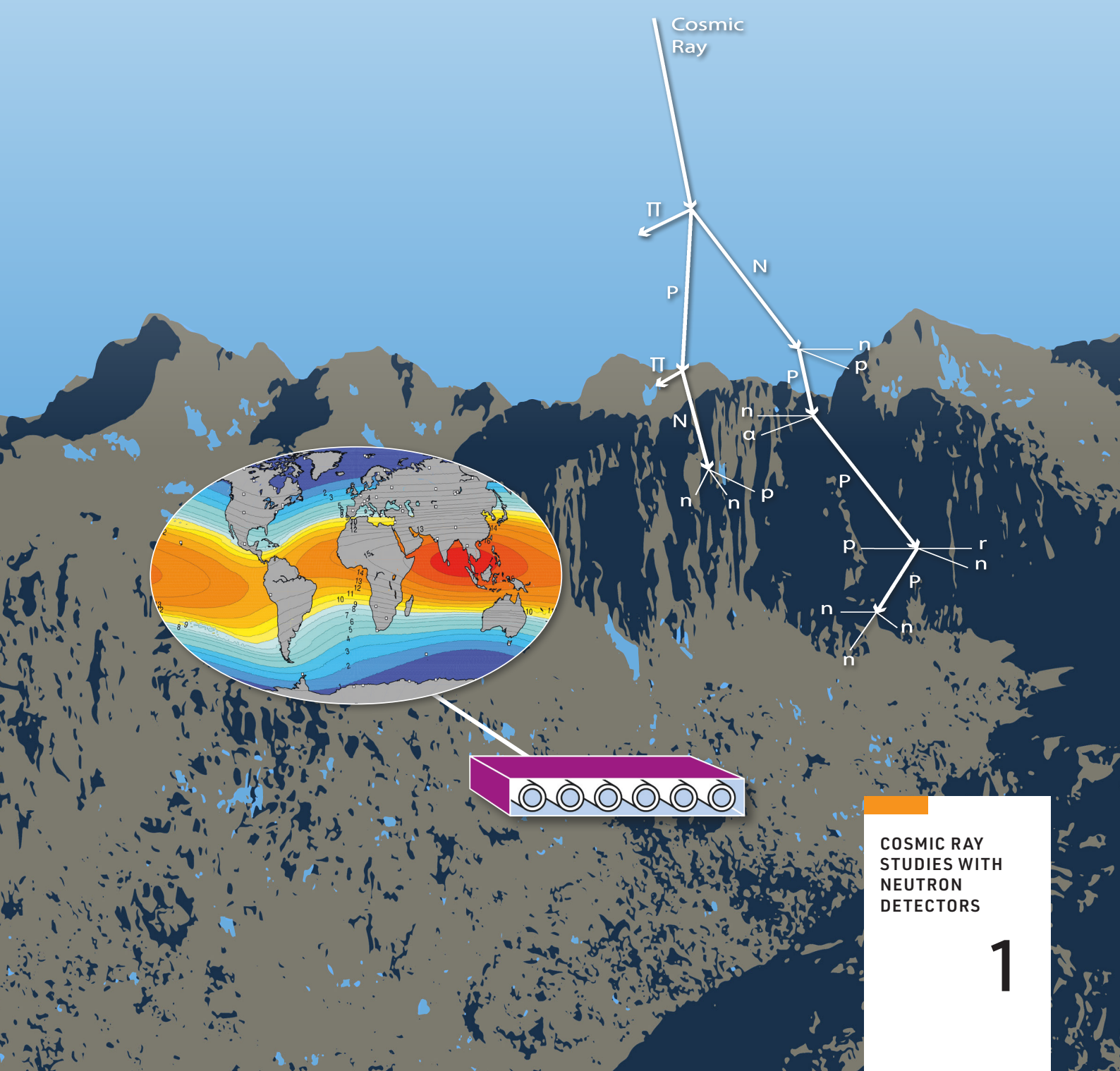

COSMIC RAY STUDIES WITH NEUTRON DETECTORS

1

Cosmic ray studies with neutron detectors
Volume 1

NMDB@HOME 2020

Proceedings of the 1st virtual symposium on cosmic ray studies with neutron detectors July 13–17, 2020

Edited by Maria Abunina, Rolf Bütikofer, Karl-Ludwig Klein, Olga Kryakunova, Monica Laurenza, David Ruffolo, Danislav Sapundjiev, Christian T. Steigies, Ilya Usoskin

Universitätsverlag Kiel
Kiel University Publishing

Cosmic ray studies with neutron detectors | Volume 1 (2021)

Edited by Maria Abunina, Rolf Bütikofer, Karl-Ludwig Klein, Olga Kryakunova, Monica Laurenza, David Ruffolo, Danislav Sapundjiev, Christian T. Steigies, Ilya Usoskin

Bibliographic information published by the Deutsche Nationalbibliothek
The Deutsche Nationalbibliothek lists this publication in the Deutsche Nationalbibliografie.
Detailed bibliographic data are available in the internet at
http://dnb.d-nb.de

The electronic open access version of this work is permanently available on MACAU:
Open Access Repository of Kiel University (https://macau.uni-kiel.de):
https://dx.doi.org/10.38072/2748-3150/v1

2021 Universitätsverlag Kiel | Kiel University Publishing
Universitätsbibliothek Kiel
Leibnizstr. 9
24118 Kiel
Germany
verlag@ub.uni-kiel.de, www.ub.uni-kiel.de

Cover: Sylvain Cnudde (Observatoire de Paris, LESIA), Wiebke Buckow
Typesetting: Wiebke Buckow

eISSN: 2748-3150
eISBN (PDF): 978-3-928794-64-0

Contents

Cosmic ray studies with neutron detectors | Volume 1 (2021)
KIEL-UP • DOI: 10.38072/2748-3150/p1

NMDB@Home2020
1st virtual symposium on cosmic ray studies with neutron detectors

Maria Abunina[1], **Rolf Bütikofer**[2], **Karl-Ludwig Klein**[3], **Olga Kryakunova**[4], **Monica Laurenza**[5], **David Ruffolo**[6], **Danislav Sapundjiev**[7], **Christian T. Steigies**[8], **Ilya Usoskin**[9]

Correspondence

[1] Pushkov Institute of Terrestrial Magnetism, Ionosphere and Radio Wave Propagation, (IZMIRAN), Moscow, Russia
[2] Physikalisches Institut, University of Bern, Switzerland
[3] Observatoire de Paris, LESIA, Université PSL, CNRS, Sorbonne Université/ Université de Paris, France
[4] Institute of Ionosphere, Almaty, Kazakhstan; P.N. Lebedev Physical Institute of the Russian Academy of Science, Moscow, Russia
[5] INAF - Istituto di Astrofisica e Planetologia Spaziali, Roma, Italy
[6] Department of Physics, Faculty of Science, Mahidol University, Bangkok 10400, Thailand
[7] Royal Meteorological Institute of Belgium, KMI-IRM, Brussels, Belgium
[8] Extraterrestrial Physics, Institute of Experimental and Applied Physics, Kiel University, Germany
[9] Space Physics and Astronomy Research Unit, University of Oulu; Sodankyla Geophysical Observatory, University of Oulu, Finland

Keywords

cosmic rays; neutron detectors; solar-heliospheric physics; space weather

Abstract

An overview on the presentations at the first virtual symposium on cosmic ray studies with neutron detectors is given. The meeting was held online in July 2020. Neutron detectors on ground are shown to provide significant contributions to research on interactions of galactic cosmic rays with magnetic fields in the Heliosphere and on the acceleration of energetic particles, as well as to a growing range of applications, including geophysics and space weather. The advent of easily accessible databases makes original data easily available to a large user community. The present overview outlines and introduces the more detailed articles contained in the proceedings.

1. Introduction

Cosmic rays at energies between several hundreds of MeV and tens of GeV play a major role for energetic and plasma processes in the Heliosphere. Various types of neutron detectors on the Earth are used worldwide to probe neutrons produced in interactions of primary cosmic rays with the atomic nuclei of the Earth's atmosphere, and to infer information on their interaction with the magnetic fields of the Heliosphere and the magnetosphere of the Earth, and on heliospheric processes of particle acceleration. While these fields of investigation have a history over more than 70 years, they gain new interest with each new space mission launched to probe heliospheric plasma processes. Their long-standing observations allow us to monitor trends of the heliospheric magnetic field over many solar activity cycles. This is of special interest since the low levels of solar activity witnessed in recent cycles go along with a significant enhancement of the flux of galactic cosmic rays (GCR) in the inner Heliosphere.

KIEL-UP • DOI: 10.38072/2748-3150/p1

Besides their role as a target of fundamental research, galactic and solar cosmic rays at GeV-energies are an issue for space weather purposes. The monitoring of radiation doses, to which the aircrew of civil aviation and airline passengers are exposed, has been receiving attention since the 1990s. While spacecraft most often monitor only particles up to a few hundreds of MeV, neutron detectors on the Earth provide an adequate tool to measure the more energetic particles that become a source of radiation in the lower atmosphere. The advent of real-time space weather services is based on neutron monitor observations and on space-borne measurements.

The lack of possibilities to have scientific meetings that became clear in late winter 2020 triggered interest in the heliospheric cosmic ray community to propose an online meeting with the aim to discuss investigations in the field of cosmic ray research based on ground-based neutron detector data, the neutron detectors themselves, and the handling and distribution of data. The meeting consisted of daily, three-hour sessions between July 13 and 17, 2020. Each session was attended by 70 to 80 persons from Africa, the Americas, Asia, Australia, and Europe. The technical organisation was at the University of Kiel (Germany).

The present paper intends to give an overview on the presentations and discussions, and to set the stage for the authors' contributions that follow. Contributions are addressed in the order of their presentation at the meeting, which may be different from the order in the present proceedings.

2. Cosmic rays in the heliosphere

The advent of measurements of cosmic rays above the atmosphere, such as from the PAMELA and AMS-2 experiments, up to rigidities of several tens of GV has provided the opportunity for yield function validation and calibration for all active neutron monitors (Koldobskiy et al), for verification of the Global Survey Method (Belov et al), and for parametrization of the spectrum of galactic cosmic ray variations and the shape during negative and positive polarity periods (a power-law spectrum of variations with strong exponential attenuation at high rigidities and a pure power-law spectrum, respectively; Yanke al.).

The leader fraction, i.e., inverse neutron multiplicity, has been used as a proxy of a cosmic ray spectral index above the cutoff rigidity to enhance the high-precision spectral information from the worldwide neutron monitor network and extend it to higher rigidity (Banglieng et al.)

On short time scales, a method of defining Forbush Decreases (FDs) and an automated process for identifying FDs in neutron monitor data have been developed and a positive correlation between FD magnitude and properties of the associated Interplanetary Coronal Mass Ejection (ICME) has been found, with decreasing correlation strength as the neutron monitor cutoff rigidity increases (Light et al). The ring of stations method has been used to investigate in detail FDs and their precursors (Abunina et al.). FD precursory signals have been observed also in events without a sudden storm commencement (Lingri et al.). This emphasises the possibility to forecast the arrival of an ICME at Earth using neutron monitor observations.

A full-orbit test-particle simulation has been developed to compute the FD amplitude and time profile resulting from the particle propagation through a magnetic cloud, whose topology has been obtained with the Grad-Shafranov reconstruction. The comparison between model results and both space- and ground-based cosmic ray measurement has suggested that particle drifts across the closed field lines within magnetic clouds have a primary role in affecting the galactic cosmic ray propagation (Benella et al.).

A long and sloping decrease of cosmic ray intensity (up to $\sim 4\,\%$) was observed in neutron monitor data during May 2019, associated with a series of small solar eruptions following each other, although the interplanetary counterpart did not hit the Earth (Trefilova et al.).

The energy spectrum of solar-diurnal variations of cosmic rays has been derived from neutron monitor and muon telescope data. It is qualitatively well described by a flat form with an upper cutoff near 100 GeV (Gololobov et al.).

KIEL-UP • DOI: 10.38072/2748-3150/p1

The wavelet analysis has been applied to investigate long-term variations (Baird and MacKinnon) and mid-term periodicities (13.3 – 298 days), which were found to depend on the neutron monitor rigidity cutoff and height (López-Comazzi and Blanco).

The long-term cosmic ray modulation has been found to be much weaker in cycles 23-24 than in cycles 21-22. This can be explained by the weakening of the solar magnetic field, and consequently an increased role of particle diffusion during propagation in the Heliosphere (Yanke et al.).

The expected cosmic ray modulation has been retrieved in the observations of the CCD imagers of the Hubble Space Telescope, as well as evidence for two spatially confined regions over North America and Australia that exhibit increased particle fluxes at the 5-sigma level (Tancredi et al.).

3. Cosmic rays in the atmosphere

Cosmic-Ray Neutron Sensing for Environmental Sciences (CRNS) is a young research field that has established a technique to monitor water content in soil by measuring the flux of sub-MeV neutrons. The water content in soil, air, snow and vegetation moderates the density of neutrons above the ground. This signal represents the average water content of an area of several hectares. Hundreds of such small neutron detectors have been installed worldwide and they provide critical input for climate research, hydrological models and irrigation management. The reliability of these measurements depends on the knowledge of the incoming cosmic radiation, which has traditionally been taken from one reference neutron monitor. As these corrections do not take into account the differences between the neutron monitor and the sensor (altitude, cutoff rigidity, etc), the CRNS community is exploring the use of the neutron monitor network to improve the quality of the soil humidity prediction and to open up new opportunities for cooperation between the disciplines (Schrön and Köhli).

4. Solar energetic particle events – GLE analysis

During powerful solar events, such as flares and coronal mass ejections (CMEs), charged particles can be accelerated to high energies. These particles are known as solar energetic particles (SEPs). If their energy spectrum extends beyond 450 MeV, the primary particles, especially protons, but sometimes also neutrons, trigger atmospheric cascades that reach the surface of the Earth. Such events are called ground level enhancements (GLEs). Ground-based instruments such as the worldwide network of neutron monitors, neutron detectors and muon telescopes allow us to observe these events and to complement satellite data, which most often pertain to lower energies.

In the “GLE analysis” session Mishev, Koldobskiy and coworkers presented a new GLE analysis method based on the neutron monitor network. The method allows to compute the trajectory of particles in the simulated magnetosphere and to calculate the main parameters of relativistic solar protons (energy spectrum, direction of the anisotropy axis, pitch-angle distribution). The method is based on new neutron monitor yield functions, which were updated and cross-calibrated with the PAMELA and AMS-02 experiments.

Bütikofer and coworkers analyzed some SEPs, registered by the EPHIN detector aboard SOHO, which were comparable in magnitude with previously recorded GLEs, but had no response in the data of ground-based detectors. In addition, for some recent GLEs and sub-GLEs, the energy spectrum was modeled and compared with the satellite data.

The possibility to use radio emission of electron beams (type III bursts) as a tracer of magnetic connectivity was discussed by Klein. The analysis was applied to GLEs in order to confirm their magnetic connection to the Earth and to discuss the constraints on the acceleration region of the non thermal electrons and relativistic protons.

KIEL-UP • DOI: 10.38072/2748-3150/p1

5. Space weather research and services

The global neutron monitor network has a long tradition in the research on cosmic ray variations and solar energetic particles. Recently, it has been used also for space weather purposes, specifically for alerts and the related assessment of the exposure of aircrew to radiation doses caused by cosmic rays. Using neutron monitor data Gil et al. showed that the increase in the superposed averaged number of failures of Polish transmission lines appears around FDs, as well as one day after the occurrence of fast halo CMEs. Fuller and coworkers reported that data of French neutron monitors at Kerguelen Island and Terre Adélie (Antarctica) are used for the monitoring of the radiation doses received by civil aircrew in France in the framework of the SIEVERT programme. Since 2019 they support the real-time space weather service for civil aviation worldwide under the auspices of ICAO (International Civil Aviation Organization). Large enhancements in the fluxes of relativistic electrons lead to spacecraft malfunctions and have in a number of cases resulted in the failure of satellites. To estimate the state of near-Earth space during dangerous relativistic electron enhancements at geostationary orbits Kryakunova et al. suggested to use data from the world-wide neutron monitor network.

With the creation in 2009 of an international database of neutron monitors, NMDB, and its subsequent development, the opportunity appeared for the first time to use the global survey method (GSM) in real-time mode (Gololobov et al.). Authors showed that such monitoring results allow us to forecast geomagnetic disturbances with a preceding time from a few hours up to 1.5 days. Using NMDB data Papailiou et al. showed that large Forbush decreases, regardless of the heliolongitude of the solar source, are accompanied by increased geomagnetic activity and increased cosmic ray anisotropy, including anisotropy before the events, which can serve as a typical precursor of Forbush decreases and geomagnetic storms.

The network of neutron monitors should be expanded for a successful solution of space weather problems. Kato and coworkers reported that a new neutron monitor started its operation at Syowa Station in Antarctica in the frame of the 59th Japanese Antarctic Research Expedition. A distinctive feature of this neutron monitor is that it is paired with a cosmic ray muon detector. For space weather tasks it makes sense to employ different types of cosmic ray detectors, such as those installed in the Space Environment Viewing and Analysis Network (SEVAN, Armenia). The first prototype of a new directional muon telescope was shipped from Spain to Antarctica. Santos et al. reported the first observations of a cosmic ray detector based on water Cherenkov radiation, which is operated at the Marambio base, Antarctic Peninsula, by the LAGO (Latin American Giant Observatory) Collaboration.

6. Neutron detectors: instrumentation, response function

A new neutron monitor station (NEMO) was installed at the Spanish Antarctic base Juan Carlos I on Livingston Island (S 62°39'46", W 60°23'20", 12 m asl) in January 2019 as part of the Antarctic Cosmic Ray Observatory (ORCA) along with a muon telescope (MITO), and integrated into the renewable energy grid of the base (Blanco et al.). The neutron monitor at Jang Bogo (74.62S, 164.2E; Jung et al.) base has been operating since December 2015 consisting of 18 tubes of three-units transferred from McMurdo station.

Electronics of neutron monitors at DOME C (Poluianov et al.) and SANAE (Strauss et al.) have been upgraded mainly for multiplicity measurements. A novel registration system (NMRENA) has been developed for counter signals, based on an FPGA and allowing for pulse height information (Böttcher et al.). A new electronic system has been realized at Princess Sirindhorn (Thailand; Mitthumsiri et al.) and Mawson (Antarctica; Saiz et al.) for measuring cross-counter time delay distributions to obtain cross-counter leader fractions (LFs), related to cross-counter neutron multiplicity, which can used as a proxy of the cosmic ray spectrum. Complementary Monte Carlo simulations have also been performed to account for large-separation LFs, suggesting that they can be attributed to multiple atmospheric secondaries from the same primary cosmic ray.

KIEL-UP • DOI: 10.38072/2748-3150/p1

Differential response functions of paraffin-moderated bare counters during 1995 and 2009 latitude surveys have been determined to estimate the spectral index for GLEs of 1989 and yield functions (Nuntiyakul et al.). The comparison between bare counters and neutron monitors provided a rather precise measurement of the spectral index, and in particular the variation of the spectral index within a given event. The determination of the paraffin bare detector function will improve the quality of future estimations of the spectral index of relativistic solar particles based on measurements of the bare counter to neutron monitor count rate ratio during ground-level enhancements detected at the South Pole.

FLUKA simulations have been performed to estimate the bare detector responses in 2009 latitude survey to vertical secondary particles (Nuntiyakul et al., poster) and the processes contributing to the count rate recorded by the second neutron monitor installed at Dourbes (Belgium) during different phases of its construction (Sapundjiev and Stankov).

The importance of the pulse height (PH) analysis for checking the long-term stability of the counters was highlighted by Evenson. For instance, PH spectra have been taken annually from one of the neutron monitors used at South Pole from 1997 to 2003. Despite the broadening of the resolution, the average PH has only been reduced by 13 % over this interval with a negligible impact on the count rate from the tube degradation.

7. Neutron detectors: databases and analysis techniques

Steigies reported that a major upgrade to the database infrastructure of NMDB was performed in the fall of 2019 to ensure the availability of this data in the future. The original setup of one main MySQL server (for receiving data from the neutron monitor stations) and several distributed mirrors (for redistributing data via NEST and direct access from dedicated mirrors for other users) has been replaced by a MariaDB Galera Cluster with currently five nodes. All nodes in the cluster can be used for reading and writing data, thus greatly improving the performance of NMDB. New nodes can be quickly added to the cluster, broken nodes are removed automatically, and rejoin the cluster after they have been repaired. ProxySQL is used to access the cluster behind the firewall and to distribute the load between the different nodes. The two ProxySQL servers at different computing centers (high-availability) share a virtual IP address that is provided by Keepalived, so that the whole cluster is accessible from the outside via a constant host name (one for reading, another one for writing data) so that no users tools have to be updated, when the IP addresses of the cluster change.

The Oulu group (Väisänen et al.) conducted an extensive data survey for inter-comparison and analysis of publicly available neutron monitor datasets since 1953 to identify the best possible data sources. Data from the same stations, but different sources, are not always equivalent, which creates a problem for the reliability and reproducibility of scientific results.
Data products and data analysis tools for cosmic ray observations are available on different web sites:

- The International GLE database (http://GLE.oulu.fi, last accessed April 7, 2021) has been revised to account for the variable galactic cosmic ray background for 58 GLEs. The GLE time profiles have been detrended and the cumulative count rates have been calculated for most of the events as well as the integral omnidirectional fluences by applying the effective rigidity method (Usoskin et al.). This work could allow more precise studies of parameters of SEP events.
- An online tool has been made available at http://cosmos.hwr.arizona.edu/Util/rigidity.php (last accessed April 7, 2021) for the computation of cutoff rigidity and particle trajectories in the magnetosphere. The expected variations of effective cutoff rigidities for neutron monitors over the period 1950 – 2050 have been estimated (S. Belov et al.).
- A database of directivity functions to describe the directional sensitivity of the detector to primary protons has been made available at http://crd.yerphi.am/Directivity_Functions (Karapetyan et al., last accessed April 7, 2021).

KIEL-UP • DOI: 10.38072/2748-3150/p1

8. Conclusion

The NMDB@Home meeting illustrated multiple applications of neutron detectors as complements of satellite observations or independent diagnostic tools: primary research on cosmic ray acceleration and propagation, the magnetic field in the Heliosphere, but also applications for geophysics and space weather. The present proceedings contain the articles of part of the presentations and the abstracts of the contributions without submitted proceeding article. The harmonisation of data distribution especially thanks to internationally organised databases allows an easy access to the measurements for users with a variety of research interests.

Acknowledgments

As the scientific organisers of the virtual symposium NMDB@Home we express our gratitude to the University of Kiel, which hosted the meeting thanks to its University Computing Center (Rechenzentrum), and which publishes these proceedings within a pilot project conducted by Kiel University Publishing. The NMDB project, which initially proposed the idea of the symposium, has been funded by the European Union's FP7 programme (contract no. 213007).

In memoriam

The participants of the symposium took note of the recent passing away of eminent members of the community.

Michel Alania passed away at the age of 85 years on May 18, 2020. He was the designer and first PI of the neutron monitor in Tbilisi, Georgia, and made long-standing contributions to cosmic ray research, especially on the solar modulation of cosmic rays, as a researcher and head of the cosmic ray group at Siedlce University, Poland. The obituary was given at the conference by Agnieszka Gil.

Roger Pyle passed away at the age of 78 years on May 21, 2020. He had been a long-standing member of the cosmic ray group at the University of Delaware, Newark, and continued working for the operation of the 'Spaceship Earth' network after his retirement in 2007. Roger Pyle undertook a dedicated effort to make neutron monitor data publicly available. The NMDB group gratefully remembers his work to integrate the University of Delaware neutron monitors into NMDB, including the provision of real-time data. The obituary was given at the conference by Paul Evenson.

While completing these proceedings, we were informed that **Evgenia A. Eroshenko** from IZMIRAN, Russia, passed away at the age of 80 years on June 3, 2021. Evgenia Eroshenko had a long-standing career with research on all aspects of cosmic ray observations with neutron monitors. She was one of the founding members of the NMDB consortium, where she ensured the participation of a wide network of neutron monitors from Russia and Asia.

We are highly indebted to the lifelong work of these colleagues whose efforts to develop research and instrumentation allow us today to pursue observations with neutron detectors for understanding cosmic rays.

Session 1:

Cosmic rays in the heliosphere: spatial and time variability

Cosmic ray studies with neutron detectors | Volume 1 (2021)
KIEL-UP • DOI: 10.38072/2748-3150/p2

Comparison of long-term variations of the cosmic ray flux from the network of ground-based detectors, PAMELA and AMS-02 data

Anatoly V. Belov, Victor G. Yanke, Raisa Gushchina, Nataly Shlyk

Correspondence
Pushkov Institute of Terrestrial Magnetism, Ionosphere and Radio Wave Propagation, (IZMIRAN) Moscow, Russia,
abelov@izmiran.ru, yanke@izmiran.ru, rgus@izmiran.ru, nshlyk@izmiran.ru

Keywords
long-term variations; PAMELA, AMS-02; ground-based detectors; balloon stratospheric sounding

Abstract
The paper presents preliminary results of a comparison of long-term variations of the cosmic ray flux using data from the network of ground-based detectors with direct flux measurements on the PAMELA and AMS-02 magnetic spectrometers and a series of balloon stratospheric soundings. The analysis showed good agreement for the entire period of continuous ground-based monitoring of cosmic ray variations.

1. Introduction

Galactic cosmic rays with rigidity up to one hundred GV are constantly modulated by the solar wind. On the one hand, this galactic cosmic rays flux is recorded by a network of ground-based detectors under the atmosphere: ionization chambers, muon telescopes, and neutron monitors. Cosmic ray variations are determined experimentally from ground-based observations at the network of cosmic ray stations, and the processing task is reduced to restoring variations in the near-Earth interplanetary space from the observational data. This problem is solved by the global spectrographical method (GSM) (Krymsky et al. 1966; Nagashima 1971; Belov et al. 1983).

Recently, more and more often, the flux of galactic cosmic rays is measured directly by spacecraft detectors at various points of the heliosphere and near the Earth's orbit.

The aim of this work is to compare the results of ground-based measurements processed by the GSM method with the direct measurements of the cosmic ray flux on spacecrafts. Such an opportunity appeared only with the launch of the PAMELA and AMS-02 magnetic spectrometers, which measure particle fluxes in a wide range of rigidities, including the effective particle rigidity of the ground network of detectors - 10 GV.

There are quite a lot of works with comparisons of direct and indirect measurements (Alanko et al. 2003; Usoskin et al. 2005, 2011, 2017; Koldobskiy et al. 2018, 2019a, 2019b). True, the ultimate goal of these works was to reconstruct the modulation potential within the force field approximation. Thus, in Usoskin et. al. 2005, the era of ground-based monitoring of cosmic radiation from 1951 to 2004 was considered. The reconstructed spectrum of cosmic rays from several neutron monitors was calibrated using the data of balloon stratospheric sounding and AMS-01. The calibrated spectrum was used to reconstruct the modulation potential values. In Usoskin et al. 2017, the data series was extended to 2010 and the data from the PAMELA magnetometer were also used for calibration.

KIEL-UP • DOI: 10.38072/2748-3150/p2

In Usoskin et al. 2011, several epochs of ground-based monitoring of cosmic radiation were considered. The period of ionization chambers (Forbush) from 1936 to 1951, the period of single neutron monitors IGY (mining) from 1951 to 1964 and the modern period of operation of the network of neutron monitors nm64, although the above-mentioned works used data from only 6-8 neutron detectors. For the same period, the modulation potential was also reconstructed from the data of stratospheric sounding. It is hoped that the use of data from detectors of the entire world network (> 40) should increase the accuracy, expand the energy range, and remove some uncertainties in the obtained results.

2. Ground monitoring and global spectrographic method GSM

The Earth is a giant natural magnetic spectrometer that separates primary charged particles according to their rigidity, so that registration of cosmic rays at different latitudes and depths in the atmosphere gives significantly different results. The ground-based network of detectors consists of more than 40 neutron monitors, 3 stratospheric sounding stations, and a dozen multi-directional muon telescopes.

The counting rates of the detectors *N* are directly measurable. The measured variations in the zero-harmonic approximation are related to the spectrum of primary variations reflecting interplanetary processes $\delta J / J_B\left(R\right)$ by the system of Fredholm integral equations of the first kind:

$$v^i = \delta N / N|_{R_c^i} = \int W\left(R_c^i, h_0^i, R\right) \cdot \delta J / J_B \cdot \mathrm{dR}, \quad (1)$$

where i = 1,.., m defines the number of the detector. Here, the coupling function $W^i\left(R_c^i, h_0^i, R\right)$ between primary and secondary variations recorded by detector *i*, located at a point with the rigidity of geomagnetic cutoff R_c^i at a depth in the atmosphere h_0^i acts as the kernel of the equation, and the spectrum of variations *dJ/J(R)* - as an unknown function. In our case, the circumstance is that the desired solution can be sought in the form of an analytical function of the spectrum of variations *dJ/J* with a certain number of parameters, which increases the stability of the found solution.

For the spectrum of variations, a parametric representation is often used in the form

$$dJ / J_B = a_1\left(R_0 + R\right)^{-\gamma} \text{ at } R \le R_u\ , \quad (2)$$

in (Belov et al. 1998) a variant of a global spectrographical method based on monthly average data is described, specially adapted for studying long-term variations in the approximation of isotropic variations.

As a result of the calculations performed for the period of cosmic ray monitoring, the amplitude and parameters of the spectrum of variations of the zero harmonic were obtained for a rigidity of 10 GV, which is close to the effective rigidity of particles recorded by neutron monitors. The result of this analysis can be found in (Yanke et al. 2020).

3. Data from the PAMELA and AMS-02 magnetic spectrometers

Direct measurements of galactic cosmic rays, including considered range of rigidities near 10 GV, were carried out using orbital detectors on the PAMELA and AMS-02 spacecraft.

The PAMELA (Adrianiet et al. 2011, 2013, 2014, 2017) (elliptical orbit 350–600 km) operated from summer 2006 to January 2014. The geometric factor of the PAMELA magnetic spectrometer is 21.5 cm^2sr (Adrianiet et al. 2017). The PAMELA operating period is divided into 83 time slots. Each time slot contains 78 energy bands.

The AMS-02 (Aguilar et al. 2015, 2018) is a magnetic spectrometer installed on board of the ISS and has been operating from 2011 to the present. Its operating period is divided into 79 time intervals.

Each time slot contains 45 energy bands. The geometric factor of the AMS-02 spectrometer is ∼ 0.5 m^2sr (Ting 2013).

The digital data of the PAMELA and AMS-02 detectors, averaged over the Carrington rotations, are available in the database (crdb 2020) and are described in (Di Felice et al. 2017). Sampling by the time or by the rigidity (t, R) is possible.

In this work energy channels close to 10 GV are important for comparison with the results of the World Network of Stations (CR Network 2020). The considered energy ranges of the PAMELA and AMS-02 detectors are given in Table 1, which also shows the average energy/rigidity values for each range.

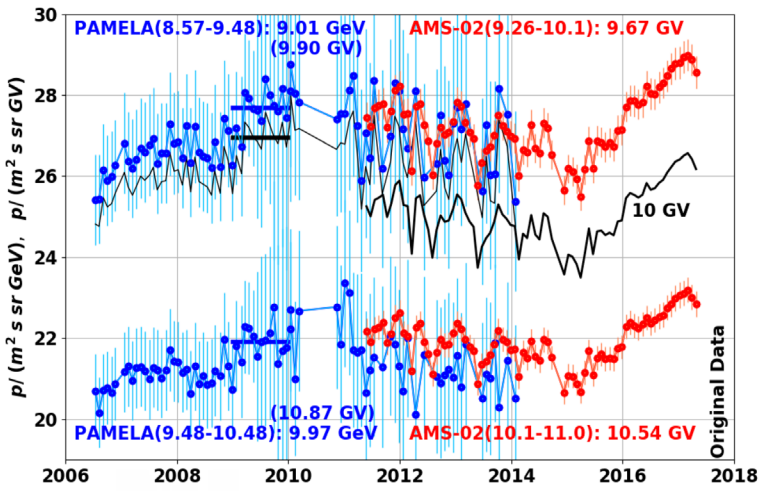

Figure 1: - a10 (% to 2009) - variations of the density of CRs with a rigidity of 10 GV (red curve with dots in the lower).

Figure 1 shows the time course of the energy ranges of the PAMELA and AMS-02 magnetic spectrometers selected in accordance with the table 1. The statistical errors of the PAMELA spectrometer data up to 2009 for the considered energies of ∼ 10 GeV are about 4%. Subsequently, the statistical error of the PAMELA data in this range almost doubled. With the same methodology, this indicates a hardware problem. The statistical errors of the data of the AMS-02 spectrometer are significantly lower and slightly exceed 1% for the rigidity of ∼ 10 GV for the entire monitoring period. The solar activity minimum in 2009 was chosen as the base period. It is shown in figure 1 by horizontal lines. The thin black curve shows temporal changes in particle flux recalculated for 10 GV for the PAMELA. The double black curve shows the AMS-02 data recalculated for 10 GV. The time dependence of the proton flux reduced to 10 GV is also shown. Temporal changes for the 10 GV rigidity will be discussed below.

PAMELA		**AMS-02**	
range, GeV	E_{evr}, GeV/R_{evr}, GV	range, GV	R_{evr}, GV
8.57÷ 9.48	9.01/ **9.90**	9.26÷10.1	**9.67**
9.48÷10.48	9.97/**10.87**	10.1÷11.0	**10.54**

Table 1: Considered energy ranges of the PAMELA and AMS-02 detectors.

KIEL-UP • DOI: 10.38072/2748-3150/p2

4. The analysis method

In order to compare the long-term changes in the cosmic ray flux from the data of ground-based detectors and the PAMELA and AMS-02 spectrometers, it is necessary to generate the PAMELA and AMS-02 data for the rigidity of 10 GV, for which there are reliable ground-based measurements of cosmic rays, and to calibrate the measurements of the unified ground-based cosmic ray detector according to direct measurements.

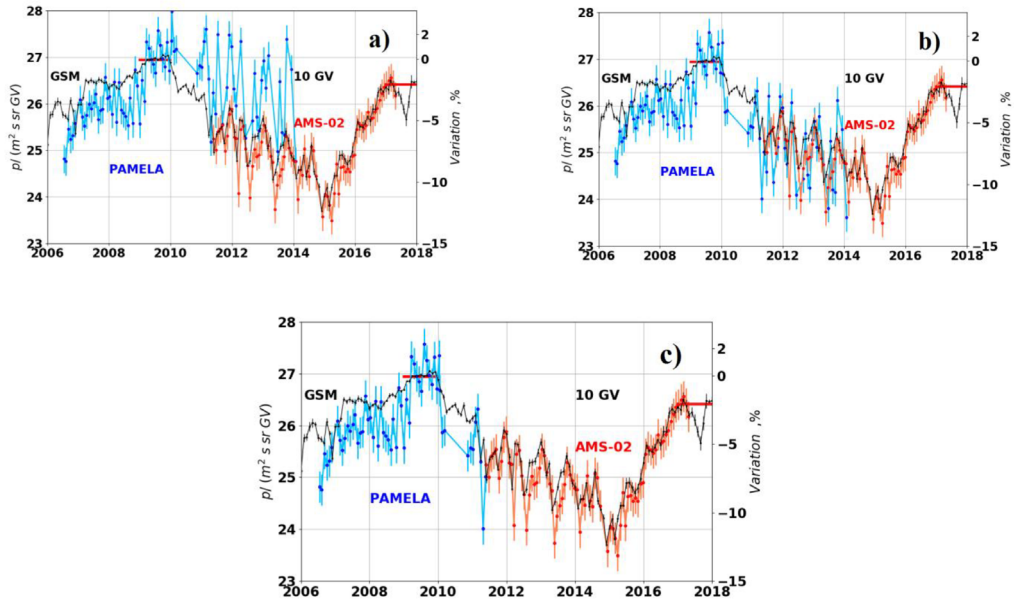

Figure 2: Comparison of the PAMELA and AMS-02 spectrometers data with the GSM data.

The flux of protons is experimentally determined in a certain range of rigidities; therefore, it is necessary to determine the average rigidity of particles in this range. In a limited range of rigidities, spectra can always be represented in a power-law form. By definition, the average rigidity $\overline{R}$ in the case of a power-law spectrum $J = aR^{-\gamma}$ in the interval $[R_1, R_2]$ is determined from the equality (Lafferty et al. 1995)

$$a \cdot \overline{R}^{-\gamma} \cdot \left(R_2 - R_1\right) = a \int R^{-\gamma} \mathrm{dR} \qquad 3)$$

But for calculating the average values $\overline{R}$, the spectrum index γ is unknown, which can be determined by solving the system of transcendental equations for two adjacent intervals $[R_1, R_2]$ and $[R_3, R_4]$ and the definition of $\overline{R}$ and γ.

Since the results of the GSM analysis are cosmic ray variations, it is necessary to directly calibrate and link the data of such a multidirectional ground-based detector to the real spectra of galactic cosmic rays.

The calibration procedure is as follows. Variations relative to the base period with the flow J_B during this period are, by definition, equal to

$$v = \left(J - J_B\right) / J_B \qquad (4)$$

KIEL-UP • DOI: 10.38072/2748-3150/p2

Variations are determined as a result of the GSM analysis. Then for calibration we get

$$J = J_B\left(v + 1\right) \tag{5}$$

The calibration was carried out relative to the base period of 2009 according to the PAMELA magnetometer data, for which $J_B = 26.94$ p/(m² s sr GV) for the rigidity of 10 GV. The result of this calibration for the entire period of continuous ground-based monitoring of cosmic rays is given in table 2. Statistical errors of the proton flux for the period after 1970 are ± 1.2 p/(m² s sr GV).

5. Comparison of the PAMELA and AMS-02 spectrometers data with the GSM data

In figure 2a we compared the initial data of the PAMELA and AMS-02 magnetic spectrometers (see figure 1), converted to 10 GV, with the calibrated GSM data in flux units (left scale) and their variations (right scale). Variations are calculated relative to the base period 2009 of the PAMELA data. We should note the weak agreement between the PAMELA and GSM data until 2009 and a completely different time course of the PAMELA data from 2010 with very large variations, and a general shift relative to the ground data. The agreement between the AMS-02 and the GSM data is good for the entire presented period. Variations in the data of the AMS-02 magnetometer were also calculated relative to the base period of 2009 using the baseline PAMELA value. Therefore, the agreement of the variations indicates the correct calibration and the absence of drift of the data of the detectors of both magnetic spectrometers at that time.

In figure 2b, it is assumed that the efficiency of the PAMELA detector after 2010-01-13 is ε = 1.0488 for 10 GV. This problem was also discussed by the authors of the PAMELA project (Martucci et al. 2018). And finally, figure 2c shows the combined data of the two detectors PAMELA and AMS-02, which generally agree well with the GSM data.

Figure 3 shows the temporal changes of the galactic cosmic ray protons flux at 1AU according to the data of the ground-based network of neutron monitors and comparison with direct measurements using the PAMELA and AMS-02 spectrometers. Dots also show some data from balloon stratospheric sounding.

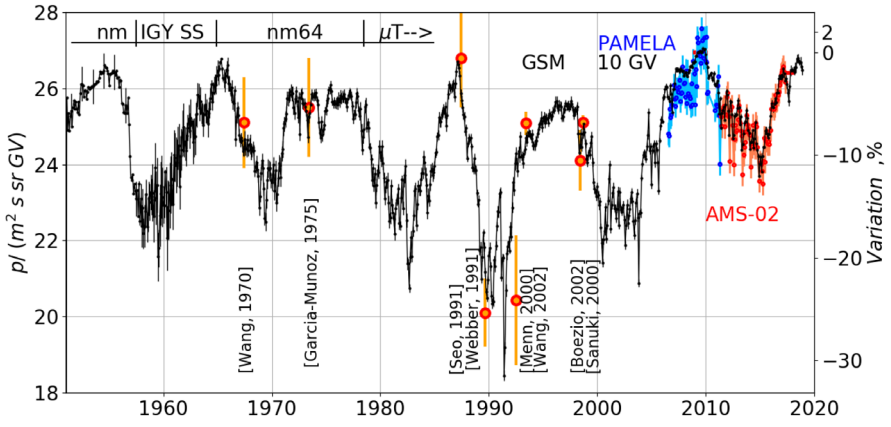

Figure 3: Time variations of the GCR proton flux at 1AU based on the data from the ground-based network of detectors .

KIEL-UP • DOI: 10.38072/2748-3150/p2

6. Discussion and conclusions

Due to its unique capabilities, the PAMELA satellite experiment made it possible to calibrate the spectrum of variations obtained as a result of continuous ground monitoring of cosmic ray variations and their GSM processing. Direct measurements of the particle flux in the PAMELA and AMS-02 experiments, as well as the data from a series of balloon stratospheric soundings, made it possible to compare it with the long-term variations of the cosmic ray flux from the network of ground-based detectors data.

The results of continuous ground-based monitoring of cosmic ray variations and the results of direct measurements of the particle flux for the entire observation period are in good agreement. Despite the doubling of the PAMELA measurement error for the period after 2009, no overall drift was observed.

The AMS-02 data for the period 2012-2014 demonstrate large, in comparison with the result of the GSM, short-period variations, which may indicate an underestimation of low energies in the GSM method.

The assessment of the cosmic ray flux outside the magnetosphere for the entire observational period obtained by the GSM method was carried out. Space radiation is a significant obstacle to manned flights. Accurate measurements of cosmic radiation are essential for planning appropriate protection measures. On the basis of ground-based monitoring, fluxes of galactic protons were retrospectively obtained with an average monthly resolution for the period of the space era (see table 2).The calibration was carried out according to the data of the PAMELA magnetic spectrometer in the base period of 2009 The same results can be obtained for the daily average and hourly average resolution.

year	Jan	Feb	Mar	Apr	May	Jun	Jul	Aug	Sep	Oct	Nov	Dec	Annual
1951		25.76	24.90	25.35	24.89	25.27	25.41	25.00	25.49	25.67	25.46	25.65	25.35
1952	25.46	25.37	25.65	25.31	25.88	26.11	26.11	26.08	25.78	25.95	25.95	25.72	25.78
1953	25.91	26.03	25.98	26.01	26.02	26.06	26.05	26.09	26.11	26.13	26.17	26.17	26.06
1954	26.17	26.28	26.45	26.39	26.43	26.41	26.46	26.61	26.56	26.54	26.46	26.38	26.43
1955	26.07	26.37	26.39	26.40	26.46	26.42	26.43	26.35	26.46	26.27	26.30	26.03	26.33
1956	26.22	26.21	25.60	25.59	25.37	25.35	25.55	25.53	25.35	25.76	25.05	24.22	25.48
1957	23.65	23.58	23.73	23.23	23.49	23.31	23.10	23.33	22.64	23.49	22.51	23.10	23.03
1958	22.38	22.86	22.19	22.38	22.77	23.21	22.35	22.70	23.10	23.01	23.27	23.15	22.78
1959	23.26	22.63	23.06	23.92	23.12	23.45	21.57	21.80	22.65	23.23	23.41	23.14	22.94
1960	22.94	22.91	23.81	23.28	22.06	22.81	22.79	23.19	23.46	23.63	22.96	23.59	23.12
1961	24.25	24.18	23.98	24.04	24.43	24.50	23.41	24.21	24.39	24.82	24.97	24.61	24.32
1962	24.54	24.36	24.75	24.96	25.20	24.88	25.21	25.13	25.07	24.58	24.70	24.74	24.84
1963	25.31	25.32	25.83	25.80	25.48	25.67	25.37	25.33	25.04	25.31	25.57	25.33	25.45
1964	25.40	25.07	25.34	25.46	25.74	26.11	25.65	25.89	26.07	26.13	26.09	26.33	25.77
1965	26.47	26.35	26.52	26.68	26.77	26.51	26.27	26.25	26.17	26.33	26.48	26.60	26.45
1966	26.12	26.12	25.96	25.86	26.01	25.64	25.62	25.93	24.66	25.26	25.48	25.29	25.66
1967	24.78	24.60	24.69	24.62	24.35	24.40	24.67	24.43	24.40	24.64	24.37	24.53	24.54
1968	24.53	24.32	24.36	24.44	24.36	23.83	23.94	24.05	23.85	23.69	22.86	23.16	23.95
1969	23.76	24.10	23.89	23.35	22.58	22.49	23.07	23.59	23.90	23.85	23.89	23.58	23.50
1970	23.52	23.74	23.99	23.30	23.84	22.99	23.21	23.65	24.04	23.97	23.66	24.28	23.68
1971	24.40	24.95	25.06	25.19	25.34	25.73	25.73	25.81	25.83	25.93	25.86	25.86	25.47
1972	25.50	25.35	25.72	25.91	25.66	25.24	25.76	24.79	25.84	25.88	25.60	25.59	25.57
1973	25.61	25.51	25.41	25.17	24.71	25.25	25.35	25.57	25.85	25.79	25.77	25.87	25.49
1974	25.78	25.89	25.67	25.57	25.11	24.83	24.69	25.13	24.76	24.92	25.03	25.41	25.23
1975	25.43	25.69	25.74	25.95	25.97	26.08	25.91	25.64	25.59	25.66	25.58	25.60	25.74
1976	25.67	25.58	25.74	25.64	25.81	25.74	25.78	25.75	25.86	25.73	25.63	25.52	25.70
1977	25.72	25.83	25.88	25.85	25.80	25.53	25.20	25.32	25.31	25.62	25.87	25.79	25.64
1978	25.42	25.27	25.46	24.89	24.39	24.71	24.91	25.52	25.56	24.97	25.10	24.97	25.10

1979	24.46	24.44	24.14	23.58	23.90	23.43	23.76	22.99	23.45	23.84	23.79	24.47	23.85
1980	24.32	24.10	24.48	24.03	23.65	23.10	23.41	23.54	23.58	22.99	22.51	22.60	23.53
1981	23.43	22.94	22.73	22.56	22.18	22.85	23.07	23.11	23.36	22.46	22.39	23.12	22.85
1982	23.60	22.85	23.57	23.72	23.96	22.53	21.40	21.40	20.75	21.56	22.08	21.58	22.42
1983	22.24	22.67	23.31	23.37	22.40	22.95	23.43	23.32	23.31	23.59	23.77	23.77	23.18
1984	24.20	24.04	23.73	23.45	22.74	23.18	23.05	23.47	23.83	23.88	23.72	23.80	23.59
1985	23.96	24.30	24.33	24.73	24.77	25.23	25.12	25.12	25.31	25.37	25.46	25.34	24.92
1986	25.51	25.00	25.29	25.84	26.09	26.03	25.99	26.00	26.06	26.12	25.78	26.13	25.82
1987	26.43	26.70	26.62	26.53	26.33	25.86	25.69	25.49	25.32	25.25	24.86	24.96	25.84
1988	24.15	24.54	24.70	24.66	24.69	24.47	23.92	23.84	24.16	23.88	23.85	23.26	24.18
1989	22.96	23.06	21.75	21.83	21.00	21.56	22.20	21.83	21.17	20.66	20.49	20.96	21.62
1990	21.59	21.81	21.31	20.53	20.34	20.39	21.49	21.32	21.86	22.37	22.77	22.75	21.54
1991	23.24	23.26	21.03	21.54	21.54	18.45	19.18	20.69	21.65	21.85	21.96	21.74	21.34
1992	22.36	22.11	22.86	23.54	23.33	24.02	24.29	24.03	23.83	24.35	24.19	24.73	23.64
1993	24.19	24.23	24.03	24.28	24.40	24.70	24.58	24.75	24.84	24.81	24.79	24.68	24.52
1994	24.80	24.49	24.49	24.49	24.62	24.62	24.80	24.93	25.04	25.07	25.22	24.97	24.80
1995	25.15	25.25	25.09	25.20	25.20	25.22	25.09	25.33	25.29	25.23	25.28	25.39	25.23
1996	25.42	25.52	25.65	25.66	25.50	25.45	25.56	25.53	25.52	25.21	25.25	25.45	25.48
1997	25.44	25.61	25.52	25.53	25.59	25.46	25.53	25.67	25.58	25.45	25.30	25.39	25.51
1998	25.40	25.44	25.52	24.80	24.31	24.51	24.80	24.46	24.78	25.07	24.85	24.55	24.87
1999	24.14	24.06	24.23	24.35	24.26	24.56	24.73	24.05	23.52	23.36	23.26	23.15	23.97
2000	23.41	23.19	22.94	23.02	22.33	21.92	21.42	22.02	22.25	22.88	22.04	22.40	22.49
2001	23.04	23.62	23.99	22.31	22.94	23.25	23.40	22.85	22.83	22.59	22.82	23.28	23.08
2002	22.40	23.28	22.81	22.75	22.86	22.94	22.54	21.88	22.40	22.94	22.45	22.66	22.66
2003	22.82	23.10	23.27	23.03	22.51	22.13	22.52	22.98	23.24	22.60	20.88	22.72	22.65
2004	22.73	23.64	24.02	24.25	24.33	24.22	24.14	24.47	24.78	25.37	24.37	24.48	24.23
2005	23.47	24.36	24.49	24.55	24.04	24.54	24.38	24.05	23.31	24.63	25.00	25.17	24.33
2006	25.13	25.76	25.78	25.98	26.05	26.03	25.77	25.74	25.66	26.07	25.85	25.37	25.77
2007	25.98	25.98	26.14	26.51	26.46	26.51	26.47	26.44	26.52	26.50	26.45	26.46	26.37
2008	26.33	26.40	26.42	26.35	26.32	26.42	26.48	26.58	26.60	26.56	26.68	26.67	26.48
2009	26.69	26.85	26.85	26.95	26.95	26.96	26.98	26.95	26.97	27.05	27.01	27.04	26.94
2010	26.89	26.67	26.56	26.27	26.32	26.37	26.40	26.28	26.21	26.39	26.10	26.07	26.38
2011	26.14	26.20	25.89	25.33	25.73	24.96	25.35	25.42	25.52	25.15	25.57	25.91	25.60
2012	25.84	25.39	24.77	25.66	25.64	25.31	24.67	24.77	25.28	25.29	25.31	25.47	25.28
2013	25.69	25.49	25.04	25.26	24.37	24.53	24.82	25.08	25.12	25.42	25.21	24.90	25.08
2014	24.82	24.40	24.58	24.59	24.89	24.44	24.67	25.11	24.55	24.38	24.21	23.70	24.53
2015	24.01	24.20	23.80	24.21	24.46	24.45	24.89	24.90	24.81	24.70	24.79	24.98	24.52
2016	25.28	25.62	25.52	25.49	25.58	25.73	25.63	25.89	25.88	26.25	26.32	26.25	25.79
2017	26.36	26.30	26.51	26.38	26.20	26.26	26.11	25.88	25.66	26.05	26.47	26.46	26.22
2018	26.48	26.48	26.42	26.54	26.55	26.77	26.80	26.72	26.68	26.68	26.57	26.47	26.60

Table 2: Average monthly flux values in p/(m2 s sr GV) in the Earth's orbit according to data from the ground network of cosmic ray stations.

Acknowledgments

This work was partially supported by the grant RFBR № 18-02-00451. Experimentally and methodologically support the project USU "Russian national network of ground stations of cosmic rays". We are grateful to all the staff of the World Network of cosmic ray stations http://cr0.izmiran.ru/ThankYou.

References

Adriani, O., Barbarino, G. C., Bazilevskaya, G. A., et al. (PAMELA Collaboration), 2011, The Astrophysical Journal, 742:102 (11pp), DOI: http://dx.doi.org/10.1088/0004-637X/742/2/102

Adriani, O., Barbarino, G. C., Bazilevskaya, G. A., et al. (PAMELA Collaboration), 2013, The Astrophysical Journal, V.765, N.2. DOI: http://dx.doi.org/10.1088/0004-637X/765/2/91

Adriani O., Barbarino, G. C., Bazilevskaya, G. A., et al. 2014, Physics Reports, 544, 4, 323.

Adriani O., Barbarino, G. C., Bazilevskaya, G. A., et al. (PAMELA Collaboration), 2017, "Ten years of PAMELA in space", Riv. Nuovo Cimento 40 473 DOI: http://dx.doi.org/10.1393/ncr/i2017-10140-x

Aguilar, M., et al. (AMS Collaboration), 2015, Phys. Rev. Lett. 114, 171103 , DOI: http://dx.doi.org/10.1103/PhysRevLett.114.171103

Aguilar, M., et al. (AMS Collaboration), 2018, Phys. Rev. Lett. 121, 051101, DOI: http://dx.doi.org/10.1103/physrevlett.119.251101

Alanko, K., Usoskin, I. G., Mursula, K., Kovaltsov, G. A., 2003, Adv. Space Res., 32 (4), 615–620, DOI: http://dx.doi.org/10.1016/S0273-1177(03)00348-X

Belov, A. V., Dorman, L. I., and Yanke, V. G., 1983, "The simplest versions of the global-spectrographical method". Proc. of 18-th ICRC, Bangalore, Vol. 10, 144-147

Belov, A. V., Gushchina, R. T., Yanke, V. G., 1998, Geomagnetism and Aeronomy, V.38, No.4, 131

CRDB (Cosmic Ray DataBase), 2020, https://tools.ssdc.asi.it/CosmicRays/chargedCosmicRays.jsp (last accessed April 8, 2021)

CR Network, 2020, nmdb: https://www.nmdb.eu/, https://www.nmdb.eu/nest/, usu: http://www.ckp-rf.ru/usu/433536, idb: http://cr0.izmiran.ru/mosc (last accessed April 8, 2021)

Di Felice, V., Pizzolotto, C., D'Urso, D., Dari, S., Navarra, D., Primavera, R., Bertucci, B., 2017,"Looking for cosmic ray data? The ASI Cosmic Ray Database" 35th ICRC, PoS 1073, Korea, https://pos.sissa.it/301/1073/pdf (last accessed April 8, 2021)

Koldobskiy, S. A., Kovaltsov, G. A., Usoskin, I. G., 2018, J. Geophys. Res. 123, 4479, DOI: https://doi.org/10.1029/2018JA025516

Koldobskiy, S. A., Bindi, V., Corti, C., Kovaltsov, G. A., Usoskin, I. G., 2019, J. Geophys. Res. 124, 2367-2379, DOI: http://dx.doi.org/10.1029/2018JA026340

Koldobskiy, S.A., Bindi, V., Corti, C., Kovaltsov, G. A., Usoskin, I.G., 2019, PoS ICRC 2019, id 1094

Krymskiy, G. F., Altukhov, A. M., Kuzmin, A. I., Krivoshapkin, P. A., Skripin, G. V., Chirkov, N.P., 1966, Geomagnetism and Aeronomy, V.6., №6, 991-996.

Lafferty, G. D., Wyatt, T. R., 1995, "Where to stick your data points: The treatment of measurements within wide bins" Nuclear Instruments and Methods in Physics Research A 355, 541-547. DOI: https://doi.org/10.1016/0168-9002(94)01112-5

Martucci, M., et al. 2018, Proton Fluxes Measured by the PAMELA Experiment from the Minimum to the Maximum Solar Activity for Solar Cycle 24, ApJL, 854: L2, DOI: http://dx.doi.org/10.3847/2041-8213/aaa9b2

Nagashima, K., 1971, Rep. of Ionosphere and Space Res. In Japan, Vol. 25, No 3, 189

Ting, S., 2013, The Alpha Magnetic Spectrometer on the International Space Station, Nucl. Phys. B, Proc. Suppl. 243-244, 12-24

Usoskin, I. G., Alanko-Huotari, K., Kovaltsov, G. A., and Mursula, K. , 2005, J. Geophys. Res., 110, A12108, DOI: http://dx.doi.org/10.1029/2005JA011250

Usoskin, I. G., Gil, A., Kovaltsov, G. A., Mishev, A. L. and Mikhailov, V. V., 2017, J. Geophys. Res. Space Physics, 122, 3875–3887, DOI: http://dx.doi.org/10.1002/2016JA023819

Usoskin, I. G., Bazilevskaya, G. A., K., Kovaltsov, G. A., 2011, Journal of Geophysical Research: Space Physics 116, A02104, DOI: http://dx.doi.org/10.1002/2016JA023819

Yanke, V. G., Belov, A. V., Eroshenko, E. A., Trefilova, L. A., Kobelev, P. G., Gushchina, R. T., 2021, "Experimental spectrum of cosmic ray variations in the range of rigidity from 1-20 GV in the Earth's orbit according to AMS-02 data", Cosmic ray studies with neutron detectors 1, DOI: https://dx.doi.org/10.38072/2748-3150/p4

Questions and answers

Ludwig Klein: Would you argue that the calibration of Pamela after 2012 is not reliable?

Answer: No, I wouldn't, it cannot be asserted. The PAMELA data up to and including 2009 and the AMS-02 data for the entire period are in good agreement with the data of neutron monitors, with the PAMELA data used as the base period of 2009. After a long break since 2010, there were problems with the PAMELA detector, it is evident from the increased statistical errors.

Mike Snow: The ~5% shift in 2010 PAMELA data is from the PAMELA collaboration or is factor that gives agreement with neutron monitor data?

Answer: A shift of 4.88% is a factor necessary for agreement with neutron monitor data, but for agreement only since 2010. The PAMELA data up to and including 2009 and the AMS-02 data for the entire period are in good agreement with the data of neutron monitors. The main conclusions of the work are not affected by the normalization of the PAMELA data after 2009.

Cosmic ray studies with neutron detectors | Volume 1 (2021)
KIEL-UP • DOI: 10.38072/2748-3150/p3

About long term modulation of cosmic rays in the 23-24 solar activity cycles

Victor G. Yanke[1], **Anatoly V. Belov**[2], **Raisa Gushchina**

Correspondence
Pushkov Institute of Terrestrial Magnetism, Ionosphere and Radio Wave Propagation (IZMIRAN), Moscow, Russia,
yanke@izmiran.ru, abelov@izmiran.ru, rgus@izmiran.ru

Keywords
cosmic rays; modulation; magnetic field

Abstract
Recently, there has been a significant trend in magnetic fields on the Sun. The total magnetic field of the Sun from the end of the 22nd cycle of solar activity (SA) has more than halved and this decrease continues. Changes in the magnetic field are the key to all the active phenomena occurring on the Sun and in the heliosphere and, accordingly, to processes in cosmic rays. In long-term CR variations in 23-24 cycles of SA the attenuation of the solar magnetic field is displayed and these variations turned out to be the smallest for the entire time of CR observations. Model calculations of CR modulation for 21-22 and 23-24 cycles of SA showed: with a slight difference in the regression characteristics obtained, the distribution of contributions to the generated CR modulation from the effects of various SA indices is strongly varies in the analyzed periods. Possible reasons for the features of the last two SA cycles are discussed.

1. Introduction

The sun is a magnetically active star. The role of the magnetic field in the dynamics of the processes occurring on the Sun is decisive and its variations are the key to all active phenomena occurring on the Sun, in the solar atmosphere and heliosphere. The solar cycle is the result of cyclical changes of the magnetic field that occur in the solar interior. The connection between the CR variations observed on Earth and the cyclic SA has been established long ago, and the variety of manifestations of which provides constant interest in solar CR modulation. Long-term changes of the characteristics of the global magnetic field of the Sun and sporadic SA indicate a decrease of SA observed more than twenty years, which starting from the end of the 22nd SA cycle. During the transition from the 22nd cycle to the 23rd, the activity of the Sun decreased quite sharply, and in the 24th cycle this decrease continued. For the entire time of observations of the Sun, there was nothing like this. This change of SA is especially manifested as a weakening of the solar magnetic field, which spreads to the solar wind and the heliosphere (Livingston et al. 2012; Ishkov 2013; Sun et al. 2015). As a result of the process of restructuring the general magnetic field of the Sun, there is a trend towards a decrease of magnetic fields of all structures on the Sun. The rate of development and the level of flare activity in the 24th cycle is significantly lower than observed in previous cycles, and there were no very large and extreme flare events at all.

The observed weakening of the global magnetic field of the Sun and the corresponding trend of heliospheric characteristics in 23-24 SA cycles (1996-2019) raises the question of the response of this phenomenon to long-term CR modulation in these cycles. This can be clarified most clearly

KIEL-UP • DOI: 10.38072/2748-3150/p3

when comparing the observed CR variations in cycles 23-24 (1996-2019) with variations in the previous 21-22 SA cycles (1976-1996). In this work, the study of long-term CR variations is based on the construction of a CR modulation model, combining several solar indices. As the main modulating characteristics of the global magnetic field of the Sun, the model proposes: the polar magnetic field of the Sun, coronal holes, characteristics of large-scale fields - the average magnetic field on the surface of the solar wind source and the field of the Sun as a star, as well as the slope of the heliospheric current sheet (corresponding justification for the choice of characteristics given in Belov et al. 2002; Gushchina et al. 2008, and links to them). The sporadic SA in the model is described using the CME index (Belov & Gushchina 2018). In the modulation model developed by us, the characteristics of the magnetic field on the surface of the solar wind source are calculated based on observations that began in 05.1976 (the beginning of the 21st cycle) at the observatory Wilcox (WSO, http://wso.stanford.edu/, last accessed April 6, 2021). The analysis of the CR modulation features in 21-24 cycles was carried out on the basis of long-term observations of the above mentioned SA characteristics and of the data of continuous CR monitoring on the world network of cosmic ray stations. The density of CR continuous ground observations of which on the world network of cosmic ray stations have been carried out using neutron monitors since 1957, in the last two cycles (23rd and 24th) is very different from what we saw in previous cycles. Firstly, the low SA minimum at the end of 2009 (minimum SA 23/24 cycle) caused a record increase in the CR density and a comparable minimum 24/25 cycle (in August 2019, according to preliminary data) is distinguished by a continuing increase of CR intensity until the end of 2019. For more than sixty years of continuous CR observations, previously ground-based observations did not achieve such CR density values which exceed the previous four CR maxima (in cycles 19-22) the value of which may approach the extraheliospheric level. Secondly, the unusually weak CR modulation in the 23rd and 24th SA cycles is surprising. The purpose of this work is to analyze the features of CR modulation in 23-24 cycles (1996-2019) and compare the results obtained with CR modulation in 21-22 cycles (1976-1996).

2. Data of CR and characteristics of SA peculiarities of time variations CR and SA indices

Here, continuing the study of long-term CR modulation those begun in a previous works (for example, Belov et al. 2002, 2005; Gushchina et al. 2008), we describe the process of long-term CR modulation separately for two periods 05.1976-10.1996 and 11.1996-12.2019 to consider the role of weakening of the solar magnetic field in CR modulation. The observed trend of the solar magnetic field to cosmic radiation is considered for the 23rd and 24th cycles of «lowered» SA and is compared with CR modulation in the 22nd cycle of the «transient» SA and in the 21st cycle of the «increased» SA (https://www.izmiran.ru/library/pushkov2019/pushkov2019abs.pdf, last accessed April 6, 2021).

The initial data for modeling CR variations are observations of the CR intensity and of a number of SA characteristics which reflect changes in the solar wind structures observed during the development of SA cycles and contribute to modulation. Long-term variations of galactic CRs in 21-24 SA cycles were obtained by global survey method based on data from the global network of ground-based detectors (~ 40 neutron monitors), data from a multi-directional telescope (Nagoya station), and the results of stratospheric sounding at three different points (Stozhkov et al. 2007). The spectrum of long-term CR variations for 1976-2019 calculated by the method (Belov, Gushchina, Sirotina 1993), further analysis was carried out using the monthly mean values of CR variations with 10 GV rigidity *(a10* is the value of long-term variations in galactic CRs). In this work, the spectrum of long-term variations was determined relative to the SA minimum in the 23rd cycle (2009).

The contribution to modulation is largely determined by the temporal changes of the solar magnetic fields of different scales (global and local) during their interaction. Since CR are charged particles, their behavior is determined by IMF and can be seen in observed variations of cosmic

radiation. The effect of SA on the observed CR modulation is described through the following chain: the magnetic field of the Sun (the dipole component of the solar magnetic field *Hpol*, which changes its sign at the maximum of the local fields cycle) - the surface of the solar wind source (the average magnetic field *Bss* - the integral energy characteristic of the SA, defined as the square of the radial component of the magnetic field, and the structural characteristic - the slope of the current sheet *hcst*), the average field of the Sun as a star *Bmf* - heliosphere (characteristic of the solar wind - interplanetary magnetic field *Bimf*) - cosmic rays (in work - the amplitude of CR variations with a rigidity of 10GV - *a10*). The time changes of the parts of this interconnected chain, which are important for CR modulation, namely, the characteristics of the global magnetic field of the Sun (according to the results of daily observations of the Sun's field on magnetographs (http://wso.stanford.edu/) and the heliospheric characteristic - the interplanetary magnetic field (https://omniweb.gsfc.nasa.gov/, last accessed April 6, 2021) associated with the solar field is shown in figure 1 (a-h), where, in addition to the above modulating CR characteristics, the characteristics of the coronal holes area effect to modulation (Gushchina et al. 2016) and sporadic solar activity (using the introduced CME index). The decrease trend in the 23-24 SA cycles (1996-2019) of the indicators of global processes on the Sun and in the heliosphere is clearly visible. A particularly significant decrease occurs in the solar magnetic field (figure 1a-e) at the boundary of the solar wind and extends to the characteristics of heliomagnetosphere, primarily by the IMF value (figure 1b), together with a change in the density and speed of the solar wind (Belov et al. 2001). Accordingly, a decrease in the SA and IMF levels leads to a change (increase) in the CR intensity observed on Earth and in near-Earth space (figure 1f). A twofold decrease of average field on the source surface *Bss* has occurred, as is clearly seen in figure 1a, in the last more than 20 years. As for the magnetic fields in the solar wind above the poles, heliophysicists have established (Ishkov 2013) that, in general, over the past 30 years, they have decreased by about three times.

3. Choice of the indices for a modulation model

Long-term CR modulation was described using a multiparameter model in which the SA parameters are linearly related to the amplitude of CR variations. When constructing the model, a combination of modulating parameters is used; the corresponding justification for the choice of which is given in (Belov et al. 2002, 2005; Gushchina et al. 2008). Figure 1 (a-h) shows the time course of the characteristics for several cycles; below (figure 2 a-c,e,f) will be presented the temporal changes of the characteristics which used to build the modulation model in the 21-22nd and 23-24th cycles to compare the CR variations (figure 2d) in them. The trend of the main parameter modulating CR - the global magnetic field of the Sun-is its significant and prolonged decreasing, ultimately leads to a trend in the characteristics of the SA and the heliospheric field. Below is a summary of the temporal changes in each index. The *hcst* (figure 1d) correlates best with CR variations and is the main parameter in the CR modulation model, the modulation depth depends on it, the current sheet is the largest magnetic inhomogeneity in the heliosphere with which CRs interact; it is the place of the most effective drift. In the last activity minima, the *hcst* values increase (from 9.3° at the 22/23 minimum to 16.6° in the period close to the 24/25 minimum). Increase of this structural characteristic at the SA minima was noted in (Gushchina et al. 2012) with the assumption of the role of the drift effect in its creation.

The square of the radial component of the magnetic field averaged over the surface of the solar source the wind *Bss* (figure 1a) has been decreasing since the end of the 22nd cycle, at the 23/24 minimum unprecedentedly low values were recorded. When using IMF data *Bimf* (figure 1b) in modeling, there is always a doubt: can the measurements of the IMF near the Earth sufficiently well characterize changes in magnetic fields in the entire heliosphere, where CR modulation occurs.

Therefore, there is a desire to find another parameter that also well complements the hcst, but, in contrast to the IMF intensity, is more global. Probably it is better idea to search for this parameter

KIEL-UP • DOI: 10.38072/2748-3150/p3

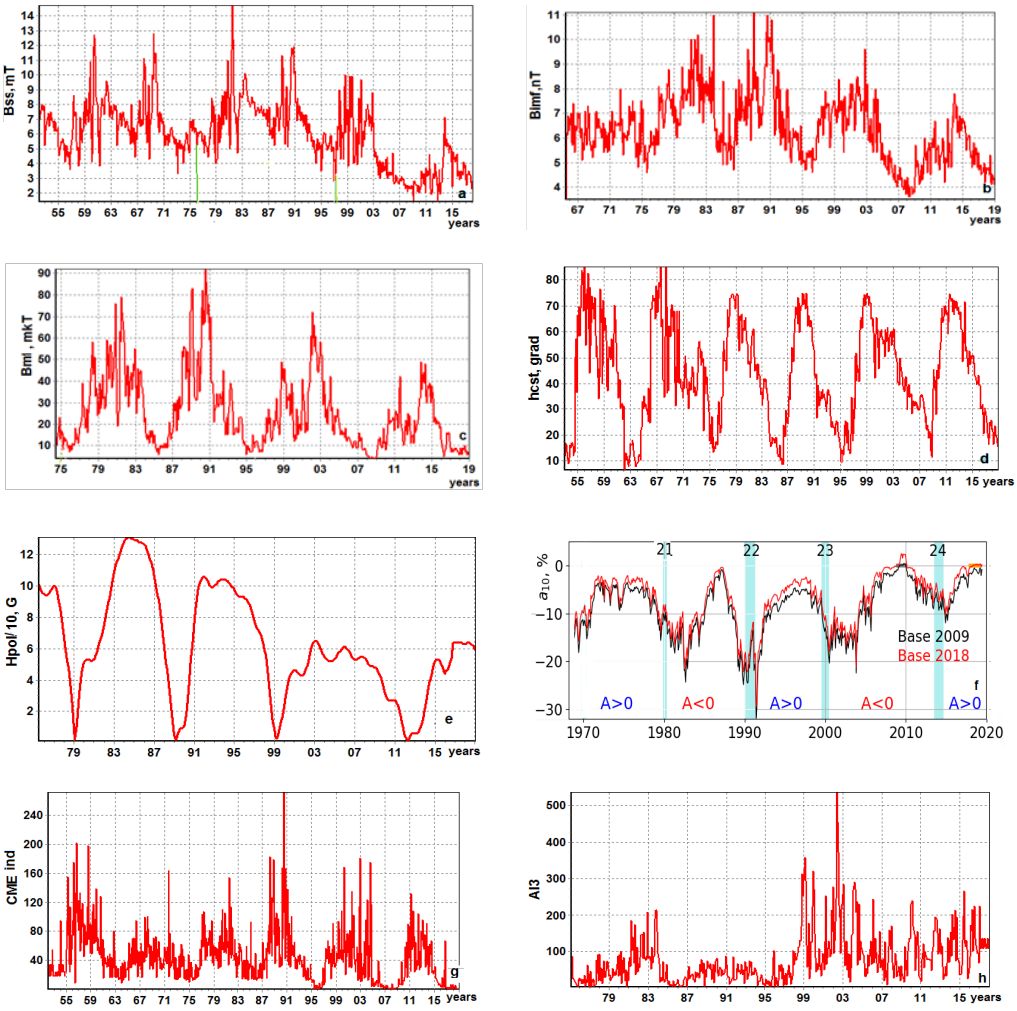

Figure 1: Cyclic variations of: a) - mean magnetic field of the Sun (*Bss*) (Obridko & Shelting 1999) b) magnetic induction of the interplanetary magnetic field near the Earth (*Bimf*); c-magnetic field of the Sun as Bmf stars); d) - the slope of the heliospheric current sheet (hcst);e) polar field of the Sun (*Hpol*) f) -variations of CR density with a rigidity of 10 GV (a10,% -); g) -CME index (Belov & Gushchina 2018); h) -area of low-latitude coronal holes (AL3) (Gushchina et al. 2016).

on the surface of the source, where the hcst is determined. The relationship between *Bss* and the modulus of the heliospheric field *Bimf*, measured near the Earth, is quite close. So interchangeability of *Bimf* and *Bss* in modulation models is revealed. It is shown at (Belov et al. 1999, 2002), that replacing the heliospheric field module *Bimf* in the empirical model by the average magnetic field *Bss* is not only possible, but even improves the quality of the model. *Hpol* (figure 1e) - the polar magnetic field of the Sun - is taken into account in the model by magnitude and by sign; in the last two cycles it has a smaller, than before, and decreasing with time amplitude; CME-index (figure 1g) - takes into account the effect of sporadic SA on CR modulation; it decreases, especially in the 24th cycle. AL3 (figure 1h) – the area of low-latitude coronal holes, the choice was justified in (Gushchina et al. 2016); it increases modulation in contrast to high-latitude coronal holes. The effect of low-latitude holes occurs in antiphase with other modulating indices. Note that in solar cycles the indices listed below behave differently, this allows us to hope that we can get a complete picture of modulation when constructing a model with complementary indices.

KIEL-UP • DOI: 10.38072/2748-3150/p3

4. Describing long-term CR variations using a model based on solar characteristics

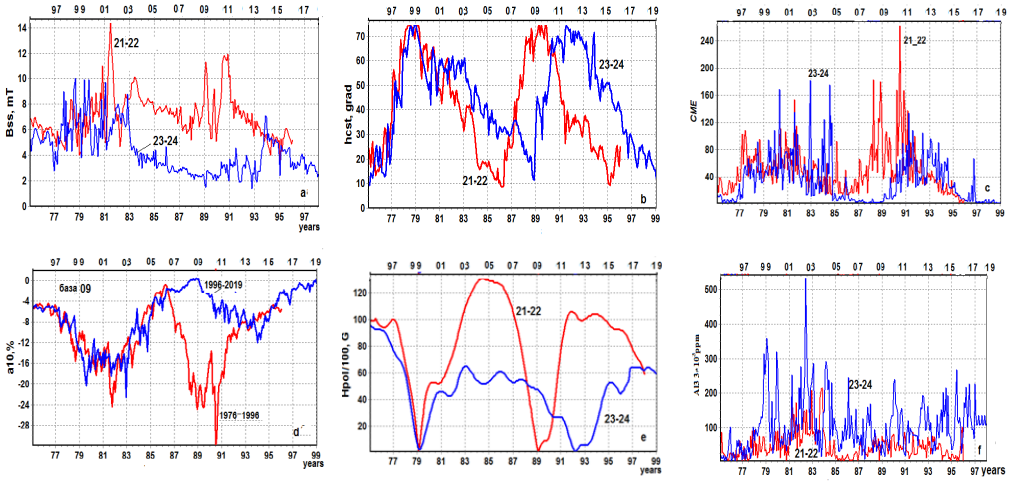

Figure: 2 (a-f) Changes of indices (red curves - 21-22 cycles; blue ones - 23-24 cycles; a, b, c-are determined on the source surface: a) - mean magnetic field of the Sun (*Bss*); b) is the slope of the heliospheric current sheet (hcst); c) -CME index; d) - variations in CR density with a rigidity of 10 GV (a10,% to 2009); e) - solar polar field (*Hpol*); f) - area of low-latitude coronal holes (AL3).

An understanding of the process of modulation of galactic CRs by the heliosphere electromagnetic fields is facilitated by modeling CR variations. Our group has proposed a semi-empirical multivariate model (Belov et al. 2002, 2018; Gushchina et al. 2008, 2016; Yanke et al. 2019), in which the long-term CR modulation is described by the mentioned above characteristics with a detailed justification for their choice. For these indices and the amplitude of CR variations with a rigidity of 10 GV *a10,%* to 2009, a multivariable regression analysis was performed taking into account the delay for each parameter and the role of each of them in CR modulation was revealed. The set of the above indices reproduces well the observed variations when describing modulation. The CR level has been growing at the last two cycles, while the 11-year cyclicity has been preserved, but the amplitude of variations has decreased. As a result of the model description of CR variations, carried out separately for 21-22 and 23-24 cycles, we obtained: correlation coefficient (r), standard deviation of the model (δ), regression characteristics (k), and delay times of CR variations relative to the SA indices (t_{delay}) (table 1).

cycles	r	δ	k_{hcst}	k_{Bss}	k_{CME}	k_{Al3}
21-22 (1976.08-6.10)	0.97	1.59	-0.19	-0.76	-0.05	0.009
t_{delay}			14	5	1	8
23-24 (1996.11-9.12)	0.96	1.60	-0.10	-1.90	0.038	0.009
t_{delay}			25	4	1	8

Table 1: Results of multivariable regression analysis for 21-22 and 23-24 cycles.

5. Discussion and conclusion

The observed and expected CR variations in 21-22 and 23-24 cycles and the contributions to the modulation model from changes in solar heliospheric characteristics are shown in figure 3. The main role in

KIEL-UP • DOI: 10.38072/2748-3150/p3

modulation in 21-22 cycles belongs to the slope of current sheet (*hcst*), and in 23-24 cycles belongs to *Bss*. (figure 3a, b). Regression coefficient for *hcst* in 23-24 cycle model is - 0.1%/°. This is ∼ 2 times less than in 21-22 cycles (-0.19%/°). The regression coefficient for *Bss* in 23-24 cycles is -1.9% / μT, and in 21-22 cycles is-0.76% / μT. The CR modulation in these SA cycles is much weaker than the modulation in 21-22 cycles. The reason is anomalies which appears on the Sun and in the heliosphere during last two cycles due to the weakening of the solar magnetic field and the state of the heliosphere.

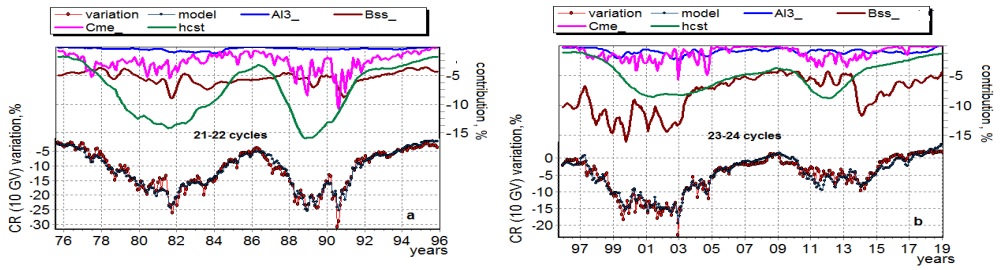

Figure 3: - a10 (% to 2009) - variations of the density of CRs with a rigidity of 10 GV (red curve with dots in the lower part of the figure) and the result of their simulation (solid black curve); upper part of the figure - the contribution from changes: the slope hcst (green curve), the mean magnetic field of the Sun *Bss* (brown), the CME index (pink) and the area of coronal holes AL3 (blue): (a) - 21-22 and (b) -23-24 cycles.

The analysis of the 23rd cycle with weak CR modulation and the 24th cycle, the lowest during the CR observation time, can be explained by the different (in comparison with other cycles) impact on CR of specific physical processes (drift, diffusion, convection, and adiabatic energy changes) which create modulation. The interaction of the main modulation mechanisms and the role of modulation characteristics in generating overall modulation changes with solar cycles (Potgieter 2013; Belov et al. 2017, Kalinin et al. 2017). In the presented modulation model, the contribution to the overall modulation from the CR drift effect in the 24th cycle is lower. In the modulation model for cycles 23-24, the aforementioned predominance of the contribution from the action of a large-scale magnetic field on the Sun on CR, expressed in the value of the *Bss* index (taking into account the relationship between *Bimf* and *Bss*), may indicate an increase in the role of CR diffusion during propagation in the heliosphere with a low IMF (Kalinin et al. 2017). In the 23-24th cycles, a decrease of the influence of the current sheet tilt angle on the CR modulation was revealed. The change in its value occurs within the same limits as in other cycles, but the effectiveness of the effect on modulation is greatly reduced (requires additional explanation!). In the 23-24th SA cycles, the general CR modulation is dominated by the effect of a large-scale magnetic field on the Sun on CR, expressed in the *Bss* index, despite a decrease in the *Bss* value itself.

Acknowledgments

Experimentally and methodologically support the project USU “Russian national network of ground stations of cosmic rays”. We are grateful to all the staff of the World Network of cosmic ray stations: http://cr0.izmiran.ru/ThankYou.

References

Belov, A., Gushchina, R., Sirotina, I., 1993, Proc. 23-rd ICRC. 3, 605
Belov, A., et al. 1999, Bulletin of the RAS. Physics, 63, 8, 1606

Belov, A., et al. 2002, Geomagnetism and Aeronomy, 42, 6, 727
Belov, A., Gushchina, R., Obridko, V. et al. 2005, Proc. 29th ICRC, 2, 235
Belov, A., Gushchina, R., Tlatov, A., Yanke, V., 2016, Geomagnetism and Aeronomy, 56, N3, 275
Belov, A., Gushchina, R., Yanke, V., 2017, Bulletin of the RAS. Physics., 81, 2, 165
Belov, A., Gushchina, R., 2018, Geomagnetism and Aeronomy, 58, 1, 3
Goddard's Space Physics Data Facility, https://omniweb.gsfc.nasa.gov/ (last accessed April 21, 2021)
Gushchina, R. et al. 2008, Geomagnetism and Aeronomy, 48, 5, 1
Gushchina, R. et al. 2012, Geomagnetism and Aeronomy, 52, 4, 1
http://www.izmiran.ru/library/pushkov2019/pushkov2019abs.pdf. DOI: https://dx.doi.org/10.31361/pushkov2019.017
Ishkov, V., 2013, J. Physics: Conference Series (JPCS). 409. 1216
Kalinin, M., Bazilevskaya, G., Krainev, M.,et. al., 2017, Geomagnetism and Aeronomy, 57, 5, 549
Livingston, W., Penn, M., Svalgaard, L., 2012, Astrophys.J. Lett., 757:L8
Obridko, V., and Shelting, B., 1999, Solar physics, 184. 187
Potgieter, M., 2013, Living Reviews in Solar Physics, 10(3), DOI: https://dx.doi.org/10.12942/lrsp-2013-3
Stozhkov, Yu., et al. 2007, Preprint M.: Phys. Lebedev inst.RAS. 55
Sun, Xudong, Hoeksema J. Todd, Liu Yang, Zhao Junwei, 2015, Astroph. J., 798, 2, 114, 8
The Wilcox Solar Observatory, http://wso.stanford.edu/ (last accessed April 6, 2021)
Yanke, V., Belov, A., Gushchina, R., Zirakashvili, V., 2019, Journal of Physics: Conf. Series 1181

Cosmic ray studies with neutron detectors | Volume 1 (2021)
KIEL-UP • DOI: 10.38072/2748-3150/p4

Experimental spectrum of the cosmic ray variations within rigidity range of 1-20 GV in the Earth's orbit by the data of AMS-02

Victor G. Yanke, Anatoly V. Belov, Liudmila Trefilova, Pavel G. Kobelev, Eugenia A. Eroshenko†, Raisa Gushchina

Correspondence

Pushkov Institute of Terrestrial Magnetism, Ionosphere and Radio Wave Propagation (IZMIRAN), Moscow, Russia, yanke@izmiran.ru, abelov@ izmiran.ru, trefilova@izmiran.ru, kosmos061986@yandex.ru, erosh@ izmiran.ru, rgus@izmiran.ru

Keywords

long-term variations; AMS-02; spectrum of variations; ground-based detectors

Abstract

For the first time, based on the experimental data of AMS-02, a three-parameter spectrum of variations of galactic cosmic rays was obtained in the range of rigidity 1- 20 GV, to which neutron monitors are most sensitive. It was found that during the period of negative polarity of the solar magnetic field, a power-law spectrum of variations is observed with a strong exponential decay in the region of high rigidity. When the polarity changes to positive at the beginning of the new 24th solar cycle, the spectrum of cosmic ray variations becomes purely power-law. The transition to the experimentally obtained spectrum of variations will make it possible to remove a number of uncertainties and increase the accuracy of the analysis of data from the ground network of detectors. This will make it possible to retrospectively obtain fluxes of galactic protons with an average monthly resolution for the period of the space era based on ground-based monitoring.

1. Introduction

Despite the significant progress achieved in recent decades, the physical mechanisms underlying the modulation of galactic cosmic rays in the heliosphere still the subject of discussion. The complex process of particle transfer creates problems for the development of a universal picture of long-term variations in galactic cosmic rays, which covers a long observational period (on the order of 70 years) of continuous monitoring of cosmic radiation.

Experimental data on flux variations over the period from the mid-1950s to the present could be obtained with good accuracy only from continuous ground-based measurements on a network of cosmic ray detectors. The need to analyze the results of such long-term ground monitoring led to the creation of special methods. One of the earliest and most successful implementations of the global method was created in Yakutsk (Krymsky 1966, 1967, 1981; Altuchov 1969) and was named the "Global Spectrographic Method" (GSM), since the calculations used data from a network of detectors distributed across the globe. Around the same time, Japanese researchers proposed their methodology (Nagashima 1971). In essence, in all variants this is a method of spherical analysis, where the expansion of the function of cosmic ray variations in spherical harmonics is used. But this takes into account cascade processes in the atmosphere and the movement of particles in the Earth's magnetosphere. With this in mind, we can say that GSM is essentially a sophisticated ver-

† deceased

KIEL-UP • DOI: 10.38072/2748-3150/p4

sion of spherical analysis. IZMIRAN has created its own version of GSM (Belov et al. 1973, 1974, 2019), which has been used for many years for a detailed and comprehensive study of variations in cosmic rays of the zero harmonic (isotropic component of cosmic ray variations), the first spherical harmonic (e.g. Belov et al., 2017), and sometimes the second harmonic of cosmic ray variations.

In the simplest case, the problem is reduced to solving a system of equations describing the cosmic ray variations at each point and obtaining the parameters of the isotropic component variation.

Directly observed variations in the count rate of the *i*-th cosmic ray detector (where N_B is the base count rate relative to which the variations are calculated) can be represented as

$$v_i = \int_{R_c^i}^{\infty} W^i\left(R, R_c^i, h_0^i\right) \cdot \frac{\delta J}{J(R)} \cdot dR + \sigma^i. \quad (1)$$

Here $W^i(R, R_c^i, h_0^i)$ is a coupling function between primary cosmic ray and variations of the secondary cosmic ray registered by detector *i* located in the point with geomagnetic cut off rigidity R_A^i on the atmospheric depth h0. The spectrum of the primary cosmic radiation and the desired spectrum of the isotropic variation are designated, respectively, as $J(R)$ and $\delta J/J(R)$. The discrepancy σ^i reflects the inadequacy of the used model of variations and possible hardware variations.

The coupling functions determine the influence of the Earth's atmosphere, and the magnetosphere effect takes into account the rigidity of the geomagnetic cutoff of the considered detector. The coupling functions of the neutron component were calculated by us (Aleksanyan et al. 1982), the coupling functions of the muon component were used from Fujimoto et al. (1976).

An important situation is when the analytical form of the desired solution is known, or the solution can be approximated with a high degree of reliability by a model built on the basis of a priori information. In this case, as a rule, the corresponding system of equations for finding a small number of unknown parameters turns out to be well conditioned. The advantage of this situation is that it is practically impossible to obtain an absurd solution if the analytical model is chosen in accordance with the process under study.

The objective of this work is to establish the analytical form of the spectrum of variation with a minimum number of parameters for use in analyzing data from the global network of ground-based cosmic ray detectors using the AMS-02 experimental data on the spectrum of protons and nuclei in the range of rigidity from several GV to several tens of GV. This will make it possible to abandon the empirically specified spectra of variation.

2. Data of magnetic spectrometer AMS-02

High-precision data of the orbital detector of cosmic rays AMS-02 for the study of dark matter and antimatter also provide a unique opportunity to measure spectral characteristics at moderate and high rigidity.

Direct measurements of galactic cosmic rays in the range of rigidities from one to several tens of GV were carried out on the PAMELA and AMS-02 spacecraft. The statistical accuracy of the data of the AMS-02 magnetic spectrometer is significantly higher, since the geometric factor of the AMS-02 is about 0.5 m2 sr, and the PAMELA spectrometer is only 21.5 cm2 sr. This work was based on the data of the AMS-02 magnetic spectrometer.

AMS-02 (Aguilar et al. 2015, 2018) is a magnetic spectrometer operating onboard the *International Space Station* from 2011 to the present. The digital data is available in the database (CRDB 2020). A description of the database can be found in Valeria et al. (2017).

Sampling by rigidity or by time (t, R) is possible with fixing one of the parameters. For a given moment in time, proton spectra can be obtained in a very wide range of rigidities. In this work, we limited ourselves to the particle rigidity in the range 1 - 20 GV, to which the network of ground-based neutron monitors is most sensitive.

KIEL-UP • DOI: 10.38072/2748-3150/p4

The entire time period is divided into 79 intervals averaged by the Carrington rotation since May 2011 (2110 rotations). For example, the time dependence of the proton flux for two energy ranges close to the rigidity of 10 GV can be found in Belov et al. (2020).

3. Ground methods

In Belov et al. (1998) a variant of the global spectrographic method is described, specially adapted for studying the long-term behavior of isotropic CR variations. The analysis is carried out using the monthly average data of neutron monitors (about 45 detectors), muon telescopes, and stratospheric sounding. In the simplest case of isotropic variations the problem is reduced to solving the system of equations (1). In the model, it was assumed that the spectrum of variations is given in a three-parameter form and is defined as:

$$\delta J / J(R) = a_1 / (R_L + R)^{\gamma} . \quad (2)$$

Area of the parameter changes $\gamma = 0 \div 2$ and: $R_L = (0 \div 4)$ GV.
A three-parameter approximation of the GCR variation spectrum is suitable for describing the spectrum of long-term variations in the 5-50 GV regions.

Figure 1 shows the parameters of the spectrum of variations in galactic CR: a_{10}, R_L and γ, obtained by this method. The bottom panel shows the standard deviations of the experimental data from the model, which make it possible to assess the adequacy of the applied variation model.

The spectrum of variations in the form (2) was chosen empirically, but other options were also considered. A direct experimental verification of the shape of the spectrum of variations in the range of rigidity from one to several tens of GV has never been carried out, since the maximum rigidity of particles in measurements of fluxes outside the magnetosphere at best reached 2 GV. Direct measurements in a wide range of rigidities using unique magnetic spectrometers will solve this problem.

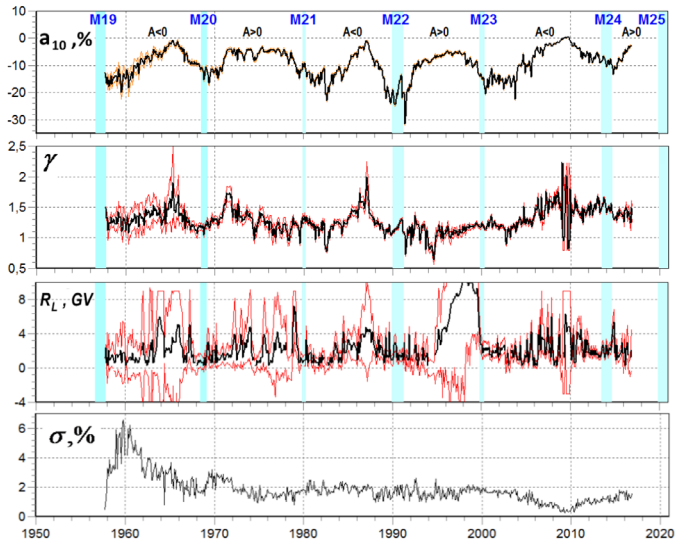

Figure 1: Parameters of the galactic cosmic rays variation spectrum: a_{10}, R_L and γ the model discrepancy is shown at the bottom.

KIEL-UP • DOI: 10.38072/2748-3150/p4

4. Method of experimental determination of the spectrum of variations

To experimentally determine the spectrum of GCR variations, we used data from the AMS-02 magnetic spectrometer for the entire period of its operation. The time course of AMS-02 flux variations relative to the 2009 base period and their comparison with the GSM results are shown in the top panel of figure 2. The period of the polarity reversal of the Sun magnetic field from the second half of 2013 to the first half of 2014 is also highlighted here (Sun 2015; Ishkov 2018). But above all, the measured flux was freed from the contribution of solar cosmic rays.

For this, the periods of solar events were excluded from the analysis: 13 SPE, including 6 GLEs (see table 1). The selection criterion for the events was the excess of the proton flux > 100 MeV threshold of 1 pfu (graphical data can be found on the website (SWPC 2020)).

Analysis shows that the contribution ($< 10^{-4}$ %) of solar cosmic rays can be neglected by considering the averaged GCR flux per Carrington revolution. In figure 2 (top left panel), the SPE and GLE moments during the AMS-02 operation period are marked with vertical segments, the length of which is proportional to the effect.

dt	Flash score	p>100 MeV, pfu	GLE, %
2011-08-04 03:41	M9.3	2	
2011-08-09 07:48	X6.9	2.5	
2012-01-23 03:38	M8.7	2.3	
2012-01-27 17:37	X1.7	11.9	7.0
2012-03-07 00:02	X5.4	70	0.1
2012-03-13 17:12	M7.9	2	
2012-05-17 01:25	M5.1	20	15.0
2013-04-11 06:55	M6.5	2	
2013-05-22 13:08	M5.0	3	
2014-01-06 07:45		4.1	3.0
2014-01-07 18:04	X1.2	4.2	
2015-10-29 02:19		2	1.0
2017-09-10 15:35	X8.2	50	6.0

Table 1: Proton enhancements for operating period of the AMS-02.

The result of the analysis in figure 2 is shown for the period of negative polarity (left) and positive polarity (right) of the Sun magnetic field, and the time point is marked with a vertical line in the upper panel of the figure.

The middle panel shows the spectrum of particles (protons) J for the considered moment of time and the spectrum of particles J_B for the base period. Due to the lack of data for a later period, January – April 2017 was selected as the base period (horizontal segment on the top panel), although the SA minimum and the maximum count rate are observed in April 2020. The results should be considered as preliminary and should be revised after updating the AMS-02 data.

Changes in the particle spectrum relative to the particle spectrum in the base period determine the spectrum of variations. By definition, the spectrum of variations for each point in time is defined as:

$$v = J / J_B - 1 \tag{3}$$

In the last expression, the variables are functions of time and rigidity, i.e. $v(t,R)$, $J(t,R)$ and $J_B(R)$. The experimental spectrum of variations, in this way determined, is shown in the lower panel of figure 2 (points and errors in their determination) for two polarities of the total magnetic field of the Sun.

KIEL-UP • DOI: 10.38072/2748-3150/p4

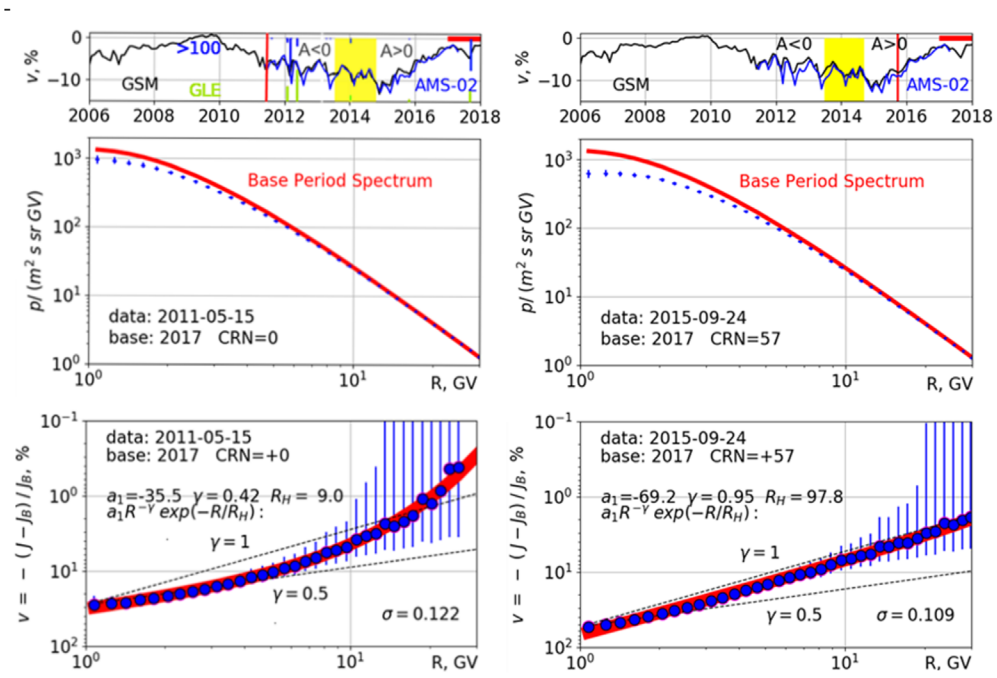

Figure 2: An example of spectra for two points in time: for a period of negative (left) and positive polarity (right) of the total magnetic field of the Sun. The middle panels show the particle spectra (obtained from AMS-02) and the spectra of variations found on their basis, shown in the lower panels.

The choice of the approximating function for the spectrum of variation depends on the rigidity range and the problem being solved. Several analytical models of the spectra of cosmic ray variations were considered, including the spectrum of variations of the form (2).

However, the most successful for approximating the experimental spectrum of cosmic ray variations in a wide range of rigidities was the power-law spectrum modulated by an exponential in the region of upper rigidities, i.e.

$$v = a_1 R^{-\gamma} \exp(-R/R_H), \tag{4}$$

where R_H -upper rigidity. Function (4) is nonlinear with respect to the parameters a_1, γ and R_H. System (4) can be reduced to linear by taking the logarithm. As a result, we obtain a system of linear equations for the parameters $\ln a_1$, γ and $1/R_H$:

$$\ln v_i = \ln a_1 - \gamma \ln(R_i) - R_i / R_H \tag{5}$$

The parameters of approximation a_1, γ and R_H for two time moments with positive and negative polarity of the total magnetic field of the Sun also presented at the bottom panels in figure 2.
More common model:

$$v = a_1 (R_L + R)^{-\gamma} \exp(-R/R_H) \tag{6}$$

In the region of lower rigidities ν is also controlled by a parameter, but the model has not yet been considered, since it remains nonlinear even after the logarithm procedure.

KIEL-UP • DOI: 10.38072/2748-3150/p4

5. Discussion of the results

The parameters of approximation a_1, γ, and R_H in the considered model (4) were obtained for each solar rotation since May 2011. In the period of negative polarity of the solar magnetic field (A < 0) before the polarity reversal, the parameter R_H is close to 10 GV, and during this period, a power-law spectrum of GCR variations with strong exponential decay in the areas of rigidity > 20 GV is observed. With a change in polarity and at the beginning of a new 24th solar cycle, the parameter R_H becomes close to 100 GV, and the spectrum turns into a purely power-law spectrum.

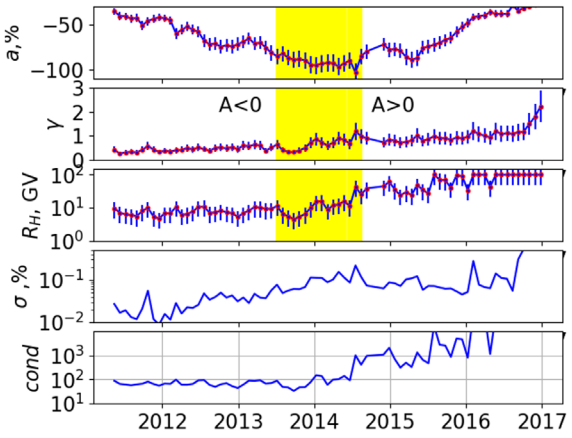

Figure 3: Time dependence of the parameters of the CR spectra variations by the AMS-02 data.

For the entire period according to AMS-02 data in figure 3 the time dependence of the parameters of the spectrum of variations in cosmic rays are presented. The values of a1, γ, and R_H were obtained as a result of approximation of the experimental spectra, which are shown in figure 2. The peculiarities of the behavior of the parameters γ and R_H in periods of different polarities of the solar magnetic field are clearly visible. The γ exponent increases linearly over the period under consideration, and the RH parameter increases abruptly from an average value of ∼ 10 GV to ∼ 100 GV after a period of polarity reversal of the solar magnetic field, which is accompanied by a transition to a power-law spectrum of cosmic ray variations. The last two panels in figure 3 show the time dependence of the model error σ and the condition number «cond». The value of the conditionality number until the end of the polarity reversal is at the level of 100, which indicates a well-conditioned system of equations (4). When approaching the base period, the condition number increases rapidly.

It can be noted that before the solar activity maximum in 2014 and the polarity reversal, the experimentally measured variations on the AMS-02 experiment in some periods are almost twice as large as the variations obtained by the GSM method from the data of ground-based detectors. This coincides with the period of negative polarity A < 0 of the solar magnetic field, in the period of positive polarity A > 0 after the polarity reversal of the solar magnetic field, this effect is not observed.

6. Summary and conclusions

Due to its unique capabilities, the satellite experiment AMS-02 for the first time made it possible to obtain an experimental spectrum of cosmic ray variations in the range of rigidities to which the ground-based network of neutron monitors is sensitive. This, in turn, will make it possible to remove the uncertainty in the choice of the spectrum of cosmic ray variations during GSM analysis, since until now the spectrum of cosmic ray variations was determined only empirically.

In this work, based on AMS-02 data, for the first time, the experimental spectrum of cosmic ray variations and its temporal changes in the range of rigidity 1-20 GV for the period from May 2011 to April 2017 are obtained. The found form of the spectrum of variations will make it possible to increase the accuracy of the reconstructed parameters of the spectrum of cosmic ray variations outside the magnetosphere from the data of the network of ground-based cosmic ray detectors.

An important result of this work is the transformation of the form of the spectrum at different periods of polarity of the interplanetary magnetic field. During the period of negative polarity $A < 0$ of the solar magnetic field, a power-law spectrum of variations with a strong exponential decay is observed in the region of upper rigidities.

When the polarity changes $A > 0$ the spectrum of cosmic ray variations transforms into a purely power-law spectrum.

In the work for the base period, the data of January – April 2017 were used, but when new data are published, including the minimum SA and the maximum count rate in April 2020, the calculations of the spectrum of variations must be updated.

Acknowledgments

The work was carried out on the experimental basis USU („Russian national network of ground cosmic ray stations“). We are grateful to all the staff of the World Network of cosmic ray stations: http://cr0.izmiran.ru/ThankYou

References

Adriani, O., Barbarino, G. C., Bazilevskaya, G. A. et al. (PAMELA Collaboration), 2017, "Ten years of PAMELA in space", Riv. Nuovo Cimento 40, 473-522, DOI: https://dx.doi.org/10.1393/ncr/i2017-10140-x; Google Scholar (last accessed April 6, 2021)

Aguilar, M., et al. (AMS Collaboration), 2015, Phys. Rev. Lett. 114, 171103; DOI: https://dx.doi.org/10.1103/PhysRevLett.114.171103

Aguilar, M., et al. (AMS Collaboration), 2018, Phys. Rev. Lett. 121, 051101, DOI: https://dx.doi.org/10.1103/physrevlett.119.251101

Alanko, K., Usoskin, I. G., Mursula, K., Kovaltsov, G. A., 2003, Adv. Space Res., 32 (4), 615–620, DOI: https://dx.doi.org/10.1016/S0273-1177(03)00348-X

Belov, A. V., Dorman, L. I. and Yanke, V. G., 1983, "The simplest versions of the global-spectrographical method". Proc. of 18-th ICRC, Bangalore, Vol. 10, 144-147

Belov, A. V., Gushchina, R.,T., Yanke, V.,G., 1998, Geomagnetism and Aeronomy, V.38, No.4, 131

Belov, A. V., Gushchina, R.T., Shlyk, N.S., Yank,e V.G.,"Comparison of long-term variations of the cosmic ray flux from the network of ground-based detectors, PAMELA and AMS-02 data", Cosmic ray studies with neutron detectors 1 DOI: https://dx.doi.org/10.38072/2748-3150/p2

CRDB (Cosmic Ray DataBase), 2020, https://tools.ssdc.asi.it/CosmicRays/chargedCosmicRays.jsp (last accessed April 6, 2021)

CR Network, 2020, nmdb: https://www.nmdb.eu/, https://www.nmdb.eu/nest/, usu: http://www.ckp-rf.ru/usu/433536, idb: http://cr0.izmiran.ru/mosc (last accessed April 6, 2021)

DiFelice, V., Pizzolotto, C., D'Urso, D., Dari, S., Navarra, D., Primavera, R., Bertucci, B., 2017, "Looking for cosmic ray data? The ASI Cosmic Ray Database" 35th ICRC, PoS 1073, Korea, https://pos.sissa.it/301/1073/pdf (last accessed April 6, 2021)

Ishkov, V. N., 2018, Geomagnetism and Aeronomy, V.58, No.6, 753-767, DOI: https://dx.doi.org/10.1134/S0016793218060051

Koldobskiy, S. A., Kovaltsov, G. A., Usoskin, I. G., 2018, J. Geophys. Res. 123, 4479, DOI: https://dx.doi.org/10.1029/2018JA025516

Koldobskiy, S. A., Bindi V., Corti C., Kovaltsov G. A., Usoskin I.G., 2019, J. Geophys. Res. 124, 2367-2379. doi: https://dx.doi.org/10.1029/2018JA026340

Koldobskiy, S. A., Bindi, V., Corti, C., Kovaltsov, G. A., Usoskin, I. G., 2019, PoS ICRC 2019, id 1094, https://pos.sissa.it/358/1094/pdf (last accessed April 6, 2021)

Krymskiy, G. F., Altukhov, A. M., Kuzmin, A. I., Krivoshapkin, P. A., Skripin, G. V., Chirkov, N. P., 1966. Geomagnetism and Aeronomy, V.6., No.6, pp.991-996.

Lafferty, G. D., Wyatt, T. R., 1995, "Where to stick your data points: The treatment of measurements within wide bins", Nuclear Instruments and Methods in Physics Research A 355, 541-547, DOI: https://dx.doi.org/10.1016/0168-9002(94)01112-5

Nagashima, K., 1971, "Rep. of Ionosphere and Space Res", Japan, Vol. 25, No 3, 189

Sun X., Hoeksema J.T., Liu Y., Zhao J., 2015, Astroph. J., 798, 2, id. 114, DOI: https://dx.doi.org/10.1088/0004-637X/798/2/114

SWPC, 2020, https://www.swpc.noaa.gov (last accessed April 6, 2021)

Ting S., 2013, The Alpha Magnetic Spectrometer on the International Space Station, Nucl. Phys. B, Proc. Suppl. 243-244, 12-24

Usoskin, I. G., Alanko-Huotari, K., Kovaltsov, G. A., and Mursula, K., 2005, J. Geophys. Res., 110, A12108, DOI: https://dx.doi.org/10.1029/2005JA011250

Usoskin, I. G., Gil, K., Kovaltsov, G. A., Mishev, A. L. and Mikhailov, V. V. , 2017, J. Geophys. Res. Space Physics, 122, 3875-3887, DOI: https://dx.doi.org/10.1002/2016JA023819

Usoskin, I. G., Bazilevskaya, G. A., Kovaltsov, G. A., 2011, Journal of Geophysical Research: Space Physics 116, A02104. DOI: https://dx.doi.org/10.1029/2010JA016105

Xudong, S., Todd, H. J., Yang, L., Junwei, Z., 2015, Astroph. J., 798, 2, id. 114, 8, DOI: https://dx.doi.org/10.1088/0004-637X/798/2/114

Questions and answers

Ludwig Klein: Would you argue that the calibration of Pamela after 2012 is not reliable?
Answer: No, I wouldn't, it cannot be asserted. The PAMELA data up to and including 2009 and the AMS-02 data for the entire period are in good agreement with the data of neutron monitors, with the PAMELA data used as the base period of 2009. After a long break since 2010, there were problems with the PAMELA detector, it is evident from the increased statistical errors.

Mike Snow: The ~5% shift in 2010 PAMELA data is from the PAMELA collaboration or is factor that gives agreement with neutron monitor data?
Answer: A shift of 4.88% is a factor necessary for agreement with neutron monitor data, but for agreement only since 2010. The PAMELA data up to and including 2009 and the AMS-02 data for the entire period are in good agreement with the data of neutron monitors. The main conclusions of the work are not affected by the normalization of the PAMELA data after 2009.

Cosmic ray studies with neutron detectors | Volume 1 (2021)
KIEL-UP • DOI: 10.38072/2748-3150/p5

Wavelet analysis of long-term variations in neutron monitor, sunspot number and interplanetary magnetic field data

Fraser Baird[1], **Alexander MacKinnon**[2]

Correspondence

[1] University of Surrey, Guildford, UK, f.baird@surrey.ac.uk
[2] School of Physics and Astronomy, University of Glasgow, UK, alexander.mackinnon@glasgow.ac.uk

Keywords

neutron monitors; wavelets; solar activity

Abstract

We use wavelet analysis to investigate the characteristic timescales appearing in neutron monitor data and their solar drivers. Wavelet analysis of Oulu NM data shows the well-known roughly 11-year variation in intensity, but with a period contracting during solar cycle 22. This is also seen in the wavelet analysis of the interplanetary magnetic field magnitude data. However, this varying period is not shown in the wavelet analysis of daily estimated sunspot numbers, a proxy for solar magnetic field strength. The time at which the wavelet transform is found to be similar for both NM and sunspot number, but not for the interplanetary magnetic field magnitude. This further highlights a complex relationship between cosmic rays, the heliosphere, and Earth.

1. Introduction

The time series produced by the count rate in a Neutron Monitor (NM) contains information on the variation of cosmic ray (CR) intensity, above the appropriate cutoff rigidity, arriving at Earth. The CR flux at Earth in turn is modulated by solar magnetic activity and its effect on the magnetosphere. When analysed using Fourier series methods, NM time series show persistent periodic behaviour on scales recognisable from the Sun: the solar rotation period; the 11-year activity cycle; and other periods found in sunspot number (e.g. Kudela et al. 1991).

Fourier methods are ideal for identifying persistent periodic behaviour in a time series. Wavelet methods (Farge 1992; Torrence & Compo 1998) go further, providing a decomposition of a time series in which the amplitude at a fixed period can vary with time. Variations of amplitude will contain information on the internal dynamics of the system being studied as well as its external drivers.

The variable appearance of a period in NM data prompts obvious questions. Do periods in NM data solely mirror the solar drivers, or is there also a component from the response of the terrestrial magnetosphere? Here we begin an analysis of such questions by comparing the time behaviour of the power at particular periods, obtained from wavelet analysis, comparing this behaviour with measures of solar magnetism, starting with sunspot number, and of the state of the solar wind at Earth. We start by presenting key wavelet ideas, before presenting wavelet transformations of NM, sunspot data and Interplanetary Magnetic Field (IMF) measurements. Differences and similarities are revealed by this process, which we discuss.

KIEL-UP • DOI: 10.38072/2748-3150/p5

2. Method

The wavelet transform is defined as the convolution of a time series with a wavelet function, dilated to a scale and translated to a time:

$$W\left(s, \tau\right) = \sum_{t=0}^{N-1} T\left(t\right) \psi_s^*\left(t - \tau\right) \tag{1}$$

Where $W\left(s, \tau\right) =$ wavelet transform
$T\left(t\right) =$ discrete time series with N data points, $\{t \in \mathbb{Z} \mid 0 \leq t < N\}$
$\psi_s^* =$ complex conjugate of the wavelet function (see eq. 2)
$s =$ scale to which the wavelet function is dilated, analogous to the period of oscillation.

In general, a wavelet function must satisfy the following conditions: be of zero mean, and be localised in time and frequency domains. For this study, the wavelet function utilised was the second derivative of a complex gaussian function:

$$\psi_s\left(t\right) = \frac{C}{\sqrt{s}}\left(4t^2 + 4it - 3\right) e^{-\left(t^2 + it\right)} \tag{2}$$

As with Fourier transforms, discontinuities in the time series cause large peaks in the wavelet transform. While this can be helpful if one wishes to identify discontinuities in the signal, the end points of the time series create artefacts near the end points of the wavelet transform. In order to screen out these edge effects, we employ a cone of influence (COI). The COI defines a minimum and maximum time index depending on scale, and values outwith the range defined by the COI are set to zero, i.e.

$$W_{COI}\left(s, \tau\right) = \begin{cases} W\left(s, \tau\right), & \tau_{min}\left(s\right) < \tau < \tau_{max}\left(s\right) \\ 0, & otherwise \end{cases} \tag{3}$$

For the wavelet function shown in eq. 2 the minimum and maximum values are given as

$$\tau_{min}\left(s\right) = \sqrt{s}, \quad \tau_{\max} = \tau_{N-1} - \sqrt{s} \tag{4}$$

Data were obtained for the interval 1964/04/01 to 2020/06/30 for three quantities: Oulu NM count rate, IMF magnitude, and estimated daily sunspot number (SSN). For each of these data the wavelet transform was computed using eq. 1 at a range of scales, $s = \left[1,\ 4096\right]$, corresponding to periods $T =$ 6 days, 28 years. This was performed using the *PyWavelets* implementation of the continuous wavelet transformation (Lee et al. 2019). The COI was applied, and the result of each of these transformations was then squared, and plotted as a scalogram. Note that prior to taking the transformation, the IMF data was filtered with a 10-day running mean, so the very first scale does not yield a physical result.

KIEL-UP • DOI: 10.38072/2748-3150/p5

3. Results

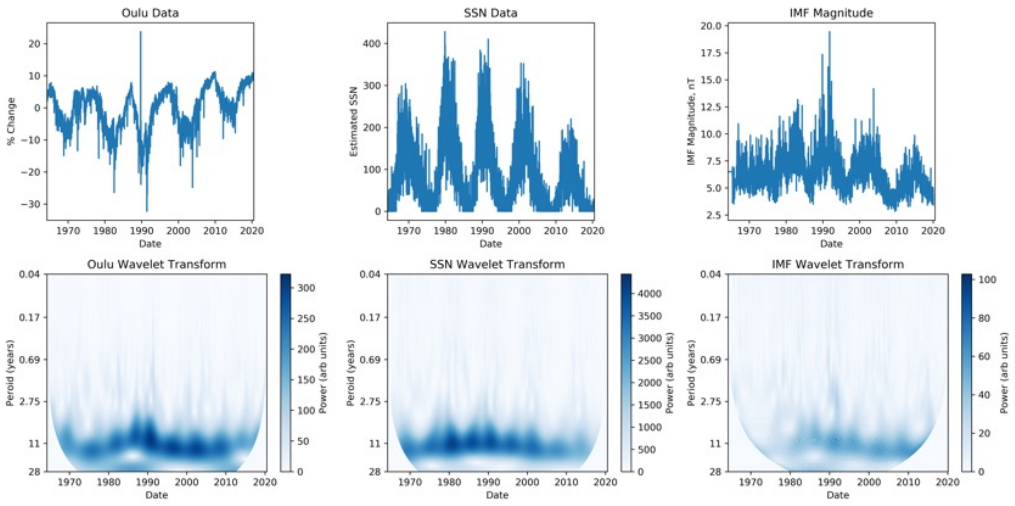

Figure 1: Data (top row) and their WT scalograms (bottom row) for Oulu NM (left column), SSN (middle column) and IMF Magnitude (right column).

The input data and resulting scalogram for all quantities are presented in figure 1. Note that the y-axis of the scalogram is a log scale. It is evident from the scalograms that each data exhibits a consistent $\sim$ 11yr variation. While the SSN scalogram shows that the period of the variation is fairly constant, this is not mirrored in the NM or IMF scalograms. The NM scalogram clearly shows a contraction in the period of variation between 1980 and 1990, before returning to a period closer to 11 years in the following decades. This behaviour is also seen in the IMF scalogram, which is of poor resolution.

While the SSN and NM scalograms differ in the constancy of period, they both show similar trends in the power of the scalogram, though they do not match exactly. While both scalograms show low power of variation from 2000 to 2020 (particularly the latter decade), the maximum power occurs around 1980 for the SSN and 1990 for the NM. Interestingly, the IMF scalogram differs completely in terms of power. The time of maximum power occurs between 2000 and 2020, and the minimum between 1970 and 1980.

4. Discussion and conclusion

As noted in the previous section, the IMF magnitude scalogram is of low quality. This is likely due to the intermittent nature of this data; since it is provided by different satellites over time, gaps in the data are inevitable due to operational challenges and periods between missions. While these gaps have been filled in with linearly interpolated values, the gaps still create sections of the data where absolutely no periodic variations are present.

It is not particularly surprising that the SSN scalogram doesn't perfectly match that of the NM or IMF magnitude – sunspots are only a proxy for solar magnetic activity and other factors will play a role in the CR activity at Earth. However, the magnitude of the difference is unexpected.

Since the strength of the IMF is associated with the modulation of cosmic rays (Beer et al. 2012), it follows that the long-term variations of the IMF should be mirrored in that of the NM data. The changing period of the long-term variation is similar in both scalograms, but the power of the variation is not similar in either scalogram. It could be that the aforementioned data gaps are the main cause of the IMF transform power.

From this study, a number of conclusions can be drawn. Firstly, that wavelet analysis has also identified the well-known persistent, long-term, periodic variation of ∼11 years in NM, SSN, and IMF magnitude data. Secondly, that the period of this variation contracts between 1980 and 1990 in the NM and IMF data, but not the SSN data. Thirdly, the time of maximum and minimum power of the NM and SSN scalograms are well matched, however the IMF scalogram does not match the other two in this regard. The physical origin of these differences will be investigated further elsewhere, together with the co-variability of NM and solar measurements at other timescales.

Acknowledgments

We thank the NMDB database (www.nmdb.eu) for providing data and the Sodankyla Geophysical Observatory (http://cosmicrays.oulu.fi/) for the Oulu NM data. We also thank WDC-SILSO, Royal Observatory of Brussels, Belgium (www.sidc.be/silso/) for providing SSN data, and NASA/GSFC Space Physics Data Facility's OMNIWeb service (https://omniweb.gsfc.nasa.gov/index.html) for provision of IMF data.

References

Beer, J., McCracken, K., von Steiger, R., 2012, Cosmogenic Radionuclides, Springer, DOI: https://dx.doi.org/10.1007/978-3-642-14651-0_5

Farge, N., 1992, Ann. Rev. Fluid Mech. 24, 395, DOI: https://dx.doi.org/10.1146/annurev.fl.24.010192.002143

Lee, G. R. , Gommers, R. ,Wasilewski, F., Wohlfahrt, K., O'Leary, A., 2019, Journal of Open Source Software, 4, 36, 1237, DOI: https://dx.doi.org/10.21105/joss.01237

Torrence, C., Compo, G. P., 1998, Bull. Amer. Meteor. Soc. 79, 61, DOI: https://doi.org/10.1175/1520-0477(1998)079%3C0061:APGTWA%3E2.0.CO;2

Kudela, K., Ananth, A. G., Venkatesan, D., 1991, JGR 96, 15871 DOI: https://dx.doi.org/10.1029/91JA01166

Cosmic ray studies with neutron detectors | Volume 1 (2021)
KIEL-UP • 10.38072/2748-3150/p6

Dynamics of energetic spectrum of solar-diurnal variations of cosmic rays in 19-24 solar activity cycles

Petr Yu. Gololobov, Vladislav G. Grigoryev, Germogen F. Krymsky, Sardaana K. Gerasimova

Correspondence
Yu.G. Shafer Institute of Cosmophysical Research and Aeronomy of SB RAS, Yakutsk, Russia,
gpeter@ikfia.ysn.ru

Keywords
cosmic rays; solar diurnal variations; energy spectrum; neutron monitor; muon telescope

Abstract
The anisotropic angular distribution of cosmic rays (CR) in the interplanetary medium manifests itself on Earth as periodic diurnal intensity variations. Ground-based detectors of CRs have different energy sensitivity to the primary CR radiation and, therefore, the amplitude and phase recorded by them are also different. This fact makes it possible to study the energy spectrum of the variations when using a sufficient number of detectors. In this work, the results of the investigation of the energy spectrum of solar-diurnal variations of CRs obtained by a network of neutron monitors and muon telescopes are presented. The network allows measuring CRs with median energies from units to hundreds of GeV. The expected values of the amplitude and phase of the daily CR variations at the selected ground-based stations for different types of the energy spectrum are shown. The calculated data are compared with experimental data for 19-24 solar activity cycles.

1. Introduction

The flux of galactic cosmic rays (CR) observed in near-Earth space is anisotropic. CR detectors located on Earth register such anisotropy as a periodic 24-hour variation of intensity, which is commonly called solar-diurnal variations (SDV). It is known that SDV reaches a maximum at 18:00 of local time and has an amplitude of about 0.5% of the total CR intensity. SDVs are observed in a wide range of energies and are found in the data of CR detectors located both high in the mountains and deep underground. At the same time, the SDV amplitude decreases with increasing energy and, according to neutron monitors (NM) data, is about ~ 0.5% (Munakata et al. 2014), and according to the underground muon telescope Matsushiro at a depth of 220 m w.e. (meters of water equivalent) - only ~ 0.05% (Munakata et al. 2010). At the same time, the exact form of the SDV energy spectrum remains insufficiently studied so far. In Ahluwalia & Ericksen (1971), Ahluwalia & Riker (1987), Jacklyn et al. (1969) and Pomerantz & Duggal (1971) an SDV rigidity spectrum was studied. For simplicity, we assume that CRs consist exclusively of protons. Then the rigidity spectra proposed in the above works can ber converted to the following form of the SDV energy spectrum

$$f_{SDV}(E) = \begin{cases} E^{\beta}, \; if \;\; E \le E_u, \\ 0, \; if \;\; E > E_u \end{cases} \tag{1}$$

KIEL-UP • DOI: 10.38072/2748-3150/p6

where the parameters E_u and β could be found by comparing the experimental data with theoretical calculations. The above studies showed that the spectrum most likely has the parameters $\beta = 0$ and $E_u = 100$ GeV, where the latter can vary depending on the solar activity cycle, reaching 50 GeV at the minimum and 150 GeV at the maximum. A later attempt (Hall et al. 1997) showed that β also ranges from -0.3 to +0.5. Also, Ahluwalia (1992) showed that E_u has a functional relationship with the strength of the interplanetary magnetic field.

This work aims to study the SDV energy spectrum (1) using measurements of ground-based and underground CR detectors based on general ideas about the interaction of CRs with the geomagnetic field and the Earth's atmosphere. At the same time, the dynamics of the spectrum with the solar activity cycle is also considered.

2. Determination of the SDV energy spectrum

2.1. Data and methods

The list of ground-based CR detectors used in this work is presented in the table 1. It includes 7 NMs located in high-, mid- and low-latitude regions of the Earth, as well as 7 ground-based and underground muon telescopes (MT). Such a set of detectors makes it possible to cover the region of median energies Emed from a few to hundreds of GeV.

The CR intensity recorded by the i-th ground-based detector can be expressed as a series of spherical harmonics as follows:

$$I^i = \sum_{n=0}^{\infty} \sum_{m=0}^{n} \left(a_n^m x_n^{m,i} + b_n^m y_n^{m,i} \right), \tag{2}$$

where $x_n^{m,i}$, $y_n^{m,i}$ are components of the so-called receiving vector $\boldsymbol{R}_n^{m,i}$, a_n^m and b_n^m are the components of the multidimensional distribution vector of the CR $\boldsymbol{A}_n^m$ (Krymsky et al. 1966, 1967). In the framework of this work, we will limit ourselves to considering the equatorial components of the diurnal anisotropy, namely a_1^1 and b_1^1, since they are easiest to observe in an experiment.

№	Station name, detector type	Abbreviation	Geographical coordinates	Altitude, m / depth, m w.e. (water equivalent)	Cutoff rigidity, GV	Emed, GeV
1	Apatity NM	APTY	67.55N 33.33E	177	0.57	15
2	Climax NM	CLMX	39.37N 106.18W	3400	2.99	11
3	Lomnicky stit NM	LMNC	49.20N 20.22E	2634	3.98	13
4	Yakutsk NM	YKTK	62.01N 129.43E	105	1.65	16
5	Thule NM	THUL	76.50N 68.7W	26	0.00	16
6	Rome NM	ROME	41.90N 12.52E	60	6.32	24
7	Haleakala NM	HALE	20.72N 156.27W	3030	12.91	29
8	Nagoya MT	NAGO	35.15N 136.97E	77 / 0 m w.e.	11.50	52
9	Yakutsk MT	Y00V	62.01N129.43E	105 / 0 m w.e.	1.65	51
10		Y07V		105 / 7 m w.e.		69
11		Y20V		105 / 20 m w.e.		104

KIEL-UP • DOI: 10.38072/2748-3150/p6

12	Misato MT	MISA	36.12N 137.50E	735 / 30 m w.e.	11.39	131
13	Sakashita MT	SAKA	35.58N 137.53E	334 / 80 m w.e.	11.50	270
14	Matsushiro MT	MATS	35.15N 136.97E	408 / 220 m w.e.	11.50	672

Table 1: Information about the NM stations and MT used in this work. Emed for MTs and NMs are determined based on response functions presented by Fujimoto et al. (1984) and Aleksan'yan et al. (1982).

As can be seen from equation (2), the amplitude and phase of the SDV observed by ground-based detectors will be determined by the vector $\boldsymbol{R}_n^{m,i}$. The calculation of the parameters $x_n^{m,i}$ and $y_n^{m,i}$ is carried out with some adaptation of the method of receiving vectors (Grigoryev et al. 2011, Yanchukovsky et al. 2016), in which the calculation results become similar to the coupling coefficients (Yasue et al. 1982; Fujimoto et al. 1984):

$$x_n^m + iy_n^m = \frac{\int_{Rc}^{\infty}\int_0^{\frac{\pi}{2}}\int_0^{2\pi} W\left(E,\theta\right) f_{SDV}\left(E\right) N\left(\theta,\varphi\right) sin\theta e^{im\Psi} P_n^m\left(sin\Phi\right) dEd\theta d\varphi}{\int_{Rc}^{\infty}\int_0^{\frac{\pi}{2}}\int_0^{2\pi} W\left(E,\theta\right) N\left(\theta,\varphi\right) sin\theta dEd\theta d\varphi}, \quad (3)$$

where $W\left(E,\theta\right)$ are the response functions, $N\left(\theta,\varphi\right)$ is the directional diagram of the device, θ, φ are latitude and longitude, **Ψ** and **Φ** are the asymptotic angles of arrival of particles. Here, the integral in the denominator is equal to the total CR intensity, and in the numerator - the intensity due to the SDV. Therefore, the amplitudes and phases of diurnal variations observed by ground-based detectors will be determined by the expressions

$$A_1^i = \sqrt{(a_1^1)^2 + (b_1^1)^2} \cdot \sqrt{(x_1^{1,i})^2 + \left(y_1^{1,i}\right)^2} \text{ and } P_1^i = \text{atan}\left(a_1^1 / b_1^1\right) - \text{atan}\left(x_1^{1,i} / y_1^{1,i}\right), \text{ respectively.}$$

2.2. Analysis of the obtained results and discussion

Assuming an 18-hour maximum anisotropy and specifying the distribution components as $a_1^1 = 1$ and $b_1^1 = 0$, we investigate the dependence of A_1^i and P_1^i on the spectrum parameters β and E_u in (1). Considering $-1.0 \le \beta \le 1.0$ we get the picture shown in figure 1 a, b. As you can see, with negative values of β, the amplitudes of daily variations observed by NMs significantly exceed MT, but with an increase of β the situation changes in the opposite direction. Only when β is close to 0 the expected amplitudes for NM and MT are mutually comparable. The difference between phases P_1^i of MTs and NMs is practically leveled when $\beta > 0$, and, on the contrary, it grows when $\beta < 0$. Comparing this picture with the SDV parameters measured experimentally in 1990-1998 (figure 1 e, f), we can conclude that β should vary near 0.

Based on the foregoing, consider the dependence of the same parameters A_1^i and P_1^i on E_u at β = 0 (figure 1c, d). It is seen that, as a result of the influence of the geomagnetic field and the Earth›s atmosphere, the primary SDVs are suppressed and phase is shifted at an early time. Moreover, A_1^i observed for MT is always lower than for NM. On the other hand, the P_1^i phase is higher for mid- and low-latitude stations than for high-latitude stations, regardless of the type of detector. It is noteworthy that the A_1^i and P_1^i of NMs strongly depend to E_u only within ~100 GeV, while A_1^i and P_1^i of MTs - within ~400 GeV.

KIEL-UP • DOI: 10.38072/2748-3150/p6

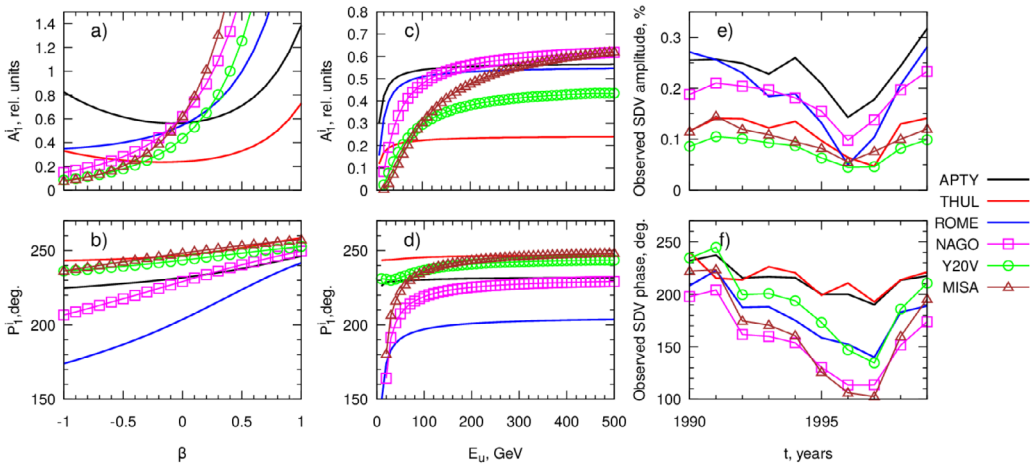

Figure 1: (a,b) - A_1^i and P_1^i expected for different values of in equation (1); (c, d) - A_1^i and P_1^i expected for different values of $E_u\left(\beta = 0\right)$; (e, f) - amplitude and phase of SDV measured by ground-based detectors (see table 1). To facilitate the perception of the picture, only a part of the detectors are presented.

The shown above result qualitatively demonstrates the applicability of the theoretical spectrum in describing experimental data. For a quantitative assessment of the effect, we consider the ratios: A_1^i / A_1^0 and $P^i = P_1^i - P_1^0$, where we will take APTY as the 0th device, due to its stability and continuity. These relationships, expected theoretically and obtained experimentally, are presented in figure 2. The figure demonstrates the relationship between E_u and the level of solar activity. At the same time, the E_u values are quite consistent with the previously obtained results of other 50 authors ($GeV \le E_u \le 150V$). However, E_u cannot be determined unambiguously.

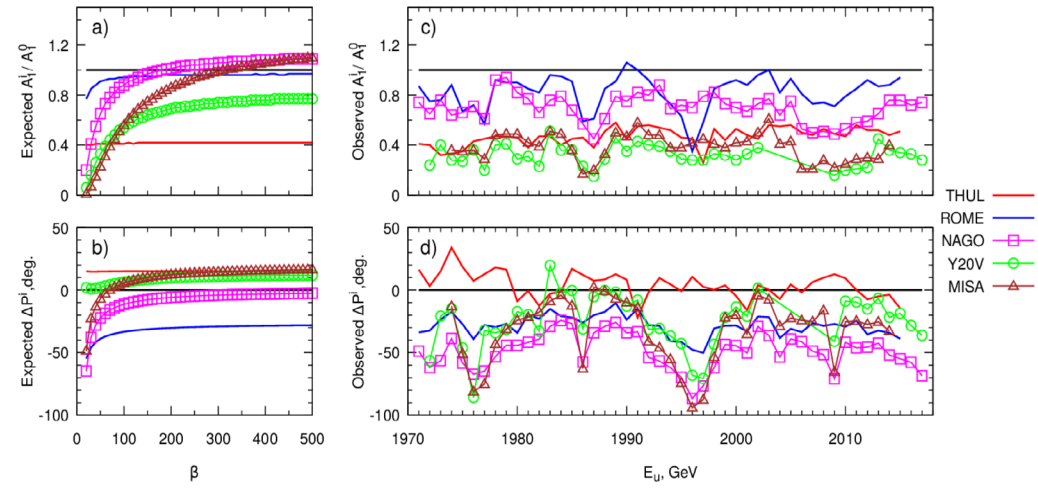

Figure 2: (a, b) - calculated values of A_1^i / A_1^0 and ΔP^i expected for different values of $E_u\left(\beta = 0\right)$. (c,d) - the same parameters obtained experimentally for the period 1971-2017.

KIEL-UP • DOI: 10.38072/2748-3150/p6

Figure 3 shows the values of the amplitude of the SDV according to the measurements of CR detectors presented in table 1, as well as, for comparison, the same parameters expected from theory. The experimental SDV was obtained separately for periods of maximum and minimum solar activity through averaging of the SDV amplitudes observed in 1980, 1990, 2000, 2013 and 1976, 1986, 1996, 2008, respectively. It can be seen that there is a mutual agreement between the experiment and theory. A closer look shows that there are some disagreements. The probable reason is the greatly simplified form of the SDV spectrum, as well as the lack of accounting of the temperature effect (for MT) and the orbital motion of the Earth (Compton-Getting effect). Also, from the figure, it is seen that the SDV amplitudes observed by LMNC and CLMX during solar activity maximum greatly differ from the estimated values. These stations are high-altitude stations and, probably, the response functions need to be estimated more precisely.

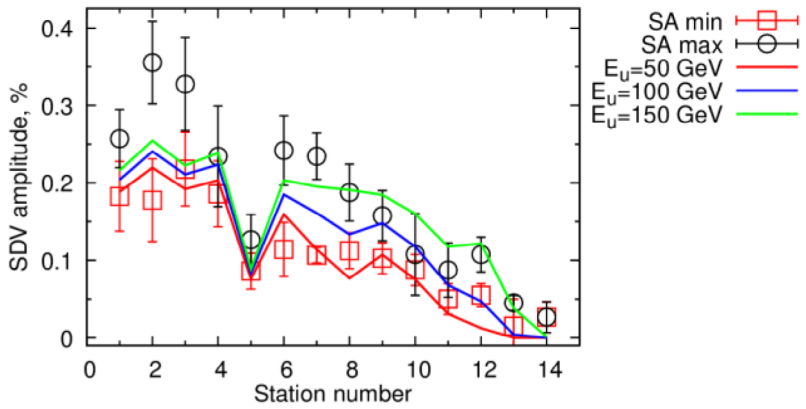

Figure 3: Expected values (solid colored curves) and experimentally observed SDV amplitudes (points) during periods of minima and maxima of solar activity. The calculation was performed at $E_u(\beta = 0)$ = 50, 100, 150 GeV. Station numbers correspond to those presented in the table 1. The errors deduced from the dispersion of the mean monthly values.

3. Conclusion

Based on NM data and ground and underground MT data, the energy spectrum of SDV was studied. The measured SDV values were compared with those theoretically expected on the selected CR detectors for the period 1971-2017. It is shown that the spectrum of a flat form with an upper cutoff $\sim$ 100 GeV is qualitatively describing the experimental data. More research is needed to determine the exact shape of the energy spectrum.

Acknowledgments

The work is carried out with partial support of the ShICRA Basic Research Program no. AAAA-A17-117021450058-6 and the RFBR grants Nos. 18-42-140002-r_a, 18-02-00451-a.

We thank WDC for Cosmic Rays[1], GMDN team[2] and Cosmic-Ray section of Solar-Terrestrial environment laboratory of Nagoya University[3] for providing their data.

1 http://cidas.isee.nagoya-u.ac.jp/WDCCR/index.html (last accessed April 20, 2021).

2 http://cosray.shinshu-u.ac.jp/crest/DB/Public/Archives/GMDN.php (last accessed April 20, 2021).

3 http://cosray.shinshu-u.ac.jp/crest/DB/Public/main.php (last accessed May 31, 2021).

KIEL-UP • DOI: 10.38072/2748-3150/p6

References

Ahluwalia, H.S., 1992, Geophys. Res. Lett. 19, 633, DOI: https://dx.doi.org/10.1029/92GL00525

Ahluwalia, H.S., Ericksen, J.H., 1971, JGR. 76, 6613, DOI: https://dx.doi.org/10.1029/JA076i028p06613

Ahluwalia, H.S., Riker, J.F., 1997, Planet. Space Sci. 35, 39, DOI: https://dx.doi.org/10.1016/0032-0633(87)90142-5

Aleksan'yan, T.M., Dorman, I.V., Dorman, L.I. et al., 1982, Izv. Akad. Nauk SSSR Ser. Fiz., 46, 1689 (in Russian)

Fujimoto, K., Inoue, A., Murakami, K., 1984, Rep. Cosmic Ray Res. Lab., No.9, 185

Grigoryev, V.G., Starodubtsev, S.A., Krymsky, G.F., et. al., 2011, Proc. 32nd ICRC. 11, 252, DOI: https://dx.doi.org/10.7529/ICRC2011/V11/0360

Hall, D.L., Duldig, M.L., Humble, J.E., 1997, ApJ. 42, 1038, DOI: https://dx.doi.org/10.1086/304158

Jacklyn, R.M., Duggal, S.P., Pomerantz, M.A., 1969, Proc. 11th ICRC, 29, 47, ed. A. Somogyi, Acta Physica

Krymsky, G.F., Kuz'min, A.I., Chirkov, et al., 1966, Geomag. Aeron. 6, 991 (in Russian)

Krymsky, G.F., Kuz'min, A.I., Chirkov, et al., 1967, Geomag. Aeron. 7, 7 (in Russian)

Munakata, K., Mizoguchi, Y., Kato, C., et al., 2010, ApJ. 712, 1100, DOI: https://dx.doi.org/10.1088/0004-637X/712/2/1100

Munakata, K., Kozai, M., Kato, C., et al., 2014, ApJ. 791, 22, DOI: https://dx.doi.org/10.1088/0004-637X/791/1/22

Pomerantz, M.A., Duggal, S.P., 1971, Space Sci. Rev. 12, 75, DOI: https://dx.doi.org/10.1007/BF00172130

Yanchukovsky, V.L., Grigoryev, V.G., Krymsky, G.F. et. al., 2016, Solar-Terrestrial Phys. 2, 103, DOI: https://dx.doi.org/10.12737/16762

Cosmic ray studies with neutron detectors | Volume 1 (2021)
KIEL-UP • DOI: 10.38072/2748-3150/p7

A novel approach in magnetic cloud-driven Forbush decrease modeling

Simone Benella[1], **Monica Laurenza**[1], **Rami Vainio**[2], **Catia Grimani**[3], **Giuseppe Consolini**[1], **Qiang Hu**[4], **Alexandr Afanasiev**[5]

Correspondence

[1] INAF-Istituto di Astrofisica e Planetologia Spaziali, Roma, Italy, simone.benella@inaf.it, monica.laurenza@inaf.it, giuseppe.consolini@inaf.it

[2] Department of Physics and Astronomy, University of Turku, Finland, rami.vainio@utu.fi

[3] DiSPeA, Università degli Studi di Urbino Carlo Bo, Urbino, Italy; Istituto Nazionale di Fisica Nucleare (INFN), Sezione di Firenze, Sesto Fiorentino, Italy, catia.grimani@uniurb.it

[4] Center for Space Plasma and Aeronomic Research, The University of Alabama in Huntsville, Huntsville, USA, qh0001@uah.edu

[5] Department of Physics and Astronomy, University of Turku, Turku, Finland, alexandr.afanasiev@utu.fi

Keywords

cosmic rays; solar-terrestrial relations; coronal mass ejections (CMEs); magnetic clouds

Abstract

Interplanetary coronal mass ejections (ICMEs) are large-scale solar wind disturbances propagating from the Sun and causing a depression of the galactic-cosmic ray (GCR) intensity known as Forbush decrease (FD). ICMEs generally contain coherent plasma structures called magnetic clouds (MCs). A unique and powerful data analysis tool allowing for the study of the quasi-3-D configuration of a MC is the Grad-Shafranov (GS) reconstruction. The aim of this work is to investigate the role played by the MC configuration in the formation of a FD. A suited full-orbit test-particle simulation has been developed in order to evaluate FD amplitude and time profile produced by the MC obtained with the GS reconstruction. Particle trajectories are computed starting from an isotropic flux outside the MC region. In addition, particle diffusion has been modeled by superimposing a small-angle scattering over the unperturbed charged particle motion at each time step. The model allows us to investigate the MC effect on GCR propagation and to study the energy dependence of the physical processes involved, as it provides an estimate of ground-based GCR counts observations at different latitudes. A comparison between model results and both space-based cosmic-ray measurements in L1 and ground-based observations suggests a major role of drifts in producing the FD and a reduced contribution of GCR particle diffusion.

1. Introduction

Interplanetary coronal mass ejections (ICMEs) are large magnetic structures connected to the Sun that during their travel can limit the cosmic-ray propagation producing galactic cosmic-ray (GCR) intensity depressions known as Forbush decreases (FDs; Forbush 1937). From a statistical point of view the 80% of ICMEs is associated with a FD (Richardson & Cane 2011). During the ICME transit it is generally possible to identify two components: the first comprises a shock front and a region of shocked and compressed solar wind plasma presenting large-amplitude magnetic field fluctuations called turbulent sheath; the second is a coherent plasma structure called magnetic cloud (MC) that is presumably connected to the Sun (see Cane 2000, and references therein). The

KIEL-UP • DOI: 10.38072/2748-3150/p7

typical signatures of a MC on the in situ spacecraft (S/C) observations are a smooth rotation in the magnetic field components, a magnetic field strength higher than the background solar wind and values of temperature and plasma-beta that are lower than average (Burlaga et al. 1990; Lepping et al. 1990, 1997). In general, the most effective physical process in generating major FDs is the interaction of GCRs with the ICME shock/sheath region, since intense shocks associated with fast ICMEs may overcome the MC effect in GCR modulation (e.g. Wibberenz et al. 1998). Otherwise, the MC effect could even be dominant since the minimum intensity occurs after the arrival of the MC (Badruddin 1986; Zhang & Burlaga 1988). Moreover, ICMEs that contain MCs cause larger FDs on average with respect to ICMEs that do not show any coherent structure (Richardson & Cane 2011). In this work we focus on slow ICMEs for which the effect of the shock/sheath and the effect of the MC on the GCR intensity could be similar. Therefore, in case of weak shock/sheath part of an ICME the FD profile depends on the magnetic configuration within the ICME. Numerous models have been developed in order to relate the properties of FDs with those of ICMEs/MCs (Cane et al. 1995; Munakata et al. 2006; Krittinatham & Ruffolo 2009; Dumbović et al. 2018; Petukhova et al. 2019). These studies are based on the analytical definition of the magnetic field components within the MC and in some cases the MC expansion is taken into account into the model. In this work we propose an novel method to model MC-driven FDs by using a realistic MC configuration starting from IMF and plasma in situ data. The quasi-3-D large-scale configuration of a MC can be found by applying the Grad-Shafranov (GS) reconstruction (Hau & Sonnerup 1999; Hu & Sonnerup 2002). The main idea of the method is to join the GS reconstruction with a suited test-particle simulation that allows us to investigate the effect of the MC configuration in modulating the GCR intensity. Finally, we present a case study for which the method can be applied successfully. In order to test the model we use ground-based GCR observations from five neutron monitor (NM) stations at different latitudes (Dome C, South Pole, Newark, Rome and Mexico City) as well as space-based measurements gathered by a radiation monitor on board the LISA Pathfinder mission (LPF; Armano et al. 2018, 2019). Space-based GCR observations in the near-Earth environment reach lower rigidities with respect to NMs and allow for the study of the fine structure of FD evolution. On the other hand, a comparative study with ground-based NM observations is crucial in order to investigate the energy dependence of this event. The paper is organized as follows. In Section 2 a description of the method is provided and a comparison between model results and observations is reported in Section 3 as a case study. Finally, our conclusions are drawn.

2. Description of the method

The method that we present is aimed to simulate the GCR variation profile of a FD event associated with the passage of a MC. In order to investigate the effect of the MC in modulating GCR particles a quasi-3-D magnetic field configuration representing the MC is necessary. The magnetic structure is obtained here by applying the GS reconstruction and it is used to initialize the particle simulation. The GS reconstruction is an advanced data analysis technique that allows to retrieve a MC topology starting from single S/C in situ data. The technique is based on the GS equation, that describes a 2D plasma structure under the hypothesis of axial invariance along the *z-axis:*

$$\frac{\partial^2 A}{\partial x^2} + \frac{\partial^2 A}{\partial y^2} = -\mu_0 \frac{d}{dA}\left(p + \frac{B_z^2}{2\mu_0}\right), \tag{1}$$

where A is the vector potential, p is the plasma pressure and μ_0 is the vacuum permeability. The first step in performing the GS reconstruction is the application of the deHoffmann-Teller (HT) analysis. This procedure is aimed to estimate the HT velocity that represents the mean velocity of the MC, used to fix the comoving reconstruction reference frame. In this reference frame the

KIEL-UP • DOI: 10.38072/2748-3150/p7

electric field vanishes and the magnetic structure is stationary, according to the Faraday's law. The z-axis orientation of the reconstruction reference frame can be estimated by using the condition that the transverse pressure

$$P_t = p + \frac{B_z^2}{2\mu_0}$$

is a single-valued function of the potential vector A. The x-axis is oriented along the S/C trajectory direction, where the magnetic vector potential $A(x,0)$ is calculated from data. The transverse pressure is then fitted with a proper combination of analytical functions and equation (1) is numerically evaluated. The GCR intensity modulation associated with the MC transit is modeled through a full-orbit test-particle simulation (Benella 2020; Benella et al. 2020). Particles injected in the simulation are only protons, that represent the 90% of the GCR composition in the inner heliosphere, approximately. The incident proton flux is assumed to be isotropic. The hypothesis of isotropy holds since we focused on slow ICMEs with no clear shock/sheath effect on GCRs. Otherwise, when the interaction between shock/sheath region and GCRs is important, the particle flux may be anisotropic at the MC start time (Tortermpun et al. 2018). The aim of this test-particle simulation is to provide a proton intensity variation profile as a function of time. First, the particle motion through the steady magnetic field is determined by drifts induced by magnetic field inhomogeneity and curvature, thus leading to fully deterministic particle trajectories, since random fluctuations of the magnetic field components are not allowed. As a second step, we evaluated the contribution of the particle diffusion in affecting the proton propagation in the simple assumption of constant diffusion coefficient D. The particle diffusion is modeled by superimposing a small-angle scattering over the unperturbed charged particle motion at each time step Δt. The scattering process varies the particle velocity vector direction with an angle θ_{sc} at each time step and preserves the particle energy. The square of the scattering angle θ_{sc} is exponentially distributed. The mean-free path of the diffusion process is defined as $\lambda = 3D / v$, where v is the particle velocity. The proton intensity variation profile obtained with and without the diffusion process are compared and discussed in the next section.

3. The 2016 August 2nd Forbush decrease

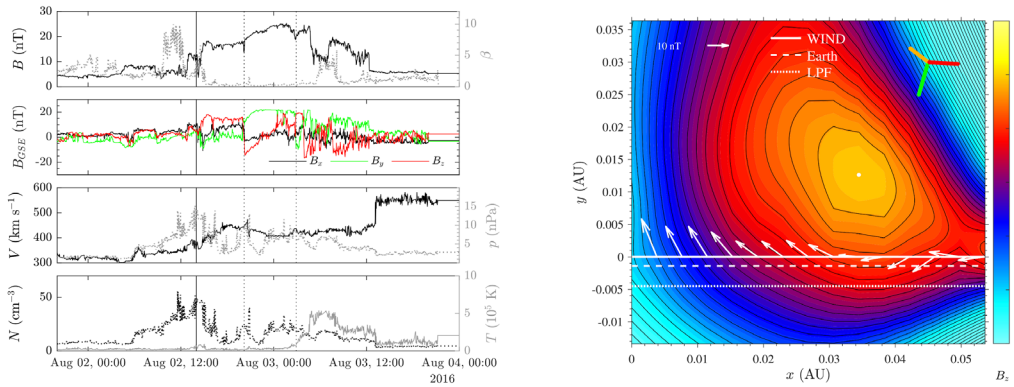

Figure 1: Left: Wind magnetic field and plasma observations for the 2016 August 2nd event. The vertical solid line indicates the ICME start time and vertical dotted lines indicate the MC transit time. Right: GS reconstruction of the 2016 August 2nd MC . Straight lines are Wind (solid dotted), Earth (dashed line) and LPF (dotted line) paths. The color map indicates the Bz and solid black lines are the level curves of the potential vector A. White arrows are the transverse magnetic field components along the Wind S/C path. A projection of the GSE reference frame is reported in the corner (x GSE in red, y GSE in yellow, and z GSE in green).

KIEL-UP • DOI: 10.38072/2748-3150/p7

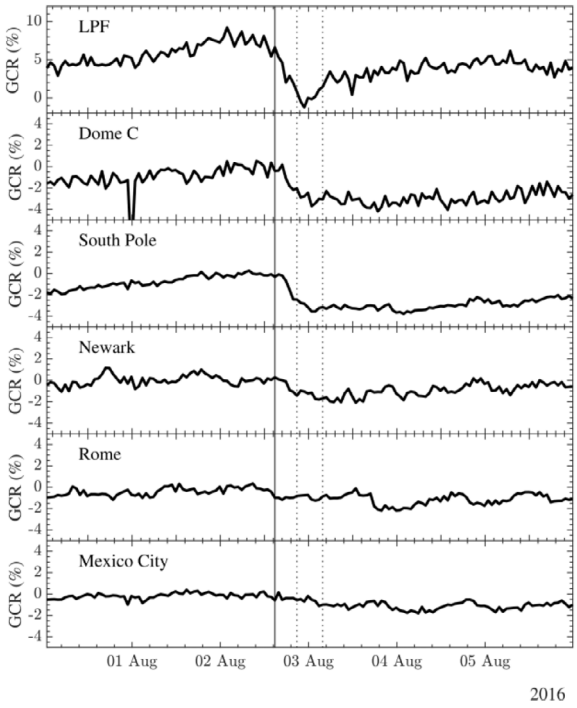

Figure 2: LPF (first panel) and NM (other panels) GCR observations for the 2016 August 2nd FD. The vertical solid line indicates the ICME start time and vertical dotted lines indicate the MC transit time.

An ICME was observed at L1 between 2016 August 2nd at 14:00 UT and August 3rd at 03:00 UT, as reported in the near-Earth ICME catalog at http://www.srl.caltech.edu/ACE/ASC/DATA/level3/icmetable2.html (last accessed April 7, 2021). In order to perform the GS reconstruction we used data from the Wind S/C that are shown in figure 1 (left panel). The MC region can be identified between 20:10 UT on August 2nd and 03:00 UT on August 3rd, where the smooth rotation of magnetic field components and low temperature and plasma beta values are present. At the ICME transit a GCR intensity FD was observed in space by a particle detector on board the LPF S/C at L1 and at

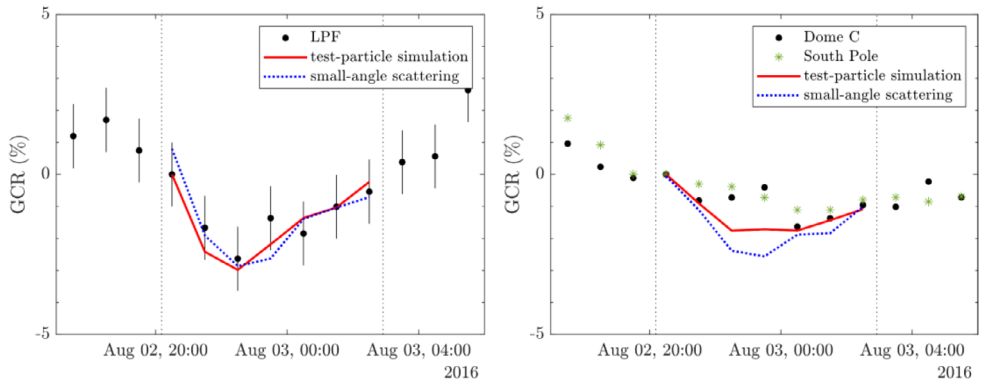

Figure 3: Left: comparison between LPF observations and the hourly-averaged intensity variation profile obtained from the simulation. Right: comparison between polar NM observations (Dome C, South Pole) and the hourly-averaged intensity variation profile obtained from the test-particle simulation. The simulation is performed without including diffusion (red solid lines) and with $D = 10^{22}$ cm^2 s^{-1} (blue dotted lines).

KIEL-UP • DOI: 10.38072/2748-3150/p7

	Dome C	South Pole	Newark	Rome	Mexico City
Geographic coordinates	75.06 S, 123.2 E	90.0 S, N/A	39.7 N, 75.8 W	41.9 N, 12.5 E	19.3 N, 260.8 E
Altitude (m)	3233	2820	50	s.l.	2274
Vertical cutoff rigidity (GV)	1.1	1.1	2.4	6.27	8.2
Observed FD amplitude (%)	3.7	2.6	1.8	1.2	1.1
Observed MC-driven FD ampl. (%)	1.7	1.2	< 1	< 1	< 1
Simulated MC-driven FD ampl. (%)	1.8	1.8	1.1	1.0	< 1

Table 1: Geographic latitude, altitude, and vertical cutoff rigidities of five NM stations. The total and MC-driven FD amplitudes of the 2016 August 2 event are compared with simulation results for the MC-driven FD amplitude.

ground-level by NMs. LPF and NM GCR observed variations are reported in figure 2. The GS reconstruction is then performed. The HT analysis returns an excellent constant velocity $V_{HT} = (-413.6, -26.4, 11.5)$ km s^{-1} and a z-axis orientation with respect to the geocentric solar ecliptic (GSE) reference frame is $\vartheta = 17.3°$ and $\varphi = 53.9°$, where ϑ and φ are the latitude and longitude angles respectively. The GS reconstruction is shown in figure 1 (right panel). Straight lines at $y = 0$, y = -1.4 × 10^{-3} AU and y = -4.4 × 10^{-3} AU indicate Wind, Earth and LPF paths through the MC, respectively. The last step of our method is the test-particle simulation. The initial proton differential flux is calculated with the Gleeson and Axford model (Gleeson & Axford 1968) by setting the proton local interstellar spectrum according to Usoskin et al. (2017). Hence, the solar modulation parameter for 2016 August is $\phi = 519$ MV. The energy interval of the protons injected in the simulation is set between 70 MeV and 100 GeV since LPF measured proton and helium nuclei above 70 MeV n^{-1}. In order to estimate the NM count rate from the simulation we cut the proton differential flux above the cutoff energy of each NM station and used the yield function proposed by Mishev et al. (2013) to take into account the instrument response. NM characteristics, observations and MC-driven FD amplitudes obtained from the simulation for these five NM stations are summarized in table 1. The signature of the MC passage on the GCR flux is a decrease of the particle intensity of 1.7% and 1.2% at Dome C and South Pole, respectively. The cutoff energy is the atmospheric cutoff of $E_c = 500$ MeV for these polar stations. The simulation outcome is a decrease of $1.8\% \pm 0.4\%$ at Dome C and South Pole locations. The FD energy dependence is obtained through the simulation as the FD amplitude goes down at higher energies as observed by NMs. Indeed, amplitudes < 1% were recorded by NM stations such as Newark, $E_c = 1.6$ GeV, Rome, $E_c = 5.4$ GeV, and Mexico City, $E_c = 7.3$ GeV. Proton variation time profiles obtained through the simulation are reported in figure 3 where are compared with data gathered by LPF (left panel) and two polar NMs (right panel). Solid red lines are the simulation outcome without diffusion. In this case the modulation of the proton intensity induced by the MC structure is due to drifts associated with the inhomogeneity and the curvature of the magnetic field. There is a good agreement between model results and observations for both FD amplitude and time profile. In general, the cosmic-ray particle diffusion due to turbulent fluctuations of the magnetic field plays an important role in particle intensity modulation in the heliosphere. On the other hand, spatial scales involved in the GCR diffusion are larger with respect to the scale of the MC under study, thus we expect that diffusion does not play an important role in the 2016 August 2nd FD. We verified this by performing a test-particle simulation, which includes the small-angle scattering for a typical value of the diffusion coefficient usually assumed in the heliosphere: $D = 10^{22}$ cm^2 s^{-1} (Potgieter 2013). In figure 3 GCR observations are compared with simulation outcomes with particle diffusion (blue dotted lines). As expected the time profile is similar to the one obtained when only drifts are considered, indicating that no effect from diffusion is present, being the associated $\lambda \sim 10^{10}$ m greater than the MC size, i.e. $\sim 8 \times 10^9$ m.

4. Conclusions

We proposed a method to study the effect of the interaction between MCs and GCRs by using the GS reconstruction technique that allows us to perform a test-particle simulation on a realistic magnetic field configuration based on in situ S/C observations. The method has been applied to the 2016 August 2nd FD. Magnetic field and plasma observations for the GS reconstruction are taken from the Wind S/C and proton variation profiles obtained from the simulation are compared to data gathered by a particle detector on board LPF and to ground-based observations of five NM stations. Simulation results and data trend show an excellent agreement in both amplitude and time profile of the FD, when particles are assumed to propagate through the MC only by means of gradient and curvature drifts, i.e., when the MC is treated as a stationary plasma structure and magnetic field fluctuations are not allowed. Moreover, we developed a test-particle simulation with a particle small-angle scattering that allowed us to evaluate the effect of the diffusion in modulating GCRs during the FD. For the typical value $D = 10^{22}$ cm^2 s^{-1} of the diffusion coefficient, that is assumed to be constant at all energies, the large scale on which the GCR diffusion takes place is greater than the size of the analyzed MC. Thus, we suggest that diffusion does not play a primary role in modulating cosmic-ray particles in this MC case study, which can be can be considered as representative of FDs associated with MCs that are not preceded by a shock/sheath region.

Acknowledgments

S.B., M.L. and G.C. acknowledge the financial support of the Italian MIUR-PRIN grant 2017APKP7T on Circumterrestrial Environment: Impact of Sun-Earth Interaction. The authors are grateful to the LISA Pathfinder Collaboration for providing the mission particle detector data. The LPF data can be downloaded from https://www.cosmos.esa.int/web/lisa-pathfinder-archive/home. R.V. and A.A. acknowledge the financial support of the Academy of Finland (projects 309939 and 312357). Data from the Wind experiment were obtained from the NASA-CDAWeb website. We acknowledge the NMDB database (https://www.nmdb.eu/) funded under the European Union's FP7 program (contract No. 213007), and the PIs of individual NM stations for providing data.

References

Armano, M., Audley, H., Baird, J., et al., 2018, ApJ, 854, 113, DOI: https://dx.doi.org/10.3847/1538-4357/aaa774

Armano, M., Audley, H., Baird, J., et al., 2019, ApJ, 874, 167, DOI: https://dx.doi.org/10.3847/1538-4357/ab0c99

Badruddin, R., 1986, SoPh, 105, 413

Benella, S., (2020), Galactic cosmic-ray recurrent and transient short-term variations: advanced data analysis and modeling (Doctoral dissertation, University of Urbino Carlo Bo, Urbino, Italy), http://hdl.handle.net/11576/2673737

Benella, S., Laurenza, M., Vainio, R., et al., 2020, ApJ, 901, 21, DOI: https://dx.doi.org/10.3847/1538-4357/abac59

Burlaga, L., Lepping, R., and Jones, J., 1990, Physics of Magnetic Flux Ropes, Vol. 58, 373, DOI: https://dx.doi.org/10.1029/GM058p0373

Cane, H., Richardson, I., and Wibberenz, G., 1995, ICRC, 4, 377

Cane, H. V., 2000, Cosmic Rays and Earth (Berlin: Springer), 55, DOI: https://dx.doi.org/10.1007/978-94-017-1187-6_4

Dumbović, M., Heber, B., Vršnak, B., Temmer, M., and Kirin, A., 2018, ApJ, 860, 71, DOI: https://dx.doi.org/10.3847/1538-4357/aac2de

Forbush, S. E., 1937, PhRv, 51, 1108, DOI: https://dx.doi.org/10.1103/PhysRev.51.1108.3

Gleeson, L., Axford, W., 1968, ApJ, 154, 1011, DOI: https://dx.doi.org/10.1086/149822

Hau, L.-N., Sonnerup, B. U., 1999, JGRA, 104, 6899, DOI: https://dx.doi.org/10.1029/1999JA900002

Hu, Q., Sonnerup, B. U., 2002, JGRA, 107, SSH, DOI: https://dx.doi.org/10.1029/2001JA000293

Krittinatham, W., Ruffolo, D., 2009, ApJ, 704, 831, DOI: https://dx.doi.org/10.1088/0004-637X/704/1/831

Lepping, R., Burlaga, L., Szabo, A., et al., 1997, JGRA, 102, 14049, DOI: https://dx.doi.org/10.1029/97JA00272

Lepping, R., Jones, J., Burlaga, L., 1990, JGRA, 95, 11957, DOI: https://dx.doi.org/10.1029/JA095iA08p11957

Mishev, A., Usoskin, I., Kovaltsov, G., 2013, JGRA, 118, 2783, DOI: https://dx.doi.org/10.1002/jgra.50325

Munakata, K., Yasue, S., Kato, C., et al., 2006, Advances in Geosciences: Volume 2: Solar Terrestrial (ST) (Singapore: World Scientific), 115

Petukhova, A. S., Petukhov, I. S., Petukhov, S. I., 2019, JGRA, 124, 19, DOI: https://dx.doi.org/10.1029/2018JA025964

Potgieter, M. S., 2013, Living Reviews in Solar Physics 10.1: 3, DOI: https://dx.doi.org/10.12942/lrsp-2013-3
Richardson, I., Cane, H., 2011, SoPh, 270, 609, DOI: https://dx.doi.org/10.1007/s11207-011-9774-x
Tortermpun, U., Ruffolo, D., Bieber, J., 2018, ApJL, 852, L26, DOI: https://dx.doi.org/10.3847/2041-8213/aaa407
Usoskin, I. G., Gil, A., Kovaltsov, G. A., Mishev, A. L., Mikhailov, V. V., 2017, JGRA, 122, 3875, DOI: https://dx.doi.org/10.1002/2016JA023819
Wibberenz, G., Le Roux, J., Potgieter, M., Bieber, J., 1998, SSRv, 83, 309, DOI: https://dx.doi.org/10.1023/A:1005083109827
Zhang, G., Burlaga, L., 1988, JGRA, 93, 2511, DOI: https://dx.doi.org/10.1029/JA093iA04p02511

Questions and answers

Ludwig Klein: How do you define „class of events"?
Answer: The class of events is defined by FDs associated with ICMEs that do not have an effective shock/sheath part, for which isotropy of the GCR at the start time of the MC passage can be reasonably assumed. Moreover, for such events the observed modulation on GCRs is mainly due to the interaction with the MC.

Hugh Hudson: Can models based on diffusive propagation do as well?
Answer: The scale of the analyzed structure suggests that diffusive propagation might play a minor role in this case. In general a diffusive propagation model is more suitable to investigate the particle propagation on larger scales.

David Ruffolo: Entry/exit of particles due to gradient & curvature drifts was also considered by Krittinatham & Ruffolo (2009).
Answer: Yes, indeed we took into account the paper by Krittinatham & Ruffolo (2009) in our study.

Cosmic ray studies with neutron detectors | Volume 1 (2021)
KIEL-UP • DOI: 10.38072/2748-3150/p8

Precursory signals of Forbush decreases with and without shock wave

Dimitra Lingri[1], **Helen Mavromichalaki**[1], **Maria Abunina**[2], **Anatoly V. Belov**[2], **Eugenia A. Eroshenko**[†2]

Correspondence

[1] Faculty of Physics, National and Kapodistrian University of Athens, Greece,
dlingri@phys.uoa.gr, emavromi@phys.uoa.gr

[2] Pushkov Institute of Terrestrial Magnetism, Ionosphere and Radio Wave Propagation (IZMIRAN), Moscow, Russia,
abunina@izmiran.ru, abelov@izmiran.ru, erosh@izmiran.ru

Keywords

cosmic ray intensity; Forbush decreases; neutron monitors; precursory signals

Abstract

Many previous studies have shown that before the beginning of a Forbush Decrease (FD) of the cosmic ray intensity, a precursor signal can be observed. All these surveys were focused on FDs that are associated with a sudden storm commencement (SSC). In this work we demonstrate that precursors could also be observed in events without a SSC that is determined by an abrupt increase of the interplanetary magnetic field. The type of precursory signals and their diversity among the events are the main purpose of this study. We try to figure out similarities and differences on the signals and the associated events from both categories in the last fifty years, from 1969 to 2019, using the same selection criteria of the under investigation FDs. Simultaneously the orientation of the upcoming solar disturbances in comparison to the way they configure the increase of the interplanetary magnetic field and create these signals are discussed.

1. Introduction

Sudden decreases that are often observed in cosmic ray (CR) intensity were first studied by Scott Forbush (1937) and from then they are called as Forbush decreases (FDs) (Forbush 1954). In most cases, a shock wave generated by a Coronal Mass Ejection (CME) expanding from the Sun to the interplanetary medium, compresses the Earth's magnetophere and a sudden storm commencement (SSC) is created (Cane 2000). So, the FD of the CR intensity starts simultaneously with the SSC record.

But there are many recorded FD events, the starts of which are not connected with a SSC. Nowadays they are assumed to be generated by high speed solar wind streams (HSSWSs) from coronal holes (CHs), although there are cases when they are related with more intense solar expanding phenomena, like solar flares, CMEs etc. In these phenomena the onset is defined by a sharp increase in the value of the interplanetary magnetic field (IMF). These events are more gradual, smoother and with a smaller amplitude than the FDs with SSC (Melkumyan et al. 2019).

The main purpose of this study is to find out if a precursory signal could also be observed, when the Earth is outside of the front of the upcoming shock. Around the start of a FD, pre-decreases and pre-increases of the CR intensity, combined with changes in the first harmonic of the anisotropy at the equatorial plane (A_{xy}) may appear some hours before the start of the event and can be useful for

† deceased

KIEL-UP •DOI: 10.38072/2748-3150/p8

forecasting the upcoming disturbance (e.g. Papailiou et al. 2012; Lingri et al. 2016b; Tortermpun, Ruffolo, and Bieber 2018; Lingri et al. 2019 and references there in). These CR intensity anomalies can be detected by applying data analysis of the neutron monitors (NMs) of the worldwide network. They can be observed from 20 h up to 1 – 2 h earlier than the start of the main phase of the Forbush decrease, which in most cases is important for the early detection of the event (e.g. Asipenka et al. 2009).

Especially, a pre-decrease is due to the "loss cone" effect, where NMs are connected with a low density region of cosmic rays come from downstream of the shock (Leerungnavarat, Ruffolo, and Bieber 2003). On the other hand, the CR particles reflected by the front of the stream are accelerated and recorded at the Earth as pre-increases (Dorman et al. 1995). The observed precursor sign for each event depends on the heliographic position of the solar source in combination with the Earth's position in the heliosphere (Kozai et al. 2016) and on the nature of the flow.

So in this work we try to answer the question if a SSC is necessary to be able to observe a precursor as it is considered until today and if it is not, which are the similarities and the differences between the two kinds of events. NMs data from the last fifty years have been examined (1969-2019) and FD events for cosmic rays of 10 GV rigidity characterized by amplitude, corrected for the geomagnetic effects, greater than 2% were selected. The cosmic ray anisotropy A_{xy} before the start of the FD was chosen to be greater than 0.8% and the interplanetary space conditions to be quite undisturbed. In Section 2 the data sources, the methodology that has been used and the selection procedure are presented. In Section 3 two characteristic events, one from each category with and without SSC that present precursory signals are analyzed Finally Section 4 contains discussion and new conclusions of this study.

2. Data selection and methodology

2.1 Data collection

In this work, the studied time period was chosen to cover four and half solar cycles (half of 20, 21, 22, 23 and 24 solar cycle), from 1969 to 2019, as to have solar, cosmic and interplanetary data simultaneously with observations of the solar disk obtained from Geostationary Operational Environmental Satellites (GOES, https://www.ngdc.noaa.gov/stp/space-weather/solar-data/solar-features/solar-flares/x-rays/goes/xrs/, last accessed April 7, 2021). It is noticed that there are some data gaps around 1985-1992, where no continuous solar wind and/or interplanetary data exist.

Forbush Effects and Interplanetary Disturbances Database (FEID), (http://spaceweather.izmiran.ru/eng/dbs.html) have been used for the FDs and their characteristic solar and interplanetary parameters, calculated for the rigidity of 10 GV, which is close to the effective rigidity of most NMs, by using the Global Survey Method (GSM) (Belov et al. 2018). Finally, the OMNIWeb site (https://omniweb.gsfc.nasa.gov, last accessed April 7, 2021) for the interplanetary and geomagnetic parameters was used.

Cosmic ray data were taken from the high resolution neutron monitor database (NMDB, https://www.nmdb.eu/, last accessed April 7, 2021; Mavromichalaki et al. 2011) and from the worldwide cosmic ray center of Nagoya University (http://cidas.isee.nagoya-u.ac.jp/WDCCR/, last accessed April 7, 2021). Some criteria for the selected NMs have been used, as the rigidity of the NM station to be smaller or equal to 3 GV and the location to be at an altitude lower than 1000m, as their measurements are affected by the cosmic ray anisotropy and density fluctuations. The sub-polar NM stations are not taken into account in this study, as they are affected by the north- south anisotropy Az (Belov et al. 2017a, 2017b). It is noticed also that the number of the used NM stations varies from time to time because new stations are founded and some others are shut down. However, in average for each studied event data were extracted from a number of around 20-25 NM stations.

KIEL-UP •DOI: 10.38072/2748-3150/p8

2.2 Methodology and selection criteria

For the selection of the events under investigation the Global Survey Method (GSM) was used, which unifies the simultaneous observations of cosmic ray intensity from terrestrial monitors and the anisotropy's variations for particles with magnetic rigidity of 10GV, which is close to the effective rigidity of the most neutron monitors (Belov et al. 2018).

The criteria that were used, are similar to those of Lingri et al. (2019), but instead of the amplitude of FD at 10 GV rigidity, we use the amplitude corrected for the magnetospheric effect by the Dst index (MagnM), as was calculated at the same rigidity (Belov et al. 2018; http://spaceweather.izmiran.ru/dbs/fds/full-list-parameters-eng.pdf, last accessed April 7, 2021). MagnM is more specific and helpful to avoid some magnetospheric alterations in the cosmic ray intensity capture. Which of them will be greater depends on the existing geomagnetic circumstances. So, the pre-conditions that are chosen for this detailed study of FDs with a precursory signal before are:

I) FDs to be (or not) associated with an SSC.

II) The MagnM to be equal or greater than 2%. As precursors are about 2σ of the FD's amplitude, this value helps us to avoid cosmic ray background fluctuations to be falsely characterized as precursor.

III) The A_{xy} component of CR anisotropy one hour before the onset to be greater that 0.8%. As the mean value of A_{xy} is around 0.52%, the value of 0.8% allows us to collect as many candidate events as we can, whose diurnal variations amplitude is close to the A_{xy} calculated values (Belov et al. 2017a).

There is the preference for the interplanetary environment to be quiet or with small fluctuations before the start of the event, so the precursors to be clearly detected. If the interplanetary magnetic field is disturbed before the start of a FD, we exclude the event from our investigation. In FEID CR intensity variations are recorded, which means that there are also some Forbush increases and Ground Level Enhancements (GLEs) for example, which may have an amplitude greater than 2% but we do not want them in our database and they have to be excluded.

Finally it has to be noted that we avoid to examine FDs, which reached their minimum amplitude two to three days after their start, because in these cases we cannot characterize the fluctuations before the onset of the FD as precursors. We should notice that in the events where an SSC does not define the start of a FD, we have to put by hand the onset of each FD that in our study is determined by the first hour when an abrupt increase of the IMF starts to be recorded.

For the determination of the precursory signals we use the Ring of Station Method – RSM, which turns the geographical longitudes to asymptotic and determines the reception cone of each station and the diurnal anisotropy variation which is recorded in each neutron monitor in connection with the asymptotic longitudes (for details see Abunina et al. 2020). RSM was used to find out the possible existence of a precursor, by plotting the asymptotic longitudinal cosmic ray distribution diagrams, in which NM data are captured which were hourly corrected for pressure. The Tsyganenko96 model for the cut off rigidity is used to calculate the asymptotic directions of each station (Tsyganenko and Stern 1996).

3. Selected Forbush decreases

FEID database includes more than 6000 events that took place in the studied time period 1969-2019. From them, if we apply the criterion MagnM to be greater than 2%, 1173 FDs remain to be examined. When all criteria are taken into account, 153 FDs associated with SSC and 74 FDs without a SSC connection remain to be investigated. About the percentage of 30% of the events of

KIEL-UP •DOI: 10.38072/2748-3150/p8

each category could be studied for precursors, as we examine each FD separately for simultaneous CR, solar and interplanetary data and for the way of how the CR intensity changes throughout the time. In the next section one characteristic event with precursors for each category is analyzed.

3.1 FD associated with SSC – The event of 15.02.2014

The event occurred on 15 February 2014 at 13:16 UT is used as an example in the category of the FDs that are associated with a shock wave. The events of this category have been analyzed in detail also in previous studies (e.g. Lingri et al. 2016a; Lingri et al. 2019). It was associated with a halo CME with velocity of 533 km $s-1$, that created a rapid increase in the solar wind speed and also in the IMF, which reached the value of 16.2 nT. The produced FD's amplitude reached the value of 4.0% for CRs of 10 GV rigidity and significant variations of the Axy component took place (figure 1). The Axy and Az components of the anisotropy were increased after the SSC arrival. Moreover the Axy changed its direction significantly after the arrival of the main ejecta and of the associated magnetic cloud (orange arrows in figure 1). Finally, it was not associated with a geomagnetic storm, as the Dst index reached the value of -37 nT.

From the figure 2 a precursor signal is observed before the shock wave arrival. A pre-increase precursor was observed from 10 to 2 hrs before the FD at an asymptotic longitude range between 110° and 320°. In the meantime a pre-decrease signal started to be recorded by the NMs about 4 hrs before the SSC in a range of 40° – 130°. This means that many stations show a significant increase of the recorded variations and a few ones present a minimum.

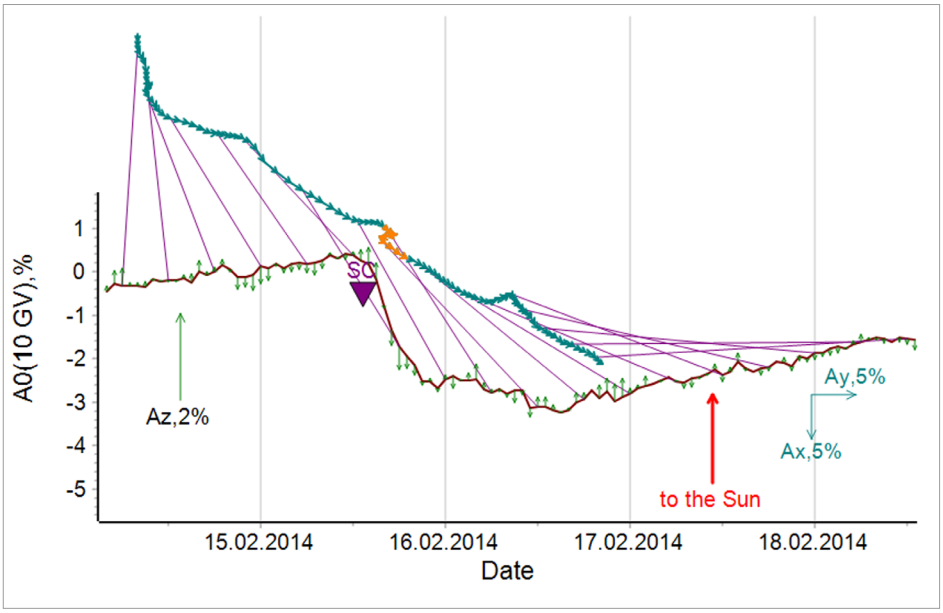

Figure 1: The anisotropy variation on the equatorial plane (Axy – blue vectors) and of the z component (Az – green vectors) during the time period of the event of 13-18 February 2014. The red line represents the CR intensity variations. The purple lines connect the same points in time on the two curves of the blue and the red lines.

KIEL-UP •DOI: 10.38072/2748-3150/p8

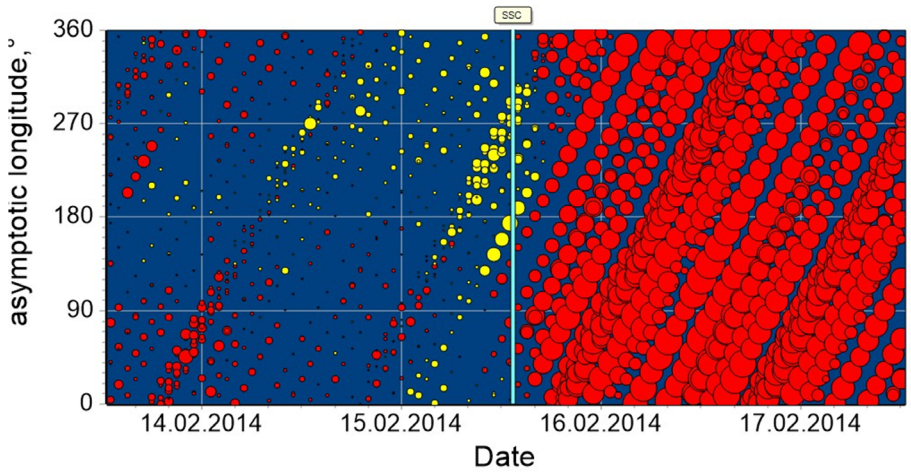

Figure 2: The asymptotic longitude of each station versus the time of the FD on 15 February 2014 is presented. The red circles represent decrease of the CR intensity, while the yellow ones represent increase. The cyan vertical line indicates the shock arrival time. The size of its bubble is proportional to the hourly recorded cosmic ray amplitude of each station.

3.2 FD without an association with SSC – the event of 21 October 2003

Forbush decrease of 21 October 2003 at 14:00 UT is an interesting example of event not connected with a SSC, but with precursory signals. It is the first of a series of intense events that took place in October 2003 (figure 3), with the last one to be the greatest FD not only of the solar cycle 23, but also of the last fifty years. As it is shown in figure 3 this FD of 21 October 2003, in contrary to the next ones, started with an onset.

In 19 October the active region 10484 had just dawned on the observable from Earth solar disk and three large solar flares are erupted (2 M-flares and 1 X-flare). The solar wind velocity reached the value of 744 km s − 1 and IMF increased to 11.8nT. It is generally considered that FDs without an association with a SSC have smaller amplitudes than the FDs that occur with a strong shock wave. This is not real and this specific event has an amplitude, corrected for geomagnetic effects, of 6.2% at the rigidity of 10 GV. Finally, a moderate geomagnetic storm was recorded, with the minimum of Dst index to be -61 nT.

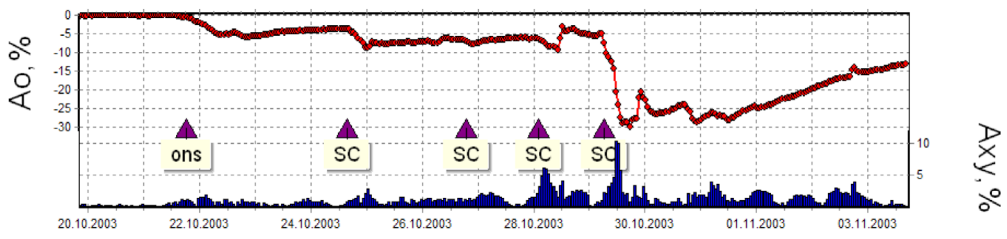

Figure 3: The CR intensity (A0) (red line) and the anisotropy on the equatorial plane A_{xy} (blue histogram) for the time period 20 October 2003 - 4 November 2003.

KIEL-UP •DOI: 10.38072/2748-3150/p8

An untypical pre-decrease precursor signal is observed before the onset of the FD. Pre-decrease sign started to be recorded by the NMs about 8h before the onset of the FD and it ranged between 110° – 360° (figure 4). It is noted that the untypical kind of precursors does not depend on the mechanism that generates the FD and is observed in both categories.

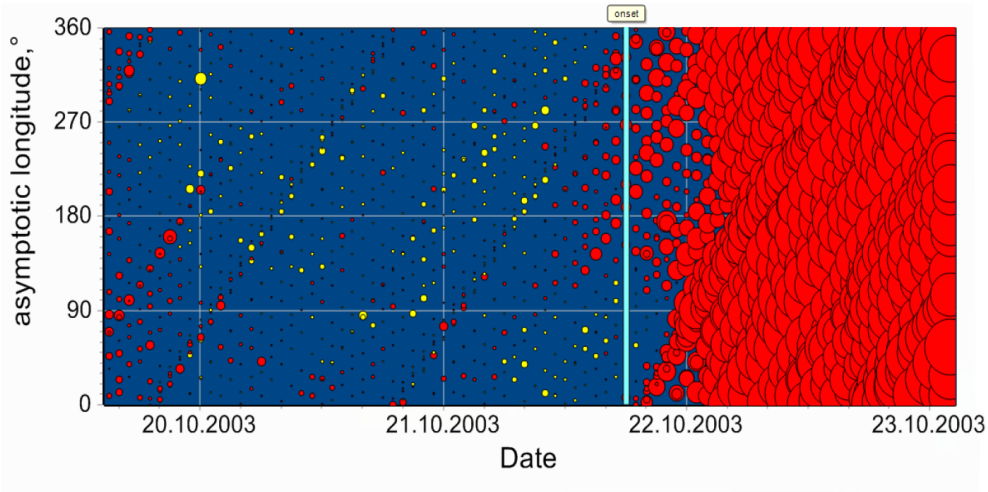

Figure 4: The asymptotic longitude of each station versus time (upper panel) of the FD on 21 October 2003. The red circles represent decrease in the CR intensity while yellow ones represent increase. Cyan vertical line is the onset time. The switching of yellow and red circles two days before the FD is the solar diurnal anisotropy record. The size of its bubble is proportional to the recorded amplitude of each station every hour.

4. Discussion and conclusion

From the study of the precursors of FDs that took place at the time period 1969 – 2019 (solar cycles 20, 21, 22, 23, 24) remarkable results were obtained. The most important and innovative of them is that indeed precursory signals could be observed before FDs which are not associated with the presence of a SSC in the upper magnetosphere. The two categories present similarities, mainly in the kind of precursor and the time period before the start of the FD where it appears. They present differences in the orientation of the solar phenomenon that generated the event and the shape of the precursory signal.

The events that are not associated with a SSC happened due to a phenomenon occurring in the eastern region of the solar disk and in some cases due to a coronal hole. On the contrary most FDs accompanied by a shock wave come from phenomena in the active regions occurring in the central and western zones of the solar disk.

Precursors are really anisotropic phenomena and can be observed as pre-decreases, pre-increases and in same events both of them are recorded (Lingri et al. 2019). It is the same in both categories, but in the case of the absence of a SSC, when a shock wave does not exist, pre-increases are rare as this phenomenon is directly connected with the front of the shock wave. The front swept out the cosmic ray particles and when there is a connection with the reception cone of the NM station a pre-increase is recorded.

It has to be noticed that typical and untypical precursors appear in both categories of FDs and they are not a point of the association or not with a SSC. In general for typical FDs without SSC, the asymptotic longitudes where the pre-decreases are observed are ranged between $\sim 0°$-$190°$ and starts about 18h before the onset, while the few pre-increases appear in a range of $\sim 190°$-$300°$, 8h

before the start of the event. On the other hand, the signals in FDs with a SSC are quiet narrower than those without a SSC, with the asymptotic longitudes where pre-decreases are observed ranging between ∼0°-160° and starting about 18h before the SSC, while pre-increases appear in a range of ∼220°-330°, 10h before the start of the event.

The shape of the signal of a typical pre-decrease starts narrow and then expands as it goes close to the onset when there is no association with a SSC, while in the other category the range of the signal is about the same throughout the time. Finally, it has to be noticed that with the new criteria in both categories ∼70% of the studied events present precursory signals, while in previous studies, for the case of FDs associated with a SSC by using different criteria, the percentages were about ∼30% and ∼47% (Papailiou et al. 2012; Lingri et al. 2019), respectively.

Acknowledgments

This research work was supported by the Hellenic Foundation for Research and Innovation (HFRI) and the General Secretariat for Research and Technology (GSRT), under the HFRI PhD Fellowship grant (GA. no. 14492). Special thanks to the colleagues of the NM stations (https://www.nmdb.eu/), last accessed April 7, 2021) for kindly providing the cosmic ray data used in this study in the frame of the High resolution Neutron Monitor database (NMDB) funded under the European Union's FP7 Program (contract no. 213007). Thanks are due to the IZMIRAN/FEID, ACE/Wind, OMNI and NOAA data centers.

References

Abunina, M., Belov, A.V., Eroshenko, E.A., et al., 2020, Solar Phys. 295, 69, DOI: https://dx.doi.org/10.1007/s11207-020-01639-7
Asipenka, A.S., Belov, A.V., Eroshenko, E.A., et al., 2009, Adv. Space Res. 43, 708, DOI: https://dx.doi.org/10.1016/j.asr.2008.09.022
Belov, A., Abunina, M., Abunin, .A., et al., 2017a, Geomagn. Aeron. 57, 389, DOI: https://dx.doi.org/10.1134/S0016793217040028
Belov, A., Abunina, M., Abunin, .A., et al., 2017b, Geomagn. Aeron. 57, 541, DOI: https://dx.doi.org/10.1134/S0016793217050036
Belov, A., Eroshenko, E., Yanke, V., et al., 2018, Solar Phys. 293, 68, DOI: https://dx.doi.org/10.1007/s11207-018-1277-6
Cane, H.V., 2000, Space Sci. Rev. 93, 55, DOI: https://dx.doi.org/10.1023/A:1026532125747
Dorman, L.I., Villoresi, G., Belov, A.V., et al., 1995, Nucl.Phys. B, Proc. Suppl. 39, 136, DOI: https://dx.doi.org/10.1016/0920-5632(95)00016-3
Forbush, S.E., 1954, J. Geophys. Res. 59, 525, DOI: https://dx.doi.org/10.1029/JZ059i004p00525
Kozai, M., Munakata, K., Kato, et al., 2016, Astrophys. J. 825, 100, DOI: https://dx.doi.org/10.3847/0004-637X/825/2/100
Leerungnavarat, K., Ruffolo, D., Bieber, J.W., 2003, Astrophys. J. 593, 587, DOI: https://dx.doi.org/10.1086/376408
Lingri, D., Mavromichalaki, H., Belov, A., et al., 2016a, Solar Phys. 291, 1025, DOI: https://dx.doi.org/10.1007/s11207-016-0863-8
Lingri, D., Mavromichalaki, H., Belov, A., et al., 2016b, in XXV ECRS 2016 Proceedings – eConf C16-09-04.3, https://arxiv.org/abs/1612.08900
Lingri, D., Mavromichalaki, H., Belov, A., et al., 2019, Solar Phys. 294, 70, DOI: https://dx.doi.org/10.1007/s11207-019-1461-3
Mavromichalaki, H., Papaioannou, A., Plainaki, et al., 2011, Adv. Space Res. 47, 2210. DOI: https://dx.doi.org/10.1016/j.asr.2010.02.019
Melkumyan, A.A., Belov, A.V., Abunina, M.A., et al., 2019, Adv. Space Res. 63, 1100, DOI: https://dx.doi.org/10.1016/j.asr.2018.10.009
Papailiou, M., Mavromichalaki, H., Belov, A., et al., 2012a, Solar Phys. 276, 337, DOI: https://dx.doi.org/10.1007/s11207-011-9888-1
Tortermpun, U., Ruffolo, D., Bieber, J.W., 2018, Astrophys. J. 852, L26, DOI: https://dx.doi.org/10.3847/2041-8213/aaa407
Tsyganenko, N., Stern, D., 1996, J. Geophys. Res. 101, 27187, DOI: https://dx.doi.org/10.1029/96JA02735

Questions and answers

Ludwig Klein: It looks like your FDs from the eastern solar hemispheres have no shocks visible at the Earth? Isn' t the shock usually supposed to be broader than the driver?

Answer: Yes, it is true. The shock is broader than the driver, but as the shock moves inside the heliosphere, following the Parker spiral, the front of the shock does not reach the Earth's magnetosphere. So, the Earth intercepts the downstream region of the shock, which indeed is not observable at the Earth.

Cosmic ray studies with neutron detectors | Volume 1 (2021)
KIEL-UP • DOI: 10.38072/2748-3150/p9

Short-term periodicities observed in neutron monitor counting rates

Alejandro López-Comazzi, Juan José Blanco

Correspondence
CaLMa - Monitor de Neutrones de Castilla-La Mancha, Universidad de Alcalá, Madrid, Spain,
alejandrofrancisco.l@edu.uah.es

Keywords
global neutron monitor; periodicities; solar wind speed; interplanetary magnetic field

Abstract
The main objective is to check whether the periodicities observed in the cosmic rays in the interval 2013-2018 are affected by the magnetic rigidity or the height at which the neutron monitors are placed. A Global Neutron Monitor (GNM) has been defined as representative of the neutron monitor global network. The Morlet wavelet analysis is applied to the GNM and the selected solar activity parameters to find out common periodicities. Short-term periodicities of 13.5, 27, 48, 92, 132 and 298 days have been observed in cosmic ray intensity. A clear inverse relationship between rigidity and spectral power has been obtained for the 13.5, 48, 92, 132-day periods. A not so clear but still observed direct relationship between the height of the neutron monitors and the spectral power for the 48, 92, 132-day periods has been also found. The periodicity of 92 days is the one which shows the highest dependence with rigidity cutoff and height. As far as we know, this is the first time that these dependencies are reported. We think that these observations could be explained by assuming some cosmic ray intensity energy dependence in such periodicities and a competitive effect between rigidity and height.

1. Introduction

The primary cosmic rays are electrically charged high energy particles, mostly originating in violent phenomena of our galaxy (such as supernova explosions, pulsars with very strong magnetic fields) and, to a lesser extent, solar or extragalactic phenomena, that continuously affect the terrestrial atmosphere with energies between 10^6 and 10^{20} eV/nucleon. When these primary CR interact with particles present in the Earth's atmosphere, other particles called secondary cosmic rays, such as protons, muons, neutrons and mesons are created. Some of these secondary particles are registered by ground-based neutron monitors and muon telescopes respectively.

The year 1964 was designated by cosmic ray investigators as the international quiet year of the sun (IQSY) and Hugh Carmichel developed a neutron monitor (NM) with a statistical accuracy of 0.1 % for hourly data called "NM64" or also known as "supermonitor", Shea and Smart (2000). These "NM64" is used as standard to obtain data which to compare with other stations.

From that date to the present day, other similar instruments have been developed along different locations on the terrestrial sphere. Most of them share their measurements through the Neutron Monitor Data Base (NMDB).

To study the solar activity through NMs requires the use of multiple stations located in different geomagnetic locations because their position with respect to the Earth's magnetic field determines

KIEL-UP • DOI: 10.38072/2748-3150/p9

the minimum energy of cosmic rays to generate counts on a given NM. This need justifies the foundation of the NMDB.

Cosmic Ray Intensity is anticorrelated to the solar activity, measured by the sunspot number, with a certain delay caused by irregularities in the Interplanetary Magnetic Field, Forbush (1958) and Usoskin et al. (1998).

2. Results

2.1 Data analysis and method

This proceeding examines the short-term periodicities, i.e. periodicities between 2-512 days, during the period 2013-2018 using the wavelet analysis. The fact that several different phenomena can contribute to different periodicities and these are not constant in time could make Fourier analysis unsuitable (Schreiber et al. 1998) and therefore it has been used wavelet analysis to observe the intrinsic temporal variation in the periods.

A set of neutron monitors with available data from 2013 to 2018 has been selected. These data are one hour pressure corrected counting rates and were collected from the NMDB web page. A check of data availability for the data provider stations in NMDB was performed initially. Only stations with less than 5% of missing values and/or outliers, i.e. clear wrong data, were selected for the study. The set of outliers and missing values were substituted by linear interpolation. Once the outliers are substituted in the data from the selected stations, the wavelet analysis is applied to their counting rates to find out periodicities in the data. This analysis decomposes a signal into a sum of wavelets which come from a "mother" wavelet function, in this case the Morlet function.

We define as Global neutron monitor (GNM) an ideal neutron monitor whose power spectrum is obtained using the averaged of the counting rates, in typified units, of all the selected neutron monitors in a particular study. Criteria based on three quality indices have been used to define the final list of stations to build the Global neutron monitor. These three quality indices are referenced as Q_j, Q_x and Q_u which, by distinct methods, compare the different stations and give us a quantitative idea of which stations have a distant behavior of the general trend. For the calculation of the averaged counting rates we only took into account the neutron monitors whose value is greater than 0.5 in the three indices.

The index as Q_j evaluate how much a single power spectrum of a certain station differs from the one that is obtained by average of all stations. Q_x is the weighted cross-correlation between a single neutron monitor counting rates and the other stations. Q_u is determined following the same procedure to calculate Q_x but it is applied to Global Wavelet Spectrum and not to the counting rates (for more information, see López-Comazzi et al. 2020). The final selection of stations comprises 22 neutron monitors at different vertical cutoff rigidity and height in meters above sea level (m.a.s.l). The positions on the Earth, latitude and longitude, of the selected neutron monitors are depicted in figure 1.

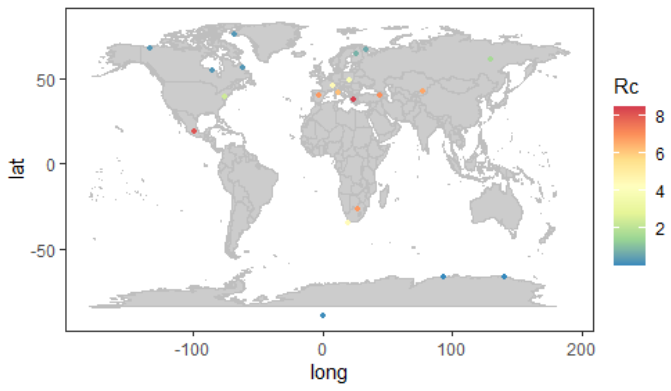

Figure 1: Map with the locations of the 22 selected neutron monitors used to build the Global Neutron Monitor (GNM).

KIEL-UP • DOI: 10.38072/2748-3150/p9

2.2 Global Neutron Monitor

Wavelet analysis applied to the neutron monitor counting rates presents, in general, similar results for all the neutron monitors. The Global Neutron Monitor (GNM) shows a representative behaviour of all stations and it can be used to describe the characteristics of the periodicities observed in cosmic rays counting rates. The detected periodicities in cosmic rays counting rates, total solar irradiance (TSI), sunspot number (SSN), solar wind speed (V) and interplanetary magnetic field (B) are listed in table 1.

The most prominent period observed in the GNM counting rates is the 27-day one and it appears throughout the complete time series except from mid-2013 to mid-2014 (figure 2). This period, related to the synodic solar rotation, was observed by the 22 stations.

A second peak, probably related with solar rotation, is centered in 13.5 days. The 13.5-day period (the second harmonic of the fundamental solar rotation) has been associated with both solar active longitudes as well as tilted dipole structure (Vipindas et al. 2016). This period presents higher power between 2014 and 2017 (figure 2) and it is especially strong in the second half of 2016 during the decreasing phase of the Solar Cycle. This periodicity is much weaker and almost undetectable from 2017 to the end of the studied time interval in coincidence with the solar minimum.

The nearly annual period is the second highest peak (figure 3). Its strength varies with time, being stronger between 2013-2015, weaker between 2015-mid 2017 and disappearing in 2018. This period is clearly observed in all the stations with similar strength. The period is peaked around 298 days.

Three minor peaks (around 132, 92 and 48 days) complete the set of relevant periodicities. All of them show a behavior depending on time disappearing after mid 2015 (figure 2). The three periods were identified between 2014-2016 with similar spectral power in all the neutron monitors and in coincidence with a lower cosmic ray intensity.

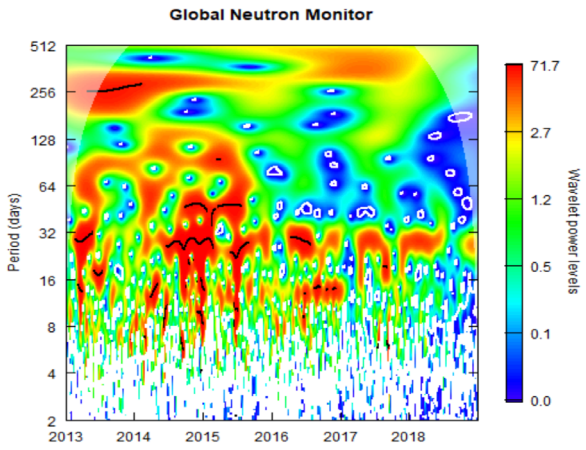

Figure 2: The Wavelet Power Spectrum of the Global Neutron Monitor (GNM).

KIEL-UP • DOI: 10.38072/2748-3150/p9

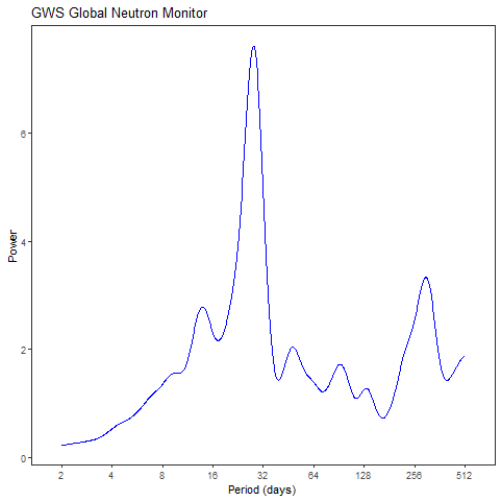

Figure 3: The Global Wavelet Spectrum of the Global Neutron Monitor (GNM).

	Period (days)					
	≈ 13.5	≈ 27	≈ 48	≈ 92	≈ 132	≈ 298
CR	14 ± 1	28 ± 3	48 ± 4	92 ± 6	132 ± 5	298 ± 16
V	13 ± 1	27 ± 3	–	88 ± 9	–	256 ± 28
V_x	14 ± 1	27 ± 3	–	88 ± 7	–	256 ± 27
V_{perp}	14 ± 1	26 ± 1		89 ± 6	–	311 ± 20
B	13 ± 1	26 ± 2	54 ± 3	107 ± 8	–	298 ± 29
B_r	14 ± 1	27 ± 3	–	–	–	–
B_z	–	25 ± 2	–	–	–	–
SSN	–	27 ± 2	44 ± 3	105 ± 7	–	300 ± 25
TSI	14 ± 1	25 ± 3	50 ± 4	94 ± 5	–	324 ± 27

Table 1: Periodicities in GNM counting rates, sunspot number (*SSN*), total solar irradiance (*TSI*), interplanetary magnetic field (*B*) and solar wind speed (V) and its components in GSE coordinates. The second line expresses the notation used to refer to each obtained periodicity in the different ranges.

2.3 Cutoff rigidity and altitude dependence with spectral power of the different periodicities

One of the open questions regarding to the observation of periodicities by neutron monitors is the role of rigidity and altitude above sea level on the relative strength of a particular periodicity. The figure 4 shows the spectral power of the 13.5, 48, 92 and 132-day peaks vs magnetic rigidity $\boldsymbol{R_c}$. A different behaviour between southern NM (green circles in figure 4) and northern NM (blue circles) has been detected. Southern stations do not show dependence but this is not truth for northern stations.

The dependence of the spectral power with the altitude of the NM site has been also studied. A direct result appears when spectral power is represented against altitude (figure 5). NM at sea level (below 200 m.a.s.l) do not show a relationship with height (green circles in figure 5). However a direct relationship emerges for stations above 200 m.a.s.l (blue circles in figure 5) for the 92 and 132-day periods.

KIEL-UP • DOI: 10.38072/2748-3150/p9

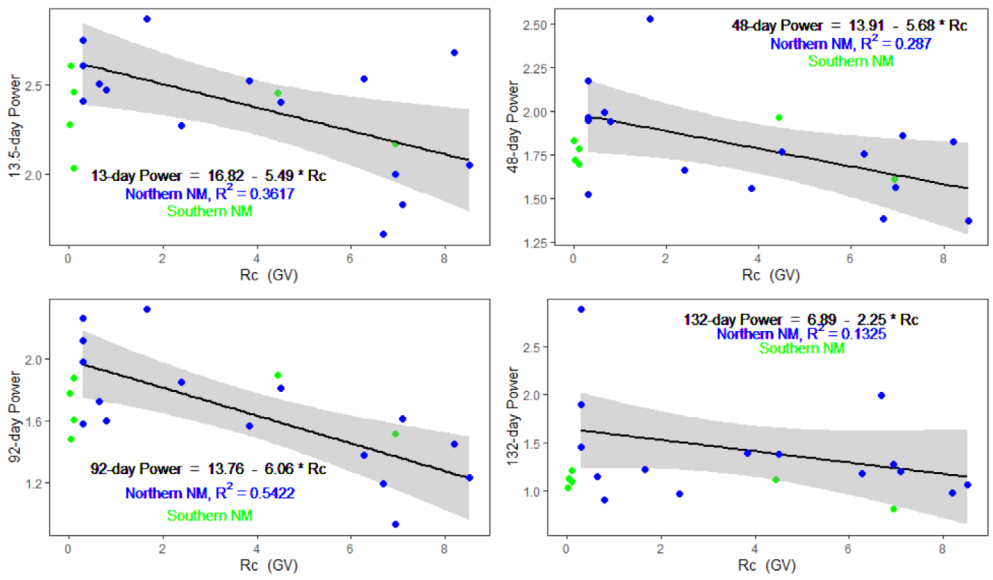

Figure 4: The spectral power of the 13.5-, 48-, 92- and 132-day period VS. magnetic cutoff rigidity R_c of each neutron monitor. In green, the neutron monitor located in the southern hemisphere and in blue the stations located in the northern hemisphere. The black line is the regression line obtained by linear adjust for the northern hemisphere neutron monitor. R^2 is the coefficient of determination obtained for the northern hemisphere stations. The grey band displays the error range of fit line.

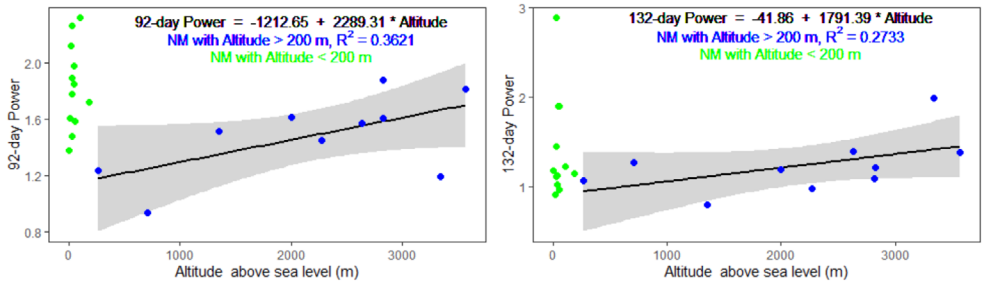

Figure 5: The spectral power of the 92 and 132-day period vs altitude of each neutron monitor in meters above sea level. In green, the neutron monitor with altitude less than 200 m and in blue the NM with altitude more than 200 m. The black line is the regression line obtained by linear adjust for the NM with altitude higher than 200 m. R^2 is the coefficient of determination obtained for stations with altitude more than 200 m. The grey band displays the error range of the fit line.

3. Discussion and conclusions

A rigidity dependence has been observed in the power of the spectral power in some of the periodicities, concretely in 13.5, 48, 92 and 132-day periods. This result could be explained if the transport conditions are changing with these periods in a way that cosmic rays with less energy are more effective affected than cosmic rays with higher energies.

The second main observation inferred from our work is that also exist a dependence with respect the height at which neutron monitor is located. This dependence is clear at heights above

200 m a.s.l and, as the rigidity dependence, only is observed for certain periodicities. These were the 92 and 132-day periodicities.

The dependence with rigidity and height shows an opposite behaviour regarding to the spectral power on GNM counting rate and both effects are observed for the 92 and 132-day periods. These effects are clearer for the 92-day periodicity.

The periodicities detected in neutron monitor counting rates are also observed in the selected parameters (table 1). We discuss now the periods in parameter and their role in forcing CRI periodicities.

The 48-day period is also observed in the module of interplanetary magnetic field, SSN and TSI while the 92-day period is registered in the same parameters in addition with the solar wind velocity. On the other hand, previous works have reported the relationship between solar wind speed and the fractional coronal hole area (Tulasi et al. 2010) and between the TSI and the presence of coronal holes (Woods et al. 2010). Maybe, this is pointing out a possible relationship between solar wind structures and the observed flux of cosmic ray which is reflected by the observed 48 and 92-day periodicities.

Close to the 92-day period observed in cosmic ray, a periodicity of 88-day has been found in the solar wind velocity. This period is only observed in the solar wind velocity and could be a harmonic of the ACE (spacecraft data used in this work) orbital period of 177 days. Nevertheless after analysing the ACE orbit, no such period of 88 days is detected, therefore it should be concluded that 88 day is a true period in the solar wind velocity. This could reinforce the hypothesis of solar wind structures producing energy depending periodic variations in the cosmic ray flux.

The 13.5 and 27-day periods, related with the solar synodic rotation, are observed in almost all the analyzed parameters. The most prominent peak in the power of the wavelet analysis for NM counting rate is in 27 days (figure 3). This period is attributed to the solar rotation commonly, and is related to the coronal holes and co-rotating interaction regions, i.e. interactions between fast and slow solar streams.

The 132-day period was only detected in CR. This could imply that this periodicity is induced by a process not related with solar wind velocity, heliospheric magnetic field, SSN or TSI. However, the relationship of this periodicity with a solar phenomenon cannot be ruled out. It has been reported the observation of the period of 134.5 days in the sunspot data of the northern hemisphere and a similar period (133 day) detected in the data of whole disk along the SC 23 (Joshi et al. 2009).

Finally, the 298-day period is detected in the magnetic field intensity, TSI, SSN and in the component V_{perp} perpendicular to the ecliptic plane in addition to GNM counting rates.

The 132 and 298-day period are very close to subharmonics of the solar synodic rotation of 27 days, the fifth 135 days and eleventh 298 days) subharmonic. Therefore, the 132 and 298-day period could related to the fifth and eleventh subharmonic of the solar synodic rotation of 27 days.

References

Forbush, S. E., 1958, J. Geophys. Res., 63, 651, https://ui.adsabs.harvard.edu/abs/1958JGR....63..651F (last accessed April 7, 2021), DOI: https://doi.org/10.1029/JZ063i004p00651

Joshi, B., Pant, P., & Manoharan, P., 2009, Astronomy and Astrophysics, 452

López-Comazzi, A. Blanco, J.J, 2020, Sol. Phys., 295, 81, DOI: https://doi.org/10.1007/s11207-020-01649-5

Schreiber, H., 1998, Annales Geophysicae, 16, 510, DOI: https://doi.org/10.1007/s00585-998-0510-2

Shea, M. & Smart, D., 2000, Space Science Reviews, 93, 229, DOI: https://doi.org/10.1023/A:1026500713452

Tulasi Ram, S., Liu, C. H., & Su, S.-Y., 2010, Journal of Geophysical Research:Space Physics, 115

Usoskin, I. G., Kananen, H., Mursula, K., Tanskanen, P., & Kovaltsov, G. A.,1998, J. Geophys. Res., 103, 9567, DOI: https://doi.org/10.1029/97JA03782

Vipindas, V., Gopinath, S., & Girish, T. E., 2016, Astrophysics and Space Sci-ence, 361, 135. DOI: https://doi.org/10.1007/s10509-016-2719-y

Woods, T. N., 2010, Astronomical Society of the Pacific Conference Series, Vol.428, Irradiance Variations during This Solar Cycle Minimum, ed. S. R. Cranmer, J. T. Hoeksema, & J. L. Kohl, 63, https://arxiv.org/abs/1003.4524

KIEL-UP • DOI: 10.38072/2748-3150/p9

Questions and answers

Monica Laurenza: Are all peaks significant? Did you estimate white or red noise?
Answer: Yes, all peaks are significant. To determine if the peaks represents real characteristics of the time series, a background spectrum is taken. In this work we taken a simple model for red noise, the univariate lag-1 autoregressive process.

Ludwig Klein: The 48 h period was reported in one of yesterday's talks. Any idea of what it means and if it's real?
Answer: I think the 48-day period is real. The 48-day period is observed in this work in neutron monitor counting rates and in the module of interplanetary magnetic field, Sunspot number and total solar irradiance. Previous works have reported the relationship between solar wind speed and the fractional coronal hole area (Tulasi et al. 2010) and between the total solar irradiance and the presence of coronal holes (Woods et al., 2010). Maybe, this is pointing out a possible relationship between solar wind structures and the observed flux of cosmic ray which is reflected by the observed 48-day period.

Ilya Usoskin: Is there correlation between altitude and cutoff rigidity Rc for the analyzed NMs? Most likely high-Rc NMs tend to be high-altitude.
Answer: This is the plot Altitude VS cutoff rigidity for the selected NMs. Green circles displays southern NMs and blue circles are northern NMs. The linear regression fit give us a coefficient of determination of $R^2 = 0.1$.

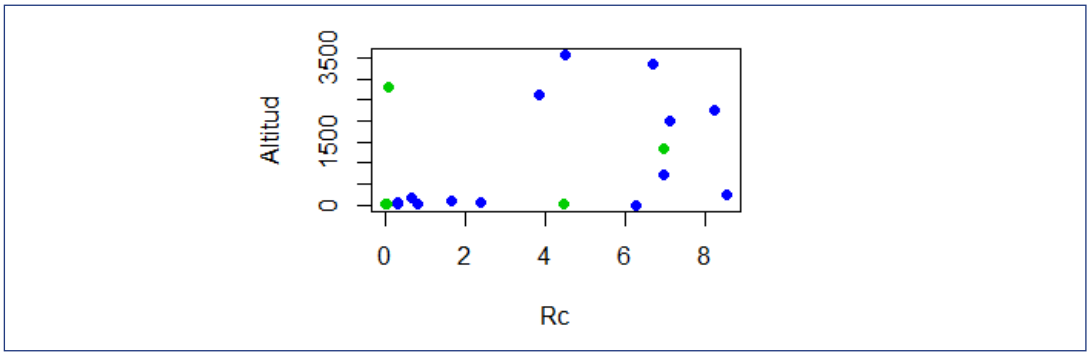

Agnieszka Gil: There is a big difference between sea-level and high-altitude NMs in the 92-day period power vs altitude plot. Any thoughts about the cause? Is the 92-day power vs cutoff rigidity dependence excluded at the plot?
Answer: Probably for stations at sea level or low altitude (less than 200 m), the effect of cutoff rigidity is the dominant factor. This fact would explain the strong dispersion of the spectral power value for these stations (NMs with altitude > 200 m). In the 92-day spectral power VS. altitude plot, the 92-day power vs cutoff rigidity dependency is not excluded.

Gonzalo Tancredi: Do you have plans to extend this work for previous years? e.g. 90's & 00's
Answer: Yes, I intend to extend the study to the entire range covered by the neutron monitors (1960-2020) and analyze the short- medium- and long-term periodicities.

Cosmic ray studies with neutron detectors | Volume 1 (2021)
KIEL-UP • DOI: 10.38072/2748-3150/p10

Unusual decrease of the cosmic ray intensity in May 2019 on the background of the minima solar activity

Liudmila Trefilova, Pavel G. Kobelev, Anatoly V. Belov, Eugenia A. Eroshenko†, Anaid A. Melkumyan, Victoria A. Oleneva, Victor G. Yanke

Correspondence
Pushkov Institute of Terrestrial Magnetism, Ionosphere and Radio Wave Propagation(IZMIRAN), Moscow, Russia,
trefilova@izmiran.ru, kosmos061986@yandex.ru, abelov@izmiran.ru, erosh@izmiran.ru,
amelkumyan6@gmail.com, olene@izmiran.ru, yanke@izmiran.ru

Keywords
solar activity; Forbush decrease; CME, cosmic ray variations

Abstract
In May 2019 there was a long and sloping decreasing of cosmic ray's intensity (up to ~4%), which was observed on neutron monitors. Despite this was a small decreasing compared to quasi-eleven-period variation, it stands out well in 24th cycle of solar activity.
According to LASCO/SOHO and STEREO-A data from spectrometer in different UHF bands and from coronograph, there was a series of CMEs which affected on modulation of cosmic rays by creating a series of Forbush decreasing, which didn't restore. This series was connected to two active regions on sun and began on April 30 from "reversed halo" CME. This CME didn't reach the earth, but led to significant additional modulation of cosmic rays, mostly on east side. Later there was a series of smaller CMEs on May 1-6, which also didn't reach the earth, but were gradually approaching to Earth. Recent CMEs on 8-9 and 12-13 created a normal Forbush decreasing.
In May 2019, cosmic rays shown again, that they can collect information about distant objects of geliosphere and transmit it to Earth. The ground-level detectors sometimes can observe an interaction of interplanetary disturbances, which didn't reach the earth. East CMEs are especially effective, because they closing magnetic field lines beyond the orbit of earth and can interfere the restoring of cosmic ray's intensity.

1. Introduction

Since July 2018, the calmest period in the minimum solar activity of the 24th solar cycle has been observed. We can notice that the first half of May 2019 stands out sharply. From April 28 to May 17, against the background of a deep minimum of solar activity, a remarkable event took place. Small (up to 4%), but prolonged decrease in the intensity of cosmic rays measured by neutron monitors (~ 10 days). This decrease is considered a relatively small change in intensity in General, but rather unusual and interesting for minimal solar activity. We can highlight it on the variations of cosmic rays at the Moscow station (figure 1) and on the time dependence of the zero harmonic A0 in figure 3, which will be discussed in detail below. It can be seen that the recovery started on 12 May, but the situation changed on May 16 and a new decline began. The next recovery started on May 17, which also lasted for 10 days. The total duration of the event is about 25 days. Such a large time interval indicates that there were significant changes in the characteristics of the interplanetary environment almost on the scale of the semi-heliosphere.

† deceased

KIEL-UP • DOI: 10.38072/2748-3150/p10

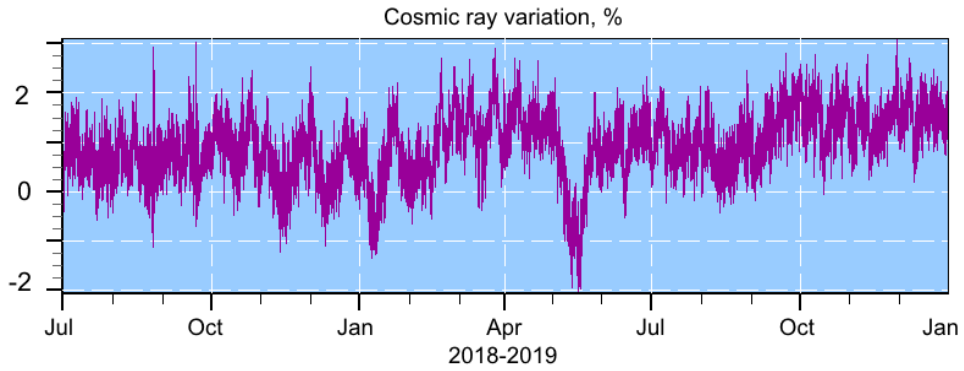

Figure 1: Hourly variations in the rate of counting cosmic rays according to the neutron supermonitor Moscow (July 2018-December 2019).

Such events are rare: a similar event was observed in September 1979 (Belov et al. 1983), but with a much greater decrease in the intensity of cosmic rays (more than 10%). It was observed during the maximum of solar activity. This events are typical for such periods. A certain similarity with the event of May 2019 was also found in several other cases – in April 1980, July 2000 and July 2006 with amplitudes of 6%, 11% and 3.5%, respectively. The first two were observed at the maximum of solar activity, the last one - at the end of the maximum- at the beginning of the minimum.

2. Data analysis

2.1 Solar and geomagnetic conditions (activity) during the reviewingperiod

According to SEEDS Monthly Catalog (http://spaceweather.gmu.edu/seeds/lasco.php, last accessed April 7, 2021), at this time (from April 28 to May 12), 13 significant CMEs were recorded (the angle of the ejection solution Angular Width $>50°$, table 1) out of 38 observed during the eighteen-month quiet period (from July 2018 to December 2019), which is $\sim$ 35%. Forbush effects observed near Earth's orbit in May 2019 according to the World network of neutron monitors, according to the "database of interplanetary perturbations and Forbush effects" (Belov et al. 2001). For each event, the maximum amplitude of the FE_{mag} effect, the maximum magnetic field and solar wind speed B_{max} and V_{SWmax}, the Axy_{min} projection of the cosmic ray anisotropy vector on the earth's Equatorial plane and the North-South projection A_z, and finally the rate of decreases D_{min} are shown at the moment of the Forbush effect. All 13 emissions came from two regions that had been active for a long time. Constant emissions (including minor ones) did not allow the cosmic rays to recover and supported the process of slow decline.

	Date Time	FEmag, %	B_{max}, nT	V_{SWmax}, km/s	Axy_{min}, %	Az, %	D_{min}, %/h
1	2019-05-01 13:00:00	0.9	9.1	569	1.08	0.81	-0.26
2	2019-05-03 18:00:00	0.6	9.8	505	0.87	1.16	-0.28
3	2019-05-07 19:00:00	0.8	11.9	380	0.96	1.21	-0.20
4	2019-05-09 06:00:00	0.5	11.9	380	0.64	1.18	-0.21

KIEL-UP • DOI: 10.38072/2748-3150/p10

5	2019-05-10 18:00:00	1.3	14.3	556	0.99	0.75	-0.33
6	2019-05-14 00:00:00	1.1	14.3	556	1.34	1.07	-0.35
7	2019-05-16 00:00:00	0.9	8.4	480	1.08	1.13	-0.28

Table 1: Forbush effects observed near Earth's orbit in May 2019.

Forbush decrease is a short-term and drastic decrease in the intensity of galactic cosmic rays. The effect is explained by the increased scattering of galactic cosmic rays by perturbations of the interplanetary magnetic field carried by the solar wind from the Sun to the borders of the heliosphere.

The strongest CMEs from these active areas were observed from April 28 to May 12, 2019. On April 28, an ejection occurred beyond the Western limb. However, this ejection did not alone create such a decrease, at this time also came the disturbance created by the flow of plasma from the coronal hole observed in the center of the solar disk on April 27. Then there was a strong release on April 30 (figure 2, source: https://sohowww.nascom.nasa.gov/explore/coronagraph.html, last accessed June 4, 2021)"

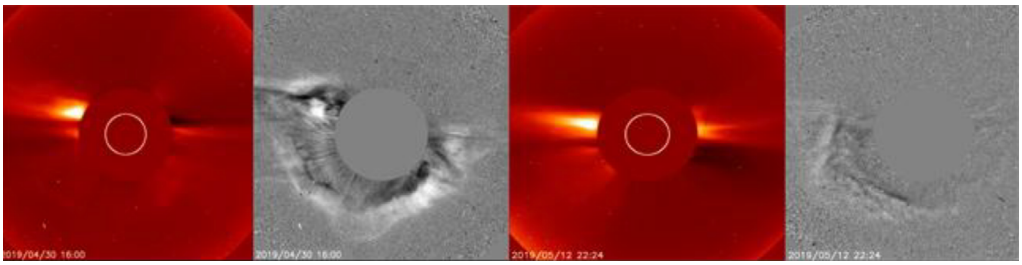

Figure 2: Reverse halo on April 30 on the SOHO coronograph.
Figure 2b: Ejection on May 12 towards the Earth on the SOHO coronograph.

On the chronograph, it was a reverse halo. The next ejection was observed for the Eastern limb on May 1. Further, from May 3 to May 5, a number of ejections were observed on the Eastern limb, which gave Forbush declines on May 6, 7 and 8. But on May 6, there was an outburst in the East of the visible solar disk, and on May 9, there was a slight Forbush decrease. On May 8 and 9, there were ejections in the visible Eastern part of the solar disk, giving a number of Forbush decreases on May 10 and 11. Such continuous CMEs did not allow the cosmic rays to recover. It was only after May 12 that the recovery started, as no significant processes were observed for several days. However, on May 12, there was again a fairly large ejection in the form of a direct halo (figure 2b), which led to a Forbush decrease on May 16, without allowing the cosmic rays to fully recover. No events were observed after May 13, and cosmic rays began to recover from May 17 and fully recovered by May 26.

KIEL-UP • DOI: 10.38072/2748-3150/p10

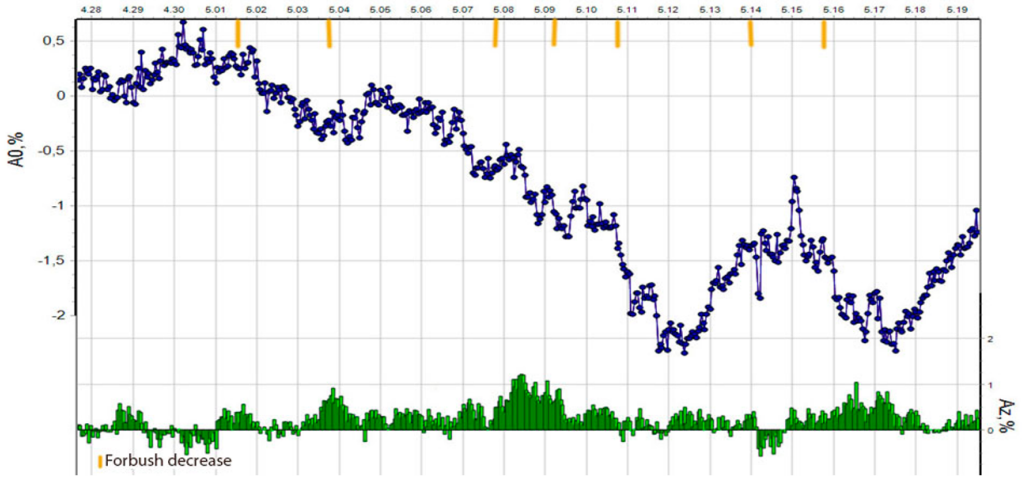

Figure 3: The Amplitude of the zero harmonic A 0 for an uncharacteristic decrease in the rate of counting cosmic rays in May 2019

2.2 Method of selecting Forbush effects for the May decrease

Here is an example for the events of May 1, where the maximum amplitude of the FE_{mag} effect reached 0.9%. Each Forbush was selected by changes in various parameters, mainly components of the magnetic field, solar wind speed, density, and temperature. Figure 4 shows a significant increase in wind speed, and the other parameters mentioned above have also increased slightly.

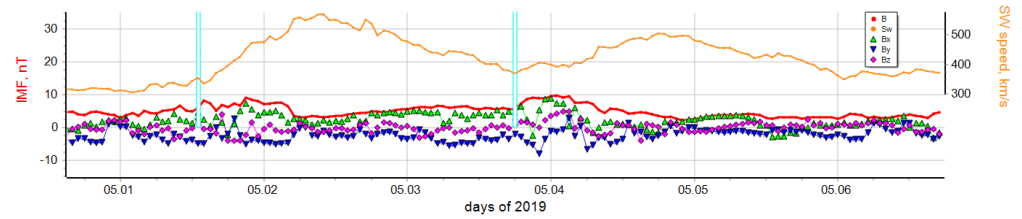

Figure 4: Solar wind parameters.

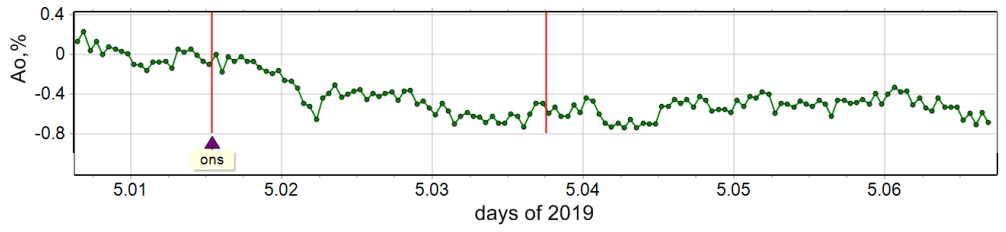

Figure 5: The amplitude of the zero harmonic A0 for an uncharacteristic decrease in the speed of counting cosmic rays in May 2019.

KIEL-UP • DOI: 10.38072/2748-3150/p10

Then there is some decrease in all indicators, which is replaced by another growth, which indicates the next Forbush decrease. Thus, we get a Forbush decrease with subsequent recovery (figure 4). By transferring the time interval to the graph of the zero harmonic amplitude (figure 5), we can see that there is a pre-reduction of the Forbush effect in this event. The same method is used for all other events.

Analysis of the characteristics of the solar wind in General allows us to see that due to the significant frequency of flares that followed the initial decrease due to the activity of coronal holes on May 1-3, and then due to emissions from active regions, cosmic rays did not have time to recover, forming a number of Forbush effects, which led to a long total decrease.

2.3 Results of the analysis of the zero harmonic of cosmic rays

Analyzing the data of neutron monitors with an effective energy of 10 GeV, we can distinguish a number of individual decreases separated by sections of elevation or plateau (figure 3). These slopes are caused by a lot of small Forbush decreases following each other, up to 1.5%. Forbush effects are considered significant from 3.5% at a proton energy of 10. However, after such small decreases, there is no recovery for a long time.

2.4 Distribution of solar wind density for CMEs in April-May

Based on the solar wind density model presented on the website http://helioweather.net/archive/2019/05/den2e4-earth_201905.mp4 (last accessed April 23, 2021), we can see its detailed distribution during outliers.

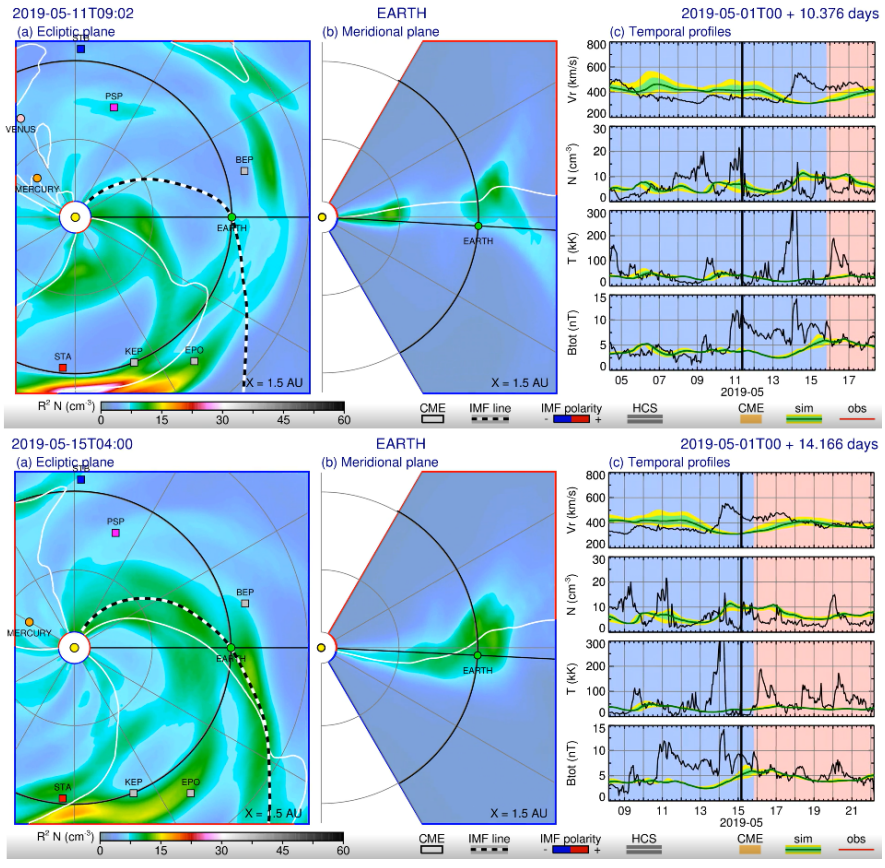

Figure 6: Behavior of solar wind density on May 11 (left), solar wind density behavior on May 15 (right).

KIEL-UP • DOI: 10.38072/2748-3150/p10

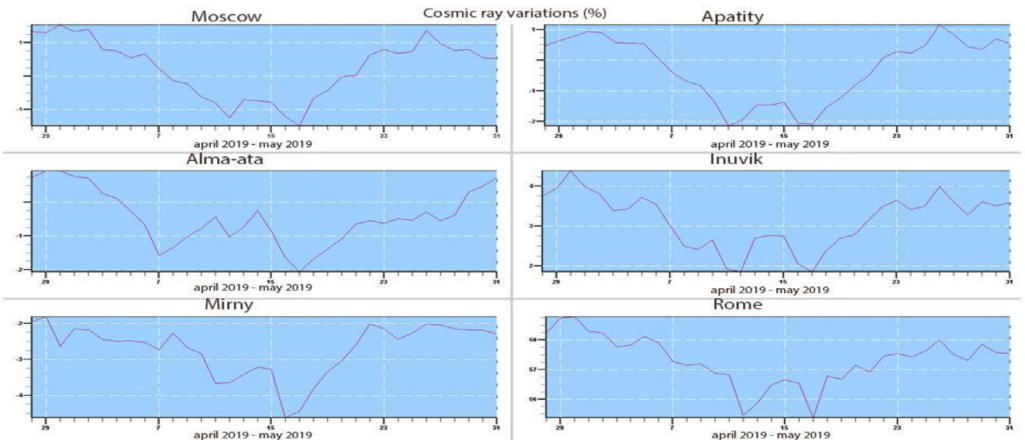

Figure 7: Daily variations in the rate of counting cosmic rays according to neutron monitors with different latitude and longitude locations.

Inside the CMEs, the solar wind density reaches much higher values than usual. High-density plasma closes the lines of force for cosmic rays in certain directions, thus reducing the number of detected particles. Figure 6a shows the ejections that occurred on April 8 behind the Eastern limb, as a result-the decrease in cosmic rays on May 11. Despite the fact that the ejections do not reach the Earth, they influenced the count rate of neutron monitors. Figure 6b shows the distribution of density from direct CMEs towards the Earth on May 12 and 13, which led to a decrease in cosmic rays on May 16-17. This minimum intensity is visible on all monitors (figure 7).

The flow of cosmic rays is strongly influenced by magnetic fields. Under normal conditions, the magnetic field can be represented as a quasi-spiral, cosmic rays move along lines of force, mostly in the direction of the sun. The ejection can be represented as a ring with a field wound on it, which has different values and is directed mostly across the magnetic lines of the sun. The lines of force are moving behind the shock wave from the release. Transverse lines of force create a kind of screen for cosmic rays, that have been involved in a gradually expanding flow cannot overcome the cross-flow. In these areas, the exchange of cosmic rays is difficult, and recovery is worse. However, cosmic rays, not being able to pass through the force line, will seek to find another path. This reduces the recovery flow compared to normal, which leads to a decrease in the intensity of cosmic rays, which is an important condition for the appearance of Forbush decreases.

2.5 The decreasing on the other planets

Looking at the location of the planets relative to the Sun in the beginning of May, we can say that dedicated emissions in considered period could influence as well as on Mars and Jupiter. We can conclude it looking at the date on figure. It could be said that investigated phenomenon has global character. There are cosmic ray variations on the Earth, Mars, and electrons from Jupiter, recorded near the Earth presented in figure 8.

A detailed description of the RAD instrument can be found in Hassler et al. (2012) and data from base (RAD, 2020). Since Mars was opposite the eastern limb, as a result of the powerful solar event April 28 in early May on the RAD detector on Mars, the probability of a significant Forbush decrease was higher than that of Earth. However, on the Martian detector, the variations had, on the whole, the same time dependence and approximately the same magnitude as near the Earth for 10 GV. However, on May 9-10 and 21-22, Forbush decreases were observed at the RAD detector, with a value of 2-3%, which indicates the global nature of the phenomena under study.

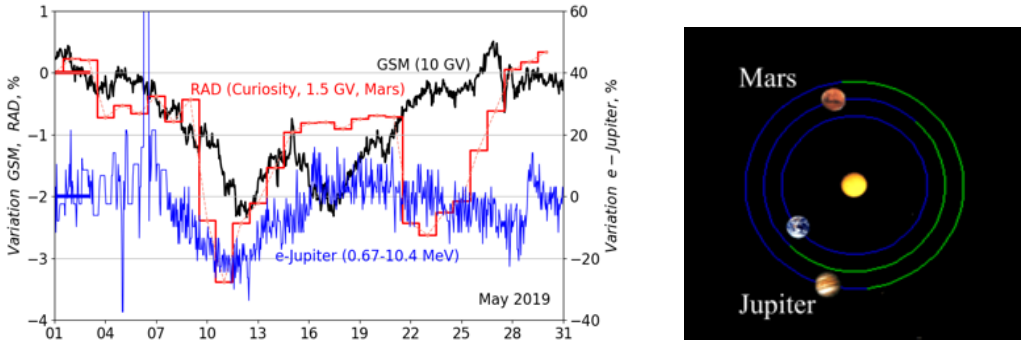

Figure 8: Cosmic ray variations on the Earth, Mars and electrons from Jupiter, recorded near the Earth.

A detailed description of the SOHO/EPHIN instrument can be found in Müller-Mellin et al. (1995) and data from base (EPHIN 2020). The variations in the electron flux of Jupiter near the Earth's orbit are an order of magnitude larger than the variations in the flux of protons 10 GV, and the time course repeats in the first half of May. But, as follows from figure 8 Earth and Jupiter were not on the same line of force at that moment. And this also testifies in favor of a global decrease in the CR intensity.

3. Discussion and conclusion

The hypothesis of series of small events followed each other was proved by analysis of global survey method, which allows us to highlight separate events from the series.

There was a period of splash during the minimum of Solar activity, that was great enough. Perhaps, we could observe one of the greatest Forbush effect in the cycle, when CME on April 30 had been directed to the Earth.

We can notice the influence of emissions on the Earth, which are not able to come there, special for eastern. Cosmic rays come from huge area therefore we can see more eastern events or even events out of nthe limb by neutron monitor data. The modulation of cosmic rays is depending on situation in whole heliosphere. There is fundamental difference between cosmic ray variations and other geophysical effects.

Acknowledgments

This work was partially supported by the grant RFBR Nº 18-02-00451. Experimentally and methodologically support the project USU *Russian national network of ground stations of cosmic rays*. We are grateful to all the staff of the World Network of cosmic ray stations http://cr0.izmiran.ru/ThankYou.

RAD is supported by NASA (HEOMD) under JPL subcontract #1273039 to Southwest Research Institute and in Germany by DLR and DLR's Space Administration grant numbers 50QM0501, 50QM1201, and 50QM1701 to the Kiel University.

The SOHO/EPHIN project is supported under grant 50OC1702 by the German Bundesministerium für Wirtschaft through the Deutsches Zentrum für Luft- und Raumfahrt (DLR).

We acknowledge the NMDB (https://www.nmdb.eu/), founded under the European Union's FP7 programe (contract no. 213007) for providing the data.

References

Abunina, M., Abunin, A.A., Belov, A.V., Eroshenko, E.A., Asipenka, A.S., Oleneva, V.A., Yanke, V.G., 2018, Relationship between the parameters of Forbush effects and heliolongitude of solar sources Geomagnetism and aeronomy, V.51, 3, P.374-389, DOI: https://dx.doi.org/10.7868/s0016794018030082

Belov, A.V., Eroshenko, E.A., Yanke, V.G., Oleneva, V.A., Abunina, M., Abunin, A., 2018, Global survey method for the world network of neutron monitors, Geomagnetism and aeronomy, V.58, 3, P.374-389, DOI: https://dx.doi.org/10.7868/s0016794018030082

Belov, A.V., 2008, Forbush effects and their connection with solar, interplanetary and geomagnetic phenomena September, Proceedings of the International Astronomical Union 4(S257):439-450, DOI: https://dx.doi.org/10.1017/S1743921309029676

Belov, A.V., Dorman, L.I., Eroshenko, E.A., Melkumyan, A.A., 1983, „Two great cosmic ray intensity decreases in August and September 1979", Cosmic Rays (Moscow, NAUKA), Vol. 23, 60-63

Belov, A. V., Eroshenko, E. A., Oleneva, V. A., Yanke, V. G., Mavromichalaki, H., 2006, Long-term variations of the cosmic ray anisotropy by the data from neutron monitor network, Proc. 20th ECRS, Lisbon, 123

Hassler, D., Zeitlin, C., Wimmer-Schweingruber, et al., 2012, The Radiation Assessment Detector (RAD) investigation. Space Sci. Rev. 170 (1–4), 503, DOI: https://dx.doi.org/10.1007/s11214-012-9913-1

Müller-Mellin, R., Kunow, H., Fleißner, V., et al., 1995, COSTEP-Comprehensive Suprathermal and Energetic Particle Analyser, Solar Physics, V.162, P.483–504, DOI: https://dx.doi.org/10.1007/BF00733437

RAD, 2020, RAD data can be found in NASA's PDS or at the RAD web page https://atmos.nmsu.edu/data_and_services/atmospheres_data/INSIGHT/insight.html (last accessed April 7, 2021)

EPHIN, 2020. The EPHIN data used in this study as well as a detailed documentation of the new data product can be found at http://ulysses.physik.uni-kiel.de/costep/level2/rl2 and in the SOHO archive at https://soho.nascom.nasa.gov/data/archive (last accessed April 7, 2021)

Questions and answers

Monica Laurenza: Did you associate an ICME counterpart for each FD?
Answer: Yes, of course. In most cases, this relationship was clearly defined.

Rolf Bütikofer: How do you explain the very short decrease on14 May 2019?
Answer: The 14 May 2019 decrease is also a Forbush effect that recovered very quickly. This is due to the Western position of the solar source.

Ludwig Klein: Why are the recoveries of these (and other) FDs rather fast, while those of large FDs are very gradual (layman's question)?
Answer: The important is not the recovery time, but the recovery speed, which is usually not very different in cases of large and small Forbush decrease.

Session 1: Abstracts

Use of AMS-02 and PAMELA experiments data for calibration of NM network and verification of NM yield function

Sergey Koldobskiy [1,2], **Ilya Usoskin** [2,3], **Gennady A. Kovaltsov** [4], **Agnieszka Gil** [5,6]

Correspondence

[1] National Research Nuclear University MEPhI, Moscow, Russia
[2] Space Physics and Astronomy Research Unit, University of Oulu, Finland
[3] Sodankyla Geophysical Observatory, University of Oulu, Finland
[4] Ioffe Physical-Technical Institute, St. Petersburg, Russia
[5] Space Research Center, Polish Academy of Sciences, Warsaw, Poland
[6] Institute of Mathematics, Siedlce University, Poland

Launch of PAMELA and AMS-02 experiments started a new era in the study of cosmic rays. One goal of these experiments was to study the cosmic-ray (CR) solar modulation and solar energetic particles phenomena. In particular, the dependence of proton and helium fluxes on solar activity was measured. This allows us to calibrate the neutron monitor response and validate neutron monitor (NM) yield functions (YF). We found that the best agreement between the satellite experiments data and NM data can be obtained using NM YF by Mishev et al. (2013, 2020). In this work we present the results of the NM YF validation and NM calibration for all active neutron monitors.

Ring of stations method in cosmic ray's variations research

Maria Abunina, **Anatoly V. Belov**, **Eugenia A. Eroshenko**†, **Artem A. Abunin**, **Victor G. Yanke**, **Anaid A. Melkumyan**, **Nataly Shlyk**, **Irina Pryamushkina**

Correspondence

Pushkov Institute of Terrestrial Magnetism, Ionosphere and Radiowave Propagation (IZMIRAN), Moscow, Russia

For over 60 years, neutron monitors have been the main standard and high precision detectors for measuring cosmic rays with energy from 400 MeV to hundreds GeV. In order to obtain sufficiently complete information about the distribution of cosmic rays outside the magnetosphere, it is necessary to have a network of detectors spaced evenly enough around the globe. The ring of stations method is one of the most useful methods for studying the properties of the angular distribution of cosmic rays without expressing the cosmic ray intensity in terms of spherical harmonics. The method allows one to get the hourly longitude distribution of the cosmic ray intensity without modeling. The main objective of this work is to expand the use of the ring of stations method, as it is a convenient and useful method of studying cosmic ray's variations. Using the ring of stations method, it is possible to study specific angular distributions of the cosmic ray's variations that are described poorly by the sum of the first spherical harmonics. The ring of stations method is primarily used to study Forbush decreases. Detailed descriptions of Forbush decreases investigation by the ring of stations method are presented in this study. The application of the method to study the precursors of Forbush decreases and cosmic ray's behavior inside the solar wind disturbances is shown.

† deceased

KIEL-UP • DOI: 10.38072/2748-3150/v1

Recurrence of galactic cosmic rays anisotropy and intensity during solar cycle 24

Renata Modzelewska [1], **Agnieszka Gil** [1,2]

Correspondence

[1] Institute of Mathematics, Siedlce University, Poland

[2] Space Research Centre, Polish Academy of Sciences, Warsaw, Poland

We study the 27-day variations of galactic cosmic ray (GCR) anisotropy and intensity in solar cycle 24 based on neutron monitor (NM) measurements. We compare solar minima: 2007-2009 and 2017-2019 characterized by the opposite polarities of solar magnetic cycle. Now we have an opportunity to re-analyze the polarity dependence of the amplitudes of the recurrent GCR variations in 2007-2008 in A<0 and to compare it with the clear periodic variations related to solar rotation in 2017-2019 in A>0. Since the GCR recurrence is a consequence of solar rotation, we analyze not only GCR fluxes, but also solar and heliospheric parameters examining the relationship between the 27-day GCR variations and heliospheric, as well as, solar wind parameters.

Tracking cosmic-ray spectral variation during 2007-2018 using neutron monitor time-delay measurements

Chanoknan Banglieng [1,2], **Hannarong Janthaloet** [1], **David Ruffolo** [*1,2], **Alejandro Saiz** [1], **Warit Mitthumsiri** [1], **Pradiphat Muangha** [1,2], **Paul Evenson** [3], **Tanin Nutaro** [4], **Roger Pyle** [5], **Surujhdeo Seunarine** [6], **James Madsen** [6], **Pierre-Simon Mangeard** [3], **Ronald Macatangay** [2]

Correspondence

[1] Department of Physics, Faculty of Science, Mahidol University, Bangkok, Thailand

[2] National Astronomical Research Institute of Thailand (NARIT), Chiang Mai, Thailand

[3] Bartol Research Institute and Department of Physics and Astronomy, University of Delaware, Newark, USA

[4] Department of Physics, Faculty of Science, Ubon Ratchathani University, Thailand

[5] Pyle Consulting Group, Inc., St. Charles, USA

[6] Department of Physics, University of Wisconsin, River Falls, USA

[*] Presenting author

We developed electronics and analysis techniques to indicate variations in the cosmic-ray spectral index using neutron time-delay data from a single station. Here we study solar modulation using neutron time-delay histograms from two high-altitude neutron monitor (NM) stations: (1) the Princess Sirindhorn Neutron Monitor at Doi Inthanon, Thailand, with the world's highest vertical geomagnetic cutoff rigidity, 16.7 GV, from December 2007 to April 2018; and (2) the South Pole NM, with an atmosphere-limited cutoff of ~1 GV, from December 2013 to April 2018. From these histograms, we extract the leader fraction L, i.e., inverse neutron multiplicity, as a proxy of a cosmic ray spectral index above the cutoff. After correction for pressure and precipitable water vapor variations, we find that L roughly correlates with the count rate but also exhibits hysteresis, implying a change in spectral shape after a solar magnetic polarity reversal. Spectral variations due to Forbush decreases, 27 day variations, and a ground-level enhancement are also indicated. These methods enhance the high-precision cosmic ray spectral information from the worldwide NM network and extend it to higher rigidity. Partially supported by Thailand Science Research and Innovation award RTA6280002 and US National Science Foundation awards PLR/ATE-1341312, PLR-1245939, PLR-1341562, and their predecessors.

KIEL-UP • DOI: 10.38072/2748-3150/v1

A particular ICME event in August 2018 observed with the ground based muon detectors and neutron monitors

Wataru Kihara[1], Kazuoki Munakata[1], Chihiro Kato[1], Ryuho Kataoka[2], Akira Kadokura[2], Shoko Miyake[3], Jozsef Kota[4], Paul Evenson[5]

Correspondence

[1] Department of Physics, Faculty of Science, Shinshu University, Nagano, Japan
[2] National Institute of Polar Research, Tokyo, Japan
[3] Department of Electrical and Electronic Systems Engineering, National Institute of Technology, Ibaraki College, Hitachinaka, Japan
[4] Lunar and Planetary Laboratory, University of Arizona, Tucson, USA
[5] Bartol Research Institute, Department of Physics and Astronomy, University of Delaware, USA

We demonstrate that global observations of high-energy cosmic rays contribute to understanding the unique characteristic of a large-scale magnetic flux rope causing a magnetic storm in August 2018. Following a weak interplanetary shock on 25 August 2018, a magnetic flux rope caused an unexpectedly large geomagnetic storm (real-time Dst index minimum = -174 nT on 26 August 2018). It is likely that this event became geoeffective because the flux rope was accompanied by the corotating interaction region and compressed by high-speed solar wind following the flux rope. In fact, a Forbush decrease was observed in cosmic-ray data inside the flux rope as expected, and a significant cosmic-ray density increase exceeding the unmodulated level before the shock was also observed near the trailing edge of the flux rope. The cosmic-ray density increase can be interpreted in terms of the adiabatic heating of cosmic rays inside the trailing edge of the flux rope, as the observed corotating interaction region is expected to prevent a free expansion of the flux rope and results in the compression near the trailing edge. The northwest-directing spatial gradient of the cosmic-ray density was also observed during the cosmic-ray density increase, suggesting that the center of the heating near the trailing edge is located northwest of Earth. This is one of the best examples demonstrating that the observation of high-energy cosmic rays provides us with unique information to observationally constrain the three-dimensional macroscopic picture of the interaction between CMEs and the ambient solar wind, which is essentially useful to predict large magnetic storms.

Interplanetary coronal mass ejection associated forbush decreases in neutron monitors

Christopher Light, Veronica Bindi, Cristina Consolandi, Claudio Corti, Christopher Freeman, Andrew Kuhlman, Matteo Palermo, Siqi Wang

Correspondence

University of Hawaii at Manoa, Honolulu, USA

Interplanetary coronal mass ejections (ICMEs) are eruptions of plasma that propagate outward through the heliosphere. ICMEs, and the shocks they drive, cause a sudden decrease in the cosmic ray flux in their local area of the heliosphere, called a Forbush Decrease (FD). A method of defining FDs is established, and an automated process for identifying FDs in neutron monitor data is created. The correlation between ICME properties and Forbush decrease magnitude in 12 different neutron monitors is examined for 91 ICME associated FD events occurring from 2001 through August 2019. A number of ICME properties show positive correlation with FD magnitude, with decreasing correlation strength as neutron monitor cutoff rigidity increases.

KIEL-UP • DOI: 10.38072/2748-3150/v1

Analysis of the rigidity spectra of variations of cosmic rays during Forbush effect on October 8, 2012

Anna A. Lukovnikova

Correspondence
Institute of Solar-Terrestrial Physics, Siberian Branch of Russian Academy of Sciences (ISTP SB RAS), Irkutsk, Russia

On October 8, 2012 Forbush effect is studied using ground observations of cosmic rays (CR) on the worldwide network of neutron monitors by the spectrographic global survey. The rigid spectrums of variations of primary CR in Earth's orbit were presented. It is shown indices of CR variation spectra in certain periods of the investigated event.

Interplanetary coronal mass ejections as the driver of non-recurrent Forbush decreases

Athanasios Papaioannou [1], Anatoly Belov [2], Maria Abunina [2], Eugenia A. Eroshenko [†2], Artem Abunin [2], Anastasios Anastasiadis, Spiros Patsourakos, Helen Mavromichalaki [3]

Correspondence
[1] IAASARS, National Observatory of Athens, Penteli, Greece
[2] Pushkov Institute of Terrestrial Magnetism, Ionosphere and Radio Wave Propagation (IZMIRAN), Moscow, Russia
[3] Nuclear and Particle Physics Department, Faculty of Physics, National and Kapodistrian University of Athens, Greece

Interplanetary coronal mass ejections (ICMEs) are the counterparts of coronal mass ejections (CMEs) that extend in the interplanetary (IP) space and interact with the underlying solar wind (SW). ICMEs and their corresponding shocks can sweep out galactic cosmic rays (GCRs) and thus modulate their intensity, resulting in non-recurrent Forbush decreases (FDs). In this work, we selected all FDs that were associated with a sudden storm commencement (SSC) at Earth, and a solar driver (e.g., CME) was clearly identified as the ICME's source. We introduce and employ the tH parameter, which is the time delay (in hours) of the maximum strength of the interplanetary magnetic field from the FD onset (as is marked via the SSC), and consequently derive three groups of FD events (i.e., the early, medium, and late ones). For each of these we examine the mean characteristics of the FDs and the associated IP variations per group, as well as the resulting correlations. In addition, we demonstrate the outputs of a superposed epoch analysis, which led to an average time profile of the resulting FDs and the corresponding IP variations, per group. Finally, we interpret our results based on the theoretical expectations for the FD phenomenon. We find that both the shock sheath and the ejecta are necessary for deep GCR depressions and that the FD amplitude (A0) is larger for faster-propagating ICMEs. Additionally, we note the importance of the turbulent shock-sheath region across all groups. Finally, we present empirical relations connecting A0 to SW properties.

† deceased

KIEL-UP • DOI: 10.38072/2748-3150/v1

Seasonal variation of cosmic ray intensity observed by ground neutron monitor

Suyeon Oh[1], **Jaesik Jeong**[2], **Jaeyoung Choi**[1], **Yunsu Kang**[1]

Correspondence

[1] Department of Earth Science Education, Chonnam National University, Gwangju, Korea
[2] Department of Statistics, Chonnam National University, Gwangju, Korea

Neutrons and muons as the representative secondary particles are generated by interaction between primary cosmic ray particles and air molecules. They experience the seasonal variation due to the meteorological effect by temperature effect in the previous studies. The intensity of neutrons has the typical modulation with the various periods and reasons such as diurnal and solar variation or transient events. This study shows the preliminary results to examine the specific position where the most cosmic ray particles enter in the orbit of revolution using the daily data at Oulu neutron monitor. We present the statistical method to eliminate the effect by solar activity across time and to normalize the daily data by different transformations. Then we report the preliminary results.

Using Cosmic Rays detected by HST as Geophysical Markers

Gonzalo Tancredi[1], **Nathan Miles**[2], **Susana E. Deustua**[2], **Germán Schnyder**[1], **Sergio Nesmachnow**[1], **Geoffrey Cromwell**[3]

Correspondence

[1] Universidad de la República, Montevideo, Uruguay
[2] Space Telescope Science Institute, Baltimore, USA
[3] Scripps Institution of Oceanography, University of California & USGS, San Diego, USA

The Hubble Space Telescope (HST) has been operational for almost 30 years and throughout that time it has been bombarded by high energy charged particles, colloquially referred to as cosmic rays (CRs). HST orbits the Earth at an altitude of ~550km over the surface, with an equatorial inclination of 28.5 deg. We have analyzed images taken by HST from 1995 until present to extract over 1.2 billion CRs. In particular, our analysis is concentrated on 75,908 dark calibration files taken as part of routine calibration programs for five different CCD imagers with operational coverage of Solar Cycle 23 and 24. Most of the dark frames were taken at positions outside the South Atlantic Anomaly. After filtering the data, we observe the expected modulation of galactic cosmic rays by solar activity. Several sporadic events are detected, when the CR flux was over 10 times higher than the mean. We analyze STIS/CCD observations taken as HST crosses over the South Atlantic Anomaly and find a peak cosmic ray flux of ~1100 CR/s/cm2. We find strong evidence for two spatially confined regions over North America and Australia that exhibit increased cosmic ray fluxes at the 5-sigma level. Finally, we correlate the measured CR flux with the data from the NMDB.

Session 2:

GLE analysis

Cosmic ray studies with neutron detectors | Volume 1 (2021)
KIEL-UP • 10.38072/2748-3150/p11

SEP spectra derived from neutron monitor data and from EPHIN space detector data during recent GLEs and sub-GLEs

Rolf Bütikofer [1], **Patrick Kühl** [2], **Athanasios Papaioannou** [3]

Correspondence
[1] Physikalisches Institut, University of Bern, Switzerland, rolf.buetikofer@space.unibe.ch
[2] Extraterrestrial Physics, Institute of Experimental and Applied Physics, Kiel University, Germany
[3] IAASARS, National Observatory of Athens, Penteli, Greece

Keywords
Ground Level Enhancements (GLEs); Solar Energetic Particles (SEPs); neutron monitors; Solar and Heliospheric Observatory (SOHO); Electron Proton Helium Instrument (EPHIN)

Abstract
The Electron Proton Helium Instrument (EPHIN) aboard the Solar Heliospheric Observatory (SOHO) observed several SEP events with protons accelerated to energies E>500 MeV, whereas no neutron monitor (NM) of the worldwide network showed a significant increase in their counting rate. For instance, the SEP event on 8 November 2000 with maximum proton intensity at 500 MeV of >0.1 $(cm^2\ s\ sr\ MeV)^{-1}$ is outstanding, as this maximum proton flux is comparable with the GLEs on 14 July 2000 and on 15 April 2001 (max. count rate increase in 5-min data of 225% at South Pole NM). In a first step we applied a forward modelling approach of the SEP event on 8 November 2000, i.e. we computed the expected NM count rate increases for selected NM stations, utilizing as input parameters the SEP spectra determined from EPHIN data as well as anticipated pitch angle distribution and apparent source direction. The simulated count rate increases for selected NM stations showed that this SEP event should have be seen as a clear GLE. To further understand this situation, we investigated in a next step recent GLEs and sub-GLEs. Consequently, a total of four SEP events were selected, two clearly identified GLEs and two sub-GLEs. We performed a "GLE analysis" based on the data of the worldwide network of NMs for each of the four SEP events and then compared the derived SEP spectra with the proton spectra as determined from EPHIN measurements.

1. Introduction

When solar energetic particles (SEPs), which originate either from a solar flare or are accelerated by shock waves associated with coronal mass ejections (CMEs), are detected at Earth by ground based cosmic ray detectors (neutron monitors (NMs)) then such an event is called GLE, for Ground Level Enhancement or Ground Level Event. Since the first observation of a GLE in 1942 a total of 72 GLEs have been observed, i.e. about one GLE per year. The occurrence rate of SEP events is much higher. More than 20 SEP events may be observed per year during years with high solar activity. Recently, Kühl et al. (2017) investigated 42 SEP events between 1995 and 2015 with protons accelerated to energies E > 500 MeV based on measurements of the EPHIN instrument onboard SOHO. NMs at sea level and at high latitude with magnetic cutoff rigidity, Rc, ≤ 1 GV, are sensitive to primary cosmic ray protons with energies E > 500 MeV. The atmospheric cutoff energy of the

polar, high altitude NM stations SOPO (2820 m asl) and DOMC (3233 m asl) is ∼300 MeV. Therefore, many of the 42 SEP events, investigated by Kühl et al. (2017), should have been observed also by the NM network, mainly if the SEP spectrum is not too soft at energies E > 500 MeV, i.e. at energies where NMs become sensitive. On 8 November 2000 an outstanding large SEP event occurred which was observed by EPHIN (Kühl et al. 2017) and by detectors on GOES at energies E > 700 MeV (Thakur et al. 2016), but by none of the NMs of the worldwide network. The maximum intensity during this SEP event at 500 MeV was larger than 0.1 $(cm^2\ s\ sr\ MeV)^{-1}$ which is comparable with the GLEs on 14 July 2000 (max. NM increase in 5-min data of almost 60% at South Pole NM) and on 15 April 2001 (max. NM increase in 5-min data of 225% at the South Pole NM).

In a first step we applied a forward modelling of the SEP event on 8 November 2000, i.e. we computed the expected count rate increases for selected high latitude NM stations. As input parameters we used the SEP spectrum as derived by Kühl et al. (2017) based on EPHIN measurements, as well as, an anticipated pitch angle distribution and an apparent source direction which corresponds to the direction of the interplanetary magnetic field during this SEP event. Our analysis showed that the simulated NM count rates led to a clear increase during the SEP event of 8 November 2000, mainly at high latitudes (> 100%). However, the actual NM measurements did not demonstrate such a behaviour. As a result, we further analysed in a next step two recent GLEs (GLE71 & GLE72) and two sub-GLEs (events on 2013-03-07 & 2014-01-06) (Poluianov et al. 2017) based on NM data, comparing the obtained SEP spectra from this analysis with the spectra derived from EPHIN data by Kühl et al. (2017).

2. Analysis

2.1 EPHIN detector

The Electron Proton Helium Instrument (EPHIN) on board the ESA/NASA spaceprobe SOHO is part of the COSTEP (Comprehensive Suprathermal and Energetic Particle Analyzer) experiment that studies the suprathermal and energetic particle populations of solar, interplanetary, and galactic origin. EPHIN is a telescope for the measurement of energy spectra of electrons from 250 keV to more than 8.7 MeV and of hydrogen and helium isotopes from 4 MeV/nucleon to more than 53 MeV/nucleon. Charged particles are registered in the sensor by ionisation. The EPHIN sensor consists of a semiconductor stack with five layers. They are enclosed by different detectors operating as anticoincidence system (Müller-Mellin et al. 1995). Kühl et al. (2015) showed that EPHIN is capable to measure proton energy spectra up to 1 GeV. However, the EPHIN channels at energies above ∼800 MeV may be corrupted by the contribution of electrons (Kühl et al. 2017). Therefore, SEP spectra derived from EPHIN are only reliable up until 800 MeV. For penetrating particles the EPHIN detector has an angle of aperture of about 65°. Nominal the symmetry axis of EPHIN has an angle towards the Sun of 45° along the nominal Parker spiral. Due to technical problems, SOHO is rotated since 2003 several times per year within a few hours by 180°. As a consequence, EPHIN is looking with an angle of 90° to the Parker spiral but still in the ecliptic plane for some months. The data on this roll maneuver are listed under: https://soho.nascom.nasa.gov/data/ancillary/attitude/roll/nominal_roll_attitude.dat (last accessed April 13, 2021).

The determination of the SEP spectra in the work of Kühl et al. (2017) is taking place as follows: for each SEP event a two hours time interval (due to the statistical limitations of the EPHIN data) is selected, with the start of this two hour time interval being 30 minutes after the SEP onset, so that the different travel times of lower (100 MeV) and higher (1 GeV) proton energies are considered.

2.2 GLE analysis with neutron monitor data

Neutron monitors can be used to determine the SEP characteristics (proton spectra, pitch angle distribution, direction of anisotropy) during a GLE in the energy range ∼500 MeV – 15 GeV. For this analysis, the NM count rate increases are computed by assuming an SEP spectrum, pitch angle distribution, and apparent source direction. By a trial and error procedure the SEP characteristics

are determined by changing the different parameters to minimize the difference between simulated and measured NM count rate increases (for details see, e.g., Smart, Shea, & Tanskanen 1971; Debrunner & Lockwood 1980; Bütikofer & Flückiger 2015; Mishev et al. 2018).

The definition of a GLE specifies that an observed SEP event is registered as a GLE when the count rates of at least two differently located NMs observe a significant increase, with at least one NM being located near sea level (Poluianov et al. 2017). One should note that in the GLE definition there are no restrictions given, concerning the time resolution of the investigated count rate increases. Typically the sampling interval in the GLE analysis is in the order of a few minutes up to about half an hour. This is because the duration of the interesting part of a GLE as measured with NMs lasts up to a few hours. However, in the present analysis, which is driven by the 2-hour averaged EPHIN values, it is mandatory to compare with NM data with identical time resolution, i.e. the "GLE analysis", carried out in this work utilized a 2-hour time interval. As expected, the statistical errors of a 2-hour NM count rate is by about a factor five lower as for a 5-minute value, hence, much smaller count rate increases may be statistically significant. On the other hand, an SEP is defined as sub-GLE when at least two high altitude, high latitude NM stations at different locations measure a simultaneous, significant count rate increase, with no near sea level NM station recording a significant count rate increase (Poluianov et al. 2017). It is self-explanatory that the results of a *GLE analysis* where only two NM stations observed a significant count rate increase is afflicted by large uncertainties.

2.3 Investigated SEP events

The SEP event on 8 November 2000 was associated with an M7.4 class solar flare with onset at 22:42 UT and was produced at N10W77 (Lario et al. 2003; Agueda et al. 2012). LASCO onboard SOHO identified a wide ($>170°$) and fast (1738 km/s) CME at 23:06 UT[1]. These eruptive events were further associated to a type III radio burst starting at 22:55 UT (see Cane, Erickson & Prestage 2002), as well as, an intense type II burst that was identified extending from metric to decametric radio waves, starting at $\sim$23:15-23:20 UT (Agueda et al. 2012). As a result, the SEP event on 8 Novenber 2000 was driven by a set of complicated and strong eruptive events. A clear increase of this SEP can be identified up until >700 MeV in GOES/HEPAD; however, this SEP event was not seen by any of the NMs of the worldwide network.

To check possible differences between the SEP spectra as derived by EPHIN and by NM measurements, we further investigated four recent SEP events that were observed by the NM network as GLEs or as sub-GLEs. In particular, in chronological order we investigated: sub-GLE on 7 March 2012, GLE71 on 17 May 2012, sub-GLE on 6 January 2014, and GLE72 on 10 September 2017.

According to the official sub-GLE definition (Poluianov et al. 2017), the SEP event on 7 March 2012 is not a sub-GLE as this event was significantly seen in the 5-minute count rates only by the high altitude NM station South Pole with maximal relative count rate increase of $\sim$3% in the 5-minute data (Mishev et al. 2017). However, one should note that the Dome C NMs started operating only in February 2015. As a result, it can be assumed that Dome C would have seen this SEP event as well. Therefore this SEP event is listed as a sub-GLE in the official GLE database, hosted and managed by the Oulu Cosmic Ray Station of the University of Oulu, Finland (Official GLE database 2014 | https://gle.oulu.fi/).

On 17 May 2012 GOES observed a moderately strong M5.1 class flare at 01:25 UT. The Earth was well connected to the active region at the Sun (N07 W88). Near 01:50 UT the worldwide network of NM detected a clear enhancement with maximum relative count rate increase in the 5-minute data of about 17% at South Pole NM station. The near sea-level, high latitude NM stations Apatity and Oulu were in excellent positions for this event with a rapid count rate increase of $\sim$15% (Papaioannou et al. 2014). Further high-latitude NM stations measured a count rate of maximal 4% in the 5-minute data (e.g. Pewanuck, Thule, Fort Smith, Terre Adelie, Kerguelen, Inuvik). This event is labeled as GLE71 and is a GLE with a quite short duration. The time to the half-maximum of the count rate increase is significantly less than one hour. The increased NM count rates remained above background during about 2 hours.

1 https://cdaw.gsfc.nasa.gov/CME_list/sepe/ (last accessed April 13, 2021).

The SEP event on 6 January 2014 occurred during a period of active Sun and during disturbed geomagnetospheric conditions. The C2.1 class flare was located behind the west limb (> W90) (whose emission was therefore most probably underestimated) was registered at 07:55 UT and a Halo and fast (1402 km/s) CME, that was marked at 08:00 UT, were the drivers of this SEP event. Typical to such active situations, a type III burst was marked at around 07:50 UT and a type II were clearly identified starting at 07:45 UT (at metric radio waves)[2]. A non-null response was observed only by the South Pole NMs (SOPO, the common NM with lead producer and the bare NM SOPB, i.e. NM without lead producer) with maximum relative count rate increase in the 5-minute values of about 3%.

Close to the end of solar cycle 24, i.e. a period with low solar activity, an interval of high solar activity occurred between 4 and 10 September 2017. A large number of bright eruptions were observed, including four associated with X-class flares. The X8.2 solar flare on 10 September 2017, peaking at 16:06 UT, situated behind the western limb (> W90), was linked to an abnormaly fast (3163 km/s) CME, giving rise to a strong SEP event measured by near-Earth spacecraft. This western limb event triggered also GLE72 with an onset at about 16:10 UT, which occurred however, during the decaying phase of a major Forbush decrease (FD) (Belov 2009) that started on 8 September 2017 and lasted for several days. The maximum relative count rate increase in the 5-minute values at the Dome C NM station was about 10%, whereas it was only about 5% at the South Pole NM. GLE72 was observed by more than 10 high latitude NM stations with count rate increases between ~2-5% in the 5-minute data.

3. Results

3.1 Backward modelling of GLEs & sub-GLEs

For the "GLE analysis" in this investigation, the data of 30-40 NM stations were available for each SEP event. The number of NM stations that observed a significant count rate increase is one NM station for the two sub-GLEs and ~15-20 NM stations for the GLEs, under investigation. However, it must be noted that also the data of NM stations with no significant count rate increase give important information for the determination of the SEP spectrum, mainly the NM stations at high geomagnetic latitudes. Figure 1 depicts the obtained rigidity spectra for the selected four SEP events as determined by Kühl et al. (2017) based on EPHIN measurements and as based on NM data of the worldwide network. The derived rigidity spectra were computed in each case for a two hours interval that starts 30 minutes after the SEP event onset. Mishev et al. (2014) investigated the sub-GLEs on 2013-03-07 and on 2014-01-06 based on NM data. Their results are shown in Figure 1 together with the spectra derived by Bütikofer within this analysis. For GLE71 the rigidity SEP spectra were investigated based on NM data by different groups (Balabin et al. 2013; Apatity/IZMIRAN, http://pgia.ru:81/cosmicray/GLE/ 2012, last accessed April 7, 2021; Kuwabara et al. 2013; Mishev et al. 2014; Plainaki et al. 2014), the results are shown in the top right graph of Figure 1 for selected time intervals (see the legend in the top right graph). The spectra derived from the NM data show the SEP intensity in the direction of the largest solar proton flux (direction of anisotropy), whereas the spectra based on EPHIN data correspond to the average fluence in the direction in which EPHIN was looking during the corresponding SEP event. Thereby, the expectation is that the SEP fluence derived from NM data should be larger than the corresponding value deduced from EPHIN measurements. However, it must also be considered that with the starting time of 30 minutes after the SEP onset and the two-hour length of the time interval, the SEP flux may already be quite isotropic and thus the expected difference in the SEP spectra derived from EPHIN and NM data could vanish. Figure 1, shows that the best agreement of the simulated NM count rate increases to the measured ones were achieved for: (a) a pure power law in rigidity for the two sub-GLEs and (b) a modified power law for the two GLEs, investigated in this work.

2 http://secchirh.obspm.fr/spip.php?page=survey&hour=day&survey_type=4&dayofyear=20140106 (last accessed April 13, 2021).

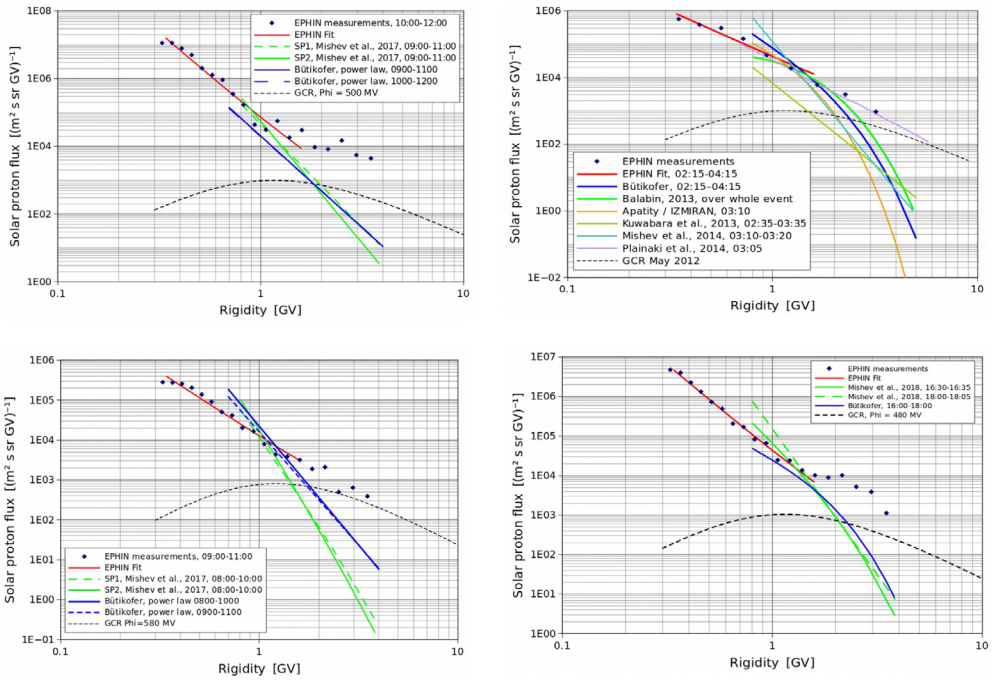

Figure 1: SEP rigidity spectra as derived from EPHIN measurements (dark blue diamonds with fits (red lines) up to 800 MeV) and determined based on NM data. **Top left:** sub-GLE on 2012-03-07, **top right:** GLE71 on 2012-05-07, **bottom left:** sub-GLE on 2014-01-06, and **bottom right:** GLE72 on 2017-09-10. For details see the text.

3.2 Significant count rate increases in hourly NM data

The plotting of hourly count rates of the NM data available during the two sub-GLEs and the two GLEs instead of higher time resolutions made apparent that more NM stations measured a significant count rate increase. Figure 2 shows as an example the relative hourly count rates of the high latitude NM stations Kerguelen, South Pole, Inuvik, and Fort Smith for 6/7 March 2012. The geomagnetic cutoff rigidity at all these four NM stations is below the respective atmospheric cutoff rigidity. The red vertical dashed line at 2012-03-07 09:00:00 gives the onset time of the SEP event in the hourly values. From figure 2 one may assume that the sub-GLE on 7 March 2012 has to be upgraded to a GLE, i.e. the data of NM stations fulfil the GLE criterion. However, Figure 2 should be treated with caution, since it is unclear if the cause of the increased count rates are indeed SEPs, as in some NM stations this raised measured cosmic ray intensity lasted for several hours. This is atypical for SEP events at the energies where NMs are sensitive. In addition, clear count rate increases were observed also at some mid-latitude NM stations as e.g. the two Moscow NM stations MCRL and MOSC with a maximum increase of about 2% in the hourly data. In fact many of the NM stations of the worldwide network showed a tendency of increasing count rate starting around beginning of 7 March 2012 which may be the pre-increase of galactic cosmic rays as it is often observed in advance of FDs (Leerungnavarat, Ruffolo, & Bieber 2003). That said, late on 7 March 2012, i.e. about one day after the SEP occurrence, a considerable FD of maximum NM count rate decline by more than 10% started.

4. Conclusions

The comparison of the derived SEP rigidity spectra as determined by Kühl et al. (2017) based on EPHIN data and as computed based on NM data by different groups does not show large discrepancies in all four SEP events investigated in the present analysis. These results show that EPHIN and

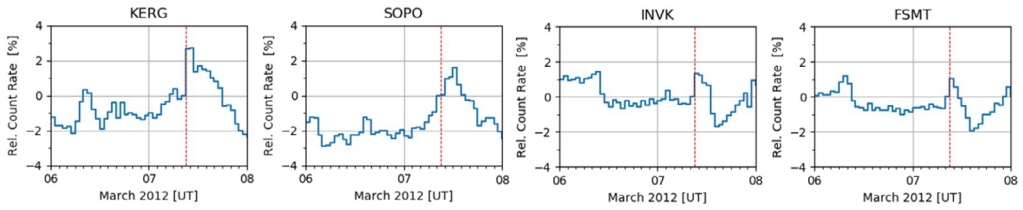

Figure 2: Relative hourly count rates of the NM stations Kerguelen (KERG), South Pole (SOPO), Inuvik (INVK), and Fort Smith (FSMT), for 6-7 March 2012. The red vertical dashed line at 2012-03-07 09:00:00 indicates the onset time in the hourly values at most NM stations.

NM data as well as the data analysis seem to result in reliable outcomes. However, this does not answer why the large SEP on 8 November 2000 was seen by EPHIN but not by the worldwide NM network. It must be investigated, if the SEP flux during that event was very anisotropic over a long time duration and if the direction of the anisotropy was not covered by the asymptotic directions of the high latitude NM stations in operation during this SEP event. Another explanation may be the greater height above the Sun of the CME formation which reduced the efficiency of the particle acceleration and therefore resulted in a steeper spectrum above 700 MeV (Thakur et al. 2016). As a consequence, the polar NMs would in this case not detect enough SEPs to observe a significant count rate increase. So far the GLE definition (Poluianov et al. 2017) does not give a criterion on the time resolution of the NM data. Based on this study, the question arises whether the GLE definition should be adapted in this regard.

Acknowledgments

The NM data were taken from the Neutron Monitor Database (NMDB, https://www.nmdb.eu). We acknowledge NMDB and in particular the PIs and teams of the NM stations from which measurement data were used for this analysis. Furthermore, we acknowledge the usage of the Official GLE database (https://gle.oulu.fi/) developed and maintained by the Oulu Cosmic Ray group at the University of Oulu. SOHO is a project of international cooperation between ESA and NASA. This work benefited by discussions during the HEROIC team meeting at the International Space Science Institute at Bern in Switzerland (Team 441; https://www.issibern.ch/teams/heroic/).

References

Agueda, N., Lario, D., Ontiveros, V., Kilpua, E., Sanahuja, B., Vainio, R., 2012, Solar Physics 281, DOI: https://dx.doi.org/10.1007/s11207-012-9959-y

Balabin, Y. V., Vashenyuk, E. V., Germanenko, A. V., and Gvozdevsky, B. B., 2013, 33rd International Cosmic Ray Conference, held 2-9 July 2013 in Rio de Janeiro, Brazil. Edited by Alberto Saa. ISBN: 978-1-5108-1008-2, 1467

Belov, A. V., 2009, IAU Symposium, Vol. 257, Universal Heliophysical Processes, ed. N. Gopalswamy & D. F. Webb, 439-450, DOI : https://dx.doi.org/10.1017/S1743921309029676

Bütikofer R., Flückiger E., 2015, J. Phys.: Conf. Ser. 632, 012053

Cane, H.V., Erickson, W.C., Prestage, N.P., 2002, J. Geophys. Res. 107, 1315

Debrunner, H., and Lockwood, J.A., 1980, J. Geophys. Res., 85 (A11), 6853-6860, DOI: https://dx.doi.org/10.1029/JA085iA12p06853

Kühl, P., Banjac, S., Dresing, N., Goméz-Herrero, R., Heber, B., Klassen, A., Terasa, C., 2015, Astron. Astrophys, 576, A120, DOI: https://dx.doi.org/10.1051/0004-6361/201424874

Kühl, P., Dresing, N., Heber, B., and Klassen, A., 2017, Solar Physics, 292:10, DOI: https://dx.doi.org/10.1007/s11207-016-1033-8

Kuwabara, T., Bieber, J., Clem, J., Evenson, P., Gaisser, T., Pyle, R., and Tilav, S., 2013, 33rd International Cosmic Ray Conference, held 2-9 July 2013 in Rio de Janeiro, Brazil. Edited by Alberto Saa. ISBN: 978-1-5108-1008-2

Lario, D., Roelof, E.C., Decker, R.B., Reisenfeld, D.B., 2003, Adv. Space Res. 32, 579

Leerungnavarat, K., Ruffolo, D., Bieber, J.W., 2003, Astrophysical Journal 593, 1, 587–596, DOI: https://dx.doi.org/10.1086/376408

Mishev, A. L., Kocharov, L. G., and Usoskin, I. G., 2014, Journal of Geophysical Research (Space Physics) 119, 670–679, DOI: https://dx.doi.org/10.1002/2013JA019253

Mishev, A., Poluianov, S., and Usoskin, I., 2017, Journal of Space Weather and Space Climate, 7(27), A28, DOI: https://dx.doi.org/10.1051/swsc/2017026

Mishev, A., Usoskin, I., Raukunen, O., Paassilta, M., Valtonen, E. , Kocharov, L., Vainio, R., 2018, Solar Phys. 293, 136, DOI: https://dx.doi.org/10.1007/s11207-018-1354-x

Müller-Mellin, R., Kunow, H., Fleißner, V., Pehlke, E., Rode, E., Röschmann, N., Scharmberg, C., Sierks, et al., 1995, Solar Phys. 162, 483.

Papaioannou, A., Souvatzoglou, G., Paschalis, P., Gerontidou, M., Mavromichalaki, H., 2014, Solar Physics, 289, DOI: https://dx.doi.org/10.1007/s11207-013-0336-2

Plainaki, C., Mavromichalaki, H., Laurenza, M., Gerontidou, M., Kanellakopoulos, A., and Storini, M., 2014, Astrophysical Journal, 785, 160, DOI: https://dx.doi.org/10.1088/0004-637X/785/2/160

Poluianov, S.V., Usoskin, I.G., Mishev, A.L., Shea, M.A., Smart, D.F., 2017, Solar Physics, 292, 176, DOI: https://dx.doi.org/10.1007/s11207-017-1202-4

Smart, D.F., Shea, M.A., Tanskanen, P.J., 1971, Proceedings of the 12th International Conference on Cosmic Rays, held in Tasmania, Australia, 16-25 August, 1971. Volume 2., 483

Thakur, N., Gopalswamy, N., Mäkelä, P., Akiyama, S., Yashiro, S., Xie, H., 2016, Solar Physics, Volume 291, Issue 2, 513-530, DOI: https://dx.doi.org/10.1007/s11207-015-0830-9

Official GLE database, 2014, http://gle.oulu.fi/#/ (last accessed April 7, 2021)

Questions and answers

Ilya Usoskin: In one of the last plots, EPHIN data above 1 GV shows a strange bump (GLE 72)

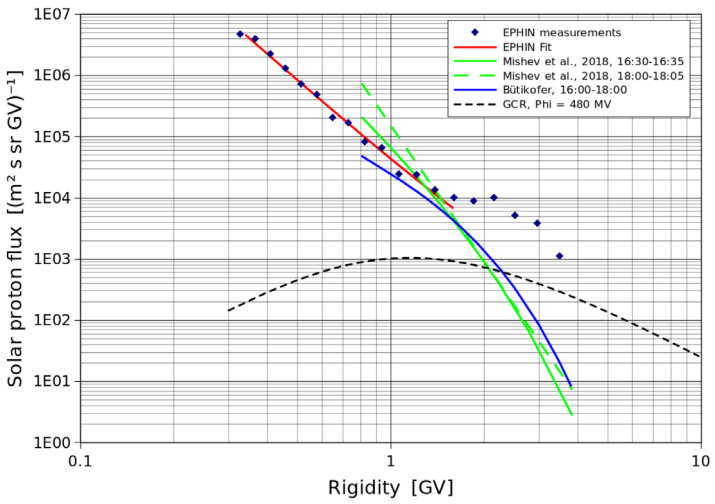

Answer: Kühl et al. (2017) pointed out that the electron contribution to the proton spectrum is negligible below about 500 MeV and is less than 20 % in the energy range between 500 and 800 MeV, but the proton energy bins above 800 MeV can be corrupted by electrons. Therefore, proton intensities >500 MeV should not be considered during SEP events.

Alexander Mishev: Just a comment. This maverick GLE on 8 November 2000 can be very anisotropic.
Answer: The SEP on 08.11.2000 was not observed by any NM station and therefore it is neither a GLE nor a sub-GLE.

James Ryan: What was the connection for the 8 November 2000?
Answer: The source is W77, thus it was a well-connected event.

Alexander Mishev: Did you try all apparent source position posibilities for the maverick event?
Answer: No, not yet. We plan to make a more comprehensive analysis of the SEP event on 8 November 2000 as well as of the other SEP events investigated in this study.

Cosmic ray studies with neutron detectors | Volume 1 (2021)
KIEL-UP • DOI: 10.38072/2748-3150/v1

Session 2: Abstracts

Application of the updated NM yield function and GLE database for an improved GLE analysis

Alexander Mishev, Ilya Usoskin, Sergey Koldobskiy, Gennady A. Kovaltsov, Leon Kocharov

Correspondence
University of Oulu, Finland

Systematic studies of solar energetic particles (SEPs) provide an important basis to understand their acceleration and propagation in the interplanetary space. During solar eruptive processes, solar ions can be accelerated to high energy. In majority of cases, the maximum energy of accelerated solar ions is several tens of MeV/nucleon, but in some cases, it exceeds 100 MeV/nucleon or even reaches a GeV/nucleon range. In this case, the energy is high enough, so that solar ions can generate an atmospheric cascade in the Earth's atmosphere, where secondary particles reach the ground, being eventually registered by ground-based detectors, specifically neutron monitors (NMs). Such events form a special class of SEP events known as ground-level enhancements (GLEs). Several methods for the analysis of GLEs, using neutron monitor data have been developed over the years. Here, we discuss a method for derivation of the spectral and angular characteristics of the GLEs using data from the world-wide NM network, namely by modeling the global NM network response with the new verified yield function computed for different atmospheric depths using records from the updated GLE database. The method is based on consecutive steps, including detailed computation of asymptotic cones and rigidity cut-off of each station used in the analysis and optimization of the global NM network response over experimental and modeled count rate increases. The method is compared with other methods, including in-situ measurements. A very good agreement between our method and space-borne measurements by the PAMELA space mission, specifically the derived fluence of solar protons during GLE 71 was achieved, providing a verification of the method is performed. Several issues of GLE analysis and possible applications are discussed.

Reconstruction of SEP fluences during GLE events: description of the new method and its application to the data

Sergey Koldobskiy[1,2], Ilya Usoskin[2,3], Gennady A. Kovaltsov[4], Alexander Mishev[2], Agnieszka Gil[5]

Correspondence
[1] National Research Nuclear University MEPhI, Moscow, Russia
[2] Space Physics and Astronomy Research Unit, University of Oulu, Finland
[3] Sodankyla Geophysical Observatory, University of Oulu, Finland
[4] Ioffe Physical-Technical Institute, St. Petersburg, Russia
[5] Space Research Center, Polish Academy of Sciences, Warsaw, Poland
[6] Institute of Mathematics, Siedlce University, Siedlce, Poland

KIEL-UP • DOI: 10.38072/2748-3150/v1

During solar eruptive events, such as solar flares and coronal mass ejections, charged particle can be accelerated from the vicinity of the Sun into the heliosphere. These particles are known as solar energetic particles (SEPs). When SEPs reach Earth, they can be registered using satellite experiments. At present, there is the AMS-02 experiment, which can be used for registration of high-energy SEP fluxes. But from the historical perspective, the only instruments that allow us to get information about SEP events over a long-term period, are neutron monitors. They register the products of SEP interaction with nuclei of atmospheric gases, if the rigidity of incoming SEP is above 1 GV. Such events are called ground level enhancements (GLE). Up to date, we know 72 GLE events (http://gle.oulu.fi). One way of GLE data representation is the reconstruction of the integral SEP fluence, which can be used in several applications, such as the study of radiation hazards, ionization of the atmosphere, etc. Here we present a new reconstruction of GLE fluences, which is based on NM yield function, updated and cross-calibrated with PAMELA and AMS-02 experiments, and a new method of non-parametric analysis of GLE data.

Relativistic solar particle events, pion decay gamma rays, and magnetic connectivity

Karl-Ludwig Klein

Correspondence
Observatoire de Paris, LESIA, Université PSL, CNRS, Sorbonne Université/ Université de Paris, France

Relativistic solar particle events detected by neutron monitors come preferentially from activity in the western solar hemisphere, but may also come from eruptions in the eastern hemisphere or from behind the solar limb. This can in principle be explained by transient interplanetary magnetic field configurations that differ from the nominal Parker spiral, especially when the heliosphere has been perturbed by numerous successive CMEs (S. Masson et al. 2012 A&A). In this contribution an attempt will be reported to use the radio emission of electrons (type III bursts) as a tracer of magnetic connectivity. A type III burst is electromagnetic emission from electron beams. At low frequencies it is observed down to the electron plasma frequency at the spacecraft, together with locally generated Langmuir waves, when the electron beams intercept the spacecraft. When the beams travel far from the spacecraft, a clear gap is observed between the low-frequency limit of the electromagnetic emission and the local plasma frequency. This feature will be applied here to GLEs, in order to confirm their magnetic connection to the Earth and to discuss the significance for identifying the acceleration region.

Session 3:

Cosmic rays and the atmosphere

Cosmic ray studies with neutron detectors | Volume 1 (2021)
KIEL-UP • DOI: 10.38072/2748-3150/p12

Analyzing atmospheric electric field by the European SEVAN network of particle detectors

Ashot Chilingarian [1], Tigran Karapetyan [1], Mary Zazyan [1], Gagik Hovsepyan [1], Balabek Sargsyan [1], Nina Nikolova [2], Hristo Angelov [2], Jaroslav Chum [3], Rony Langer [4]

Correspondence

[1] Artem Alikanyan National Lab (Yerevan Physics Institute), Armenia, chili@aragats.am
[2] Institute for Nuclear Research and Nuclear Energy, Bulgarian Academy of Sciences, Sofia, Bulgaria nina.nklv@googlemail.com
[3] Institute of Atmospheric Physics of the Czech Academy of Sciences, Prague, Czech Republic, jachu@ufa.cas.cz
[4] Institute of Experimental Physics, Slovak Academy of Sciences, Košice, Slovakia, langer@ta3.sk

Keywords

atmospheric electric field; thunderstorm ground enhancement; muon stopping effect

Abstract

Particle detectors of the European SEVAN network located on mountain heights in Aragats (Armenia), Lomnický štít (Slovakia) and Musala (Bulgaria) are well suited for the detection of thunderstorm ground enhancements (TGEs, enhanced fluxes of electrons, gamma rays, neutrons). The modulation of charged particles flux by the electric field of the thundercloud results in a sizable change in the count rate of detectors, which measure fluxes of electrons, gamma rays, and high energy muons in the near-vertical and near-horizontal directions. The relation between electric field strength and changes of particle flux count rates is nonlinear and depends on many unknown parameters of atmospheric electric field and meteorological conditions. Nonetheless, employing extreme TGEs as a manifestation of the strong electric field in the thundercloud and by measuring fluxes of three species of secondary cosmic rays (electrons, gamma rays, and muons) by SEVAN detectors located at altitudes of ≈ 3 km we study the extreme strength of the atmospheric electric field. With the simulation of particle traversal through the electric field with CORSIKA code (https://www.iap.kit.edu/corsika/index.php, last accessed April 21, 2021), we derive a maximum potential difference in the thunderous atmosphere to be ≈ 500 MV.

1. Introduction

Understanding the maximum potential difference (voltage) inside thunderstorms is one of the fundamental problems of atmospheric physics directly connected with enigma of the lightning initiation. In 1925 C.T.R. Wilson estimated the maximum potential difference in the atmosphere to be one gigavolt: “A particle may thus acquire energy corresponding to the greater part of the whole potential difference between the poles of the thundercloud, which may be of the order of 10^9 V” (Wilson 1925). In the speech to Franklin Institute in 1929 (Wilson 1929) he presents detailed calculations: “The value found for the maximum potential difference in the cloud depends on the vertical thickness, i.e. the distance through which the maximum field extends. We can hardly be wrong as to the order of magnitude if we take this height as one kilometer. If a field of 10,000 volts per centimeter extends through one kilometer the whole potential difference is 10^9 volts, i.e. one million kilovolts“. Based on such a huge potential difference Wilson estimates the maximum energy that electron can gain

KIEL-UP • DOI: 10.38072/2748-3150/p12

in the electric field to be 1 GeV: "The general effect of an accelerating field is that a beta-particle, instead of dying as it were a natural death by gradual loss of energy, is continually acquiring more and more energy and increasing its chance of surviving all accidents other than direct encounters with the nuclei of atoms" (Wilson 1925). Of course, in 1925 the particle cascade theory was not yet developed, and the measurements of the electric field in thunderclouds were not done, and C.T.R. Wilson overestimated the scale of electron acceleration. He thought that electrons could gain unlimited energy from the electric field, however, that is not possible, due to abundant radiation losses of electrons with energies greater than 50 MeV. The runaway electron (Gurevich et al. 1992) differential energy spectrum first measured in 2009 faded around 50-60 MeV (Chilingarian et al. 2010). The Intracloud electric field measured with the balloon experiments does not exceed 3,000 volts per centimeter. Thus, a potential difference as large as 1000 MV seems to be not feasible according to direct measurements: "Inside thunderstorm clouds the voltages ranged between -102 and + 94 MV (Stolzenburg & Marshall 2001). However, the estimate of maximum voltage based on the balloon soundings can be biased, because, first of all, balloon flights are rare, and second the balloon path within the thundercloud is a random walk depending on the updraft and wind speeds and hardly corresponds to the maximum possible voltage.

From the empirical relation between the first return stroke peak current and charge brought to ground, an empirical equation connecting the stroke current and voltage was derived (eq. 3 of Cooray & Rakov 2012). If we assume the extremal stroke current to be 200 kA, the maximum voltage will be approximately 200 MV. Another possibility to estimate maximum voltage is connected with the estimation of the mean electric field and its spatial extent in the cloud (like Wilson estimate). It was found that the electric field strength measured just before a lightning flash in the balloon flights, can exceed the runaway breakdown threshold by factors of 1.1 – 3.3 (Stolzenburg et al. 2007, figures 3 and 4). The height of the main negative layer above Aragats according to the satellite and radar measurements, also confirmed by the simulations of relativistic runaway electron avalanches (RREA), can reach 2 - 3 km. The height of the lower positive charged region for the largest thunderstorm ground enhancement (Chilingarian et al. 2011, 2017) events is 25-100 m. Consequently, assuming maximum strength of the electric field 2.4 kV/cm (32% above RREA threshold) and field extension 2 we obtain the maximum potential difference 480 MV by multiplying the assumed 2.4 kV/cm electric field strength to 2 km. Of course, this estimate is an upper limit of maximum voltage: we hardly can expect a 2.4 kV/cm field for the whole 2 km length. Therefore, we come to large uncertainty in the estimation of maximum voltage in the thundercloud from 100 to 480 MV. Direct monitoring of the intracloud electric field with any of spaceborne or ground-based technologies is not feasible yet, hence, we suggest to use the monitoring of particle fluxes modulated by the electric field to estimate the attainable value of the potential drop. Measurements of the modulation of cosmic ray flux traversing the electrified cloud provide a new type of evidence on cloud electrification and, possibly, allows to obtain more tight limits on the maximum potential difference in thunderclouds. The big advantage of the "particle" approach is multiyear 7/24 monitoring of different species of cosmic rays available from the measurements of high-mountain research stations. In contrast, balloon flights cannot provide continuous observations of a thunderous atmosphere and can miss extremely large voltages. TGEs observed on mountain peaks during strong thunderstorms comprise millions of particles (electrons, gamma rays, and neutrons), enhancing the intensity of ambient flux of cosmic rays up to a hundred times (Chilingarian et al. 2010, 2011, 2020, Chum et al. 2020). The same field that accelerates electrons downward in the direction of the earth will reduce the flux of muons, due to enhanced positive over negative muon flux. Simultaneous monitoring of these species of secondary cosmic rays gives a possibility to select from the multiyear continuous observations of cosmic rays on Aragats in Armenia, Musala in Bulgaria, and Lomnický štít in Slovakia most violent TGEs corresponding to extreme values of the electric field. Recently we published the analysis of the 10-year largest TGE observed on Aragats on 4 October 2010 and estimate the upper boundary of maximum potential difference to be 350 MV (Chilingarian et al. 2021). We will demonstrate in the present paper, the world largest TGEs registered in Slovakia and Bulgaria on the keen mountain tops not only confirm this result but prove that the voltage can reach 500 MV.

KIEL-UP • DOI: 10.38072/2748-3150/p12

2. Registration of TGEs with SEVAN particle detectors on Musala and Lomnický štít mountains

A network of particle detectors, known as SEVAN (Space Environment Viewing and Analysis Network (Chilingarian et al. 2018a), was developed in the framework of the International Heliophysical Year (IHY-2007) and now operates and continues to expand within the International Space Weather Initiative (ISWI). The SEVAN network is designed to measure fluxes of neutrons and gamma rays, of low energy charged particles and high-energy muons. The rich information obtained from the SEVAN network will allow estimating the solar modulation effects posed on different species of Galactic cosmic rays and fluxes of charged and neutral particles from the Solar energetic proton events (SEP). SEVAN modules located on mountain tops are actively participating in the research in the newly emerging field of high-energy physics in the atmosphere. Thus, with the same detector, we can investigate both the solar-terrestrial relations and atmospheric high-energy physics. Cheap and reliable SEVAN detectors can be installed at different locations to participate in the global network of monitoring Solar-terrestrial relations and atmospheric electricity. Observational data from SEVAN particle detectors located on mountain tops Musala (Altitude: 2925 m, Latitude/Longitude: 42°11'N, 23°35'E) in Bulgaria, and Lomnický štít (Altitude: 2634 m, Latitude/Longitude: 49°12'N, 20°12'E) in Slovakia reveal extreme TGE events. They comprise enormous enhancement of the electron and gamma ray fluxes and simultaneous decrease of muon flux. In figure 1 we show the chart of the SEVAN detector. The detector is assembled from standard slabs of plastic scintillators of 50 x 50 x 5 cm^3 size. Thick 50 x 50 x 20 cm^3 scintillator assembly (5 slabs) and two 100 x 100 x 5 cm^3 lead filters are located between 2 identical assemblies of 100 x 100 x 5 cm^3 scintillators (4 slabs). The data stream from the SEVAN comprises 1-minute count rates (or 1-sec count rates) from 3 scintillator layers. All combinations of signals from detector layers are stored as well: "100" combination means that the signal was only in the upper layer (low energy particles); "111" – that signal comes from all 3 layers (high-energy muons), "011" – near-horizontal muons). The "010" combination selects mostly neutral particles – gamma rays and neutrons.

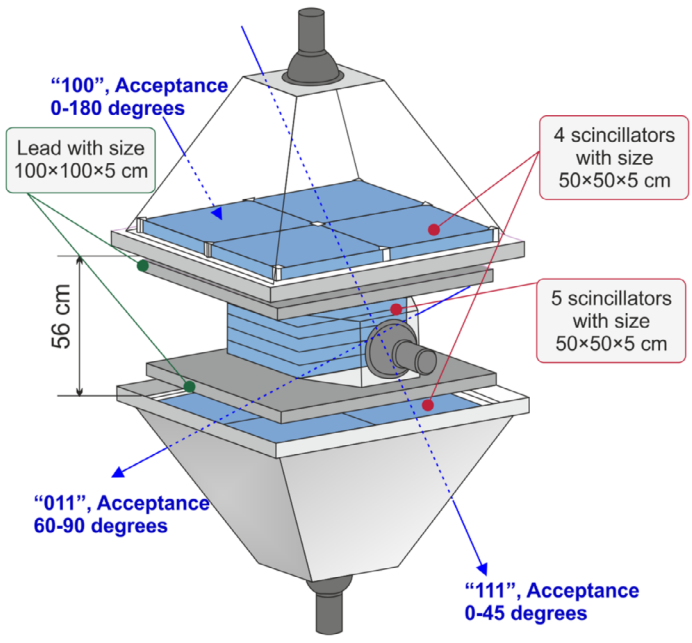

Figure 1: The module of the European "Space Environmental Viewing and Analysis Network" (SEVAN), first published in: Phys. Rev. D 103, 043021, DOI: https://doi.org/10.1103/PhysRevD.103.043021.

KIEL-UP • DOI: 10.38072/2748-3150/p12

The purity of particle selection by SEVAN coincidences was estimated by simulations, (see figure 4 in Chilingarian et al. 2018). The purity of muon selection is rather high ∼95%, due to a 10 cm thick lead filter between first and third scintillators. The energy threshold of the upper detector is ∼ 7 MeV. The minimum energy of muons ("111" combination) is ∼250 MeV. The measurement of changing fluxes of different species of the ambient population of cosmic rays, all of which are modulated by the solar activity and by the atmospheric electric field provides the possibility to investigate correlations between different species of cosmic rays and the electrified atmosphere. The atmospheric electric field, which is especially large during violent thunderstorms accelerates and decelerates charged particles dependent on the field direction and particle charge. The extreme TGEs occurred when the electric field accelerates electrons in the direction to the earth's surface; thus, the counts of "100" combination of SEVAN get enormous bust, enhancing the fair-weather count rate 250 times! Simultaneously, the same field that accelerates electrons downwards causes muon flux depletion ("111" combination) due to an abundance of positively charged muons upon negative ones (see for discussion and references Chilingarian et al. 2021). Another evidence of the large electric field in the thundercloud is the large depletion of the inclined trajectories, "011" combination comprises inclined high energy muons. The TGE particle, due to the vertical orientation of the atmospheric electric field arrives in the near-vertical direction; from the near-horizontal direction can arrive only high-energy muons, that can traverse large distances in the atmosphere without absorption. Described above modulation effects registered by SEVAN detectors in Slovakia and Bulgaria are shown in figures 2 and 3.

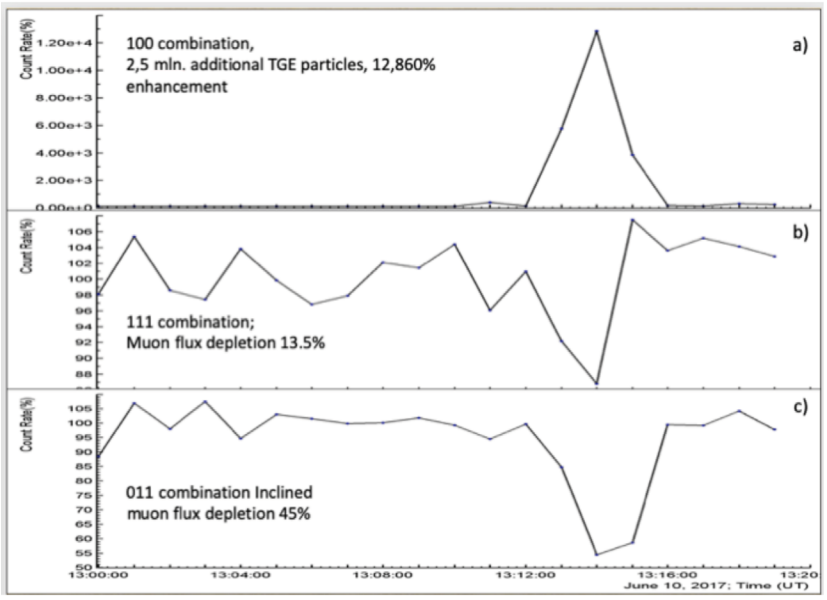

Figure 2: Extreme TGE event detected by SEVAN detector located on Lomnický štít mountain: a) – TGE particles – electrons and gamma rays; b) high energy muons; c) inclined muons, first published in: Phys. Rev. D 103, 043021, DOI: https://doi.org/10.1103/PhysRevD.103.043021.

The extreme event was recorded in Slovakia on 10 June 2017 at 13:12 UT (Chum et al. 2019): the enhancement of the count rate of "100" combination at the minute 13:12-13:13 UT was enormous and reached 12,860% (12 thousand 860 percent, figure 2a) of the fair-weather value. TGE was terminated by multi-stroke discharge at 13:14:35 UT. This world ever-largest TGE was reached only in one minute, the electric field was enormously large, unleashing a huge electromagnetic avalan-

KIEL-UP • DOI: 10.38072/2748-3150/p12

che; sure, such an enormous potential drop initiates a lightning flash that stops TGE. In the balloon flights adversely impacted by lightning, the electric field before the flash exceeded the runaway breakdown field by factors of 1.1 to 3.3 (Stolzenburg et al. 2007).

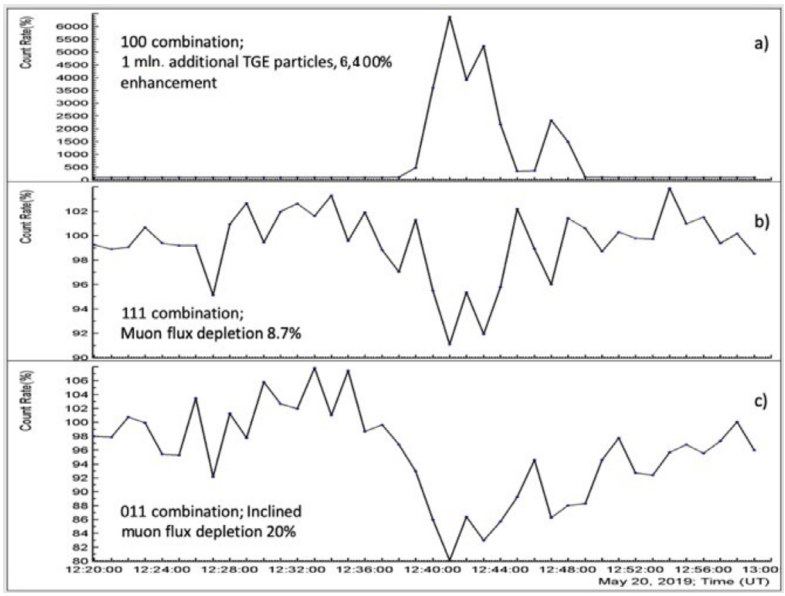

Figure 3: Extreme TGE event detected by SEVAN detector located on Musala mountain: a) – TGE particles – electrons and gamma rays; b) high energy muons; c) inclined muons, first published in: Phys. Rev. D 103, 043021, DOI: https://doi.org/10.1103/PhysRevD.103.043021.

The maximum electric field occurred a few seconds before the flash. These very large values of the electric field support the idea that the TGE may initiate lightning flashes (Chilingarian et al. 2017b). The muon flux depletion at the same minute was 13.5%, (see figure 2b), it was twice larger than for the strongest event ever observed in Aragats on 4 October 2010 (Chilingarian et al. 2021). The depletion of inclined muons was much larger 45%, see figure 2c. For the one-minute time series, the maximum enhancement of TGE particles coincides with the minimum of the muon flux; for one-second time series, the extreme values of fluxes can be shifted from each other because fast-changing electric field on the second time-scale can influence differently fluxes of near-vertical avalanche particles and the flux of cosmic ray muons coming within much broader angular acceptance.

Importantly, the count enhancement of about 50 times was observed for combination «010», which indicates neutrons and high energetic gamma-rays (Chilingarian et al. 2012a). A tremendous enhancement of neutron flux (130%) was measured by the neutron monitor at the same location. Neutron monitor evidence is very important as an independent observation and as a prove of intense photonuclear reactions of high energy gamma rays born in the TGE (previous highest neutron flux detected on Aragats was only 5.5% (Chilingarian et al. 2010)).

An extreme, however, a bit smaller, event was recorded in Bulgaria on 20 May 2019 (Nikolova 2019). The shape of the event was more complicated demonstrating 3 peaks in 10 minutes (due to 3 terminations of TGE by the lightning flashes at 12:42:18 UT, 12:46:13 UT, and 12:50:07 UT). The increase of the count rate of "100" combination during one minute, at 12:41-12:42 UT reaches ≈6,400% (6 thousand 400 percent, see figure 3a) of the fair-weather value. The muon flux depletion at the same minute was ≈9%, figure 3b. The depletion of inclined muons was 20%, see figure 3c. A highly enlarged count rate of the Liulin detector (Dachev et al. 2010) located in the same place confirms this extreme event.

KIEL-UP • DOI: 10.38072/2748-3150/p12

3. Estimation of the atmospheric electric field

In table 1 for convenience we show both the mean 1-minute and 1-second count rates measured just before the extremely large event at Lomnický štít and count rates measured at the minute of the maximum flux. As we can see from the table the count rates of the upper SEVAN scintillator and combination "100" (signal only in the upper scintillator) highly exceed fair-weather count rates, the enhancement is more than 100 times (N) or 10,000% (2 last columns of table 1).

Name	Mean 1/min	σ	Mean 1/sec	13:14 1/sec	13:14 1/min	%	N
Upper	25047	171	417	42233	2,534000	10,013	101
Coincidence 111 muons	1929	48	32.2	27.8	1666	87	
Coincidence 100	19550	142	326	42,100	2,526000	12,890	130
Coincidence 010 gamma	1468	39	24.5	55.5	3326	225	2.3

Table 1: Mean values of the count rates of Lomnický štít SEVAN and extreme values at maximum flux minute registered on 10 June 2017, first published in: Phys. Rev. D 103, 043021, DOI: https://doi.org/10.1103/PhysRevD.103.043021.

As usual, along with the enhancement of the electromagnetic component of the TGE, we register depletion of muon flux due to, so-called, muon stopping effect ("111" combination, Chilingarian et al. 2021). Measured high-energy gamma ray and neutron fluxes (combination 010) were also the largest ever measured by the particle detectors located on the earth's surface.

Proceeding from the maximum enhancements of particle fluxes we pose the problem of estimation of the atmospheric electric field that can enable such a huge multiplication and acceleration of the seed electrons from the ambient population of cosmic rays. We recognize, that the relation between electric field strength and disturbances of particle fluxes is nonlinear and depends on many unknown parameters of atmospheric electric field and meteorological conditions (topology of charged layers, the height of the cloud, wind speed, etc). However, extremely large particle fluxes measured by SEVAN detector allows us to make, as we think, relevant estimate by the detailed modeling of experiment with well-known GEANT4 and CORSIKA codes widely used in the high-energy physics and astrophysics communities. CORSIKA version 7.7400, which takes into account the effect of the electric field on the transport of particles was used in simulations. As it was already demonstrated by CORSIKA and GEANT4 simulations (Chilingarian et al. 2018b), the multiplication and acceleration of electrons of cosmic rays, the RREA process (Gurevich et al. 1992) is a threshold process and avalanches started when the atmospheric electric field reaches the threshold value that depends on the air density (for instance ≈1.63 kV/cm at 4600 m). The extent of the electric field also should be sufficiently large to ensure avalanche development. The simulation of the RREA was done within the vertical region of the uniform electric field with strengths exceeding the runaway breakdown threshold on 2.6-4.6 km height in the atmosphere. Uniformity of the electric field extending 2 km leads to the change of the surplus to threshold energies at different heights according to particular air density value. Thus, the 2.4 kV at 4.6 km height is ≈32% larger than critical energy, and at 2.6 km height is only ≈15% larger. Therefore, we provide a smooth decrease of the electric field (in sense of critical energy) with enlarging of the depth in the atmosphere. The largest TGEs occurred when the distance to the cloud base (a proxy of electric field lower boundary) was 25 – 100 m (see figure 17 in Chilingarian et al. 2020), thus the electromagnetic avalanche continued propagation in the dense air above the detector 25, 50 and 100 meters before registration. To avoid

KIEL-UP • DOI: 10.38072/2748-3150/p12

contamination by the MOS process (modification of electron energy spectra, see details in Chilingarian, Mailyan, & Vanyan 2012b) simulations for simplicity were performed with vertical beams of 1 MeV electrons, as seed particles for the relativistic runaway avalanche. In this way we obtain a reliable estimate of the maximum energy achieved by the RREA gamma rays; the MOS process generates additional high-energy bremsstrahlung gamma rays from high energy electrons of the ambient population of cosmic rays. The electron energy spectrum at energies corresponding to the minimum of ionization losses is rather flat, thus our approximation does not introduce large bias.

Simulation trials include 10^4 events for the electric field strengths 1.8-2.3 kV/cm and 200 for the strengths – 2.4 and 2.5 kV/cm. Electrons and gamma rays were followed in the avalanche until their energy decreased down to 0.05 MeV. The energy spectra of RREA electrons and gamma rays were obtained as a result of each simulation trial. We perform, as well, the calculation of the SEVAN detector response function with the GEANT4 package.

As a result of comparison of the simulations and experimental data we can conclude that for the measured at Lomnický štít extreme TGE the potential difference in the atmosphere should be 480 - 500 MV.

4. Conclusions

The emergence and evolution of the intracloud electric field govern both the high-energy particle flux and lightning occurrences. The atmospheric electric field modulates charged particle fluxes enormously enhancing electron and gamma ray fluxes and depleting muon flux. The muon stopping effect (Chilingarian et al. 2021), observed by the particle detectors at Aragats, Musala, Lomnický štít implicates the abrupt decline of count rate of high energy muons (at near-vertical and at inclined incidences). The muon depletion measured at Lomnický štít and Musala was much larger than on Aragats, therefore we expect a larger potential difference (voltage) during extreme TGEs measured in Slovakia and Bulgaria. Analyzing TGE measured in Slovakia we use the enormous enhancement of gamma ray and electron flux for revealing correspondent potential difference. The observed enhancements of gamma ray and electron fluxes were compared with CORSIKA simulations of the relativistic runaway electron avalanches and imply ≈500 MV potential difference present in the atmosphere during the minute of the highest flux (and consequently highest strength of the electric field) measured by the SEVAN detector at Lomnický štít on 10 June 2017.

Acknowledgments

We thank the staff of the Aragats, Musala, Lomnický štít high-altitude research stations for the operation of the SEVAN network particle detectors. We thank S.Chilingaryan for maintaining the ADEI knowledge base (K.Avakyan et al. 2016) allowing multiple comparisons and statistical analysis of data from remote detectors located in different countries. The data for this study is available on the Website of the Cosmic Ray Division (CRD) of the Yerevan Physics Institute: http://adei.crd.yerphi.am/adei.

References

Avakyan, K., Chilingaryan, S., Chilingarian, A., and Karapetyan, T., 2016, Physical analysis of multivariate measurements in the Atmospheric high-energy physics experiments within ADEI platform, Proceedings of 6-th TEPA symposium, 3-7 October 2016, Nor Amberd, "Tigran Metz", 56

Chilingarian, A., Daryan, A., Arakelyan, K., et al. 2010, Ground-based observations of thunderstorm-correlated fluxes of high-energy electrons, gamma rays, and neutrons, Phys Rev D 82, 043009

Chilingarian, A., Hovsepyan, G., and Hovhannisyan, A., 2011, Particle bursts from thunderclouds: Natural particle accelerators above our heads, Phys. Rev. D 83, 062001

KIEL-UP • DOI: 10.38072/2748-3150/p12

Chilingarian, A., Bostanjyan, N., Karapetyan, T., Vanyan, L., 2012a, Remarks on recent results on neutron production during thunderstorms, Physical Review D 86, 093017

Chilingarian, A., Mailyan, B., and Vanyan, L., 2012b, Recovering of the energy spectra of electrons and gamma rays coming from the thunderclouds, Atmos. Res. 114–115, 1

Chilingarian, A., Hovsepyan, G., Mailyan, B., 2017a, In situ measurements of the Runaway Breakdown (RB) on Aragats mountain, NIM A, 874, 19

Chilingarian, A., Chilingaryan, S., Karapetyan, T., Kozliner, L., Khanikyants, Y., Hovsepyan, G., Pokhsraryan, D., and Soghomonyan, S., 2017b, On the initiation of lightning in thunderclouds, Sci. Rep. 7, 1371

Chilingarian, A., Babayan, V., Karapetyan, T., et al. 2018a, The SEVAN Worldwide network of particle detectors: 10 years of operation, Adv. Space Res. 61, 2680

Chilingarian, A., Hovsepyan, G., Soghomonyan, S., Zazyan, M., and Zelenyy, M., 2018b, Structures of the intracloud electric field supporting origin of long-lasting thunderstorm ground enhancements, Physical review 98, 082001

Chilingarian, A., Hovsepyan, G., Karapetyan, T., et al. 2020, Structure of thunderstorm ground enhancements, PRD 101, 122004

Chilingarian, A., Hovsepyan, G., Karapetyan, G., and Zazyan, M., 2021, Stopping muon effect and estimation of intracloud electric field, Astroparticle Physics 124, 102505

Cooray, V., Rakov, V., 2012, On the upper and lower limits of peak current of first return strokes in negative lightning flashes, Atmospheric Research 117, 12–17

Chum, J., Langer, R., Baše, J., Kollárik, M., Strhárský, I., Diendorfer, G., and Rusz, J., 2020, Significant enhancements of secondary cosmic rays and electric field at high mountain peak during thunderstorms, Earth, Planets and Space, 72:28, https://doi.org/10.1186/s40623-020-01155-9

Dachev, Ts., Dimitrov, Pl., Tomov, B., et al. 2010, Liulin-Type Spectrometry-Dosimetry Instruments, Radiation Protection Dosimetry, 1-5

Gurevich, A., Milikh, G., and Roussel-Dupre, R., 1992, Runaway electron mechanism of air breakdown and preconditioning during a thunderstorm, Phys. Lett. A 165, 463

Marshalland, T. C., Stolzenburg, M., 2001, Voltages inside and just above thunderstorms. JGR 106(D5), 4757-68

Nikolova, N., Private communication, http://www.crd.yerphi.am/adei/ (last accessed April 8, 2021)

Stolzenburg, M., Marshall, T. C., Rust, W. D., Bruning, E., MacGorman, D. R., and Hamlin, T., 2007, Electric field values observed near lightning flash initiations, Geophys. Res. Lett., 34, L04804

Wilson, C.T.R., 1925, The electric field of a thundercloud and some of its effects, Proc. R. Soc. London, Ser. A 37, 32D–37D

Wilson, C.T.R., 1929, Some thundercloud problems, J. of Franklin Inst., 208, 1

Cosmic ray studies with neutron detectors | Volume 1 (2021) 109
KIEL-UP • DOI: 10.38072/2748-3150/p13

Cosmic radiation exposure of aviators for solar cycles 23 and 24

Pavlos Paschalis [1], **Anastasia Tezari** [1,2], **Helen Mavromichalaki** [1], **Pantelis Karaiskos** [2], **Norma Crosby** [3], **Mark Dierckxsens** [3]

Correspondence

[1] Athens Cosmic Ray Group, Faculty of Physics, National and Kapodistrian University of Athens, Greece, ppaschalis@phys.uoa.gr, anatez@med.uoa.gr, emavromi@phys.uoa.gr

[2] Medical Physics Laboratory, Faculty of Medicine, National and Kapodistrian University of Athens, Greece, anatez@med.uoa.gr, pkaraisk@med.uoa.gr

[3] Royal Belgian Institute for Space Aeronomy (BIRA-IASB), Brussels, Belgium, norma.crosby@aeronomie.be, mark.dierckxsens@aeronomie.be

Keywords

space weather; radiation dosimetry; atmospheric cascades; aviation

Abstract

Assessing the radiation exposure of aviators and frequent flyers requires the study of the cosmic ray showers inside the Earth's atmosphere. DYASTIMA / DYASTIMA-R is a Geant4 based software application, implemented by the Athens Cosmic Ray Group which allows the study of the evolving secondary particles cascades inside the atmosphere, as well as radiation dosimetry calculations (ambient dose equivalent rate) at different atmospheric altitudes, geographic coordinates and magnetic cut-off rigidity. Results for various scenarios, as calculated by DYASTIMA/DYASTIMA-R, are provided as a federated product through the European Space Agency Space Situational Awareness of the Space Radiation Service Centre Network, while the DYASTIMA software is provided through the Athens Neutron Monitor Station (A.Ne.Mo.S.) portal. Initial results for the assessment of the radiation exposure during the last Solar Cycles 23 and 24 are presented in this work, covering the most usual flying altitudes. The results indicate the dependence of the dose rate on the magnetic cut-off rigidity threshold, with higher dose rates at high geographic latitudes, as well as the anti-correlation of cosmic ray intensity with the solar activity, as higher dose rates are observed during solar minimum conditions.

1. Introduction

As primary cosmic radiation interacts with the atmospheric matter, atmospheric showers of secondary cosmic ray particles are created. Understanding these cascades may provide useful insights for the study of various Space Weather phenomena and effects, such as the ionization of the atmosphere. At the same time, atmospheric showers can be used for the radiation assessment of technological systems, such as the prevention of damages on avionics, as well as human health, such as the radiation protection of aviation crews and passengers during commercial air-flights.

Under this scope, a free software application for the study of the secondary particles cascades inside the Earth's atmosphere has been created by the Athens Cosmic Ray Group, called Dynamic Atmospheric Shower Tracking Interactive Model Application (DYASTIMA) (Paschalis et al. 2014). This application is based on Geant4 software (Agostinelli et al. 2003; Allison et al. 2006, 2016) and is

KIEL-UP • DOI: 10.38072/2748-3150/p13

provided by the Athens Neutron Monitor Station (A.Ne.Mo.S.) portal (http://cosray.phys.uoa.gr/index.php/dyastima, last accessed April 8, 2021). DYASTIMA has already been successfully used for the study of the cascades inside the Earth's atmosphere (Paschalis et al. 2014), the estimation of the Earth's atmosphere ionisation during the Ground Level Enhancement (GLE71) on 17 May 2012 (Dorman et al. 2015) and the calculation of the ion production rate inside the Venusian atmosphere (Plainaki et al. 2016).

The latest version of DYASTIMA includes a new feature, DYASTIMA-R, which allows radiation dosimetry calculations due to atmospheric showers inside the atmosphere of Earth (Paschalis et al. 2016, 2018; Tezari et al. 2019, 2020). DYASTIMA / DYASTIMA-R have been validated according to international accepted standards, as provided by ICRP 132 (ICRP 2016) and ICRU Report 84 (ICRU 2010) documents. More specifically, dosimetry calculations were performed for three time periods (January 1998, January 2000, January 2002) covering different solar activity periods (early ascending phase and solar maximum of Solar Cycle 23 respectively), eighteen vertical cut-off rigidities (Rc = 0 GV – 17 GV) covering the whole energy spectrum, and three frequent commercial flying altitudes (FL310 (9.45 km), FL350 (10.67 km), FL390 (11.89 km)). These calculations were compared to reference data and the discrepancy observed did not exceed in general the acceptable limit of 30%, for cut-off rigidities up to 10 GV (Paschalis et al. 2016, 2018; Tezari et al. 2019, 2020). Therefore DYASTIMA-R can be a reliable tool for assessing the ionizing cosmic radiation exposure of aviation crews and frequent flyers during air flights. The results for specific flight scenarios, as calculated by DYASTIMA / DYASTIMA-R, are provided through the European Space Agency Space Situational Awareness Space Weather Service Centre Network (http://swe.ssa.esa.int/web/guest/dyastima-federated, last accessed April 8, 2021) as a federated product.

2. Dosimetry calculations with DYASTIMA / DYASTIMA-R

2.1 DYASTIMA configuration

DYASTIMA software is based on a graphical user interface (GUI), allowing the user to perform easy parameterization of both the input parameters and the simulation environment. Several input parameters are required, all defined by the user (Athens Cosmic Ray Group 2019). These parameters concern the general characteristics of the planet as well as the atmospheric structure and temperature profile. More specifically, the atmospheric profile is based on the International Standard Atmosphere model (ISO 2007), while the mean annual values for the North, East and Vertical components of the magnetic field are provided by the National Oceanic and Atmospheric Administration (NOAA), based on the International Geomagnetic Reference Field (IGRF) (https://www.ngdc.noaa.gov/geomag/, last accessed April 8, 2021) at mean sea level. One of the most crucial input parameters are the primary cosmic ray spectra, which can be extracted by various models and tools. For the calculations presented in this work, the primary cosmic ray spectra (^{1}H, ^{4}He, ^{12}C, ^{16}O, ^{28}Si, ^{56}Fe) are based on the ISO15390 model (ISO 2004) and the model by Nymmik et al. (1996). More specifically, ISO was used for lower energies (below 10 MeV/nuc), while the Nymmik et al. (1996) model was used for higher energies, since these models are quite similar for energies above 10 MeV/nuc. The effect of the geomagnetic field continuous evolution for various geographic coordinates is also taken under consideration by using vertical cut-off rigidity values in the primary spectra calculations, as calculated with the IGRF for Epoch 2000.0 (Smart & Shea 2007). It should be noted that the primary spectra in this work is provided by OMERE software offered by TRAD (http://www.trad.fr/en/space/omere-software/, last accessed April 8, 2021). The geometry model, the division of the atmosphere into layers, the appropriate Geant4 physics lists and the definition of the tracking atmospheric altitudes should also be taken into consideration by the user.

By performing a simulation with DYASTIMA, all the information concerning the cascade is available to the user, such as the energy of the secondary particles, the energy deposition on the different atmospheric layers, the time of arrival etc. This output can be used as input to a second Monte Carlo simulation, performed with DYASTIMA-R, in order to perform radiation dosimetry calculations

KIEL-UP • DOI: 10.38072/2748-3150/p13

(dose rate and equivalent dose rate) for various flight scenarios covering different geographic coordinates, atmospheric altitudes and solar activity periods. The radiation weighting factors used for the calculation of the equivalent dose rate are according to ICRP standards (ICRP 2007, 2016). The parameters of the simulation, including the characteristics of the cylindrical phantom simulating the human body, the number of iterations and the reference Geant4 physics lists, are also defined by the user.

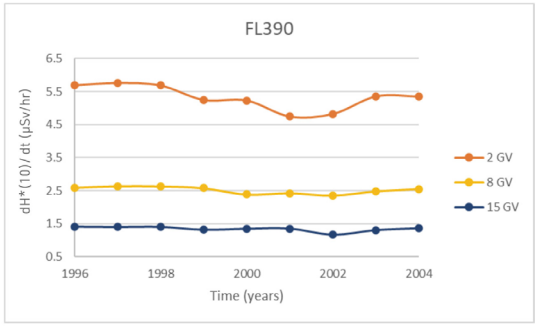

Figure 1: Ambient dose equivalent rate as a function of cut-off rigidity (Rc) and time covering 1996-2004 for the specific flying altitude (FL390).

2.2 Initial results

The average annual ambient dose equivalent rate dH*(10)/dt (μSv / hr) for FL390 and different cut-off rigidity values (Rc = 2 GV, 8 GV, 15GV) for the time period 1996 – 2004 (covering almost the whole Solar Cycle 23) is given in figure 1. It is observed that the dose rate presents high variation at higher geographic latitudes (low cut-off rigidity) and little or no variation at areas of middle geographic latitudes and equatorial regions (high cut-off rigidity). This phenomenon is also observed on the two panels of figure 2, where the dH*(10)/dt as a function of cut-off rigidity for three flying altitudes for specific years (1997 and 2004 respectively) is presented. Due to the dependence of the dose rate on the geographic latitude, it is evident, dH*(10)/dt decreases as the rigidity threshold increases. This effect is more dominant at higher atmospheric altitudes.

Finally, the dH*(10)/dt on annual basis, for the rigidity threshold of 2 GV and for three flying altitudes (FL310, FL350, FL390), is presented in figure 3, for the time period 1996-2019 covering the two recent Solar Cycles 23 and 24. The anti-correlation of the cosmic ray intensity with the solar activity is clearly observed, as the higher dose rate takes place during the extended solar minimum between the two solar cycles, while the lower dose rate is observed during the solar maximum of Solar Cycle 24.

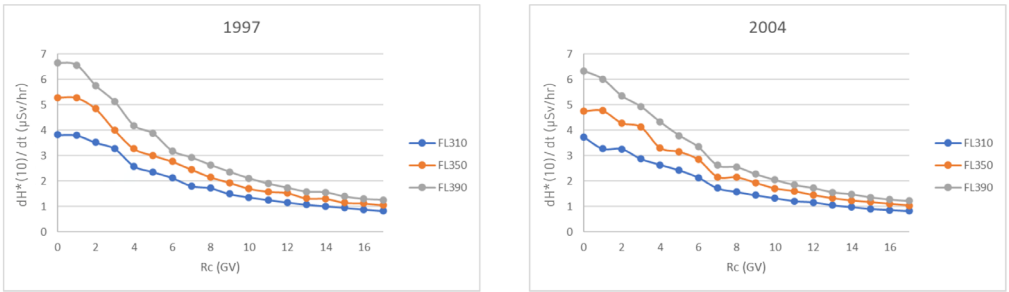

Figure 2: Ambient dose equivalent rate as a function of cut-off rigidity Rc for 1997 (left panel) and 2004 (right panel) for three frequent flying altitudes (FL310, FL350, FL390).

KIEL-UP • DOI: 10.38072/2748-3150/p13

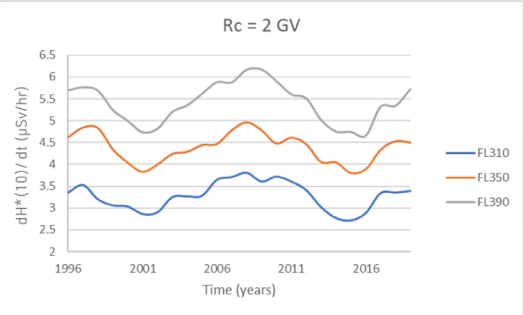

Figure 3: Ambient dose equivalent rate as a function of time for a specific cut-off rigidity (Rc=2 GV) for 3 frequent flying altitudes (FL310, FL350, FL390), covering Solar Cycles 23 and 24 (1996-2019).

3. Discussion and conclusion

DYASTIMA / DYASTIMA-R can be a useful tool for the reliable radiation assessment of aviators and passengers during air flights. The initial results are very promising clearly indicating the dependence of the dose rate on the cut-off rigidity threshold and the period of solar activity, with the dose rate decreasing with the increase of the cut-off rigidity threshold and the increase of solar activity.

So far, DYASTIMA simulations have been performed for specific points inside the Earth's atmosphere (specific geographic coordinates, cut-off rigidity and atmospheric altitudes). Future steps include dosimetry calculations performed during a whole flight, by considering the flight route as well as the time period and duration of the flight. Simulation of the atmospheric cascades in other planets will also be performed, such as the atmosphere of Mars, after the identification of the proper input parameters. These results may be useful for the evaluation of the radiation exposure of spacecraft crews.

Acknowledgments

This work is supported by ESA SSA SWE Space Radiation Expert Service Centre activities (ESA contract number 4000113187/15/D/MRP). The European Neutron Monitor Services research is funded by the ESA SSA SN IV-3 Tender: RFQ/3-13556/12/D/MRP. A.Ne.Mo.S is supported by the Special Research Account of Athens University (70/4/5803). A.T. thanks the Hellenic State Scholarship Foundation (IKY) for supporting her with a doctoral scholarship through the Operational Programme «Human Resources Development, Education and Lifelong learning» in the context of the project "Strengthening Human Resources Research Potential via Doctorate Research – 2nd Cycle" (MIS-5000432), co-financed by Greece and the European Union (European Social Fund- ESF).

References

Agostinelli, S., Allison, J., Amako, K., Apostolakis, J., et al., 2003, Nucl. Instrum. Methods A 506, 250-303
Allison, J., Amako, K., Apostolakis, J., et al., 2006, IEEE Trans. Nuclear Sci. 53, 270-278
Allison, J., Amako, K., Apostolakis, J., et al., 2016, Nucl. Instrum. Methods A A 835, 186-225
Athens Cosmic Ray Group, 2019, DYASTIMA Software User Manual
Dorman, L. I., Paschalis, P., Plainaki, C., Mavromichalaki, H., 2015, Proc. 34th ICRC, The Hague, Netherlands, PoS(ICRC2015)202
ICRP, 2007, Ann. ICRP 37, ICRP Publication 103
ICRP, 2016, Ann. ICRP 45(1), ICRP Publication 132
ICRU, 2010, Journal of the ICRU 10, Report 84, Oxford University Press
ISO, 2004, Space environment (natural and artificial)-Galactic cosmic ray model 15390:2004
ISO, 2007, Standard Atmosphere 2533:1975

Nymmik, R. A., Panasyuk, M. I., Suslov, A. A., 1996, Adv. Space Res. 17(2), 19-30
OMERE, http://www.trad.fr/en/space/omere-software/ (last accessed August 30, 2019)
Paschalis, P., Mavromichalaki, H., Dorman, L. I., Plainaki, C., Tsirigkas D., 2014, New Astron. 33, 26-37
Paschalis, P., Tezari, A., Gerontidou, M., Mavromichalaki, H., Nikolopoulou, P., 2016, XXV ECRS 2016 Proc. - eConf C16-09-04.3
Paschalis, P., Tezari, A., Gerontidou, M., Mavromichalaki, H., Karaiskos, P., 2018, Proc. 27th HNPS Annual Symposium, Athens, Greece
Pelliccioni, M., 2000, Rad. Prot. Dosimetry 88(4), 279–297
Plainaki, C., Paschalis, P., Grassi, D., Mavromichalaki, H., Andriopoulou, M., et al., 2016, Ann. Geophys. 34, 595-608
Smart, D. F., Shea, M. A., 2007, Proc. 30th ICRC, Mexico
Tezari, A., Paschalis, P., Mavromichalaki, H., Karaiskos, P., Crosby, N., Dierckxsens, M., 2019, Proc. 70th IAC, Washington DC, USA
Tezari, A., Paschalis, P., Mavromichalaki, H., Karaiskos, P., Crosby, N., Dierckxsens, M., 2020, Rad. Prot. Dos. 190, 427-436

Questions and answers

Ludwig Klein: How do you validate your model (you alluded to validation in the paper in press)?

Answer: DYASTIMA-R has been validated according to ICRP standards (ICRP 132, 2016) and the reference data found at Report 84 by ICRU (2010). The validation process is discussed in the recent publication by Tezari A., Paschalis P., Mavromichalaki H., Karaiskos P., Crosby N., and Dierckxsens M. at Oxford Academic Journal Radiation Protection Dosimetry (DOI: https://dx.doi.org/10.1093/rpd/ncaa112).

Cosmic ray studies with neutron detectors | Volume 1 (2021)
KIEL-UP • DOI: 10.38072/2748-3150/v1

Session 3: Abstracts

Monitoring environmental water with ground albedo neutrons from cosmic rays

Martin Schrön [1], **Markus Köhli** [2]

Correspondence

[1] Helmholtz Centre for Environmental Research GmbH - UFZ, Monitoring and Exploration Technologies, Leipzig, Germany

[2] Heidelberg University, Physikalisches Institut, Heidelberg, Germany

In the last 10 years the young research field of Cosmic-Ray Neutron Sensing for Environmental Sciences has established a technique to monitor local dynamics of water content in soils and snow by measuring the albedo flux of sub-MeV neutrons. The moderation power of water in soil, air, snow and vegetation determines the density of neutrons above the ground in the energy range from 1 eV to 100 keV. The signal represents an area-average water content within tens of hectares due to the diffusion of neutrons in air, and within tens of decimeters in depth. This turns a small neutron detector into a smart sensor for root-zone soil moisture at the field scale. Hundreds of small neutron detectors have been installed on natural and agricultural sites all across the globe. Climate research, hydrologic models and irrigation management rely on this data. A critical factor for the reliability of such data is the knowledge of the dynamics of incoming cosmic-ray neutrons. Conventionally, independent data from neutron monitors are consulted to serve as a reference for the correction of the local detectors. However, the performance of this comparative correction approach is often unreliable, as it does not account for displacement (cutoff rigidity, altitude), different energy window, or potential other effects on the referenced neutron monitor. The presentation shows how ground albedo neutrons from cosmic-rays are applied to environmental research, and emphasizes the need for a reliable correction for the incoming cosmic-ray flux. Being part of a young adjacent community, we rely on the neutron monitor network as our backbone, so we are interested to understand better the data provided by individual instruments and discuss approaches that account for spatio-temporal variations of incoming cosmic rays on Earth. On the other hand, our findings on the response of cosmic-ray neutrons to environmental factors as well as the large network of instruments could open new opportunities for potential cooperations between the disciplines.

Comparison between Daejeon neutron monitor data and clouds data during 2012-2018

Jongil Jung [1], **Suyeon Oh** [2], **Yu Yi** [1]

Correspondence

[1] Department of Astronomy, Space Science and Geology, Chungnam National University, Daejeon, Korea; Korea Polar Research Institute, Incheon, Korea

[2] Department of Earth Science Education, Chonnam National University, Gwangju, Korea

KIEL-UP • DOI: 10.38072/2748-3150/v1

Cosmic ray particles are the high-energy ions, mostly protons to enter the Earth from the space. They can be observed on ground base as the secondary particles produced by colliding with atmospheric particles. This collision process begins at an altitude of approximately 30 km from the ground. Because many neutrons as the secondary particles are generated by interaction with cosmic rays and atmospheric particles, cosmic ray particles are considered as the cloud condensation nuclei in the previous studies. For that reason, we examine the relation between cosmic ray flux and cloud production. We present the result by analyzing the cosmic ray intensity of Daejeon neutron detector operated from October 2011, and cloud data of East Asia in Communication Ocean and Meteorological Satellite (COMS) during the period from 2012 to 2018.

Session 4:

Space weather research and services

Cosmic ray studies with neutron detectors | Volume 1 (2021)
KIEL-UP • DOI: 10.38072/2748-3150/p14

Signs of geoeffective space weather events in cosmic rays during the first half of the solar cycle 24

Agnieszka Gil [1,2], **Renata Modzelewska** [1], **Szczepan Moskwa** [3], **Agnieszka Siluszyk** [1], **Marek Siluszyk** [1,4], **Anna Wawrzaszek** [2], **Anna Wawrzynczak** [5,6]

Correspondence

[1] Institute of Mathematics, Siedlce University of Natural Sciences and Humanities, Poland, gila@uph.edu.pl
[2] Space Research Centre, Polish Academy of Sciences, Warsaw, Poland, agil@cbk.waw.pl
[3] AGH University of Science and Technology, Krakow, Poland
[4] Military University of Aviation, Deblin, Poland
[5] Institute of Computer Sciences, Siedlce University of Natural Sciences and Humanities, Poland
[6] National Centre for Nuclear Research, Otwock, Poland

Keywords

Forbush decreases; transmission lines failures; geomagnetic storms; space weather effects

Abstract

Solar originating events are continually evident in galactic cosmic ray (GCR) flux registered at the ground by neutron monitors. We analyze time intervals of sporadic Forbush decreases (Fd) observed by neutron monitors (NM) during the first half of solar cycle 24. We consider NMs data, as well as, solar, heliospheric and geomagnetic activity parameters, around those periods, using different mathematical tools. Subsequently, an impact of space weather phenomena on energy infrastructure is well known, in the further step we consider logs from one of the Polish transmission lines operators during the time intervals of Fds. Based on the data from the Institute of Meteorology and Water Management-Polish National Research Institute we exclude from the analysis the weather-related failures. We found that the increase in the superposed averaged number of failures appears around Forbush decreases.

1. Introduction

The influence of space phenomena on functioning satellites systems (European Galileo, American GPS, Russian GLONASS and others) and space probes, communication systems, on astronauts, as well as crew and frequent passengers of aircraft, or ground energetic electrical systems and even on climate, make the understanding of the solar-terrestrial links an imperative matter (e.g. Wang et al. 2016). Variability of the Sun, continuously measured from 16th century, affects the Earth in a number of ways, depending on the level of solar activity. During the solar maximum transient phenomena as solar flares and coronal mass ejections are very frequent, leading to an increase in the injection, acceleration, and transport of solar energetic particles. Short and medium-term changes in the Sun have been identified as the cause of severe geomagnetic disturbances. A strong magnetic storm affects the normal operation of ground located electronic and electrical systems and causes damages of satellites and its equipment. These phenomena reinforce each other during the maximum of solar activity (e.g. Kudela 2009; Gopalswamy 2016; Pulkkinen 2017, and references therein). There are signatures that solar storms evolving to geomagnetic storms affect transmission lines in Poland (Gil et al. 2019, 2020a).

KIEL-UP • DOI: 10.38072/2748-3150/p14

In this context, the stream of particles of galactic cosmic ray (GCR) constantly reaching the Earth is a unique available source of information on the state of interplanetary space. In addition, terrestrial apparatus used to measure the GCR particle stream is not exposed to the influence of sudden processes on the Sun and interplanetary space and most importantly, GCR particles carry information about the global conditions prevailing in the heliosphere, and not just at one particular point, as in the case with in situ measurements made by space probes. The GCR particle flow is/was measured using various space probes, such as Voyager 1 and 2, Ulysses, ACE / CRIS, Pamela, etc., as well as unmanned balloon flights and ground detectors: neutron monitors (NMs) and muon telescopes (MTs). The global network of NMs is a unique 'instrument' for observing GCR particles in the energy range from $\sim$ 0.5 GeV to $\sim$ 50 GeV, continuously 'scanning' the entire sky. Because NMs are located at different latitudes, they provide information about the energy spectrum of the GCR, and this in turn gives information about the size of the heliosphere in which the cosmic rays at a given moment are modulated by the Sun. Thanks to the Neutron Monitor Data Base (NMDB), the realtime monitoring of space weather is possible (e.g. Grigoryev et al. 2019), predicting geomagnetic field disturbances with estimated preceding time from a few hours up to 1.5 days (Starodubtsev et al. 2019).

2. Forbush decreases

For the maxima and near maxima epochs of solar activity after the powerful coronal mass ejecta and solar flares, there are observed short period disturbances (shock waves, magnetic clouds, etc.) in the interplanetary space with the drastically massive range changes of the solar wind velocity, density and the components of the IMF. As a rule, the powerful disturbances in the interplanetary space go along with the short period decreases (called Forbush decreases, Fds) of the GCR intensity. The classical, sporadic Fds appear randomly in time, rarely without any regularity. However, they are more likely to occur in the ascending and descending phases of the solar sunspot cycle. They are characterized by the rapid decrease in the GCR intensity during one-two days (as observed on Earth) followed by its gradual recovery in 5–7 days (Forbush 1937). The usual amplitude (maximum GCR intensity reduction with respect to the GCR intensity in the Fds onset in %) of the Fds is about 5-20% for the GCR particles' energy of 10 GeV (e.g. Wawrzynczak & Alania 2010, 2005). Using these Fds characteristics, we have listed the sporadic Fds in the years 2010-2014. We have compared the times of appearance of Fds with electrical grids failures using the superimposed epoch analysis.

Superposed epoch analysis is a method reviling relationships between the analysed time series (Chree 1913). Denton et al. (2005), investigating the correlation of the geomagnetic storm phase with a temporal variation of plasma found at geosynchronous orbit, showed that one of the crucial factors for the plasma sheet density is the phase of the solar cycle. Liemohn et al. (2008) studied magnetic storms features, as their occurrence time or strength. Gil et al. (2019) had shown that the increase in the superposed averaged number of electrical grids failures (EGF) appears around one day after the fast halo CME occurrence, on the day of sudden storm commencement (SSC), as well as around zero-day or the day after when the Kp index was greater or equal 5.

KIEL-UP • DOI: 10.38072/2748-3150/p14

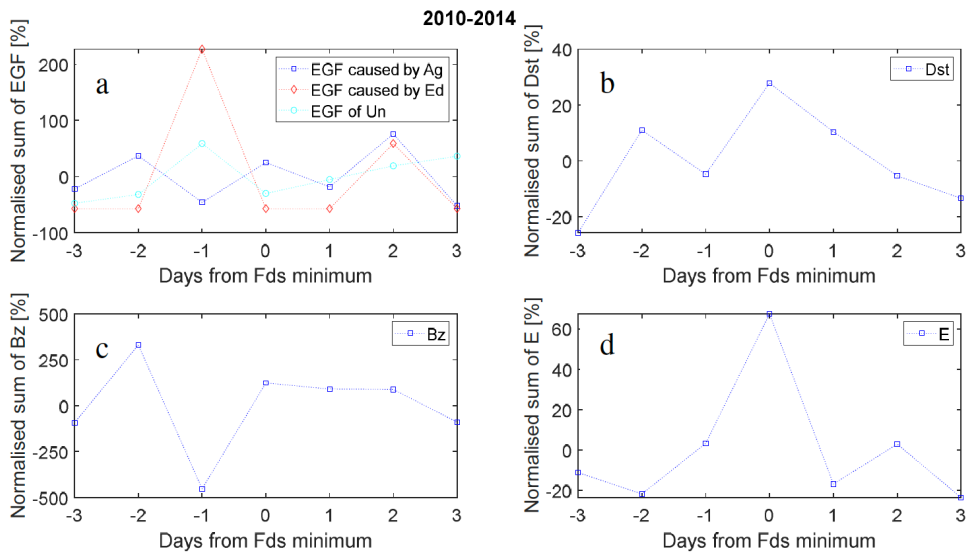

Figure 1: The superposed averaged values of (a) electrical grids failures number (caused by the aging, electronic devices breakdowns and having unknown reasons), (b) Dst-index changes, (c) Bz component of the HMF, and (d) geoelectric field E, with a key time connected to the minimum time of Forbush decreases. The value of 0 on the Y axis denotes the normalized average value around Fds.

We define the so-called zero days as a key time, among the data of minimum phase of the Forbush decreases. Next, we extract subsets of data of EGFs in South Poland in January 2010- July 2014 (of a particular type, for details see Gil et al. 2020a) 3 days before and after each key time. Subsequently, we superpose all extracted subsets of failures synchronizing all zero days. Our results are shown in figure 1a. To visualise the overall situation in the Earth vicinity we perform the Chree analysis for the same days using the data of geomagnetic Dst-index [nT] (figure 1b), heliospheric magnetic southward component Bz[nT] (figure 1c) and computed geoelectric field, E [mV/km] (figure 1d). Details of $E = \sqrt{E_X^2 + E_Y^2}$ computations are given below.

Figure 1 shows that the day before the Fd minimum phase there was a 200% growth in the EGF connected to the electronic devices, which was a day after the $\sim$350% increase in the Bz value. Two days after the Fds minima there was $\sim$100% growth in all three groups of EGF.

3. Case study-failures during the 'Battle of Grunwald day'

We analyze the geomagnetic storm which happened on July 15 of 2012 in the 602 anniversary of the famous Polish Battle of Grunwald. Thus we propose the name for this event 'Battle of Grunwald day' (Gil et al. 2020b). According to the NOAA scale, it was a G3 geomagnetic storm with the Bz heliospheric magnetic field component dropping to -20 nT, Dst index -139 nT, AE index to 1368 nT and Ap index 132 nT. It was preceded by the solar flare of X1.4 class on 12 of July. This geomagnetic storm was accompanied by the fast halo coronal mass ejection at 16:48:05UT on 12 of July-the first C2 appearance, with the sky plane speed 885 km/s and peak speed 1415 km/s (Gopalswamy et al. 2016, 2014). This geomagnetic storm was classified as the fourth of the strongest geomagnetic storms from the solar cycle (SC) 24. During this storm, the Fd was registered.

The interplanetary fast forward shock was registered on 14 July at 17:39:09 UT (www.cfa.harvard.edu, last accessed April 8, 2021). The consequences of the disturbances in the heliosphere are also seen

KIEL-UP • DOI: 10.38072/2748-3150/p14

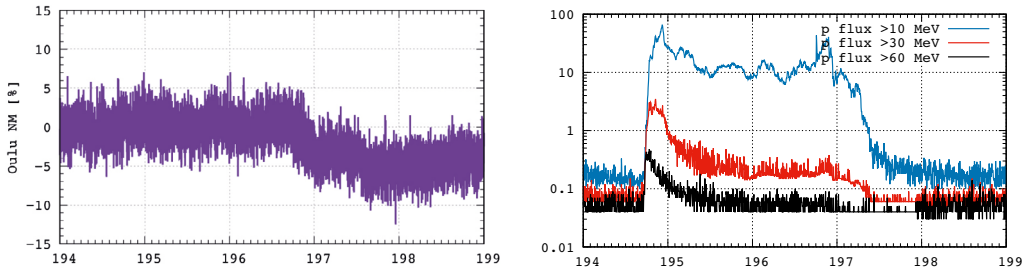

Figure 2: (a) Galactic cosmic ray intensity by Oulu neutron monitor in [%] with 1-minute resolution, (b) 5-minute integrated proton flux from OMNI, for 12-16 July 2012, DOY 194-198

in the cosmic ray flux variability. Figure 2 presents the cosmic ray proton fluxes measured in situ (figure 2b) and by Oulu neutron monitor (NM; figure 2a) for 12 – 16 July 2012.

Figure 2b shows the significant growth of proton flux on 12 July 2012 (DOY194) as a consequence of the solar flare. At 06:00 UT on 14 July 2012 (DOY196), the subsequent peak is seen in the integral proton flux > 10 MeV/n. Starting on 15 July 2012 (DOY 197), due to the CME passage, the depression in cosmic ray flux variability was observed. This decrease in cosmic ray intensity was also recorded by ground neutron monitors up to ∼10- 15 GeV as confirmed by Oulu NM (figure 2a) for which the maximum depression rate was ∼12%.

The evolution of this CME in the Earth vicinity simulated by Community Coordinated Modeling Center (CCMC) using ENLIL Model (Odstrcil, Smith, & Dryer 1996) of the dynamical 3-dimensional heliospheric conditions is shown in figure 3 (this CCMC animation of CMEs can be found in http://helioweather.net/archive/2012/07/, last accessed April 8, 2021). Figure 3b illustrates the interplanetary conditions measured and modeled: the solar wind radial velocity Vr, the proton density N and temperature T, as well as the heliospheric magnetic field strength |B| showing their rapid growth during the studied event.

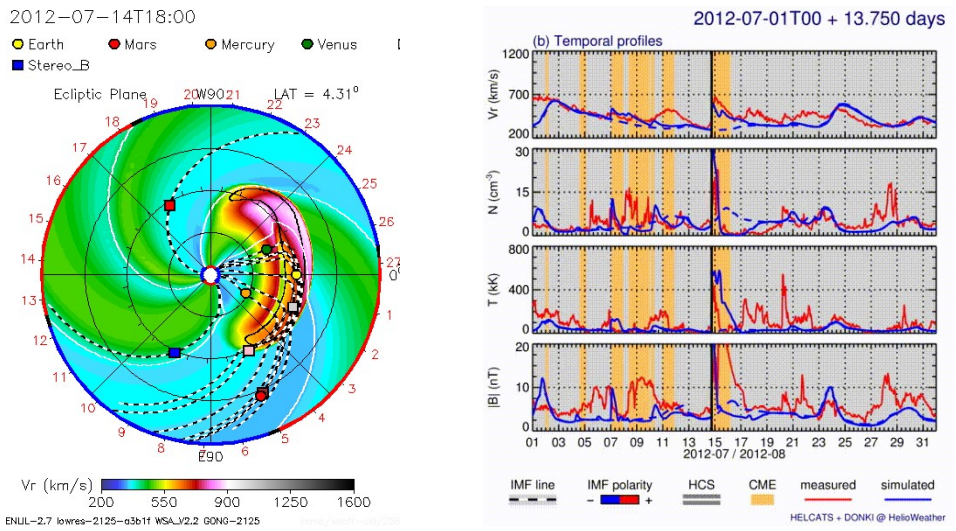

Figure 3: (a) Solar wind radial velocity contour plots in the ecliptic planes on 14 July 2012 at 18 UT, and (b) time profiles of the solar wind radial velocity Vr, proton density N and temperature T, the heliospheric magnetic field strength |B| for July 2012 with the black vertical line on 15 July 2012 at 0 UT (http://helioweather.net/archive/2012/07/vel3e1.html, ccmc.gsfc.nasa.gov, last accessed April 8, 2021)"

KIEL-UP • DOI: 10.38072/2748-3150/p14

The above-described situation was mirrored in the behaviour of Earth's magnetosphere. The dissipation processes in the CME-driven shocks (e.g., Reames et al. 1996) compressed geomagnetosphere and there appeared on July 14, 2012 at 18:09 the sudden storm commencement (SSC, http://www.obsebre.es, last accessed April 15, 2021). Firm compression of the magnetosphere, related to the above-mentioned CME arrival and passage, was detected. It was clearly visible in the horizontal B_X (N-S direction) and B_Y (E-W) geomagnetic field components measured in Belsk observatory, which served as basic data for computations of the geoelectric field with the induced surface geoelectric field according to the methodology introduced by Boteler (1994) and later developed (Boteler 2013).

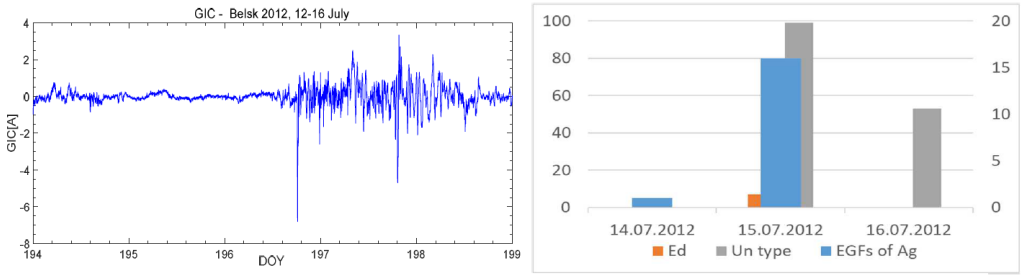

Figure: 4 (a) Computed geomagnetically induced currents (1-min resolution) for 12-16 July 2012, DOY 194-198, (b) electrical grids failures (1-h resolution), for 14-16 July 2012, DOY 196-198.

We applied the layered Earth model with resistivity according to Adam et al. (2012). Computations of the geomagnetically induced currents GIC presented in figure 4a were done by formula with $GIG = a \cdot E_x + b \cdot E_y$ (a, b) = (−62.3,133.2) Akm/V, following Wik et al. (2008). We can observe strong fluctuations in the computed GIC during the presented event.

Around that time in Polish electric transmission lines infrastructure, there was observed significant growth of the number of failures (figure 4b), which reasons might be of solar origin, namely, caused by the aging, electronic devices breakdowns and having unknown reasons (a detailed description can be found in Gil et al. 2020a). The appearance of some delay between the EGFs increase and solar disturbances in the Earth's vicinity is discussed in Švanda et al. 2020, Gil et al. 2019, and Zois 2013.

4. Summary

Analysis of each individual geoeffective event in the framework of transmission lines failures can be a clue in revealing a collective characteristic of the state of the near heliosphere, ionosphere, geomagnetosphere, which may contribute to the number of failures increase.

Acknowledgments

Data of cosmic rays are from OULU station (http://cosmicrays.oulu.fi). Data of geomagnetic field components are from Belsk observatory, the part of INTERMAGNET (http://rtbel.igf.edu.pl), heliospheric data are from OMNI (https://omniweb.gsfc.nasa.gov). The ENLIL simulation results have been provided by the Community Coordinated Modeling Center at Goddard Space Flight Center (http://ccmc.gsfc.nasa.gov). The ENLIL Model was developed by Dusan Odstrcil, now at the George Mason University - Space Weather Lab and NASA/GSFC - Space Weather Lab. We acknowledge the financial support by the Polish National Science Centre, grant no. 2016/22/E/HS5/00406.

References

Adam, A., Pracser, E., Wesztergom, V., 2012, Acta Geod. Geophys. Hung., 47, 377, DOI: https://dx.doi.org/10.1556/ageod.47.2012.4.1

Boteler, D.H., 2013, IEEE Power & Energy Society General Meeting, Vancouver, BC, 2013, 1-5. DOI: https://dx.doi.org/10.1109/PESMG.2013.6672717

Boteler, D. H., 1994, IEEE Trans. Magn., 30, 172, DOI: https://dx.doi.org/10.1109/20.312255

Chree, C., 1913, Philosophical Transactions of the Royal Society of London. Series A, Containing Papers of a Mathematical or Physical Character, 212, 75

Denton, M. H., Thomsen, M. F., Korth, H., et al. 2005, J. of Geophysical Research, 110, A07223, DOI: https://dx.doi.org/10.1029/2004JA010861

Gil, A., Modzelewska, R., Moskwa, Sz., et al. 2020a, Energies, 13, 2359, DOI: https://dx.doi.org/10.3390/en13092359

Gil, A., Modzelewska, R., Moskwa, Sz., et al. 2020b, Solar Physics, 295, 135, DOI: https://dx.doi.org/10.1007/s11207-020-01703-2

Gil, A., Modzelewska, R., Moskwa, Sz., et al. 2019, Journal of Mathematics in Industry, 9, 7, DOI: https://dx.doi.org/10.1186/s13362-019-0064-9

Forbush, S. E., 1937, Phys. Rev., 51, 1108–1109

Gopalswamy, N., Yashiro, S., Thakur, N., et al. 2016, Ap. J., 833 2, article id. 216, DOI: https://dx.doi.org/10.3847/1538-4357/833/2/216

Gopalswamy, N., 2016, Geoscience Letters, 3, article id.8, DOI: https://dx.doi.org/10.1186/s40562-016-0039-2

Gopalswamy, N., Xie, H., Akiyama, S., et al. 2014, Earth, Planets and Space, 66 104, DOI: https://dx.doi.org/10.1186/1880-5981-66-104

Grigoryev, V. G., Starodubtsev, S. A., Gololobov, P. Yu., 2019, Solar-terrestrial physics, 5, 3, 93

Kudela, K., 2009, Acta Phys. Slovaca, 59, 537

Liemohn, M. W., Zhang, J.-C., Thomsen, M. F., et al. 2008, Geophysical Research Letter, 35, L06S06, DOI: https://dx.doi.org/10.1029/2007GL031717

Odstrcil, D., Smith, Z., Dryer M., 1996, Geophys. Res. Lett. 23, Issue 18, 2521, DOI: https://dx.doi.org/10.1029/96GL00159

Pulkkinen, A., Bernabeu, E., Thomson, A., et al. 2017, Space Weather, 15, 7, 828, DOI: https://dx.doi.org/10.1002/2016SW001501

Reames, D. V., Barbier, L. M., Ng, C. K., 1996, Astrophysical Journal, 466, 473-486, DOI: https://dx.doi.org/10.1086/177525

Starodubtsev, S. A., Grigoryev, V. G., Gololobov, P. Yu., 2019, Journal of Physics. Conference Series, 1181, 012011, DOI: https://dx.doi.org/10.1088/1742-6596/1181/1/012011

Švanda, M., Mourenas, D., Žertová, K., et al. 2020, J. Space Weather Space Clim., 10, 26 DOI: https://dx.doi.org/10.1051/swsc/2020025

Wang Ch., Rosen, I. G., Tsurutani, B. T., et al. 2016, J. Space Weather Space Clim., Volume 6, A5, DOI: https://dx.doi.org/10.1051/swsc/2015046

Wawrzynczak, A., Alania M. V., 2010, Advanced in Space Research, 45, 5, 622-631, DOI: https://dx.doi.org/10.1016/j.asr.2009.09.005

Wawrzynczak, A., Alania M. V., 2005, Advanced in Space Research, 35, 682-686, DOI: https://dx.doi.org/10.1016/j.asr.2004.12.055

Wik, M., Viljanen, A., Pirjola, R., et al. 2008, Space Weather, 6, 7, DOI: https://dx.doi.org/10.1029/2007SW000343

Zois, J. P., 2013, J. Space Weather and Space Climate, 3, A32, DOI: https://dx.doi.org/10.1051/swsc/2013055

Questions and answers

Rolf Bütikofer: How can we use this result for spwx purposes?
Answer: This work still needs to be continued, but in a future it could be used in practice: transmission lines operators, who would gain knowledge about the increased risk of small power grids failures, which would be associated with the upcoming geomagnetic storm, could organize more energy-rescue-teams at that time, which would have resulted in the shortening the duration of these minor breakdowns, and thus reducing the costs related to non-delivered electricity.

Ludwig Klein: Are there comparisons with countries at comparable latitudes as to the occurrence of failures?
Answer: There are paper showing even more south countries than Poland, e.g. Czech Republic (e.g. Švanda et al. 2020, DOI: https://dx.doi.org/10.1051/swsc/2020025), Greece (e.g., Zois 2013, DOI: https://dx.doi.org/10.1051/swsc/2013055) or Italy (e.g. Tozzi 2019, DOI: https://dx.doi.org/10.1029/2018SW002065).

Cosmic ray studies with neutron detectors | Volume 1 (2021)
KIEL-UP • DOI: 10.38072/2748-3150/p15

Relationship of the characteristics of large Forbush decreases and the heliolongitude of their sources

Maria Papailiou[1], **Maria Abunina**[2], **Anatoly Belov**[2], **Eugenia A. Eroshenko**[†2], **Victor Yanke**[2], **Helen Mavromichalaki**[1]

Correspondence

[1] Nuclear and Particle Physics Department, Faculty of Physics, National and Kapodistrian University of Athens, Greece, mpapahl@phys.uoa.gr, emavromi@phys.uoa.gr

[2] Pushkov Institute of Terrestrial Magnetism, Ionosphere and Radiowave Propagation (IZMIRAN), Moscow, Russia,
abunina@izmiran.ru, abelov@izmiran.ru, erosh@izmiran.ru, yanke@izmiran.ru

Keywords

Forbush decreases; solar sources; heliolongitude; cosmic ray anisotropy

Abstract

In this investigation the different features and characteristics of Forbush decreases, with emphasis on large Forbush decreases (≥4%) and their association to solar sources, are being examined. According to the heliolongitude of the solar source, the events under study were separated into three subcategories: western (21° ≤ heliolongitude ≤ 60°), eastern (-60° ≤ heliolongitude ≤ -21°) and central (-20° ≤ heliolongitude ≤ 20°). The selected events cover the time period 1967 - 2017. The 'Global Survey Method' was used for analyzing the Forbush decreases, along with data on solar flares, solar wind speed, geomagnetic indices (Kp and Dst), and interplanetary magnetic field. In addition, the superimposed epoch method was applied in order to plot the time profiles for the aforementioned group of events. This detailed analysis reveals interesting results concerning the features of cosmic ray decreases in regard to the heliolongitude of the solar sources. Moreover, it is also shown that large Forbush decreases, regardless of the heliolongitude of the solar source, are accompanied by increased geomagnetic activity and increased anisotropy, including anisotropy before the events, which can serve as a typical precursor of Forbush decreases.

1. Introduction

The Forbush decrease (FD) effect can be defined as 'the result of the effect of coronal mass ejections (CMEs and ICMEs) and/or high speed solar wind streams originating from coronal holes on cosmic rays' (Papaioannou et al. 2010; Belov et al. 2014; Kryakunova et al. 2015). FDs are observed as a short term and steep decrease of the galactic cosmic ray intensity which is followed by a relatively slow recovery (e.g. Melkumyan et al. 2018) lasting up to one week (Cane 2000; Usoskin et al. 2008; Melkumyan et al. 2019). The study of FDs reveals a wide variety of these events in regard to the amplitude and the duration of the events, the anisotropy, the fast or gradual decrease, the complete recovery or absence of recovery phase, the completion in one or two steps, the simple or complicated time profile, etc. The diversity of the solar sources related to them may be one factor that could provide interesting results about the aforementioned variety and the various manifestations of their characteristics. In this study the different features and characteristics of FDs, with emphasis on large FDs and their association to solar sources are being examined. In particular, this

† deceased

KIEL-UP • DOI: 10.38072/2748-3150/p15

work focuses mainly on the influence of solar sources position on the FD magnitude (i.e., on the variation of the cosmic ray density) and on the maximum anisotropy of cosmic rays.

2. Data and method

The Forbusheffects and interplanetary disturbances database (FEID) of IZMIRAN (http://spaceweather.izmiran.ru/eng/dbs.html, last accessed April 8, 2021) has been used for this study (Abunin et al. 2013). Cosmic ray parameters (density, anisotropy, etc.) in this database are calculated by the 'Global Survey Method' (Belov et al. 2018). In addition to solar-wind parameters (solar wind speed and interplanetary magnetic field intensity) and geomagnetic indices (Ap, Kp and Dst) that were obtained from the OMNI database (http://omniweb.gsfc.nasa.gov, last accessed April 8, 2021), the list of sudden storm commencements (SSCs) (http://isgi.unistra.fr/data_download.php, last accessed April 8, 2021) and of the solar flares data (class, location, time) reported in the solar geophysical data (ftp://ftp.swpc.noaa.gov/pub/indices/events/, last accessed April 8, 2021) were also used (Belov et al. 2014).

3. Analysis and results

In this study, the selection of events and their grouping was made using the combination of four criteria. The criterion for group A is the SSC, for group B, apart from the SSC, the magnitude is also considered, whereas the FDs of group C are being investigated with respect to SSC, magnitude, quiet background and presence of an identified solar source. Moreover, the FDs of group C were further divided into three subcategories, according to the heliolongitude of the solar source. As a result, the categories were organized in table 1. In this table, Group C includes 100 events associated with sources with heliolongitude -90° – 90°, but since FDs associated with sources from the far eastern (-90° – -61°) and far western (61° – 90°) regions are not being considered in the particular study, the remaining 87 FDs are organized in groups C-W, C-E, and C-C.

Categorization	Criteria	Number of events
Group A	FDs with SSC	1515
Group B	FDs with SSC and magnitude greater than 4%	335
Group C	FDs with SSC, magnitude >4%, evolved in a quiet background (no other events were registered for 48 hours before and 18 hours after the onset of each FD) and connected to identified solar sources:	100
Group C-W	western sources ($21^{o} \leq$ heliolongitude $\leq 60^{o}$)	23
Group C-E	eastern sources ($-60^{o} \leq$ heliolongitude $\leq -21^{o}$)	28
Group C-C	central sources ($-20^{o} \leq$ heliolongitude $\leq 20^{o}$)	36

Table 1: The criteria for grouping the FDs registered from 1967 – 2017 used in this study.

KIEL-UP • DOI: 10.38072/2748-3150/p15

3.1 Time profiles of FD groups

Averaged time profiles for some parameters concerning the aforementioned groups of events were plotted. Specifically, cosmic ray density A0 and the magnitude of the component Axy of the first harmonic of anisotropy along with the interplanetary magnetic field intensity and the solar wind speed and geomagnetic indices Dst and Kp for the groups C-W (figure 1), C-E and C-C were plotted as result of the application of the superimposed epoch method. These profiles cover a time period of 48 hours before and 120 hours after the SSC. In figure 1, the particularity of the changes in density 44 – 30 hours before the onset of the events is not associated with modulation effects but is a consequence of GLEs, which quite often precede large FDs from western solar sources. Four of the selected events are related to GLEs (13 October 1981, 26 October1989, 04 November 2003, 14 December 2006).

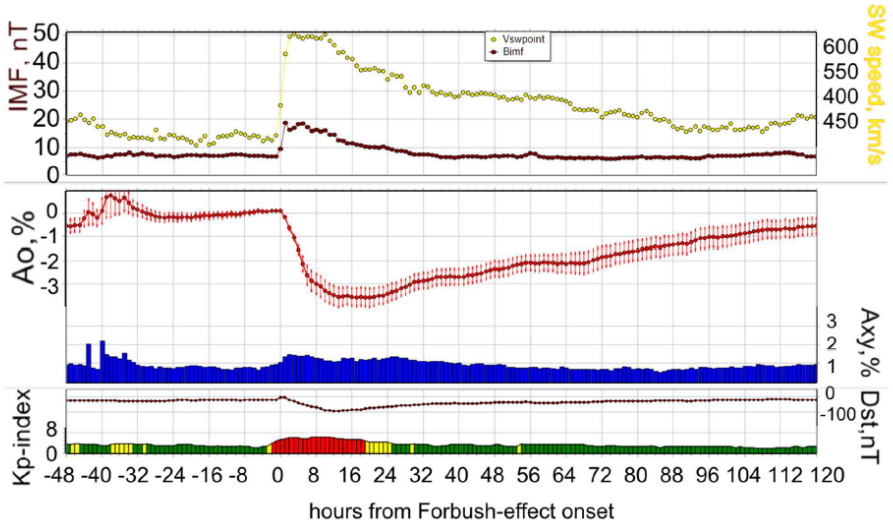

Figure 1: Variations of the interplanetary magnetic field and the solar wind speed (upper panel), the cosmic ray density A0 (points) and the magnitude of the component Axy of the first harmonic of anisotropy (columns) (middle panel) and the Dst and Kp indices (bottom panel) for the time periods before and after the arrival of the SSC, as they were calculated for 23 FDs connected to western sources with magnitude ≥4% and SSC by the superimposed epoch method. 0 suggests the recording time of the SSC.

The results from the superimposed epoch method are organized in table 2. The most interesting parameters are the FD magnitude (AF, %), the maximum value of the equatorial component of the first harmonic of CR anisotropy (A_{xymax}, %), the anisotropy one hour before the onset (A_{xyb}, %), the minimum value of the geomagnetic index Dst (Dst_{min}), the maximum value of the interplanetary magnetic field intensity (B_{max}) and the maximum value of the solar wind speed (V_{max}) averaged by the superimposed epoch method over all events and finally, the variation during the last hour before the onset of each event $\Delta B = B_0 - B_b$ and $\Delta V = V_0 - V_b$, where B_0 and V_0 are the interplanetary magnetic field intensity and solar wind speed values at the time of the SSC registration and B_b and V_b are the interplanetary magnetic field intensity and solar wind speed values one hour before the onset of the event respectively.

KIEL-UP • DOI: 10.38072/2748-3150/p15

Parameter	1515 FDs SSC	335 FDs SSC Magn. ≥4%	87 FDs SSC, A_F ≥4%, quiet background, identified solar source (−60° ≤ heliolong. ≤ 60°)		
			Western sources	Eastern sources	Central sources
A_F %	1.75 ± 0.06	4.57 ± 0.15	3.7 ± 0.45	4.37 ± 0.52	5.01 ± 0.31
A_{xymax} %	0.96 ± 0.02	1.48 ± 0.05	1.47 ± 0.19	1.36 ± 0.18	1.70 ± 0.15
A_{xyb} %	0.76 ± 0.01	0.93 ± 0.04	0.94 ± 0.14	0.96 ± 0.09	0.70 ± 0.06
Dst_{min} nT	-44.2 ± 1.3	-84.6 ± 4.17	-92.4 ± 15.46	-74.6 ± 12.38	-90.4 ± 12.1
B_{max} nT	13.24 ± 0.22	19.28 ± 0.63	18.66 ± 1.70	20.88 ± 2.43	20.04 ± 2.11
ΔB nT	2.31 ± 0.20	3.92 ± 0.48	2.71 ± 1.10	3.35 ± 1.17	4.09 ± 0.97
V_{max} km s^{-1}	492.8 ± 4.0	603.9 ± 10.6	619.7 ± 42.1	583.9 ± 27.3	627.0 ± 24.5
ΔV km s^{-1}	25.9 ± 4.4	42.5 ± 11.5	56.7 ± 35.6	25.8 ± 19.2	59.3 ± 22.7

Table 2: Results from the superimposed epoch analysis for the categories of the events under study.

The magnitude of the events connected to western solar sources (3.7%) is obviously smaller than that of the events connected to eastern (4.37%) or central sources (5.01%) (Abunina et al. 2013a). The typical value for the parameter of anisotropy during quiet conditions is 0.53% (Abunina et al. 2013b). Moreover, the usual value of anisotropy 1 hour before the FD is ∼0.7% (Belov et al. 2008), which agrees with the result for FDs with SSC (0.76%) and the FDs related to central sources (0.70%). However, for the large FDs there is an observed increase of the A_{xyb} almost up to 1%. As seen in table 2 the anisotropy one hour before the onset of the FD is almost the same (0.94 and 0.96), regardless of the location of the solar source (western or eastern) and its value significantly exceeds the typical value of anisotropy during quiet conditions (Abunina et al. 2013b). This, apparently, is a consequence of an increase of the CR density gradient in this part of the solar wind disturbance. This confirms the assumption that increased vector anisotropy is one of the typical precursors of FDs (Belov et al. 2008; Papailiou et al. 2012).

3.2 FDs in relation to solar sources

Average values of different parameters connected to the FDs under investigation are shown in table 3. Central and eastern sources not only provide more FDs, but also the FDs related to those sources are significantly larger regarding the magnitude in comparison to western sources (Belov 2008).

	87 FDs SSC, AF ≥ 4%, quiet background, identified solar source (−60° ≤ heliolong. ≤ 60°)		
Parameter	Western sources	Eastern sources	Central sources
A_F (%)	5.16 ± 0.56	5.59 ± 0.61	6.64 ± 0.57
A_{xymax} (%)	2.58 ± 0.2	2.22 ± 0.14	2.73 ± 0.18
A_{xyb} (%)	1.350 ± 0.143	1.296 ± 0.139	1.262 ± 0.144
Kp_{max}	6.75 ± 0.30	6.42 ± 0.25	6.8 ± 0.23
Ap_{max} (2nT)	138.6 ± 15.9	121.6 ± 15.0	139.9 ± 13.0
Dst_{min} (nT)	-115.7 ± 15.3	-105.7 ± 13.4	-135.9 ± 14.8
B_{max} (nT)	22.56 ± 2.29	24.77 ± 2.20	27.07 ± 1.75
V_{max} (km s^{-1})	660.5 ± 36.3	614.5 ± 26.9	660.2 ± 23.2
t_{min} (hour)	18.35 ± 2.28	22.61 ± 2.12	20.42 ± 1.67

Table 3: Average values of different parameters of the large FDs related to western, eastern and central sources.

However, FDs related to western sources are characterized by higher values of A_{xyb} (Papailiou et al. 2013). On the other hand, the maximum anisotropy for central sources is the highest (table 3), but there is a noteworthy difference between A_{xymax} for western (2.58%) and eastern sources (2.22%). FDs connected to central sources evolved in a more disturbed interplanetary medium (highest values for solar wind speed and IMF intensity are 660.2kms^{-1} and 27.07nT respectively) and are accompanied by strong geomagnetic activity, i.e. Dst_{min} = -135.9nT, Kp_{max} = 6.8 and Ap_{max} = 139.9. Geomagnetic activity is more pronounced for FDs related to western sources (Dst_{min} = -115.7nT, Kp_{max} = 6.75 and Ap_{max} = 138.6) rather than those connected to eastern sources (Dst_{min} = -105.7nT, Kp_{max} = 6.42 and Ap_{max} = 121.6), although the difference is not so big. Moreover, FDs connected to western sources reach the minimum more rapidly (t_{min} = 18.35hrs) than those related to eastern or central sources, which develop more slowly (t_{min} = 22.61hrs and t_{min} = 20.42hrs) (Abunina et al. 2013a).

4. Discussion and conclusion

This study refers to a group of large FDs, i.e. FDs with magnitude ≥4% for particles of 10GV which evolve in a quiet background (with a time difference of 48 and 18 hours from the previous and next event respectively), with identified solar sources and which were accompanied by an SSC. The FDs were selected from the IZMIRAN Forbush effects and interplanetary disturbances database and cover the time period from 1967 to 2017. These events were grouped into three categories according to the heliolongitude of their solar sources.

The features of the events with different solar sources are highlighted and summarized as follows: a) Large FDs (≥4%) related to central or eastern sources are more often observed, whereas events from western sources are the rarest, b) The magnitude of the FDs connected to western solar sources seems to be somewhat smaller than that one of eastern or central sources, c) FDs connected to western sources have a shorter life span in comparison to FDs connected to eastern or central sources which present a slower development, d) The averaged anisotropy one hour before the SSC is increased for all groups, e) The anisotropy one hour before the SSC is somewhat greater in FDs related to western sources than those related to eastern or central sources, f) Increased vector anisotropy is one of the typical precursors of FDs, g) FDs related to central sources evolved in more disturbed interplanetary conditions, which is reflected in a larger IMF increase, h) In general large FDs (≥4%) are accompanied by moderate geomagnetic storms, however, some events are related to severe or even extreme geomagnetic conditions.

References

Abunin, A., Abunina, M., Belov, A., et al. 2013, J. Physics: Conf. Series, 409, DOI: https://dx.doi.org/10.1088/1742-6596/409/1/012165

Abunina, M., Abunin, A., Belov, A. et al. 2013a, Geomagn. Aeronomy 53, 10, DOI: https://dx.doi.org/10.1134/S0016793213010027

Abunina, M., Abunin, A., Belov, A. et al. 2013b, Geomagn. Aeronomy 53, 561, DOI: https://dx.doi.org/10.1134/S0016793213050022

Belov, A.V., 2008, Gopalswamy, N., Webb, D.F. (eds.), Universal Heliophysical Processes, Proc. IAU Sympos, 257, Cambridge Univ. Press, 439, DOI: https://dx.doi.org/10.1017/S1743921309029676

Belov, A., Dryn, E., Eroshenko, E., et al. 2008, Kiraly, P., Kudela, K., Stehlik, M., Wolfendale, A.W. (eds.), Proc. 21st ECRS, Institute of Experimental Physics, Slovak Academy of Sciences, Kosice, Slovakia, 347

Belov, A., Abunin, A., Abunina, M., et al. 2014, Solar Phys. 289, 3949, DOI: https://dx.doi.org/10.1007/s11207-014-0534-6

Belov, A., Eroshenko, E., Yanke, V., et al. 2018, Solar Phys, 293, 68, DOI: https://dx.doi.org/10.1007/s11207-018-1277-6

Cane, H., 2000, Space Sci. Rev. 93, 55, DOI: https://dx.doi.org/10.1023/A:1026532125747

Kryakunova, O., Belov, A., Abunin, A., et al. 2015, J. Physics: Conf. Series, 632, DOI: https://dx.doi.org/10.1088/1742-6596/632/1/012062

Melkumyan, A., Belov, A., Abunina, M., et al. 2018, Geomagn. Aeronomy 58, 615, DOI: https://doi.org/10.1134/S0016793218050109

Melkumyan, A., Belov, A., Abunina, M., et al. 2019, Solar-Terres. Physics, 5, 28, DOI: https://dx.doi.org/10.12737/stp-51201904

Papailiou, M., Mavromichalaki, H., Belov,A., et al. 2012, Solar Phys. 276, 337, DOI: https://dx.doi.org/10.1007/s11207-011-9888-1

Papailiou, M., Abunina, M., Mavromichalaki, H., et al. 2013, Solar Phys. 283, 557, DOI: https://dx.doi.org/10.1007/s11207-013-0231-x

Papaioannou, A., Malandraki, O., Belov, A., et al. 2010, Solar Phys. 266, 181, DOI: https://dx.doi.org/10.1007/s11207-010-9601-9

Usoskin, I.G., Braun, I., Gladysheva, O. G., et al. 2008, J. Geophys. Res. Space Phys. 113, DOI: https://dx.doi.org/10.1029/2007JA012955

Cosmic ray studies with neutron detectors | Volume 1 (2021)
KIEL-UP • DOI: 10.38072/2748-3150/p16

Local intermittency measure analysis of neutron monitor data

Alexander MacKinnon[1], **Sam Rennie**[2]

Correspondence
[1] School of Physics and Astronomy, University of Glasgow, UK, alexander.mackinnon@glasgow.ac.uk
[2] Department of Physics and Mathematics, Nottingham Trent University, UK; School of Physics and Astronomy, University of Glasgow, UK, sam.rennie99@googlemail.com

Keywords
wavelets; time series; neutron monitors

Abstract
Local Intermittency Measure (LIM) is a development of wavelet analysis particularly suited to the diagnosis of isolated, intermittent events in time series. We construct LIM scalograms of Neutron Monitor (NM) data for an example each of a large GLE and a Forbush decrease. Both kinds of event show distinctive LIM signatures. In the case of the Forbush decrease the method also identifies a second, much smaller event that took place in the same time period. LIM may thus be a useful tool for automated or semi-automated detection of such events in NM data.

1. Introduction

The data provided by the global neutron monitor (NM) network offer a detailed look at many aspects of solar high-energy phenomena and solar-terrestrial interactions. Semi-regular changes in count rates reflect known periodicities in solar phenomena: the solar rotation rate, the activity cycle. Fourier and wavelet decompositions of the NM count rate time series have been used to extract information about such quasi-periodic behaviour (e.g. Kudela et al. 2010). Some of the most interesting features of NM data, however, are exceptional, one-off events such as ground level enhancements (GLE) and Forbush decreases (FD). Time series analysis methods focusing on quasi-periodic behaviour may not be the best tools for studying them. Here we suggest that Local Intermittency Measure (LIM) may be a useful tool for identifying and characterising such events in NM data. LIM is an application of wavelet analysis first introduced in the study of turbulence in fluids (Farge et al. 1990; Farge, 1992). It has been applied to solar wind data (Bruno et al. 1999), to AE-index data (Consolini & Chang 1994) and to solar flare X-ray (Dinkelaker & MacKinnon 2013a, b) and microwave (Gimenez de Castro et al. 2016) data. Here we give a preliminary exploration of its utility for characterising intermittent events in NM data. In the next section we give more details of LIM formalism and what it says about a time series before applying it to NM data to show that it can be effective at identifying GLEs and FDs. Section 4 offers some concluding comments.

KIEL-UP • DOI: 10.38072/2748-3150/p16

2. LIM introduced and applied to NM data

2.1 Wavelets and LIM

Let X_j be a series of measurements at equally spaced times j = 1…N. Assuming a wavelet basis function $\psi(t)$ the time *(t)* and scale (τ) dependent amplitudes A(t,τ) are constructed (e.g. Torrence & Compo 1998) as

$$A(t,\tau) = \sum_{j=1}^{N} \psi^* \left(\frac{(j-t)}{\tau} \right) X_j \tag{1}$$

We calculate the mean (time-averaged) power at each scale:

$$W(\tau) = \frac{1}{N} \sum_{j=1}^{N} \left| A(j,\tau) \right|^2 \tag{2}$$

and define the LIM $\Lambda(t,\tau)$ as

$$\Lambda(t,\tau) = \frac{\left| A(t,\tau) \right|^2}{W(\tau)} \tag{3}$$

Thus LIM renormalises the wavelet amplitudes in such a way that $\Lambda(t,\tau) > 1$ picks out times at which fluctuations on some scale t are over-represented, compared to the average behaviour of the time series. The square of the LIM gives an estimator for the contribution to the kurtosis K_4 of the distribution of time series increments from fluctuations on scale t (Meneveau 1991). $K_4 = 3$ for a gaussian distribution so the requirement $\Lambda^2(t,\tau) > 3$ identifies times and scales at which the time series looks inconsistent with a gaussian random walk. See Bruno et al (1999), Dinkelaker and MacKinnon (2013a), and MacKinnon and Rennie (in preparation) for more on interpretation.

Results below are obtained using the Morlet wavelet function which we adopted as standard for this work after some experimentation. We find that it offers a reasonable compromise between accuracy in time-space and in scale-space which is necessary for estimating both the onset times and durations of intermittent events.

KIEL-UP • DOI: 10.38072/2748-3150/p16

2.2 GLE of 6 November 1997

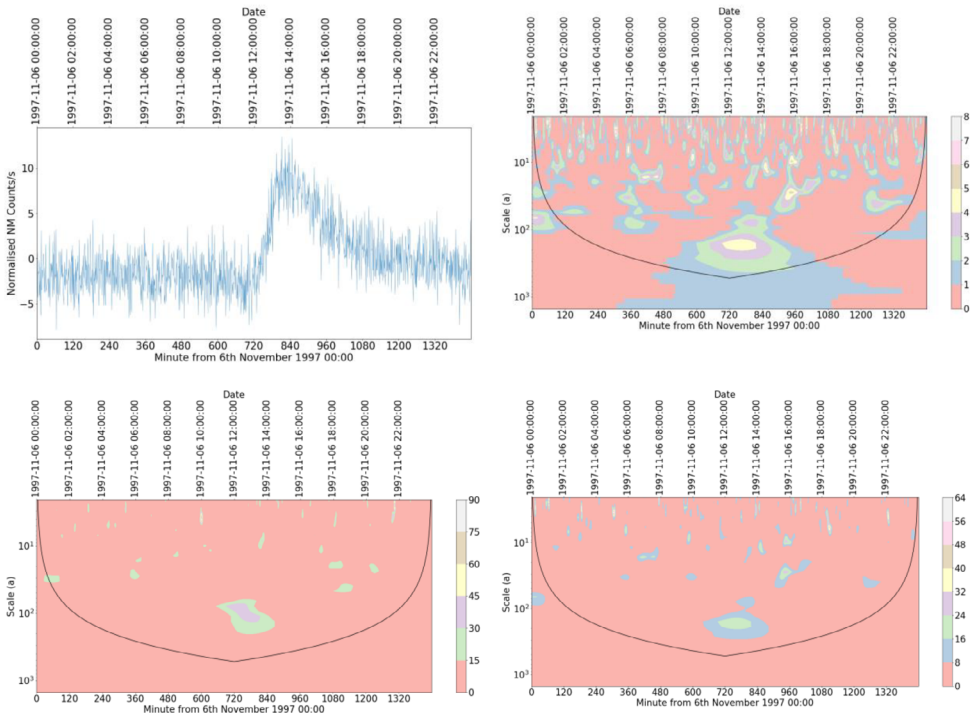

Figure 1: Clockwise from top left: Oulu NM count rate during GLE55 on 6 November 1997; Scalogram showing LIM of Oulu data as a function of time and scale during GLE55; LIM² calculated from Oulu data; LIM² calculated from data from the Terre Adelie NM.

Here we investigate the LIM signatures of a couple of large transient events, firstly GLE55 which took place on 6 November 1997. Figure 1 shows data for this event from the Oulu NM together with scalograms showing the time and scale behaviour of LIM and LIM² during this event. The scalograms show only values satisfying $\Lambda > 1$ or $\Lambda^2 > 3$ as discussed above. The occurrence of the GLE is clearly seen as an episode of large LIM values centred on $\sim$1230 on 6/11/97, at scales of about 200 min which corresponds well with the sudden observed spike in and consequent initial recovery of the secondary cosmic ray flux. Random fluctuations naturally result in many briefer episodes with smaller amplitudes. Most of these are eliminated with the more stringent $\Lambda^2 > 3$ criterion. The LIM² signature of the GLE is also seen in a scalogram calculated using data from the Terre Adelie NM. We can be confident in the reality of this feature since it is present in scalograms constructed using data from two different NM.

KIEL-UP • DOI: 10.38072/2748-3150/p16

2.3 Forbush decreases: 14 – 18 February 2011

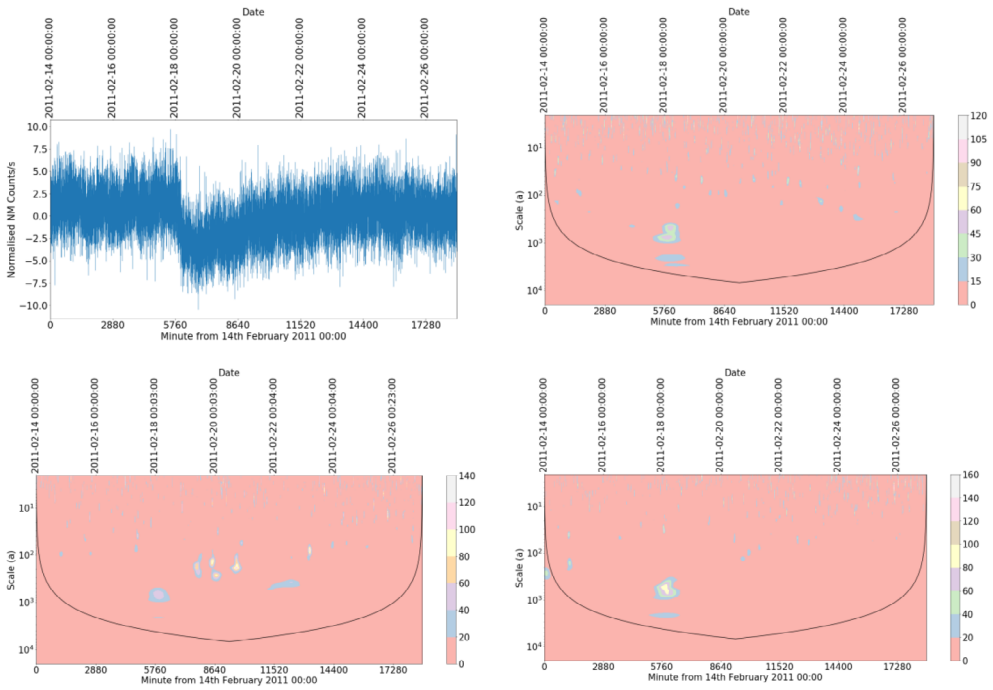

Figure 2: Clockwise from top left: Oulu NM data for 14-26 February 2011; LIM² scalogram of the Oulu data; LIM² scalogram of Moscow NM data for the same interval; LIM² scalogram of Kerguelen NM data for the same interval.

Figure 2 shows data from the Oulu NM for the period 14 – 26 February 2011, clearly showing the large Forbush decrease that took place on 18 February (Lingri et al. 2016). We show LIM² scalograms calculated using these data as well as data from the Kerguelen and Moscow NMs. All three scalograms show a well-defined peak in LIM at the time of the Forbush decrease, at a scale of about 800-900 min which seems to correspond well with the initial, sudden observed decrease in the neutron monitor count rate. All three also show many other features but these are mostly unique to a single NM and thus attributed to data noise. However the scalograms from the Oulu and Kerguelen NM's both show a local maximum on a scale of $\sim$100 min, at about 0000 on 15 February. There are maxima in the Moscow data at similar scales at about the same time and similar features are seen in scalograms from several other NMs (Rennie, 2019). These features coincide with the occurrence of a small FD, identified in the Izmiran online catalogue (http://spaceweather.izmiran.ru/eng/dbs.html, last accessed April 8, 2021) and attributed to a coronal hole. We conclude that the LIM technique has identified the occurrence of this FD, even though it is barely evident to the eye in the high resolution Oulu data shown in figure 2.

3. Discussion and conclusions

LIM takes the established method of wavelet analysis and asks when the distribution of increments becomes statistically inconsistent with the previous, average behaviour. In this sense it is similar to the automated FD method described by Light et al. (2020), while also yielding information on the dominant scales in identified events.

KIEL-UP • DOI: 10.38072/2748-3150/p16

The GLE and FD studied here were selected as random examples. We found that, while local maxima of LIM arise, as expected, from data noise, the events studied here gave rise to well-defined signatures in data from more than one NM. The LIM^2 scalograms also picked out a much weaker FD, in addition to the large event deliberately selected for study. We conclude that LIM appears to be a promising technique for automated detection of transient events in NM data. We are now testing its performance on a larger sample of data and exploring further its potential for yielding novel diagnostics of space weather events. Results of this fuller study will be reported elsewhere in due course.

Acknowledgments

We thank the NMDB project (https://www.nmdb.eu/) and the PIs of the Moscow, Terre Adelie, Oulu and Kerguelen NM for providing the data and enabling access. Computer code to construct and display LIM was developed from the wavelet software provided by C. Torrence and G. Compo, available at URL: http://atoc.colorado.edu/research/wavelets/.

References

Bruno, R., Bavassano, B., Pietropaolo, E., Carbone, V., Veltri, P., 1999, Geophys. Res. Letts. 26, 3158
Consolini, G., Chang, T., 2002, JASTP 64, 541
Dinkelaker, A., MacKinnon, A. L., 2013a, Sol. Phys. 282, 471
Dinkelaker, A., MacKinnon, A. L., 2013b, Sol. Phys. 282, 483
Farge, M., 1992, Ann. Rev. Fluid Mech. 24, 395
Farge, M., Holschneider, M., Colonna, J. F., 1990, Moffatt, H. K. (ed.), Topological Fluid Mechanics, Cambridge University Press
Gimenez de Castro, G., Simões, P. J. A., Raulin, J.-P., Guimarães, O. M., 2016, Sol. Phys. 291, 2003
Kudela, K., Mavromichalaki, H., Papaioannou, A., Gerontidou, M., 2010, Sol. Phys. 266, 173
Light, C., Bindi, V., Consolandi, C., Corti, C., Freeman, C., Kuhlman, A., Palermo, M., Wang, S., 2020, ApJ 896, 133
Lingri, D. Mavromichalaki, H., Belov, A., Eroshenko, E., Yanke, V., Abunin, A., Abunina, M., 2016, Sol. Phys. 291, 1025
Meneveau, C., 1991 J Fluid Mech. 232, 469
Rennie, S, 2019, MSc project report, University of Glasgow
Torrence, C., Compo G. P., 1998, Bull. Am. Met. Soc. 79, 61

Cosmic ray studies with neutron detectors | Volume 1 (2021)
KIEL-UP •DOI: 10.38072/2748-3150/p17

NMDB database and global survey method

Petr Yu. Gololobov, Sergey A. Starodubtsev, Vladislav G. Grigoryev, Anton S. Zverev

Correspondence
Yu.G. Shafer Institute of Cosmophysical Research and Aeronomy of SB RAS, Yakutsk, Russia, gpeter@ikfia.ysn.ru

Keywords
cosmic rays; neutron monitor; global survey method

Abstract
The method of a global survey developed in the 1970s allows using a world-wide network of neutron monitor stations as a single multidirectional device. Wherein, receiving characteristics of each device, which reflects their geometries and geographical positions, are taken into account. Such an approach makes it possible to define the first two angular moments of the distribution function of cosmic rays in the interplanetary space at each hour of observation. With the creation in 2008/2009 and subsequent development of an international database of neutron monitors NMDB, for the first time it appeared an opportunity to use the global survey method in real-time mode. Such a situation creates a unique possibility to use the results not only for scientific researches but also for space weather forecasting. To use the data of the world-wide network of neutron monitors it is necessary to carry preliminary preparations. Thereby, in the current work, the main attention is attracted to a solution to some practical questions that arise when using the NMDB in real-time.

1. Introduction

Global Survey Method (GSM) (Altukhov et al. 1969) was developed in the late 1960s in the Yu.G. Shafer Institute of Cosmophysical Research and Aeronomy and allows using the entire world network of neutron monitor (NM) stations as a single multidirectional device oriented at each measured moment in different directions. This approach makes it possible to determine the dynamics of the angular distribution of cosmic rays (CRs) with a temporal resolution that depends on the capabilities of the network devices. The use of such methods makes it possible to carry out studies of various short-term processes of solar-terrestrial relationships and space weather using CR measurements.

Despite the long existence, more than half a century, of the method, the modernization of the GSM continues to this day. One of the important stages in the development of the GSM is associated with the creation of the international database NMDB in 2007. This database made it possible to implement the GSM in real-time, which meant the application of the method for monitoring and forecasting space weather. Subsequent studies in this direction are presented in the works by Grigoryev et al. (2015, 2017, 2019). This paper presents the current state of the method and focuses on some practical issues of the implementation of the GSM based on NMDB data.

2. Method

2.1 Global survey method

GSM is a variant of the spherical analysis of experimental NM data and is based on so-called receiving vectors (Krymsky et al. 1981). The angular distribution of CR, when represented as a series

KIEL-UP • DOI: 10.38072/2748-3150/p17

of spherical functions, will be described by the multidimensional vector $\vec{A} = (a_n^m, b_n^m)$, where a_n^m and b_n^m are the decomposition coefficients, and $n \geq m \geq 0$. Determining the corresponding receiving vectors $\overrightarrow{z_n^{m,j}} = (x_n^{m,j}, y_n^{m,j})$, taking into account the relationship between the primary CR distribution and the intensity measured by ground-based detectors I^j, we have:

$$I^j = \sum_{n=0}^{\infty} \sum_{m=0}^{n} \left(a_n^m x_n^{m,j} + b_n^m y_n^{m,j} \right). \tag{1}$$

If there is a sufficient number of NM stations, it is possible to construct a system of independent equations, the solution of which will make it possible to determine the required angular distribution of CR $\vec{A}$ from the NM measurements. If it is required to determine the first spherical harmonic (diurnal anisotropy), it is necessary to have data from at least 4 evenly spaced NM stations, and for the second spherical harmonic (semidiurnal anisotropy) - 9.

Since the used NM stations have different energy sensitivities, it is necessary to introduce normalizing factors that bring the instrument readings to a certain nominal one:

$$k_n^j = \frac{\int_{R_c^j}^{\infty} W^j(E) f_n(E) dE}{\int_{R_c^j}^{\infty} W^0(E) f_n(E) dE}, \tag{2}$$

where E is the particle energy, $W^j(E)$ is the coupling coefficient (Dorman 1957) of the j-th NM station and $f_n(E)$ is the assumed energy spectrum of the n-th order variations.
Based on the above the equation (1) becomes:

$$I^j = \sum_{n=0}^{\infty} \sum_{m=0}^{n} \left(a_n^m x_n^{m,j} + b_n^m y_n^{m,j} \right) k_n^j. \tag{3}$$

Reducing equation (3) to matrix form, we obtain:

$$I = MA, \tag{4}$$

where M is the matrix of receiving vectors, and I and A are vectors of the observational data and the expected CR distribution, respectively. The solution to equation (4) has the form:

$$I = \left(M^T M \right)^{-1} M^T I \tag{5}$$

The resulting system of equations is solved by the least-squares method under the assumption that the series is rapidly decaying.

In practice, the CR intensity included in equation (3) observed by the detector may contain oscillations that are not associated with variations in the primary intensity, for example, low-frequency instrumental oscillations. Therefore, when solving (3), the high-frequency component of the intensity $I_{h.f.}$ is used, which is found from the equation

$$I_{h.f.}(t) = I(t) - \sum_{t'=t+T}^{t+T} \frac{I(t')}{(2T+1)}, \tag{6}$$

where $I(t)$ is the observed intensity, and T is the number of points of moving average, which can be taken equal to 18 hours.

KIEL-UP • DOI: 10.38072/2748-3150/p17

2.2 Using NMDB data in the global survey method

The database of neutron monitors NMDB (https://www.nmdb.eu/nest/help.php#helpstations, last accessed April 8, 2021) was created in 2007. The value of such a database lies, first of all, in the presentation of data from the global NM network in real-time, as well as the provision of high temporal resolution data in a unified form. Over 50 stations are presented in NMDB, which are distributed throughout the planet (figure 1). The description of the database, as well as the areas of scientific problems in which it is applied, are presented in the work (Mavromichalaki et al. 2011).

It is important to note that the effective CR energies recorded by the NMDB can be roughly estimated as 10-25 GeV.

Implementation of the GSM using the NMDB data allows tracking the dynamics of the CR angular distribution in real-time. However, this may pose some obstacles. First, the selection of the high-frequency component by equation (6) loses its meaning due to the absence of subsequent points; secondly, the often occurring registration errors (hardware failures) at various NM stations can significantly affect the result of the implementation of the GSM. Therefore, to take into account these problems, the following methods of processing primary data and analyzing the final results are used. In contrast to equation (6), the primary filtering method is replaced by using a linear trend for the last 24 hours, which is determined by the least-squares method. In this case, $I_{h.f.}(t)$ will be determined as the difference between the observed variations and the trend. Errors in the registration of individual stations of the NM network can be taken into account by analyzing the output data of the GSM. Comparing the obtained solutions of the system (5) and the primary equation (4), it is possible, using Chauvenet's criterion (Taylor 1985), to exclude those NM stations whose data are more divergent from the rest.

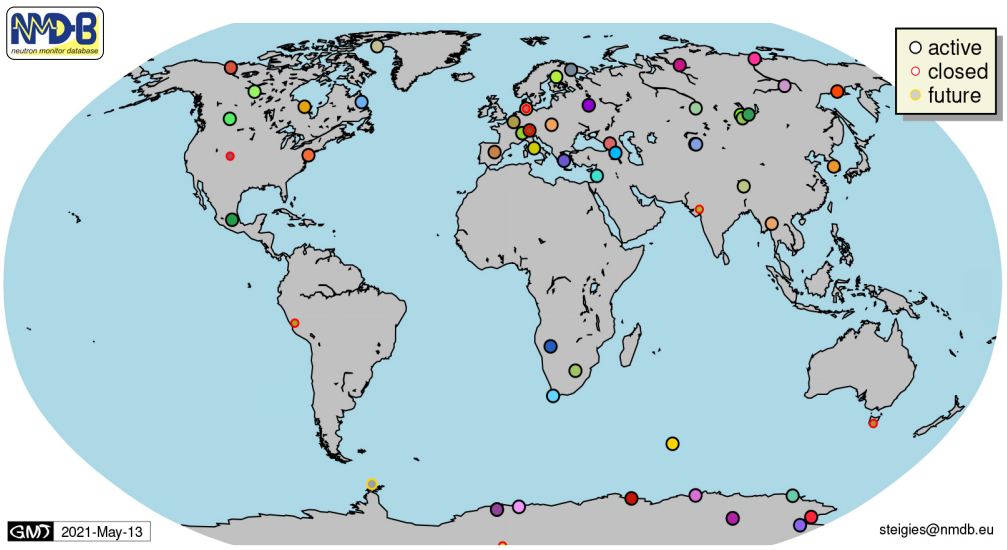

Figure 1: Geographic distribution of NM stations included in the NMDB. Station locations are marked with colored circles, ©2021 Christian T. Steigies.

2.3 Forecasting geomagnetic storms

The creation of the NMDB network in 2007 served as an impetus for the implementation of the GSM method in real-time and in the study of the possibilities of the practical application of its results. The work carried out over the past 10 years in this direction (Grigoryev et al. 2011a, 2015, 2017, 2019; Starodubtsev et al. 2019) showed that it is possible to predict geomagnetic storms. As it turned out, the parameters of the angular distribution of CRs, identified using the GSM, actively respond to the approach of geoeffective disturbances of the interplanetary medium to the Earth. Analysis of the results of the GSM for 2012-2018 made it possible to establish that anomalous changes in the magnitude and direction of the first harmonic vector (a_{11} and b_{11}) and the amplitudes of the zonal (north-south) components (a_{00}, a_{10} and a_{20}) of the CR distribution can serve as predictors of geomagnetic disturbances. For the zonal components, the critical values of individual positive values or their sums were determined, the excess of which, with a probability of 75%, is a precursor of a sharp decrease of Dst-index at the beginning of the geomagnetic storm (Grigoryev et al. 2019).

The results of the implementation of the GSM according to the NMDB data are presented online in real-time at the link http://www.ysn.ru/ ~ starodub/SpaceWeather/global_survey_real_time.html (last accessed April 8, 2021). Here, the behavior of the main parameters of the CR distribution for the last 72 hours is presented: isotropic intensity I, the modulus of the harmonic vector and the sums of positive and negative values of the zonal harmonics, as well as the values of the components and vectors of the first and second harmonics in the GSE coordinate system.

3. Conclusions

A brief description of the implementation, based on data from the world network NMDB, of the GSM in real-time is given. Based on the analysis of the obtained parameters of the CR angular distribution, the state of the interplanetary medium is monitored and geomagnetic disturbances are predicted. Monitoring results in real-time are displayed on the internet through the Web link http://www.ysn.ru/ ~ starodub/SpaceWeather/global_survey_real_time.html (last accessed April 8, 2021).

Acknowledgments

The work is carried out with partial support of the ShICRA Basic Research Program no. AAAA-A17-117021450058-6 and the RFBR grants Nos. 18-42-140002-r_a.
We acknowledge the NMDB database (https://www.nmdb.eu/), founded under the European Union's FP7 programme (contract no. 213007) for providing data.

References

Altukhov, A. M., Krymsky, G. F., Kuzmin, A. I., 1969, Acta Physica, 29, 457

Dorman, L. I., 1957, Variatsii kosmicheskikh luchei [Cosmic Ray Variations], Gostekhizdat Publ. (in Russian)

Grigoryev, V. G., Starodubtsev, S. A., 2011a, Proc. 32nd ICRC, 11, 99, DOI: https://dx.doi.org/10.7529/ICRC2011/V11/0359

Grigoryev, V. G., Starodubtsev, S. A., Krymsky, G. F., et al., 2011b, Proc. 32nd ICRC, 11, 9, https://galprop.stanford.edu/elibrary/icrc/2011/papers/SH3.6/icrc0360.pdf (last accessed May 20, 2021)

Grigoryev, V. G., Starodubtsev, S. A., 2015, Bull. of the RAS: Physics, 79, 649, DOI: https://dx.doi.org/10.3103/S1062873815050226

Grigoryev, V. G., Starodubtsev, S. A., Gololobov, P. Yu., 2017, Bull. of the RAS: Physics, 81, 200, DOI: https://dx.doi.org/10.3103/S1062873817020198

Grigoryev, V. G., Starodubtsev, S. A., Gololobov, P. Yu., 2019, Solar-Terrestrial Physics, 5, 93, DOI: https://dx.doi.org/10.12737/stp-53201911

Krymsky G. F., Kuzmin, A. I., Krivoshapkin, P. A., et al., 1981, Kosmicheskie luchi i solnechniy veter [Cosmic rays and solar wind], ed. Shafer, G.V., Nauka Publ. (in Russian)

Mavromichalaki, H., Papaioannou, P., Plainaki, C., 2011, Advances in Space Research, 47, 2210, DOI: https://dx.doi.org/10.1016/j.asr.2010.02.019

KIEL-UP • DOI: 10.38072/2748-3150/p17

Starodubtsev, S. A, Grigoryev, V. G., Gololobov, P. Yu., 2019, Journal of Physics: Conference Series, 1181, 012011, DOI: https://dx.doi.org/10.1088/1742-6596/1181/1/012011

Taylor, J. R., 1982, An Introduction to Error Analysis: Study of Uncertainties in Physical Measurements, ed. McGuire, A., University Science Books Publ.

Questions and answers

Rolf Bütikofer: Do you issue spwx alarms by SMS or e-mail ? Who are the stakeholders of your application?
Answer: The only technique of alert is the link https://www.ysn.ru/~starodub/SpaceWeather/global_survey_real_time.html (last accessed April 8, 2021).

Hazel Bain: Does the method forecast the dst value?
Answer: The method predicts the geomagnetic storms with Dst<-50 nT.

Monica Laurenza: What is the false alarm rate?
Answer: Statistical analysis of the results shows that the effectiveness of forecasting ~75%. It strongly depends on the critical values that are selected.

Christian T. Steigies: How do you access real-time data from NMDB? Via NEST or the real-time files?
Answer: The real-time files.

Christopher Light: Are you predicting that a geomagnetic storm will occur? Or are you predicting the magnitude of the dst disturbance?
Answer: Yes, we predict that a geomagnetic storm will occur. And Dst<-50 nT.

Eugenia Eroshenko: What do you do with occasional spike or drift in the stations if it occurs?
Answer: They can be eliminated using Chauvinet's criterion (see the text for details)

John Clem: How is the accuracy of your SW predictions dependent on the global NM viewing resolution?
Answer: The accuracy is highly dependent on the distribution of stations. This especially applies to the station collecting CRs from the regions of the Pacific Ocean and Earth's poles.

Cosmic ray studies with neutron detectors | Volume 1 (2021)
KIEL-UP • DOI: 10.38072/2748-3150/v1

Session 4: Abstracts

Extension of the global NM network: optimization for space weather purposes

Aleksandar Mishev, Ilya Usoskin

Correspondence
Space Physics and Astronomy Research Unit, University of Oulu, Finland

Over the years the global neutron monitor (NM) network was successfully used to study cosmic ray variations and fluxes of solar energetic solar particles (SEPs). Recently, it has been used also for space weather purposes, specifically for alerts and the related assessment of exposure to radiation. Here, we review the current status and applications of the global NM network and discuss its capability to study SEPs, namely assessment of their spectral and angular distribution, during large ground level enhancements. We discuss the existing regional gaps in the network and propose an improvement of space weather services and application of the global NM network by a plan for an extension of the existing network with several new monitors. We discuss the ability of the optimized global NM network to study various populations of SEPs and to provide reliable space weather services.

High-energy magnetospheric electron enhancements in 22-24 solar activity cycles and Forbush effects

Olga Kryakunova [1], Anatoly Belov [2], Artem Abunin [2], Nikolay Nikolayevskiy [1], Maria Abunina [2], Uakaskan Baideldinov [1], Suleimen Sultangazinov [1], Botakoz Seifullina [1], Irina Tsepakina [1]

Correspondence
[1] Institute of Ionosphere, Almaty, Kazakhstan
[2] Pushkov Institute of Terrestrial Magnetism, Ionosphere and Radio Wave Propagation (IZMIRAN), Moscow, Russia

The behavior of high-energy magnetospheric electrons with an energy >2 MeV in geostationary orbits in 22-24 solar activity cycles is considered. The daily fluence is selected as the main characteristic of the behavior of electrons measured by GOES satellites. In this work, we assumed that the electron flux begins to grow when the daily fluence exceeds 10^8 electrons/(cm^2 sr day). It is shown that the largest number of electron increases occurs in the declining phase of solar activity cycles, when there are more geoeffective coronal holes. It was obtained that in general in 2003-2015 there is a correspondence between the behavior of the number of electron increases, the square of geoeffective coronal holes and magnetic flux from them. It was shown that during very big electron enhancements, big Forbush effects recorded by the ground-based network of neutron monitors are observed.

KIEL-UP • DOI: 10.38072/2748-3150/v1

Status of a European network of SEVAN detectors

Ashot Chilingarian[1], **Tigran Karapetyan**[1], **Johannes Knapp**[2], **Balabek Sargsyan**[1], **Michael Walter**[2]

Correspondence
[1] A.I. Alikhanyan National Science Laboratory (Yerevan Physics Institute), Armenia
[2] Deutsches Elektronen-Synchrotron (DESY), Zeuthen, Germany

The Space Environment Viewing and Analysis Network (SEVAN) aims to improve fundamental research on particle acceleration in the vicinity of the sun, on space weather and on high-energy physics in the atmosphere and lightning initiation. This new type of particle detector simultaneously measures fluxes of secondary cosmic rays (electrons, photons, muons and neutrons) from solar modulation and particle acceleration in a thunderstorm atmosphere. SEVAN modules are operating at the Aragats Space Environmental Center (ASEC) in Armenia, Croatia, Bulgaria, Slovakia, the Czech Republic, and Germany (DESY sites in Hamburg and Zeuthen, since 2019). SEVAN detectors provide advantages over detectors measuring only individual particles. Simultaneously and with high time resolution, they measure count rates of low energy charged, neutral particles and high energy muons. With SEVAN detectors we probe different populations of primary cosmic rays with rigidities up to GV; provide spectra of solar energetic particles (SEPs) and their spectral features; record ground level enhancements (GLEs) initiated by solar protons and neutrons; show energy dependences of the barometric coefficients and diurnal waves; enlarge the reliability of Space Weather alerts due to simultaneous detection of fluxes of different particles; detect thunderstorm ground enhancements (TGEs) in gamma ray and charged particle fluxes; shed light on cloud electrification by measuring surges and deficits of particle fluxes; record runaway electron acceleration during thunderstorms and lightning initiation. We present the detectors and their performance over 10 years of operation and give an overview of a wide range of results that have been achieved with such a simple and cheap detector system.

A new directional muon telescope for space weather application

Sindulfo Ayuso, **Juan José Blanco**, **Juan Ignacio García Tejedor**, **Oscar García Población**, **Iván Vrublevskyy**, **José Medina**

Correspondence
Universidad de Alcalá, Castilla-La Mancha Neutron Monitor, Spain

Primary cosmic rays (CR) are modulated by solar disturbances like coronal mass ejections (CME) and shock waves before they reach the Earth. The interactions of primary cosmic rays with air molecules nuclei at the top of the atmosphere originate a shower of secondary particles including muons and neutrons which reach the Earth's surface. This phenomenon is very useful in space weather since geomagnetic storms can be forecasted several hours in advance by ground-based cosmic ray detectors like neutron monitors and muon telescopes. Earth-bound CMEs and shock waves are detectable with multidirectional muon telescopes earlier than with neutron monitors because muon detectors respond to higher energy cosmic rays. Furthermore, the study of directionality may provide additional and valuable information about cosmic rays modulating events. However, multidirectional muon telescopes, as those of Nagoya (Japan), are not easily affordable because of their size and cost. In this work, we present the MITO design concept, useful in space weather, which uses only two scintillators (1 m^2) and eight photomultipliers (PMT). It has been conceived not only to achieve

KIEL-UP • DOI: 10.38072/2748-3150/v1

muon flux registering, but also muon arrival directions through the capture and analysis of multiple PMT pulse amplitude data. In this way, the number of scintillators and electronic components is reduced, simplifying its design and construction and reducing volume, weight and cost in comparison to other directional telescopes based on two-layer matrices, but obtaining similar angular resolution. The first prototype was shipped from Spain to Antarctica where it is now recording data and some preliminary results are also presented.

Kerguelen and Terre Adélie neutron monitors - a status report

Nicolas Fuller, Karl-Ludwig Klein

Correspondence
Observatoire de Paris, LESIA, Université PSL, CNRS, Sorbonne Université/ Université de Paris, France

We give a status report about the neutron monitors at Kerguelen Island and Terre Adélie (Antarctica), operated by the French Polar Institute (IPEV) and exploited by Paris Observatory. They contribute to the observational coverage of the Southern hemisphere of the Earth and are key elements of the implication of Paris Observatory in space weather activities. These include the monitoring of the radiation doses received by civil air crew in France in the framework of the SIEVERT programme conducted by the French Institute for Radio Protection and Nuclear Safety (IRSN) and the French contribution, within the Australia-Canada-France-Japan consortium, to the real-time space weather service for civil aviation worldwide under the auspices of ICAO. Ongoing activities with the two instruments will be outlined, together with technical problems that affect the reliable functioning of the instruments.

Cosmic ray stations of ISTP SB RAS

Anna Lukovnikova

Correspondence
Institute of Solar-Terrestrial Physics, Siberian Branch of Russian Academy of Sciences (ISTP SB RAS), Irkutsk, Russia

The global network includes 4 CR stations of ISTP SB RAS, equipped with NM64 neutron supermonitors: IRKUTSK, IRKUTSK 2, IRKUTSK 3 and NORILSK. The stations record the intensity of cosmic rays neutron component (statistical accuracy of hourly measurements ~ 0.1%) and pressure (accuracy of measurements ~ 0.1 mb). The Sayan spectrographic complex of cosmic rays was created in the 1970s, it includes the following CR stations: IRKUTSK (IRKT, Irkutsk), IRKUTSK 2 (IRK2, 2000 m, the Eastern Sayan), IRKUTSK 3 (IRK3, 3000 m, the Eastern Sayan). Server cgm.iszf.irk.ru is located in Irkutsk. The server collects data from 4 CR stations, processes them, publishes on each CR station web page, and transfers the data to NMDB. We consider the current state of our cosmic ray stations.

Session 5:

Neutron detector instrumentation

Cosmic ray studies with neutron detectors | Volume 1 (2021)
KIEL-UP • DOI: 10.38072/2748-3150/p18

A new neutron monitor at the Juan Carlos I Spanish Antarctic Station (Livingston Island-Antarctic Peninsula)

Juan José Blanco[1], **Óscar García Población**[1], **Juan Ignacio García Tejedor**[1], **Sindulfo Ayuso**[1], **Alejandro López-Comazzi**[1], **Iván Vrublevskyy**[1], **Christian T. Steigies**[2]

Correspondence
[1]CaLMa - Monitor de Neutrones de Castilla-La Mancha, Universidad de Alcalá, Madrid, Spain, juanjo.blanco@uah.es
[2]Extraterrestrial Physics,Institute of Experimental and Applied Physics, Kiel University, Germany

Keywords
cosmic ray; neutron monitor instrumentation

Abstract
Last January 2019, a new neutron monitor was installed at Juan Carlos I Spanish Antarctic Station (62° 39′ 46″ S, 60°23′20″ W, 12 m asl) located in Livingston Island (South Shetland Archipelago) close to the Antarctic Peninsula. The vertical rigidity cut-off for this new station is estimated as 3.52 GV. This new station (ORC) is composed of a BF3-based 3NM64 (ORCA) and 3 bare BF3 counters (ORCB). The neutron monitor is complemented by a muon telescope sharing a common room in a single stack. ORCA and ORCB with the Castilla-La Mancha neutron monitor (CaLMa) are the Spanish contributions to the Neutron Monitor Data Base. Because Juan Carlos I station is a summer station, one minute data is providing once a day during the Antarctic summer. One hour data are sent once a day during Antarctic winter. First measurements and future plans are provided in this work.

1. Introduction

Neutron monitors are not uniformly distributed around the World. The stations are concentrated mostly on the Northern hemisphere and Antarctica. Each neutron monitor is characterized by its altitude above sea level (asl) and vertical cut-off rigidity. Two of these neutron monitors are maintained by the Space Research Group of Alcalá University. One of then, CaLMa, is operating since mid 2012 in Guadalajara (Spain) 40°38'N, 3°9'W and 708 m above sea level (Medina et al. 2013). The second one, ORCA, has been recently installed (January 2019) at Juan Carlos I Spanish Antarctic Base (BAE). Both neutron monitors are part of the Neutron Monitor Data Base (NMDB 2009) although ORCA is not providing data yet.

2. Antarctic Cosmic Ray Observatory (ORCA)

2.1 ORCA location

Juan Carlos I Spanish Antarctic Base (BAE) is a summer research base located in Livingston Island, South Shetland Islands, Maritime Antarctica 62°39'46''S, 60°23'20''W, and 12 m asl. The location of the base and the penumbra analysis is shown in figure 1. The rigidity values at Juan Carlos I Spanish Antarctic Base on 2019-02-02 12:00:00 UT are R_L = 2.221 GV, R_U = 2.673 GV according to the results of the calculator at https://tools.izmiran.ru/ (last accessed May 31, 2021) using the IGRF

KIEL-UP • DOI: 10.38072/2748-3150/p18

model. For a flat spectrum, the effective rigidity of geomagnetic cutoff is R_{eff} = 2.487 GV. Its location, close to the Antarctic Peninsula, covers a gap in the global distribution of neutron monitors. LARC neutron monitor (Cordaro et al. 2012) was operative at King George Island, 134 km apart from Livingston Island, covering such gap in the neutron monitor global network but it is switched off nowadays. Close to the scientific module in BAE Juan Carlos I, in a thermally insulated container, the Antarctic Cosmic Ray Observatory (ORCA) was installed at the beginning of January 2019.

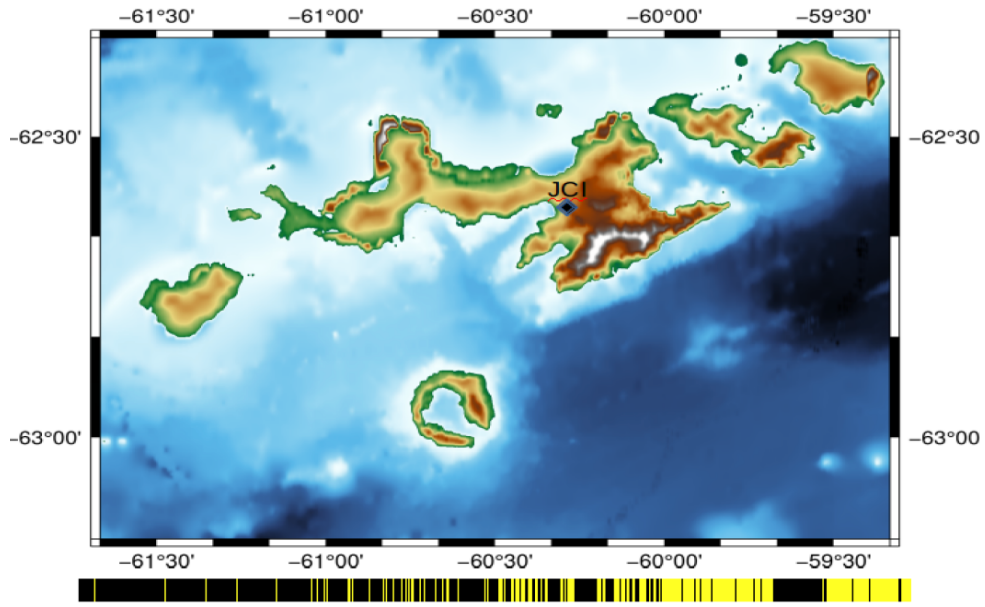

Figure 1: Map of Juan Carlos I location at Livingston Island with Penumbra at date 2019-01-02 12:00:00 UT. RL = 2.221 GV and RU = 2.673GV.

2.2 ORCA description

The Antarctic Cosmic Ray Observatory (ORCA) is an instrument to monitor the cosmic ray flux by the observation of secondary cosmic rays at ground level. It was designed to be operated at Juan Carlos I Spanish Antarctic Base and is made by a set of detectors with different targets and capabilities. ORCA is composed of a neutron detector (NEMO) and muon telescope (MITO) installed in a 20 feet container which is thermally isolated and environmentally controlled (figure 2).

The Neutron Monitor (NEMO) is composed of two groups of three proportional detectors. The counters in the first set are BP-28 detectors (NEMO-3NM64) and follow the NM64 standard, i. e. an outer reflector made of polyethylene, with lead producers in the form of lead rings around the moderator, a moderator also of polyethylene and the counter tube surrounded by the moderator. The second set is integrated by three bare, i. e. without a lead producer or polyethylene, LND2061 counters (NEMO-3BNM). NEMO-3NM64 and NEMO-3BNM measure neutrons at two different energy thresholds (bare versus lead surrounding counters). The signals from the proportional counter are preprocessed in a signal conditioning system before reaching the data acquisition system. This system consists of an FPGA with an IP core specifically designed for this application, and an embedded Linux Beaglebone Black system in which the capture code is executed, as well as the necessary corrections, the editing of the data and its subsequent publication in a database (Población et al. 2014). This system keeps its local clock synchronized using an NTP server equipped with a

KIEL-UP • DOI: 10.38072/2748-3150/p18

GPS receiver. Additionally, it also controls a Vaisala meteorologic station PTU301 Transmitter which provides pressure, temperature and relative humidity. The temperature/humidity probe composed of a Pt100 RTD Class F0.1 IEC 60751 and Vaisala HUMICAP 180C respectively (table 1).

The Muon Impact-Tracer Observer (MITO) is a telescope made by a stack of two (MITO-top and MITO-bottom) BC-400 organic scintillators (100 cm x 100 cm x 5 cm, poly-vinyl-toluene with 65% anthracene). Four photomultipliers (PMTs) are coupled to each scintillator by means of a pyramidal light guide. Each PMT collects the light reaching the lateral surface and generates a pulse which carries information about the distance between the particle impact point and the corresponding lateral surface of the BC-400 scintillator. Track impact point is calculated by comparison of the pulse height detected in the PMTs when they are working in coincidence. The two scintillators, impact points give us information about the muon incident direction. Both scintillators are placed at the top and bottom of a metallic structure 136,5 cm apart from each other with a 10 cm lead layer in between (figure 3).

MITO has two data acquisition systems operating in parallel, SAS and Aracne. SAS counts the impacts on the scintillator keeping those that follow four different coincidence channels, Top: the four PMTs in the upper scintillator, Bottom: the four PMTs in the bottom scintillator, coin8: the eight PMTs, i.e. particles that cross both scintillators, and Lateral: a combination of two PMTs in the upper scintillator located at a common lateral side and two PMTs in the bottom scintillator but at the opposite lateral side of the previous ones. Aracne records the highest pulse of all the PMTs gathered in particle detection. From them, it can select the events under the same coincidence channels as SAS. The pulse height analysis allows one to determine the impact point on the scintillators and with the two impact points, the particle trajectory throughout MITO can be reconstructed. MITO is operating in a one minute counting mode with four coincidence channels and an event to event storage of the pulse height recorded in every PMT simultaneously with a time resolution of 25 ns.

	NEMO 3NM64(ORCA)	**NEMO 3BNM(ORCB)**
Counter Type	BP28	LND2061
Effective diameter (mm)	148.5	149.1
Effective length (mm)	1908.0	1956.3
Cathode material	Stainless steel	Stainless steel
Gas filling	BF_3 (96% ^{10}B)	BF_3 (96% ^{10}B)
Gas pressure (mmHg)	200	200
Operational voltage (V)	-2700	1800
	MITO Top	**MITO Bottom**
Scintillator	BC400	BC400
Dimension (cm)	100x100x5	100x100x5
Operational voltage (V)	1200-1400	1000
PMT	4 R2154	4 R2154
	Vaisala Meteorologic station	
PTU 301	500-1100 hPa	±0.05 hPa
Pt100	-40 to 60 °C	±0.2 °C
HUMICAP 180C	0-100%	±1%

Table 1: ORCA instruments.

KIEL-UP • DOI: 10.38072/2748-3150/p18

2.3 Data handling

ORCA is measuring with a cadence of one minute as a general approach. Neutrons, muons and environmental values, pressure, temperature and humidity, are recorded with a temporal resolution of one minute. Additionally, MITO can work in a specific mode to acquire the complete pulse shape during a time interval. The duration of this interval depends on the amount of data that can be stored in every moment because for every particle incoming on MITO volume eight complete pulse signals are gathered.

Throughout the period when Juan Carlos I Base is open (Antarctic summer), real time data are sent to a web server and also are stored in a massive hard disc. Nevertheless, no real time data can be sent in winter when the base is closed although a set of data can be gathered once a month remotely.

2.4 Atmospheric corrections

NEMO and MITO measurements, i.e. secondary neutrons and muons, are strongly affected by the air pressure, the more pressure the less counting rate, and the usable counting rate value has to be corrected taking into account this fact. The correction factor β is obtained fitting the counting rate to an exponential law of pressure. From the fits for the 3NM64 group and the 3BNM group the $\beta_A = 0.00735 hPa^{-1}$, $\beta_B = 0.00639 hPa^{-1}$ for 3NM64 and 3BNM respectively. The result of the fit procedure is shown in figures 5 and 6.

Figure 3: ORCA configuration into the maritime container.

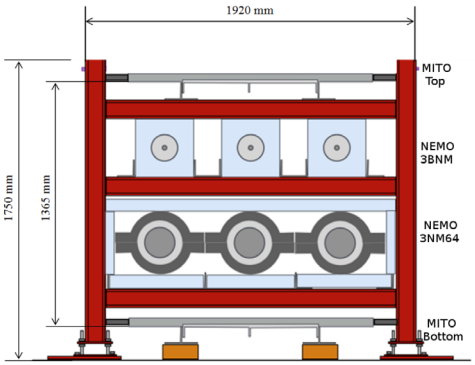

Figure 4: NEMO and MITO layout.

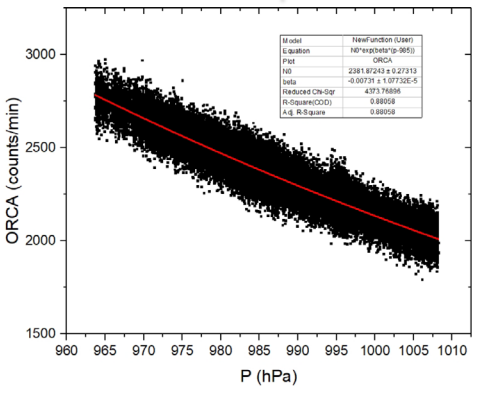

Figure 5: 3NM64 pressure correction.

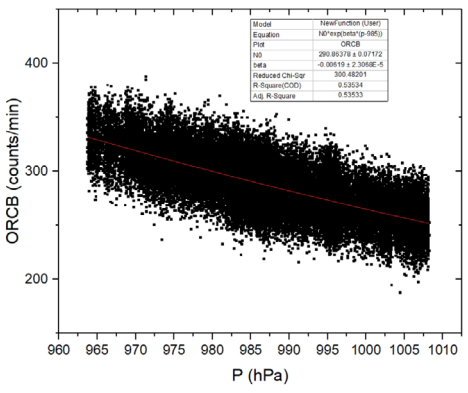

Figure 6: 3BNM pressure correction.

KIEL-UP • DOI: 10.38072/2748-3150/p18

A similar procedure is performed for the MITO coincidence modes, i. e., Top, Bottom, Coin8 and Lateral being the obtained factor, 0.00234 hPa^{-1}, 0.00177 hPa^{-1}, 0.00179 hPa^{-1} and 0.00141 hPa^{-1}, respectively.

2.5 Data product

ORCA can observe neutrons and muons in a continuous way giving counting rates with a maximum temporal resolution of one minute. Real time data can be produced while the Juan Carlos I base is operative and once a month during the Antarctic winter. Muon impact point and incoming

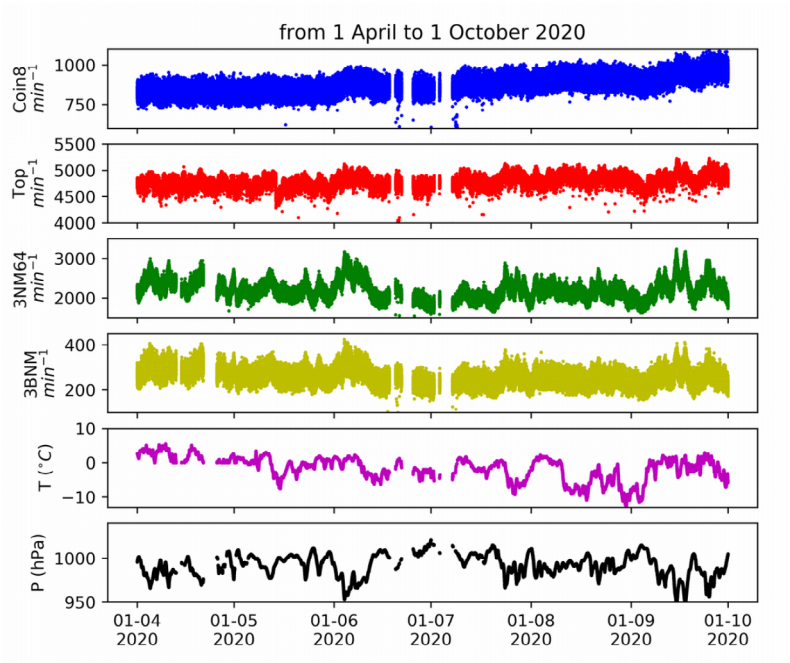

Figure 7: NEMO and MITO counting rates, temperature, pressure and humidity along the Antartic winter.

direction are also produced. Examples of this are shown in figures 7 and 8. Data was collected throughout the winter except for two weeks when renewable energy was discontinued. Pressure uncorrected counting rates are presented from two MITO coincidence modes and NEMO-3NM64 and NEMO-3BNM. Temperature inside the container and pressure are also shown.

3. Conclusions

ORCA is in nominal phase since January 2019 at Juan Carlos I Antartic Base in Livingston Island (Antarctica) at a rigidity cut-off of 2.487 GV. It can provide real time data when Juan Carlos I Base is open (Antarctic summer) and download data once a month when the Base is closed.

Neutron counting rates at two different energy thresholds are provided by 3NM64 and 3BNM modules. Muon counting rates and incident directions are measured by MITO, a new muon telescope design with minimum power consumption and maintenance.

ORCA is expected to be part of the NMDB with the following identifiers ORCA for the 3NM64 module and ORCB for the bare counters module (3BNM).

KIEL-UP • DOI: 10.38072/2748-3150/p18

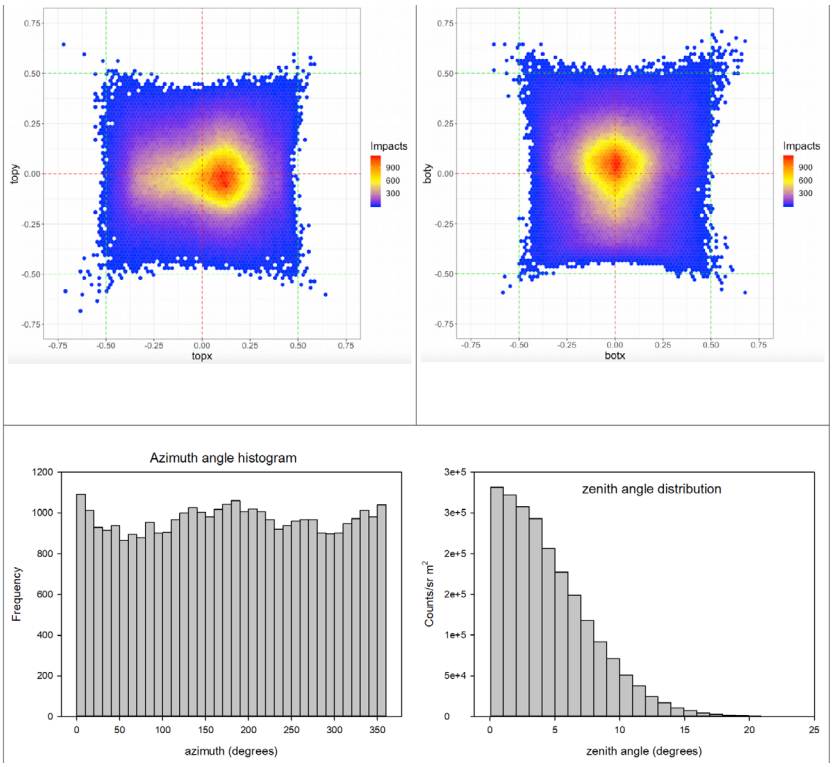

Figure 8: Top left and top right impact point on MITO Top and MITO Bottom respectively. Bottom, azimuth and zenith of incoming tracks thorught MITO.

Acknowledgments

Thanks to project CTM2016-77325-C2-1-P funded by Ministerio de Economía y Competitividad and by the European Regional Development Fund, FEDER.

References

Cordaro, E.G., Olivares, E., Galvez, D., Salazar-Aravena, D., and Laroze, D., 2012, Advances in Space Research, 49(12):1670-1683

Medina, J., Blanco, J. J., García, O., Gómez-Herrero, R., Catalán, E. J., García, I., Hidalgo, M. A., Meziat, D., Prieto, M., Rodríguez-Pacheco, J., and Sánchez, S., 2013, Nucl. Instrum. Methods Phys. Res. A, 727:97–103, DOI: https://doi.org/10.1016/j.nima.2013.06.028

Población, Ó. G., Blanco, J. J., Gómez-Herrero, R., Steigies, C. T., Medina, J., Tejedor, I. G., and Sánchez, S., 2014, Journal of Instrumentation, 9(08):T08002–T08002, DOI: https://doi.org/10.1088/1748-0221/9/08/t08002

Neutron Monitor Database, 2009, https://www.nmdb.eu/(last accessed September 11, 2020)

Cosmic ray studies with neutron detectors | Volume 1 (2021)
KIEL-UP • DOI: 10.38072/2748-3150/p19

A new cosmic ray observation at Syowa Station in the antarctic

Chihiro Kato[1], **Wataru Kihara**[1], **Yukino Ko**[1], **Kazuoki Munakata**[1], **Shin-ichi Uchida**[1], **Sou Kaimi**[1], **Ryuho Kataoka**[2], **Akira Kadokura**[2], **Paul Evenson**[3], **Yoshiaki Nakamura**[4], **Kiyoka Murase**[5], **Shoko Miyake**[6]

Correspondence

[1] Physics Department, Shinshu University, Matsumoto, Japan, ckato@shinshu-u.ac.jp
[2] National Institute of Polar Research, Tokyo, Japan
[3] Bartol Research Institute, Department of Physics and Astronomy, University of Delaware, USA
[4] Key Laboratory of Particle Astrophysics, Institute of High Energy Physics, Chinese Academy of Sciences, Beijing, China
[5] Department of Polar Science, The Graduate University for Advanced Studies, SOKENDAI, Hayama, Japan
[6] Department of Electrical and Electronic Systems Engineering, National Institute of Technology, Ibaraki College, Hitachinaka, Japan

Keywords

muon detector; neutron monitor

Abstract

A set of Cosmic Ray detectors was newly installed in Syowa Station, in the Antarctic, to observe CR neutrons and muons simultaneously at the same location. The observing system has started working in February 2018 and is in stable operation with a high operation rate, >90%. We describe the new systems and show its stability.

1. Introduction

It is well known that cosmic ray (CR) network observation is the only way to derive data for CR anisotropy analysis of space weather phenomena. Two network observations on the globe are in operation. One is Space Ship Earth (SSE) Neutron Monitor (NM) network, which observes atmospheric neutrons with energy of about 10 GeV as median energy. The other is Global Muon Detector Network (GMDN), Muon Detector (MD) network, which observes secondary muons with the energy of about 60 GeV as median energy. These two observation projects have attained some progress in space weather study individually (e.g. Bieber et.al. 2004; Munakata et.al. 2018). Since the SSE and the GMDN observe different energy regions, integration analysis of these two network observation data would provide valuable information for space weather study. For this purpose, it is necessary to observe the same direction at the same time with MD and NM for normalization between these two network observation projects.

KIEL-UP • DOI: 10.38072/2748-3150/p19

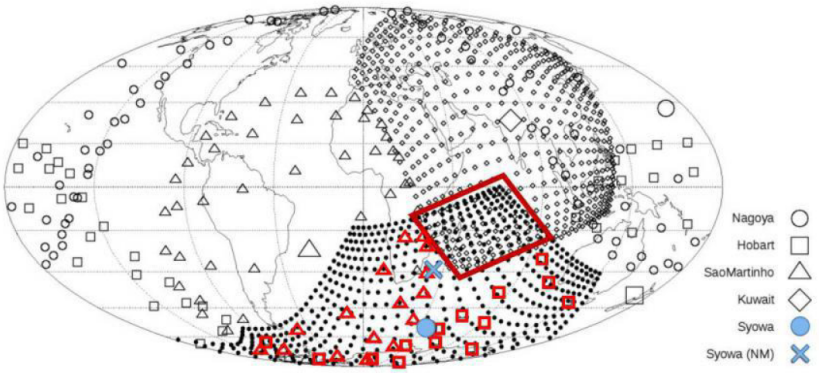

Figure 1: FOV of the GMDN and Syowa MD, and asymptotic direction of the Syowa NM. Symbols indicate asymptotic viewing directions of incident CRs with median rigidity for every directional component of the GMDN, Syowa MD, and Syowa NM. Syowa MD and Syowa NM observe the same direction. Superposed red mark indicates overlapping direction between the GMDN and Syowa MD.

The Syowa Station is located on East Ongul Island, Lützow-Holm Bay and the GMDN stations are located at Nagoya (Japan), Hobart (Australia), Sao Martinho (Brazil), and Kuwait City (Kuwait). The distribution of the asymptotic viewing directions of incident CRs with median rigidity observed by each directional channel at the GMDN station and Syowa MD, and Syowa NM is shown in figure 1. Open symbols are for the GMDN stations and the closed symbol is for the Syowa MD. Large symbols indicate vertical directional channels at each station. The blue cross symbol indicates the asymptotic viewing direction of Syowa NM. The asymptotic direction of Syowa NM is in the FOV of Syowa MD. Thus, Syowa NM and Syowa MD can observe the same direction. Furthermore, there are overlapping viewing directions between Syowa MD and GMDN, which are shown by superposed red symbols. Therefore, Syowa CR observation system can be used not only for normalization between the GMDN and the SSE but also among the GMDN stations. The observation was started in February 2018. In this paper, the new CR observation system at Syowa Station is described.

2. New detector system

The detector system was installed by the 59th Japanese Antarctic Research Expedition (JARE59) from the end of 2017 to the beginning of 2018. The system is located at (latitude, longitude, altitude) = (-69.01°, 39.59°, 24.7 m). Characteristics of the detectors are summarized in table 1.

Directional Channel	Cutoff Rigidity Pc [GV]	Median Rigidity Pm [GV]	Asymptotic directions @Pm	Correction coefficient β [%/hPa]	Average Count rate x10^4 [Counts/hr]
Syowa NM					
Omni	0.4	15.2	30S38E	-0.76	31.8
SyowaMD					
V	2.5	53.6	56S53E	-0.16	26.9
N	2.8	58.5	29S35E	-0.16	3.8
S	2.8	58.5	70S115E	-0.16	3.8

KIEL-UP • DOI: 10.38072/2748-3150/p19

E	2.8	58.5	32S81E	-0.16	6.4
W	2.8	58.5	60S8W	-0.16	6.4
NE	3.2	63.6	16S60E	-0.15	1.0
NW	3.2	63.6	34S4E	-0.16	1.0
SE	3.2	63.6	42S110E	-0.16	1.0
SW	3.2	63.6	80S77W	-0.16	1.0

Table 1: Characteristics of Syowa NM and Syowa MD.

The detectors are assembled in two refrigeration containers as shown in figure 2. Schematic views of the frame of the detector system are also shown in figure 2. Six NM64 and sixty proportional counter tubes (PCTs), which diameter is 10cm, are used for NM and MD, respectively. Three NM64 are housed in a polyethylene box after covering individually with a thin polyethylene shell and lead at the top of the frame.

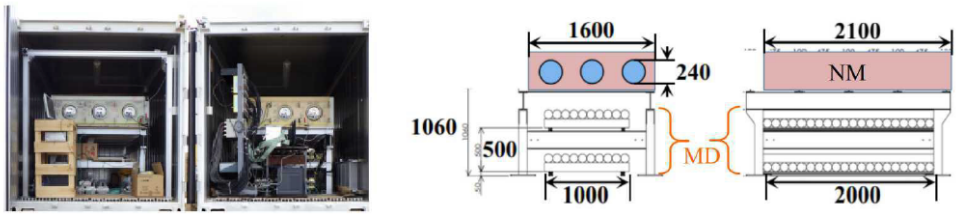

Figure 2: Left: Inside of the refrigeration containers.
Right: Schematic view of the detector system. Numbers are in mm.

The MD is placed under the NM. There are PCTs of two different lengths, which are 1 m and 2 m, to fit in the container. Since MD records directional counts, PCTs are set into four layers. How to determine the incident direction by 4 fold coincidence can be seen in figure 3. Layers of 1 m and 2 m PCTs are paired up in an orthogonal arrangement. The upper and lower pair of the PCTs give a set of (x, y) coordinates for the incident muon. Thus incident direction can be determined. The x- and y-directions are following the long and short sides, respectively. The y-direction is off from North by 20.06 degrees at a clockwise angle. It should be noted that MD is assembled in only one container because of the budget constraints. The observation started on 1 February 2018.

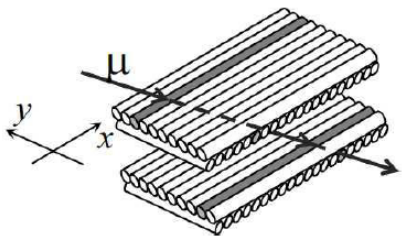

Figure 3: Conceptual diagram of 4 fold coincidence of Syowa MD. X-, y-directions are following the long and short sides, respectively.

KIEL-UP • DOI: 10.38072/2748-3150/p19

Because the containers are outside, the inside temperature of the container dropped close to -20 degrees Celsius during the first winter. One of the data taking PC failed once during this winter by an unknown cause. But to protect the PC and the other electronics, a heating system was installed in each container to maintain the interior temperature of the containers after one year of operation. The PCs are also covered by an insulator. This system maintains the interior temperature of the containers about 0 – 7 degrees and around the PCs about 10 – 17 degrees.

3. Data flow of the detector system

Figure 4 is showing the data flow of these observations. The NM records integrated counts every minute. The MD records counts/minute and counts/10minutes data. Recorded data is automatically transferred to the data server at Shinshu University, Japan through satellite communication and the internet. Frequencies of the data transfer are once a day for NM and every hour for MD. Hourly counts data are created automatically from the counts/10minutes data on the data server after the correction of the atmospheric pressure effect. It is planned to provide NM data to World Data Center (WDC) and Neutron Monitor Data Base (NMDB). Hourly count data of NM and MD's vertical channel are provided to the QL server at the National Institute of Polar Research in Japan[1].

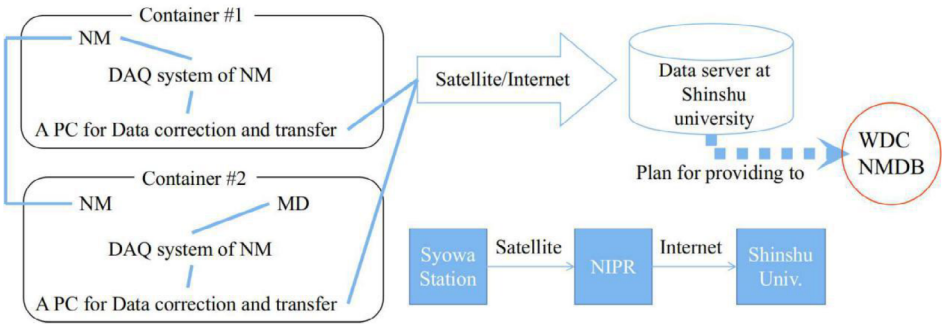

Figure 4: Data-flow diagram of SyowaMD and SyowaNM. Data is transferred via satellite communication and the internet and stored in the data server at Shinshu University.

4. Summary

Since observation started on 1 February 2018, observation is stable and operation rates are 99 % for MD and 91 % for NM. The lower rate for NM is because of PC trouble in the first winter and in the middle of 2020. The later trouble was related to the internet connection. The daily averaged count of NM and of the vertical channel of MD are shown in figure 6 from 2018.2 to 2020.7. Deviation from average is plotted. Data accumulating for two and half years shows temperature effect on the muon count as expected. The neutron count rate is consistent with South Pole NM. This is one of the collateral evidence that Syowa MD and Syowa NM are functioning correctly.

We conclude that the new CR observation system is working correctly and stable to carry out long-term observation. The new system will provide data for integrated analysis of SSE and GMDN and for a detailed study of the difference of atmospheric effect on NM and MD.

1 http://polaris.nipr.ac.jp/~cosmicrays (last accessed April 19, 2021).

Figure 5: Daily averaged count data of SyowaNM (upper panel) and SyowaMD: vertical channel (lower panel). The operation rates are 91% for NM and 99% for MD. The atmospheric temperature effect can be seen on MD data.

References

Bieber, J., Evenson, P., Dröge, W., and Pyle, R., 2004, Spaceship Earth Observations of the Easter 2001 Solar Particle Event, Astrophys. J., DOI: https://doi.org/10.1086/381801

Munakata, K., Kozai, M., Evenson, P., Kuwabara, T., et. al., 2018, Cosmic-Ray Short Burst Observed with the Global Muon Detector Network (GMDN) on 2015 June 22, Astrophys. J., DOI: https://doi.org/10.3847/1538-4357/aacdfe

Questions and answers

Question: Does the lead above the MD affect the incident direction by scattering?

Answer: It is important to estimate with MC simulation because it is unclear for Syowa MD. Currently, several papers are found in which scattering of muon in thin lead target is reported by accelerator beam experiment (e.g. Paoloni, A., Pupilli, F., 2015, IEEE Transactions on Nuclear Science, DOI: https://doi.org/10.1109/TNS.2015.2473674).

Alayman: How can the directions be the same, given that the median energies differ between a NM and a MD located at the same place?

Answer: Geomagnetic field at high latitude does not make a significant difference on orbit deflections of CR for NM and MD unlike in the case of lower latitude.

Cosmic ray studies with neutron detectors | Volume 1 (2021) 161
KIEL-UP • DOI: 10.38072/2748-3150/p20

Calibration of the operative cosmic ray detector at Marambio Base in the Antarctic Peninsula

Noelia Santos[1], Sergio Dasso[1,2,3], Adriana M. Gulisano[2,3,4], Omar Areso[2] and Matías Pereira[2], for the LAGO collaboration[5]

Correspondence

[1] Facultad de Ciencias Exactas y Naturales (FCEN), Departamento de Ciencias de la Atmósfera y los Océanos (DCAO), Grupo LAMP, Universidad de Buenos Aires (UBA), Argentina, nsantos@at.fcen.uba.ar

[2] Consejo Nacional de Investigaciones Científicas y Técnicas (CONICET), Instituto de Astronomía y Física del Espacio (IAFE), Grupo LAMP, Universidad de Buenos Aires, sdasso@conicet.gov.ar

[3] Facultad de Ciencias Exactas y Naturales (FCEN), Departamento de Física (DF), Grupo LAMP, Universidad de Buenos Aires (UBA), Argentina

[4] Instituto Antártico Argentino, Dirección Nacional del Antártico, Grupo LAMP, Universidad de Buenos Aires (UBA), San Martín, Argentina

[5] http://lagoproject.net/collab.html

Keywords

cosmic ray detector; water Cherenkov detector; space weather

Abstract

During 2019 an Antarctic Space Weather Laboratory was deployed at Marambio base in the Antarctic Peninsula. The main instrument installed was a cosmic ray detector based on water Cherenkov radiation (WCD). This detector is the first permanent Antarctic node of the LAGO (Latin American Giant Observatory) Collaboration. Long-term calibrated observations of the WCD will be presented here. Finally, the global galactic cosmic rays variability observed with the WCD will be compared with observations of a neutron monitor with similar rigidity cut off than the Marambio site.

1. Introduction

The flux of low-energy galactic cosmic rays (GCRs) is modulated by transient solar events. Thus, particle detectors at ground level that record temporal variations of the flux of secondary cosmic rays (SCRs) could provide important information for Space Weather studies. For instance, Forbush Decreases (FDs) are observed by neutron monitors (NMs) as well as by water Cherenkov detectors (WCDs) (The Pierre Auger collaboration, 2011). WCDs operating in a counting mode are highly sensitive to FDs (e.g., The Pierre Auger collaboration 2011, and Dasso & Asorey 2012). WCDs have the advantage of being able to discriminate SCRs by their deposited energy into the detector. They are robust, low-cost (Allekotte et al. 2007) and last but not least, easy maintenance and eco-friendly.

We will present the WCD set up at the Marambio Argentinian Base in the Antarctic Peninsula for space weather studies that is part of the LAGO network (http://lagoproject.net/, last accessed April 9, 2021; Asorey & Dasso 2015; Dasso at al. 2015; Sidelnik 2016). The advantage of having a detector in Antarctica is that low energy particles can reach the site due to its low magnetic rigidity cut off. This is one of a few WCDs at the Antarctic soil that is measuring operationally since its installation in March 2019, with IceTop and IceCube similar detectors (e.g., Karle 2008).

KIEL-UP • DOI: 10.38072/2748-3150/p20

In Section 2 we describe the detector and its calibration. In Section 3 we present the first observations of the pressure-corrected count rate. In Section 4 we compare WCD count rate observations with the ones from Oulu NM. Finally, in Section 5 we present a summary and conclusions.

2. A water Cherenkov detector for space weather studies

An Antarctic Space Weather Laboratory was deployed by the LAMP group (Laboratorio Argentino de Meteorología del esPacio, http://spaceweather.at.fcen.uba.ar/2/lamp, last accessed April 9, 2021) at Marambio in the Antarctic Peninsula, between January and March 2019. Marambio is an Argentinian Antarctic base located at 64.24S-56.62W and 196 m a.s.l. Its vertical geomagnetic rigidity cut off is 2.32 GV (Masías-Meza & Dasso 2014). The main instrument installed was a WCD called Neurus. The laboratory also has a magnetometer, a GPS system to make the time stamp of observations, a meteorological station and a telemetry system which provides 5-minutes real-time monitoring at the serves of the group at Buenos Aires.

This is the first permanent Antarctic detector of the LAGO Collaboration. The LAGO Project (Latin American Giant Observatory) is an extended Astroparticle Observatory based on WCDs spanning over Latin America (Asorey & Dasso 2015). It is mainly oriented to basic research in three branches of Astroparticle Physics: the Extreme Universe, Atmospheric Radiation at ground level and Space Weather Phenomena. The LAGO Space Weather program is directed towards the study of how the variations of the flux of SCRs at ground level are linked with the heliospheric and geomagnetic modulations (Asorey & Dasso 2015).

The Neurus WCD consists of a stainless steel cylindrical tank (diameter = 0.96 m, height = 1.20 m) which is full of purified water. When charged particles enter the detector with a speed greater than the speed of light in water they produce Cherenkov radiation which is detected by a photomultiplier tube (PMT). An internal coating made from Tyvek® assures the reflection and diffusion of the Cherenkov photons inside the tank. Through simulations it is known that WCDs enable the possibility of measure the muonic and electromagnetic components of the Extensive Air Showers (EAS), essentially dominated by $\mu \pm$, $e \pm$ and γ (e.g., Sarmiento-Cano et al. 2019). Pictures of the detector can be seen in the left panel of figure 1.

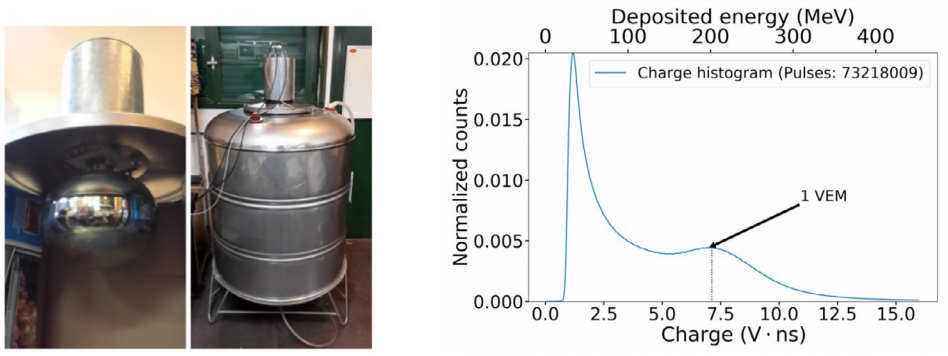

Figure 1: Left: Pictures of the Neurus WCD (from Dasso et al. 2015). Right: Calibrated charge histogram.

KIEL-UP • DOI: 10.38072/2748-3150/p20

Since 2019, and during the first year of operations, two parallel acquisition systems have been working. On one hand, an oscilloscope in the rate mode counts the pulses that exceed a peak threshold and then this rate is recorded by a communication system. The threshold was chosen in such a way as to detect SCRs with deposited energy associated with the electromagnetic component. These data will be presented in the next section. On the other hand, a Red Pitaya STEMlab board in oscilloscope mode records the trace of three sample pulses per second, limited by the acquisition speed of Red Pitaya and the communication with the computer. The area of each voltage pulse V(t) (or charge) represents the energy deposited by each particle.

The charge histogram for pulses recorded during the first 10 months of the uninterrupted operation of the detector, between 25 March 2019 and 11 January 2020, is shown in the right panel of figure 1. To generate this histogram, we consider 300 bins and the 73218009 pulses recorded. The first peak is related to the trigger threshold and is mainly generated by the electromagnetic component of the EAS. Intermediate values, evidenced by a characteristic peak called the *muon hump*, are dominated by single muons through the detector. Higher values of charge in the histogram correspond to simultaneous entrance of multiple particles to the detector called mini-showers (e.g., Asorey & Dasso 2015). This second maximum corresponds to the deposited energy by vertical muons. The charge histogram can be re-interpreted as a function of the deposited energy by vertical muons, assuming that a single muon deposits 2 MeV cm^{-1} in water (e.g., Asorey 2011) and knowing that the water level in the tank is 100 cm. With this calibration the value of 1 VEM (Vertical Equivalent Muon) in electronic units is obtain; in our case 1 VEM = (200 ± 10) MeV. This calibration enables the study of the time evolution of transient heliospheric events for different bands of deposited energy (e.g., Asorey 2011).

3. SCRs corrected count rate

The oscilloscope in the rate mode counts the total number of particles that enter the tank. The largest contribution to these rates corresponds to low-energy SCRs. Its average is around 160 counts per second. In this work we build the hourly average for the count rate *(S)* and for the atmospheric variables for the same time period of the previous section.

The flux of low-energy SCRs at ground level is influenced by atmospheric conditions. It is essential to remove these effects before studying its relationship with space weather events. As a first approach, we performed a pressure correction that is based on a linear regression of *S* and the surface pressure measurement *(P)*:

$$\frac{\Delta S}{S_0} = \beta \, \Delta P \tag{1}$$

where $\Delta S = S\text{-}S_0$ and $\Delta P = P\text{-}P_0$. S_0 and P_0 are the mean count rate and pressure, respectively, during the time period considered and β is the barometric coefficient, which depends on many factors, such as the nature of the secondary component and the altitude where the observation is performed (Dorman 2004).

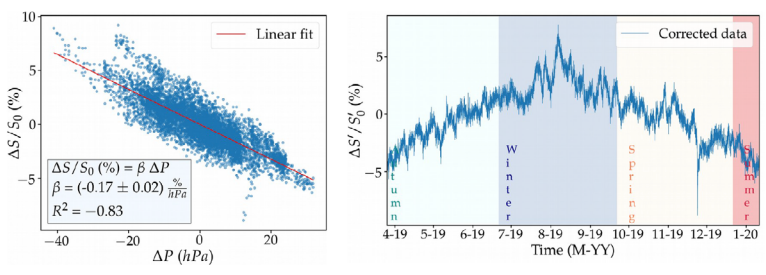

Figure 2: Left: Negative correlation between pressure deviation and the count rate relative deviation during the period considered. Right: Time series of the corrected count rate relative deviation for the same period.

KIEL-UP • DOI: 10.38072/2748-3150/p20

Left panel in figure 2 shows the negative correlation found between the count rate relative deviation and the atmospheric pressure variation. Using a least-squares fitting method, we found that the barometric coefficient in Marambio is β = - (0.17 ± 0.02) %/hPa. After removing the pressure effect, a correction due to the indoor temperature was performed. Right panel in figure 2 shows the time series of $\Delta S'/S_0'$ (the count rate relative deviation corrected for pressure and indoor temperature). It is clear that it shows a seasonal modulation with a maximum in winter and a minimum in summer. This is consistent with what has been discussed in e.g., De Mendonça (2013) and Serap Tilav (2009), and it will be considered in the future to evaluate an adequate correction of this seasonal atmospheric effect.

4. Comparison with neutron monitor

We performed a preliminary comparison of Neurus with data from the Oulu neutron monitor (65.05N – 25.47E). The Oulu vertical geomagnetic rigidity cut off is about 0.8 GV (Usoskin et al. 2001), similar and a bit lower than the one at Marambio. To be able to compare the time series, we remove the seasonal effect of the Neurus data and both data bases were normalized in such way that they have null mean and standard deviation equal to one. These two normalized time series for April 2019 are shown in figure 3. We see that they are in good agreement.

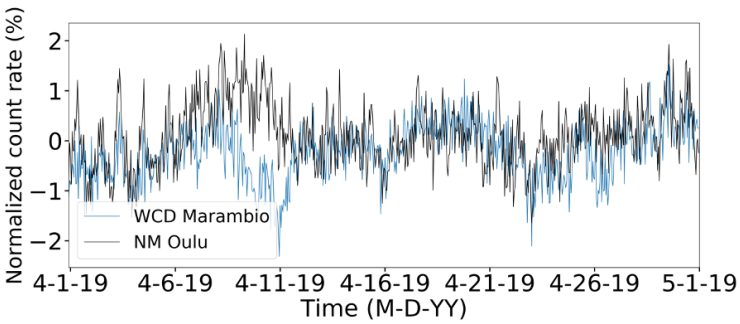

Figure 3: Normalized corrected count rate of Neurus WCD (blue line) compared to corrected count rate of Oulu NM (black line) for April 2019.

5. Discussion and conclusion

In this work we have presented a new cosmic ray detector for space weather studies based on Water Cherenkov effect, installed in the Antarctic Peninsula in 2019, as part of the LAGO detection network. We selected the first ten months of operation in order to calibrate its count rate. The expected anticorrelation between the count rate and the atmospheric pressure was corrected and we obtained a barometric coefficient: β = - (0.17 ± 0.02) %/hPa. A seasonal modulation was observed. We present the calibration of the charge histogram of Neurus and also made a comparison between Neurus WCD and Oulu NM on April 2019, which results in good agreement.

Since the upgrade made at the beginning of 2020, we are recording the trace of all particles that reach the detector, and we are able to make deeper analysis of the Neurus measurements as for instance to analize the variability of the charge histogram with much higher time cadence.

KIEL-UP • DOI: 10.38072/2748-3150/p20

Acknowledgments

The authors acknowledge for the support from the Argentinean grants UBACYT (UBA) and PIP-11220130100439CO (CONICET). The LAGO collaboration is very grateful to all the participating institutions and The Pierre Auger collaboration for their continuous support. Acknowledgments to the NMDB database (https://www.nmdb.eu/), founded under the European Union's FP7 programme for providing data, as well as to the Oulu neutron monitor webpage at http://cosmicrays.oulu.fi and the Sodankyla Geophysical Observatory.

References

Allekotte, I., et al., 2007, Nucl. Instrum. Methods Phys. Res Section A 586, 409-420

Asorey, H., 2011, Proceedings of the 32nd International Cosmic Ray Conference (ICRC2011) 11, SH3-SH4, 467

Asorey, H., Dasso. S, 2015, Proceedings of the 34th International Cosmic Ray Conference – PoS (ICRC2015) 236, 247

Dasso, S., Asorey, H., 2012, Adv. Space Res 49, 1563-1569

Dasso, S., et al., 2015, Proceedings of the 34th International Cosmic Ray Conference – PoS (ICRC2015) 236, 105

De Mendonça, R. R. S., et al., 2013, J. Geophys. Res: Space Physics 118, 1403-1409

Dorman, L. I., 2004, Cosmic Rays In The Earth's Atmosphere And Underground, Dordrecht: Kluwer Acad. Publ.

Karle, A., 2009, Nucl. Instrum. Methods Phys. Res Section A 604, S46-S52

Masías-Meza, J. J., Dasso, S., 2014, Sun and Geosphere 9, 41-47

Sarmiento-Cano, C., et al., 2019, Proceedings of the 36th International Cosmic Ray Conference – PoS (ICRC2019) 358, 412

Sidelnik, I., 2016, Proceedings of the 34th International Cosmic Ray Conference – PoS (ICRC2015) 236, 665

The Pierre Auger collaboration, 2011, Journal of Instrumentation 6, 1003

Tilav, S., et al., 2010, Proceedings of the 31st International Cosmic Ray Conference (ICRC2009)

Usoskin, I.G, Mursula, K, Kangas, J., 2001, Proceedings of the 27th International Cosmic Ray Conference (ICRC2001), Copernicus Gesellschaft, 3842

Cosmic ray studies with neutron detectors | Volume 1 (2021)
KIEL-UP • DOI: 10.38072/2748-3150/p21

Upgrade of electronics of neutron monitors DOMC and DOMB

Stepan Poluianov [1,2], **Ilya Usoskin** [1,2], **Du Toit Strauss** [3]

Correspondence
[1] Sodankylä Geophysical Observatory, University of Oulu, Finland
stepan.poluianov@oulu.fi, ilya.usoskin@oulu.fi
[2] Space Physics and Astronomy Research Unit, University of Oulu, Finland
[3] Centre of Space Research, North-West University, Potchefstroom, South Africa
dutoit.strauss@nwu.ac.za

Keywords
cosmic rays; neutron monitor; data management

Abstract
DOMC and DOMB neutron monitors (NM) operate at the Concordia research station (Dome C on the Antarctic plateau, 75°06'S, 123°23'E, 3233 m a.s.l.) since 2015. Their high elevation and proximity to the geomagnetic pole provide low atmospheric and geomagnetic cutoffs and, therefore, the exceptionally high sensitivity to low-energy cosmic rays. The instruments are the so-called mini neutron monitors with BF_3-filled counter tubes. DOMC has the standard design with a lead neutron multiplier and DOMB is a so-called "bare" (lead-free) unit. We report on a recent upgrade of the electronics heads of these instruments. The new heads have a modular architecture, built upon a single-board computer Raspberry Pi. The upgrade increases the capabilities of the instruments in two aspects: (1) measurements, particularly, of cosmic ray multiplicity; (2) remote control and monitoring. The new electronic heads register each pulse from a detector, giving a timestamp with microsecond precision, which is crucial for multiplicity measurements. Many important parameters (e.g., high voltage, pulse detection thresholds) can be controlled and adjusted remotely with the new design. High computing power allows performing data processing on the fly. The upgrade increases the capability of DOMC and DOMB in cosmic ray measurements and improves control of the operation of the neutron monitors.

1. Introduction

DOMC and DOMB are two mini neutron monitors (NM) located at the polar, high-altitude Concordia research station (Dome C on the Antarctic plateau, 75°06'S, 123°23'E, 3233 m a.s.l.) – see figures 1 and 2. The instruments are described in detail in Poluianov et al. (2015). Both neutron monitors were built with the same design, however, there is a difference in the lead neutron producer layer. DOMC is standard (with lead) and DOMB is so-called "bare" (lead-free) instrument. In 2019, they got a significant upgrade with new electronics heads, providing new abilities in data analysis and instrument control (Strauss et al. 2020).

KIEL-UP • DOI: 10.38072/2748-3150/p21

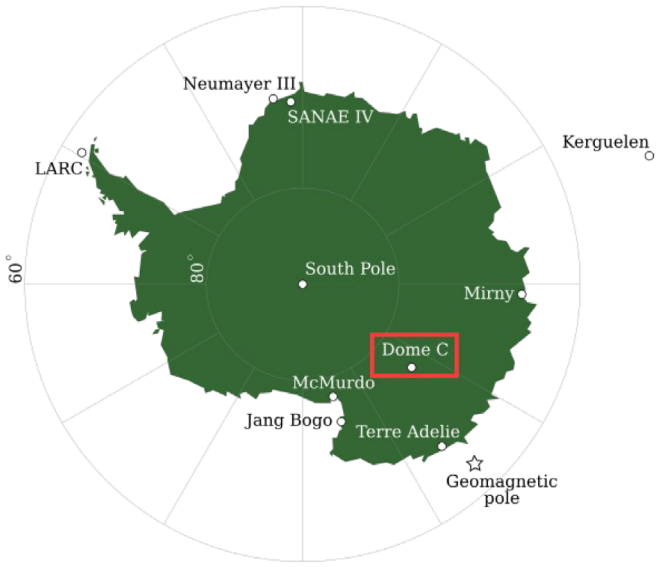

Figure 1: Location of DOMC and DOMB NMs.

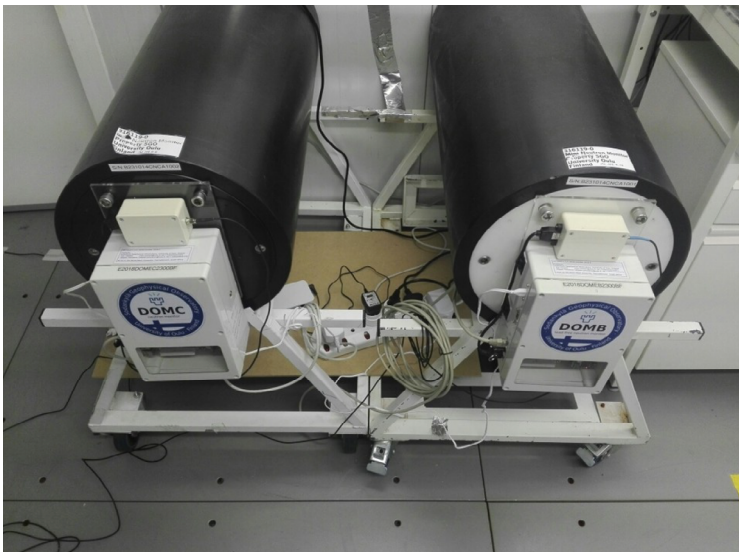

Figure 2: DOMC and DOMB NMs.

2. New electronics heads

The electronics heads (as well as the neutron monitors earlier) were made by the Centre for Space Research, North-West University (Potchefstroom, South Africa). Each head is built around a single-board Raspberry Pi 3 B computer and has a modular design. There is an ADC board responsible for the digitization of pulses from the detector, an amplifier, a high-voltage module, pressure/temperature/humidity sensors, a GPS-module for time synchronization.

KIEL-UP • DOI: 10.38072/2748-3150/p21

2.1 New features

The new head is a fully-functional computer with GNU/Linux onboard, thus, it makes interactions between the instrument and other servers very easy. It is possible to operate the instrument via SSH and FTP/SFTP protocols, and therefore to use virtually any standard methods applicable to a GNU/Linux computer.

More important parameters (high voltage at the detector, pulse height and length discriminators) can be set up remotely. This is possible because all parts of the head, responsible for pulse handling and power supplying of the detector, are controlled by the central Raspberry Pi board.

GPS time synchronization is optional. The internal clock of the head can be set up with the network time protocol (NTP) or manually.

The new head registers each pulse from the detector individually: it records its timestamp, length, maximum magnitude and fully digitized time profile in volts (figure 3).

The pulse timestamp is recorded with the microsecond precision, while the earlier version of the electronics could record it with the millisecond resolution.

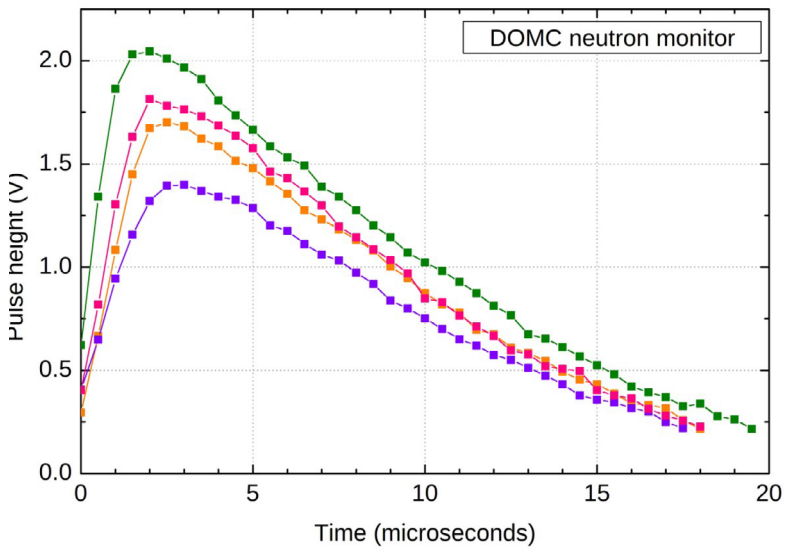

Figure 3: Examples of pulse time profiles.

2.2 Data coming from DOMC and DOMB

A new electronic head sends the following data: count data (timestamp, length, maximum magnitude and profile of every pulse), atmospheric pressure/temperature/humidity from two sensors, high voltage value, GPS coordinates, log data.

New features of the electronics lead to a significant increase of the amount of data produced by an instrument: for example, DOMC with the average count rate 1300 cts/min sends about 400 Mb/day of raw uncompressed data. To handle increased volumes, the data management system at the Oulu cosmic ray station has been upgraded (see the proceedings Poluianov et al. “Data management at the Oulu cosmic ray station” at this symposium).

2.3 New opportunities in the data processing

The new electronics, thanks to its microsecond resolution in pulse timing, allow analyzing the cosmic ray multiplicity in DOMC and DOMB records. Pulse height/length discrimination is possible

KIEL-UP • DOI: 10.38072/2748-3150/p21

not only in real time by the head's ADC board but also retrospectively from raw data files (figure 4). It may be useful if the noise level changes. Pulse height histograms are also available and they are an important tool in monitoring the NM operation.

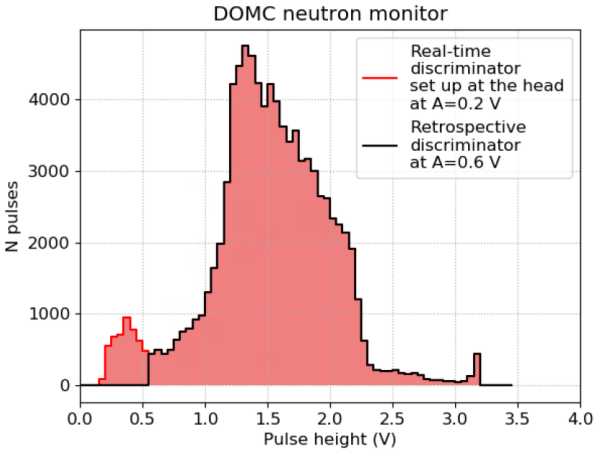

Figure 4: Pulse-height histogram from DOMC data (1 March 2020).

2.4 New opportunities in remote control

Since Raspberry Pi in the NM head is a fully-functional Linux computer, standard methods are applicable for its administration. This makes integration of the instrument to existing computer infrastructure very easy. At the Concordia station, DOMC and DOMB NMs are connected to the Concordia-NM server via local network. The server, in turn, sends data to the Oulu cosmic ray station via HERMES (a system for data transfer from Antarctica). The NM is fully controlled via SSH over the Concordia-NM server and Concordia VPN (figure 5).

It is also possible to remotely set up/adjust parameters important for CR measurements such as high-voltage, pulse height and length discriminations.

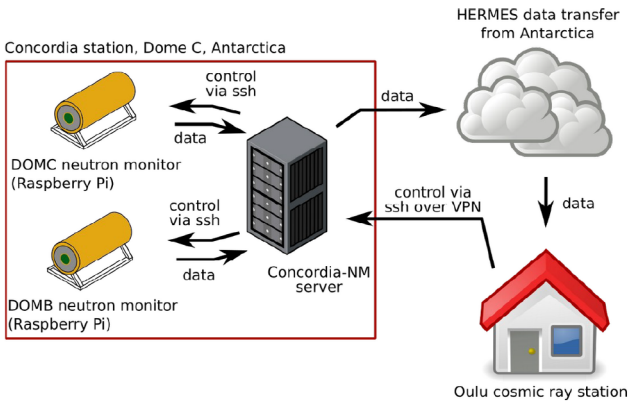

Figure 5: Dataflow of DOMC and DOMB NMs.

KIEL-UP • DOI: 10.38072/2748-3150/p21

3. Summary

DOMC and DOMB NM received new electronics in 2019. The upgraded instruments can be fully controlled remotely, which is a big advantage in operation in Antarctica. Registration of pulses with microsecond precision, as well as of their profiles, opens new opportunities in cosmic ray multiplicity measurements and fine control of the operation of the instruments.

Acknowledgments

The work was partly supported by FINNARP and Academy of Finland (projects 264378 CRIPA, 304435 CRIPA-X, ReSoLVE and 321882 ESPERA). We are thankful for the hospitality of the Italian Polar Programme PNRA (via the LTCPAA PNRA 2015/AC3 project) and the French Polar Institute IPEV.

References

Poluianov, S., Usoskin, I., Mishev, A., Moraal, H., Kruger, H., et al., 2015, Mini Neutron Monitors at Concordia Research Station, Central Antarctica, J. Astron. Space Sci., 32, 281-284, DOI: https://doi.org/10.5140/JASS.2015.32.4.281

Strauss, D. T., Poluianov, S., van der Merwe, C., Krueger, H., Diedericks, C., et al., 2020, The mini-neutron monitor: a new approach in neutron monitor design, J. Space Weather Space Clim., 10, 39, DOI: https://dx.doi.org/10.1051/swsc/2020038

Cosmic ray studies with neutron detectors | Volume 1 (2021)
KIEL-UP • DOI: 10.38072/2748-3150/p22

Study of individual pulses at the Antarctic high-altitude neutron monitor DOMC

Markus Similä , Stepan Poluianov , Ilya Usoskin

Correspondence
Sodankylä Geophysical Observatory, University of Oulu, Finland
markus.simila01@gmail.com, stepan.poluianov@oulu.fi, ilya.usoskin@oulu.fi

Keywords
neutron monitor; atmospheric cascade; cosmic rays

Abstract
A pair of neutron monitors (NMs) is installed on the high Central Antarctic plateau, at the Concordia station (3200 m altitude) and measures the nucleonic component of nucleonic-muon-electromagnetic cascades induced by high-energy cosmic rays in the atmosphere. The installation includes two NMs: DOMC, a standard mini-NM, and a bare (lead-free) DOMB NM. The newly installed data acquisition (DAQ) system records individual pulses corresponding to mostly neutrons in the detector's counting tube. Here we analyze different types of pulses and study the distribution of the waiting times between individual pulses as well as the pulse height, recorded by the DOMC NM during a quiet period of January 2020. The distribution appears double-peaked with peaks corresponding to the frequency of individual atmospheric cascades and the intra-cascade variability, respectively. We discuss also the nature of different components contributing to the pulses and separation of the signal from noise. It is shown that the waiting-time distribution has distinguished timescales, >30 ms defined by the cosmic-ray induced atmospheric cascades, and <10 ms reflecting the intra-cascade variability. The new DAQ system allows one to study the development of the atmospheric cascade.

1. Introduction

A neutron monitor (NM) is a proportional counter designed to measure the nucleonic component of complex cascades induced by energetic cosmic-ray particles in the atmosphere (Moraal et al. 2000; Simpson 2000). NMs of the standard design count the number of pulses on the central wire per unit time (count rate). The DOMC NM is a mini-NM built following the standard NM design, viz. including two layers of moderator and a lead shield (Poluianov et al. 2015). It is located on the Central Antarctic plateau at the Franco-Italian Concordia station (3200 m altitude) and has the world´s highest access for low-energy cosmic-ray particles on the ground. Since late 2019, a new data acquisition system (DAQ) operates on the DOMC NM, digitizing each pulse with the 2-MHz sampling frequency (Strauss et al., Poluianov, Usoskin & Strauss, this issue). Most of the pulses have a 0.2—2.5 V height and 10—40 μs duration. The latter corresponds to a typical NM dead time. Here we provide results of the first analysis of the waiting-time distribution of individual pulses for DOMC NM, for a very quiet period (1-27 January 2020), in relation to the development of the nucleonic cascade in the atmosphere.

KIEL-UP • DOI: 10.38072/2748-3150/p22

2. Pulse analysis

In total, about 60 millions of individual pulses have been recorded by the new DAQ system of DOMC NM during January 2020. The distribution of the amplitude and duration of pulses is shown in figure 1. Four different branches can be observed: A – the main branch, where each pulse has a well-defined shape and can be clearly separated from the others (figure 2A) so that pulse drops below the detection threshold before the new pulse starts; B – noise dominated branch, where pulses are low, short and not shaped (figure 2B); C – multiple (typically double) well-defined peaks where the second one starts before the first one drops below the threshold (figure 2C); D – multiple (can be numerous) high-amplitude peaks following with very short (10–30 μs) time separation (figure 2D), we argue that it is likely to be caused by multiple intra-counter avalanches. About 93 % of all pulses lies in the branches A and C, branch B comprises $\sim 7\,\%$, and D accounts for only 0.05 % of all pulses. We note that increasing the detection threshold to 0.5–0.6 V reduces the noise (branch B) by an order of magnitude. In the following, we have performed an analysis of the data by applying a threshold of 0.5 V, so that the contribution of unwanted branches B and D is reduced to $< 1\,\%$.

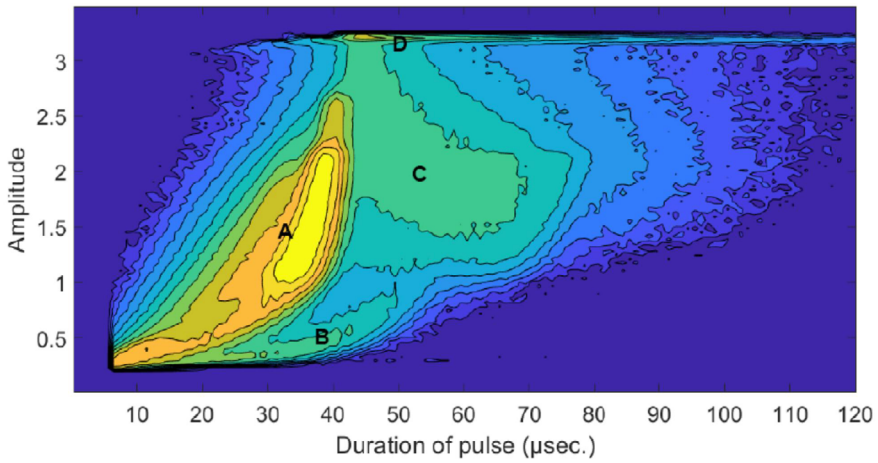

Figure 1: Amplitude (in volts) versus duration (in microseconds) log-distribution of ~60 millions of pulses recorded by DOMC NM in January 2020. The detection threshold is set for 0.2 V. Four main branches are indicated: A – the main branch where well-shaped pulses can be clearly separated; B – noise-dominated region; C – multiple pulses originated from the atmospheric cascades; D – intra-detector cascades. Examples of pulse's time profiles are shown in figure 2.

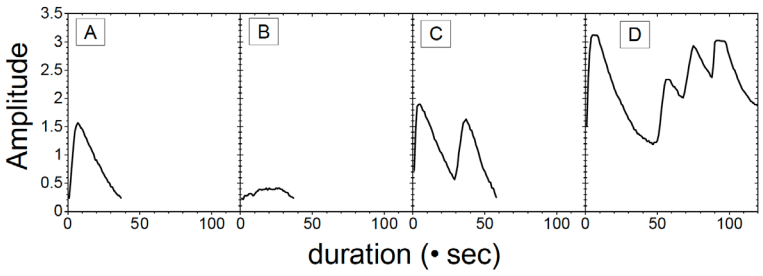

Figure 2: Typical pulse profiles (amplitude in volts vs time in microseconds) for the four branches A–D in figure 1 (as indicated by the panels).

KIEL-UP • DOI: 10.38072/2748-3150/p22

Next, we computed the waiting time, defined as the time interval between onsets (zero-times in figure 2) of subsequent pulses. The distribution (weighted with the bin width for better visibility) of the waiting times is shown in figure 3. One can see that it has two distinct scales. One peak in the distribution corresponds to ∼2 ms (0.3–10 ms) and is close to the log-normal shape. The other peak corresponds to the waiting times greater than ∼30 ms followed by a purely exponential tail corresponding to the mean count rate (∼20 Hz) of the detector. Smooth behaviour is observed in between. Here we note that the second peak corresponds to the expected standard distribution for cosmic-ray induced atmospheric cascades.

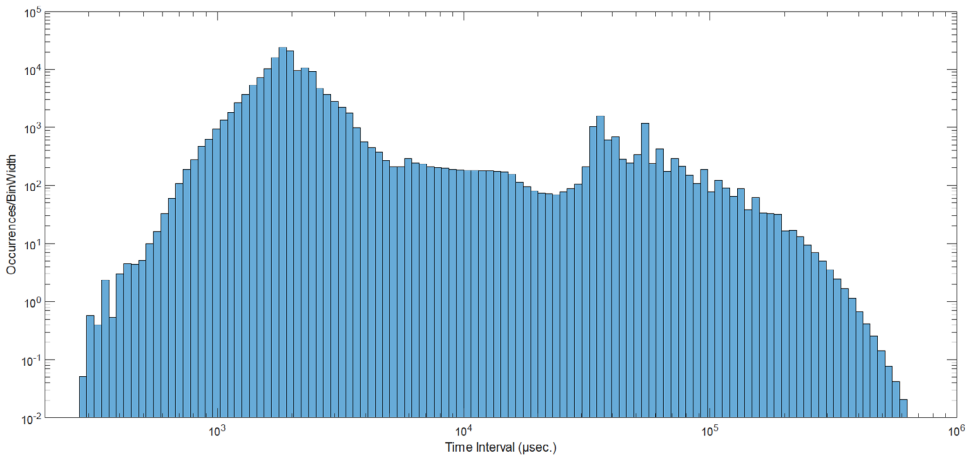

Figure 3. Distribution (histogram weighted with the bin width) on waiting times between consequent pulses (threshold 0.5 V) as measured at DOMC during January 2020.

The waiting time is defined by the waiting time between individual cascades caused by different cosmic-ray primary particles and reflects the behaviour of the cosmic-ray flux impinging on the Earth's atmosphere. The second peak dominates the count rate of the NM (because of the weighting, it looks smaller than the first one). The first peak with smaller waiting times corresponds to the intra-cascade multiplicity, viz. multiple secondary particles arriving from the atmospheric cascade induced by the same primary particles and mostly reflects the development of the cascade in the atmosphere. We note that, because of the high-altitude location of the DOMC NM, the first intra-cascade peak may be enhanced, but it may be smaller at sea level but more intense at higher cutoffs (lower latitudes). By analysis of individual pulses, one can study details of the atmospheric transport of cosmic rays.

3. Discussion and conclusion

We have analyzed the amplitude and waiting-time distribution of ∼60 millions of individual pulses digitized by DAQ of DOMC NM during a quiet period of January 2020. We have shown that the raw data contain several types of pulses: single and multiple pulses from the atmospheric cascade (∼93% of all pulses), multiple pulses from the intra-detector avalanches (<0.1%), and low-amplitude noise (∼7%). Noise can be significantly reduced by increasing the discriminator threshold from the built-in 0.2 V to 0.5 V. Two distinct peaks can be clearly identified in the waiting-time distribution of pulses: one, with a purely exponential tail, lies in the time range of longer than 30 ms reflecting the frequency of individual atmospheric cascades and corresponding to the mean count

KIEL-UP • DOI: 10.38072/2748-3150/p22

rate of DOMC NM (∼ 20 Hz); the other, with the time range of 1—10 ms and a nearly log-normal distribution, corresponds to the variability of secondary particles within the same atmospheric cascade, viz. intra-cascade variability. Similar results were obtained for different values of the discriminator threshold, ranging from 0.2—2.0 V.

The proposed method can clearly distinguish between intra- and inter-cascade variability and can be used to study multiplicities and details of the development of the nucleonic cascades induced by energetic particles in the atmosphere.

Acknowledgments

The work was partly supported by FINNARP and Academy of Finland (projects 264378 CRIPA and 304435 CRIPA-X).

References

Moraal, H., Belov, A, Clem, J., 2000, Space Sci. Rev., 93, 285-303, DOI: https://dx.doi.org/10.1023/A:1026504814360

Poluianov, S., Usoskin, I., Mishev, A., et al., 2015. J. Astron. Space Sci., 32, 281, 2015, DOI: https://dx.doi.org/10.5140/JASS.2015.32.4.281

Simpson, J.A., 2000, Space Sci. Rev. 93, 11–32, DOI: https://dx.doi.org/10.1023/A:1026567706183

Strauss, D.T., Poluianov, S., van der Merwe, C., et al., J. Space Weather Space Clim., 10, 39, 2020, DOI: https://dx.doi.org/10.1051/swsc/2020038

Cosmic ray studies with neutron detectors | Volume 1 (2021)
KIEL-UP • DOI: 10.38072/2748-3150/v1

Session 5: Abstracts

Measuring single and multiple atmospheric secondary particles from cosmic rays using cross-counter neutron time delay distributions from the Princess Sirindhorn neutron monitor

Warit Mitthumsiri[1], Alejandro Sáiz[1], David Ruffolo[1,2], Paul Evenson[3], Pierre-Simon Mangeard[3], Waraporn Nuntiyakul[4,2]

Correspondence

[1] Department of Physics, Faculty of Science, Mahidol University, Bangkok, Thailand
[2] National Astronomical Research Institute of Thailand (NARIT), Chiang Mai, Thailand
[3] Bartol Research Institute and Department of Physics and Astronomy, University of Delaware, Newark, USA
[4] Department of Physics and Materials Science, Faculty of Science, Chiang Mai University, Chiang Mai, Thailand

The Princess Sirindhorn Neutron Monitor in Thailand had its electronics upgraded in 2015 for absolute timing capability across its 18 counter tubes. This has enabled us to record the distributions of time delay between two successive counts in any pair of tubes and deduce the overall associations of the detected counts. Analyzing results from measurements and simulations, we find that associated counts between two nearby tubes (no more than 4 tubes apart) are dominated by a single atmospheric secondary interacting within the monitor, while the associated counts between two tubes with large separations (more than 4 tubes apart) are mainly from multiple atmospheric secondaries produced by the same primary cosmic ray. We calculate the fraction of unrelated counts, the 'leader fraction,' for the large-separation case and corrected for the atmospheric and water vapor pressure to observe its time variation between September 2018 to December 2019. This is a novel technique to study cosmic-ray spectral properties and multiplicities of secondary particles in the air showers using a single neutron monitor station. This research project is partially supported by Thailand Science Research and Innovation grant RTA6280002 and Research Grant for New Scholar MRG6280155.

Novel registration system for neutron monitors

Stephan I. Böttcher[1], Christian T. Steigies[1], Rolf Bütikofer[2]

Correspondence

[1] Extraterrestrial Physics, Institute of Experimental and Applied Physics, K iel University, Germany
[2] Physikalisches Institut, University of Bern, Switzerland

We present a novel registration system for counter signals based on an FPGA and a µC with USB, serial Port, and Ethernet interfaces. An interface board for up to 24 counter channels can be configured for a wide range of signal levels. Each channel comes with a programmable discriminator. The FPGA reports the observed pulse length, for frontends that encode pulse height information.

KIEL-UP • DOI: 10.38072/2748-3150/v1

Recent upgrade of the neutron monitor at Mawson, Antarctica

Alejandro Sáiz[1], Pradiphat Muangha[1,3], Marcus Duldig[2], David Ruffolo[1,3], Warit Mitthumsiri[1], Kullapha Chaiwongkhot[1], Waraporn Nuntiyakul[4,3], Paul Evenson[5], John Humble[2]

Correspondence

[1] Department of Physics, Faculty of Science, Mahidol University, Bangkok, Thailand
[2] School of Natural Sciences, University of Tasmania, Hobart, Tasmania, Australia
[3] National Astronomical Research Institute of Thailand (NARIT), Chiang Mai, Thailand
[4] Department of Physics and Materials Science, Faculty of Science, Chiang Mai University, Chiang Mai, Thailand
[5] Bartol Research Institute and Department of Physics and Astronomy, University of Delaware, Newark, USA

During the Austral Summer of 2019/2020, two scientists from Mahidol University, Thailand, joined the expedition to the Australian base of Mawson, Antarctica, to perform several upgrades to the neutron monitor at the Mawson Cosmic Ray Laboratory. Changes in the data acquisition system included both updated electronic firmware and computer software. The most relevant addition to the data stream is the measurement of waiting times between pulses, which can be used to detect cosmic ray spectral changes. Besides the same-counter waiting times, values for cross-counter waiting times are also recorded, which may be used to study the structure of atmospheric showers. The detector was also extended to include 6 extra BP28 counters as a lead-free counter array, which will also give valuable spectral information, especially during GLEs. In this presentation, details of this upgrade will be given and an initial analysis of the new data products will be presented. Partially supported by Thailand Science Research and Innovation award RTA6280002 and Research Grant for New Scholar MRG6280155.

Refurbishment of the SANAE neutron monitor

Du Toit Strauss, Corrie Diedericks, Cobus van der Merwe, Hendrik Kruger, Katlego Moloto, Helena Kruger

Correspondence

Center for Space Research, North-West University, Potchefstroom, South Africa

We present results of the recent upgrade of the SANAE (South African National Antarctic Expedition) neutron monitor (NM). We have retro-fitted a 3NM64 with electronics, originally designed for our mini-NM program, which have the ability to record individual cosmic ray pulses down to the low micro-second level. We briefly discuss the retro-fitting process and present initial results for the first year of operation, including, amongst others, measurements of the multiplicity spectrum and the level of tube degradation. We also discuss the data analysis we implemented to combine the counts from each tube into a near-real-time time series.

KIEL-UP • DOI: 10.38072/2748-3150/v1

Reformatting of neutron monitor to increase its effectivity

Victor G. Yanke

Correspondence
Pushkov Institute of terrestrial magnetism, ionosphere and radio wave propagation (IZMIRAN), Moscow, Russia

Global changes of climate, including the gradually decreasing thickness of ice, lead to objective difficulties for organizing annual Arctic North Pole expeditions on drifting ice. To solve this problem, an all-weather Arctic-class self-propelled research platform for year-round expeditions is currently under construction. On such an icebreaker on the upper deck in a sea container, one section of the 6NM64 neutron supermonitor will be placed. But for solar cosmic rays, first of all, it is desirable to have good statistical accuracy of the data. To place a larger number of sections does not allow the weight inherent in the project. Therefore, the task of the work is to increase its efficiency by reformatting a neutron detector. The key points of this reformatting are the transition to helium counters, the rejection of lead ring-shaped multiplier and the transition to brick. This allows us to increase the number of used counters and neutron collection. The latter, however, increases the cost of the detector, but leads to an increase in its efficiency by 1.5 - 2.5 times, depending on the helium counters used. In addition, the asymptotic directions of particle arrival in the geomagnetic field are calculated for possible drift points of the North Pole station, on the one hand, and the expected trajectory of the Earth's North magnetic pole, on the other hand. During the movement of the North Pole floating platform when registering a specific event, we may be at the best point, we may be at the worst point, but in any case it will be a unique region for conducting cosmophysical research.

Installation of Jang Bogo neutron monitor in Antarctica

Jongil Jung[1,2], Suyeon Oh[3], Yu Yi[1,5], Paul Evenson[4], Gunhwa Gee[5], JeongHan Kim[5], Changsup Lee[5]

Correspondence
[1] Department of Astronomy, Space Science and Geology, Chungnam National University, Daejeon, Korea
[2] Polar Research Institute, Incheon, Korea
[3] Department of Earth Science Education, Chonnam National University, Gwangju, Korea
[4] Department of Physics and Astronomy, University of Delaware, Newark, USA
[5] Korea Polar Research Institute, Incheon, Korea

The Jang Bogo research base is secondary base of South Korea and built in February 2014 and located in Terra Nova Bay, Northern Victoria Land, Antarctica. It is a state-of-the-art research station that provides easy access to central and coastal areas of Antarctica. It is also possible to produce various data and study specialized research such as climate change, topographical and geological, the upper atmosphere and space science. We have been operating the neutron monitor at Jang Bogo base since December 2015. Its location is 76.62S, 164.2E in geophysical coordinate and 79.86N, 52.46W in geomagnetic coordinate. Jang Bogo neutron monitor (JBGO) has the cutoff rigidity of about 0.1 GV. It consists of 18 tubes of three-units which were transferred from McMurdo station (MCMU) at a distance of 300km from Jang Bogo. One of three units was relocated in 2015 and the rest of units was transferred in the summer season of 2017-2019. Currently, JBGO is running well without a big problem. We respect that JBGO gives the good information to understand the space environment in the polar region. In this study, we present the installation of JBGO and preliminary scientific results using the JBGO data.

Session 6:

Neutron detector response function

Cosmic ray studies with neutron detectors | Volume 1 (2021)
KIEL-UP • DOI: 10.38072/2748-3150/p23

Snow effect on the neutron monitor network for 2018-2019

Pavel G. Kobelev[1], **Liudmila Trefilova**[1], **Lev I. Dorman**[1,2], **Lev A. Pustilnik**[2], **Anatoly V. Belov**[1], **Eugenia A. Eroshenko**[†1], **Victor G. Yanke**[1]

Correspondence

[1]Pushkov Institute of Terrestrial Magnetism, Ionosphere and Radio Wave Propagation (IZMIRAN), Moscow, Russia, kosmos061986@yandex.ru, trefilova@izmiran.ru, lid010529@gmail.com, abelov@izmiran.ru, erosh@izmiran.ru, yanke@izmiran.ru

[2]Israel Cosmic Ray and Space Weather Center, Tel Aviv University, Israel, levpust2149@gmail.com

Keywords

snow effect; neutron monitor; variations; barometric effect

Abstract

In this article, the influence of the surrounding snow cover on the neutron monitors count rate of the world network of neutron monitors was estimated using the method of reference stations. The applied technique also makes it possible to estimate the snow cover thickness at the observation point, which was done for more than two dozen stations. A comparison of the data correction results for snow is carried out for the case of automatic correction, based on the developed algorithm, and for manual one, with an error estimate.

1. Introduction

For some stations, especially mountain ones, snow is a big problem, because due to high humidity it effectively accumulates above and around the detector. For most of these stations, it is not possible to mechanically remove the snow. Therefore, the monitoring data for the neutron component, which are significantly distorted by a variable snow layer, are not suitable for studying many types of variations and require appropriate correction for further use. The registration accuracy of the 18NM64 neutron monitor is about 0.15% for the hourly-averaged interval. And already one centimeter of thick snow 0.5 cm of water equivalent above the detector leads to a distortion of the observed variations by 0.5%. Indeed, the effect is approximately determined by multiplying the barometric coefficient ($\sim$ 0.7%/hPa) on the absorber thickness.

The nature of the snow effect is twofold. The snow cover above the detector is an additional absorber, and this leads to a decrease of count rate. In addition, the neutron monitor registers a certain fraction of neutrons that are generated in the substance surrounding the detector, in particular in the ground. The snow cover shields this neutron source, which also leads to count rate decreasing. The effect of snow has been considered in many works, for example, (Korotkov et al. 2011, 2013), which also review earlier works.

† deceased

KIEL-UP • DOI: 10.38072/2748-3150/p23

2. Data and method

We have learned how to exclude the barometric effect, which has a similar nature, by using precision measurements of atmospheric pressure. Therefore, it is possible to make appropriate corrections by measuring the thickness of the snow cover. Indeed, if, in the absence of snow, the counting rate of the detector is N_i^{cor}, then the counting rate of the detector due to absorption with some effective range L (assuming that L does not depend on energy) in the snow depth x_i is equal to $N_i = N_i^{\text{cor}} \cdot \exp\left(-x_i / L\right)$. Thus, the restored count rate

$$N_i^{\text{cor}} = N_i / \varepsilon_i \text{, where } \varepsilon_i = \exp\left(-x_i / L\right) \tag{1}$$

where ε_i can formally be considered a change of the detector efficiency, i.e. a change in some properties of a detector or observation conditions. If we knew the thickness of the snow cover, then the data could be easily corrected for the effect of snow (Blomster & Tanskanen 1969). But precise data on the thickness of the snow cannot be obtained due to the inaccessibility of the stations. At the same time, we are always talking about a certain effective thickness of the snow cover, which accumulates around the detector in the most bizarre way. On the sunny side, the snow melts faster, thereby further increasing the snow mass's unevenness near the detector. Therefore, we need to look for other approximate methods. One of them is based on comparing the variations recorded at the station under consideration with the variations without snow (considered as reference). This is not an ideal solution, since a detector surrounded by snow has slightly different coupling functions than a reference one, but this method is a fairly good approximation, as the practical application has shown.

Based on (1), the variations ν_i^{cor} of count rate at detector i relative to the base count rate value N_B, corrected for the snow effect and expressed in terms of the measured variations ν_i can be written as

$$\nu_i^{\text{cor}} = \frac{N_i^{\text{cor}}}{N_B} - 1 = \frac{N_i / \varepsilon_i}{N_B} - 1 = \frac{\nu_i + 1}{\varepsilon_i} - 1 \tag{2}$$

It can be seen from (2) that in order to determine the snow-corrected variations ν_i^{cor} from the measured variations ν_i, it is necessary to evaluate the efficiency ε_i. For this purpose, we will use the data of the reference detector with count rate S, which records approximately the same variations ν^S as the detector exposed to the influence of snow ν^{cor}, i.e. $\nu^S \simeq \nu^{\text{cor}}$ The selection criterion for a reference detector is discussed below. If this condition is applied to some averaged time interval, then we can write that

$$\frac{\bar{S}}{S_B} - 1 = \frac{\bar{N} / \varepsilon}{N_B} - 1 \text{ or } \varepsilon = \frac{\bar{N} / N_B}{\bar{S} / S_B} = \frac{\bar{\nu} + 1}{\bar{\nu}^S + 1} \tag{3}$$

When determining the average values of counting rate $\bar{N}$, $\bar{S}$ and accordingly variations $\bar{\nu}$, $\bar{\nu}^S$ (S_B is the value of reference detector's counting rate), the averaging interval is also important. We applied a filter of moving average (Smith 2002). The optimal filter length is n = 23. If one-way filters are applied, then this technique can be applied in real time (Smith 2002).

In an ideal case, the detectors are identical and located at the same point, which guarantees the same variation. The selection of a closely located reference station is not always possible, since, as we will see, almost all mid- and high-latitude stations are affected by snow. A universal, although somewhat laborious, is the estimation of the expected variations based on the analysis of the world neutron monitor network data.

In other cases, it is necessary to take into account their differences, using the reception coefficients C_0 of these detectors (Kobelev et al. 2011, 2013). Variations for each detector in the

KIEL-UP • DOI: 10.38072/2748-3150/p23

zero harmonic approximation can be written as $\nu^S = a_{10} C_0^S$ and $\nu = a_{10} C_0$, so $\nu^S / C_0^S = \nu / C_0$. Considering that

$$\left(\frac{\bar{S}}{S_B} - 1\right)\frac{1}{C_0^S} = \left(\frac{\bar{N}/\varepsilon}{N_B} - 1\right)\frac{1}{C_0} \quad , \tag{4}$$

instead of (3) we get

$$\varepsilon = \frac{\bar{\nu} + 1}{C_0 / C_0^S \cdot \bar{\nu}^S + 1} \tag{5}$$

The final corrections from the effect of snow variations in the detector should be carried out using expression (2), which involves the efficiency ε obtained from equation (5). The receiving coefficients of the zero harmonic for some detectors (lines 1 and 2), which must be freed from the snow effect and for the reference stations involved (lines 3 and 4), are given in table 1.

ESOI	**Magadan**	**Moscow**	**Jungfraujoch**	**AlmaAta**	**LomnitskyStit**	**Nain**	**Peawanuck**
0.4324	1.0044	0.9331	0.8924	0.6442	0.9113	1.1195	1.1194
Rome	**Mexico**	**Thailand**	**Jungfraujoch1**	**Athens**	**Potchefstrom**	**Tsumeb**	**Kiel**
0.5440	0.4518	0.2815	0.8924	0.4360	0.5383	0.4406	0.9505

Table 1: The receiving coefficients of the zero harmonic for some detector.

Several options for a reference station were considered. The Rome reference station option is chosen as the best (guaranteed there is no snow, long observation range, stable operation, good statistics of the 17nm64 detector).

3. Discussion of the results

The effective thickness of the snow cover at the ESOI station reaches 15 g/cm² (middle panel of Figure 1 – right). Effective snow depth is formed from the snow on the surface of the Faraday cage

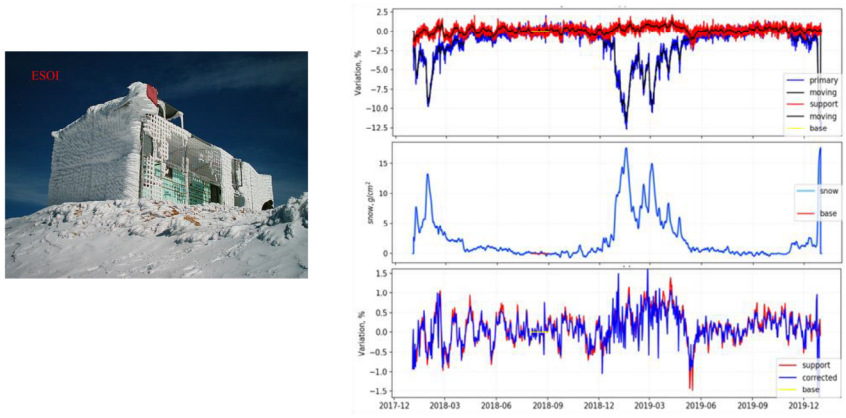

Figure 1: Station ESOI and snow effect: comparing of uncorrected and corrected variation (upper panel), snow thickness (middle panel), comparing the variation of ESOI (blue line) and Rome (red line) for 2018-2019 (bottom panel).

KIEL-UP • DOI: 10.38072/2748-3150/p23

and the snow surrounding the station. It can be assumed that the notches in the middle panel in figure 1 are associated with the periodic growth and melting of snow on the surface of the Faraday cage, and also that 1/3 of the effect is due to the snow surrounding the station.

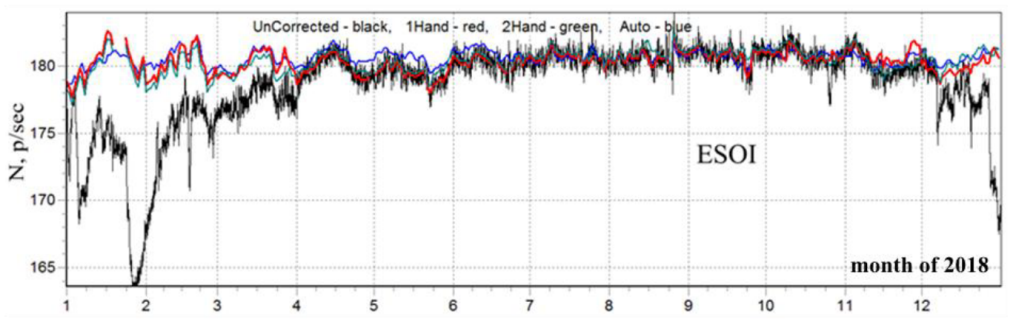

Figure 2: Comparing manually and automatically corrected data.

Figure 2 compares data adjusted by the method under discussion and data adjusted manually by two independent operators. The spread averaged over a year is no more than 0.1%.

From mid-latitude stations (Moscow, Novosibirsk, Magadan, Irkutsk, Peawanuck, Nain), one can consider the Moscow station. Despite the fact that the detector at the station is located in a building with a hipped roof, the effective snow thickness reaches 2 cm w.e. (figure 3), and the contribution from each of the 4 sections of the neutron monitor is the same. This indicates that the collection of neutrons occurs from a sufficiently large area and the unevenness of its coverage is imperceptible. The meteorological data can be found on the resource (Ventusky 2020).

High-latitude cosmic ray stations can be divided into two groups. The stations of the first group are close to mid-latitude detectors in terms of the snow effect. The effective thickness of the accumulated snow for such stations is 2-3 cm w.e. and they are located in the polar latitudes, where the

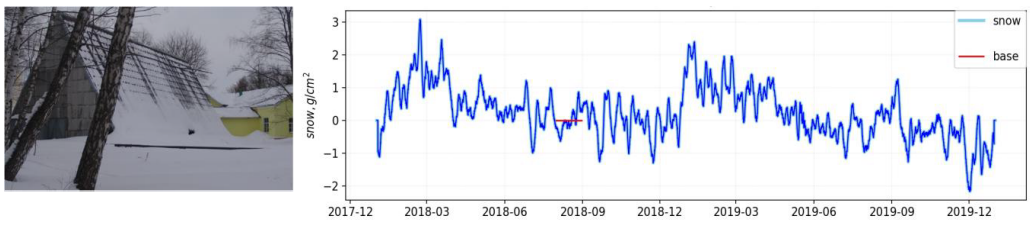

Figure 3: Station Moscow and effective snow thickness. Reference station is Rome

humidity of the air of the Gulf Stream is felt. Due to special conditions, this group also adjoins the Antarctic stations: Mirny (Fig.4), Terre Adelie, Mawson, YanBogo, Concordia, Sanae.

High-latitude stations of the second group are located in an area with sufficiently low humidity, where dry snow accumulates less on the roof and near the stations. These stations include Norilsk, Apatity, Tixie Bay, Cape Schmidt, Inuvik, where the snow effect is insignificant and close to the method error, i.e. 0.5 cm w.e. during the winter period.

KIEL-UP • DOI: 10.38072/2748-3150/p23

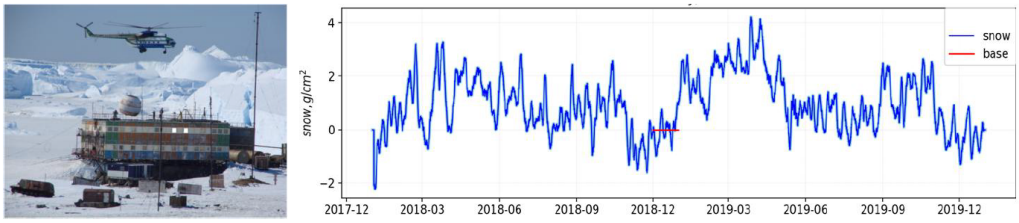

Figure 4: Station Mirny and effective snow thickness. Reference station is Rome.

The influence of snow cover near the detectors on their count rate was studied. Snow affects the data of all mountain, mid-latitude and most high-latitude detectors, which can be divided into groups.

For mountain stations, the effective thickness of the snow cover in winter reaches 10 cm of water equivalent (cm w.e.), which leads to significant errors of observed variations of cosmic rays, up to ~ 10% (figure 5).

4. Conclusions

The influence of snow cover near the detectors on their count rate was studied. Snow affects the data of all mountain, mid-latitude and most high-latitude detectors, which can be divided into groups.

For mountain stations, the effective thickness of the snow cover in winter reaches 10 cm of water equivalent (cm w.e.), which leads to significant errors of observed variations of cosmic rays, up to ~ 10%.

For mid-latitude and high-latitude stations, despite the use of hipped roofs, the effective thickness of the snow cover reaches about 2 cm w.e., which leads to errors of the observed variations in cosmic rays by up to 3%.

However, some of the high-latitude stations are located in areas with sufficiently low humidity, and dry snow accumulates less on the roof and near the stations. These stations include Norilsk, Tixie Bay, Cape Schmidt, Inuvik, Fort Smith.

The method of reference stations used in this work makes it possible to recover actual data almost automatically, by excluding the effect of snow influence. The error, in this case, depends on the thickness change rate of the snow cover (the characteristic time is a day). If the changes are slow (several days), then the errors introduced during data recovery can be neglected. If the

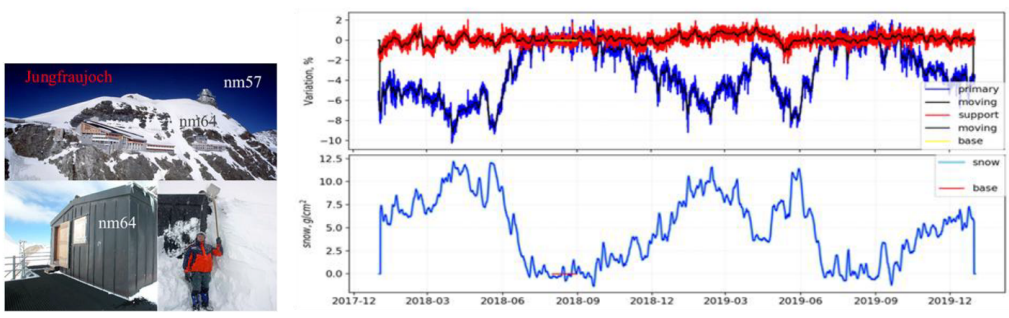

Figure 5: Station Jungfraujoch and effective snow thickness. Primary – station Jungfraujoch; reference (support) station - Rome; black lines – result of moving average filter.

changes are fast (several hours), then the errors that arise should be investigated especially, since they can increase the errors of the original data several times. But rapid changes are rare – only in moments of heavy snowfall, intense snow melting, or mechanical snow removal. The technique described in this work makes it possible not only to exclude the effect of snow, but also to estimate the effective thickness of the snow cover with an accuracy of 0.5 cm w.e.

The reference station method is good for solving the problem of automatic excluding of the surrounding snow cover influence on the counting rate of neutron detectors. But it is almost impossible to find an ideal reference station (closely located, snowless, working without interruptions during the period under consideration). Therefore, in order to ensure the guaranteed absence of snow, it is necessary to use mid-latitude or even low-latitude stations and introduce corrections for isotropic variations using the method of reception coefficients.

Acknowledgments

This work was partially supported by the grant RFBR № 18-02-00451. Experimentally and methodologically support the project USU „Russian national network of ground stations of cosmic rays“. We are grateful to all the staff of the World Network of cosmic ray stations http://cr0.izmiran.ru/ThankYou. We acknowledge the NMDB database (https://www.nmdb.eu/), founded under the European Union's FP7 programe (contract no. 213007) for providing the data.

References

Blomster, K., Tanskanen, P., 1969. "The influence of snow and water on the different multiplicities as observed in a neutron monitor NM-64 in Oulu", Proceedings of the 11th ICRC, Budapest, Vol. 2. Acta Physica, Supplement to Volume 29, 627

Kobelev, P., Belov, A., Mavromichalaki, E., Gerontidou, M., Yanke, V., 2011, "Variations of Barometric Coefficients of the Neutron Component in the 22-23 Cycles of Solar Activity", Proc. 32nd ICRC, id 654, Beijing, August, V. 11, 382–385, DOI: https://dx.doi.org/10.7529/ICRC2011/V11/0654

Kobelev, P., Belov, A., Eroshenko, E., Yanke, V., 2013. Reception coefficients and energy characteristics of the ground level cosmic ray detectors. Proc 33rd ICRC, Rio de Janeiro, id 0878, http://spaceweather.izmiran.ru/descriptions/cc.pdf (last accessed April 8, 2021)

Korotkov, V., Berkova, M., Belov, A., Eroshenko, E., Kobelev, P., Yanke, V., 2011, "Effect of snow in cosmic ray variations and methods for taking it into consideration" //, Geomagnetism and Aeronomy, Volume 51, Issue 2, 247-253, DOI: https://dx.doi.org/10.1134/S0016793211020095

Korotkov, V., Berkova, M., Belov, A., Eroshenko, E., Yanke, V., Pyle, R., 2013, "Procedure to emend neutron monitor data that are affected by snow accumulations on and around the detector housing", JGR: Space Physics, Vol. 118, 6852-6857, DOI: https://dx.doi.org/10.1002/2013JA018647

Smith, S.W., 2002, Digital Signal Processing: A Practical Guide for Engineers and Scientists

Ventusky, Web-application for meteo data visualization, https://www.ventusky.com (last accessed November 23, 2020)

Questions and answers

Rolf Bütikofer: How do you determine the snow thickness and the density of the snow?
Answer: The method directly gives the thickness of the snow in terms of the amount of substance. We don't need snow density. Linear snow thickness is required to determine density.

Rolf Bütikofer: Yes, I know very well that it is difficult to determine the water equivalent of snow. But Rome NM is not ESOI NM.
Answer: The method directly gives the thickness of the snow in water equivalent. Yes, ESOI NM is not Rome NM or any other detector. The difference should be taken into account using the reception factors for the two detectors. But in order to minimize the error, it is desirable to use the closest detectors.

Christian T. Steigies: The variations could also come from wind, water vapour, or other things?
Answer: Yes, wind accounting is especially important for high-latitude and mountain stations.

KIEL-UP • DOI: 10.38072/2748-3150/p23

Ludwig Klein: Do you have examples of wind corrections?
Answer: Yes, we dealt with the wind effect according to Mirny and Mawson data (using ground-based weather stations at the same points). However, the wind effect has not been reliably estimated: there is both a good correlation and its absence.

Kazuoki Munakata: I know only a correction using the free-air-pressure by nearby radiosonde measurements.
Answer: Perhaps, but in this case, higher layers of the atmosphere create the wind effect.

Cosmic ray studies with neutron detectors | Volume 1 (2021)
KIEL-UP • DOI: 10.38072/2748-3150/v1

Session 6: Abstracts

Responses of bare neutron counters to cosmic rays during 1995 and 2009 latitude surveys

Waraporn Nuntiyakul[1,2], Pierre-Simon Mangeard[3], Alejandro Saiz[4], David Ruffolo[4,2], Paul Evenson[3], John W. Bieber[3], John Clem[3], Allan Hallgren[5], James Madsen[6], Roger Pyle[7], Marc Duldig[8], John Humble[8], and Serap Tilav[3]

Correspondence
[1] Department of Physics and Materials Science, Faculty of Science, Chiang Mai University, Thailand
[2] National Astronomical Research Institute of Thailand (NARIT), Chiang Mai, Thailand
[3] Bartol Research Institute and Department of Physics and Astronomy, University of Delaware, Newark, USA
[4] Department of Physics, Faculty of Science, Mahidol University, Bangkok, Thailand
[5] Department of Physics and Astronomy, Uppsala University, Sweden
[6] Wisconsin IceCube Particle Astrophysics Center, University of Wisconsin-Madison, USA
[7] Pyle Consulting Group, Inc., St. Charles, USA
[8] School of Natural Sciences, University of Tasmania, Hobart, Tasmania, Australia

Ground-based neutron counters are a standard tool for detecting atmospheric showers from GeV range primary cosmic rays of either solar or galactic origin. Bare neutron counters, a type of lead-free neutron monitor, function much like standard neutron monitors but have different yield functions primarily because they are more sensitive to neutrons of lower energy. When operated together with standard monitors, the different yield functions allow estimates to be made of the energy spectrum of galactic or solar particles. At any given location, the magnetic field of the Earth excludes particles below a well-defined rigidity (momentum per unit charge) known as the cutoff rigidity, which can be accurately calculated using detailed models of the geomagnetic field. By carrying a neutron detector to different locations, e.g., on a ship, the Earth itself serves as a magnet spectrometer. We will present the responses to cosmic rays of bare neutron counters operated on board a ship during 1995 and 2009 survey years over a wide range of magnetic latitudes, that is, a latitude survey. In the 1995 survey, we carried an NM64 neutron monitor with three counter tubes, that is, a 3NM64, together with three bare neutron detectors. In the 2009 survey, two bare neutron detectors were operated on a ship where they ultimately were installed at the South Pole in 2010 to operate together with 3NM64 there.
This study is supported in part by the Thailand Science Research and Innovation via Research Team Award 6280002 and Research Grant for New Scholar MRG6280155 and the U.S. National Science Foundation Awards OPP0838838, PLR-1245939, and PLR1341562.

KIEL-UP • DOI: 10.38072/2748-3150/v1

Variability of effective cutoff rigidities for neutron monitors during 1950 – 2050

Lev Dorman[1,2], **Anatoly Belov**[1], **Eugenia A. Eroshenko**[†1], **Raisa Gushchina**[1], **Lev Pustilnik**[2], **Victor G. Yanke**[1]

Correspondence

[1] Pushkov Institute of Terrestrial Magnetism, Ionosphere and Radio Wave (IZMIRAN), Moscow, Russia

[2] Cosmic Ray and Space Weather Center, Tel Aviv University, Israel Space Agency with E. Segre Observatory on Mt. Hermon, Israel

Modern development of the experiment requires more rigorous studies of magnetospheric effects in terms of both the duration of observations and the accuracy of the experimental data. This is associated, for example, with the fact that the geomagnetic field has decreased by about 4% for the more than sixty-year period of cosmic ray observations, and it decreases at a different rate in different regions. Impresses that the contribution of high harmonicas of the geomagnetic field for this period, on the contrary, increased by about 30%. Besides, magnetic anomalies have the common tendency to a drift to the west and to the equator with an average speed of approximately 0.15 degrees per year. For practical purposes to estimate consequences of such big reorganization of a magnetic field from the point of view of magnetospheric effects of cosmic rays, it is necessary to receive planetary distributions of effective geomagnetic cutoff rigidities for the network of neutron monitor stations for each year and estimate the expected century variations of CR neutron component caused by geomagnetic variations.

Comparison between the observed and the computer modeled neutron monitor count rates

Danislav Sapundjiev, **Stanimir M. Stankov**

Correspondence

Royal Meteorological Institute of Belgium, KMI-IRM, Brussels, Belgium

Understanding the neutron monitor observations (its count rate) and the relation to the particle intensities in the space and atmospheric radiation environments is necessary for the application and use of these instruments for space weather research. The principal processes are neutron production and diffusion within the atmosphere and within the different components of the neutron monitor. A unique opportunity to understand the theory of the neutron monitors presented itself during the construction of the second neutron monitor in Dourbes (Belgium). Given the available modern computational techniques and the recorded measurements during the construction phases, we modeled the processes contributing to the count rate of the instrument. This work covers the first two stages of the construction - the assembly of the neutrons reflector and the installation of the lead producer. The results obtained from Monte-Carlo calculations of the modeled instrument compared with the corresponding observed count rates will be presented.

† deceased

KIEL-UP • DOI: 10.38072/2748-3150/v1

FLUKA simulation of neutron detector responses in latitude surveys to vertical secondary particles from cosmic rays

Waraporn Nuntiyakul[1,2], Audcharaporn Pagwhan[3], Kanokkarn Fongsamut[1], Peng Jiang[4], Pierre-Simon Mangeard[5], Alejandro Saiz[6], David Ruffolo[6,2], Paul Evenson[5], Kazuoki Munakata[7], James Madsen[8], Pongpichit Chuanraksasat[2], Boonrucksar Soonthornthum[2], Siramas Komonjinda[1], Ronald Macatangay[2]

Correspondence

[1] Department of Physics and Materials Science, Faculty of Science, Chiang Mai University, Thailand
[2] National Astronomical Research Institute of Thailand (NARIT), Chiang Mai, Thailand
[3] Graduate School, Chiang Mai University, Thailand
[4] Polar Research Institute of China, Pudong, Shanghai, China
[5] Bartol Research Institute and Department of Physics and Astronomy, University of Delaware, Newark, USA
[6] Department of Physics, Faculty of Science, Mahidol University, Bangkok, Thailand
[7] Department of Physics, Faculty of Science, Shinshu University, Nagano, Japan
[8] Wisconsin IceCube Particle Astrophysics Center, University of Wisconsin-Madison, Madison, USA

In the standard neutron monitor (NM64) design, there are lead rings to generate evaporation neutrons that are moderated by polyethylene before being detected in the neutron-sensitive proportional counter. A proportional counter without the lead, sometimes called a "lead-free" or "bare" counter, responds to lower energy particles on average and can be used in conjunction with an NM64 to estimate the energy spectrum of the primary cosmic rays. The objective of this work is initially to refine the understanding of the lead-free neutron monitor operation in latitude surveys using FLUKA Monte-Carlo simulations. Simulation of the responses to neutrons and other atmospheric particles, accounting for the dead time, will also be reported. This study is supported in part by the Thailand Science Research and Innovation via Research Team Award 6280002 and Research Grant for New Scholar MRG6280155.

Calculations of the sensitivity of the SEVAN network to galactic and solar cosmic rays

Mary Zazyan, Ashot Chilingarian

Correspondence

Artem Alikhanyan National Lab (Yerevan Physics Institute), Armenia

To understand the sensitivity of the new type of particle detectors to the highest energy solar ions we investigate the response of the SEVAN basic units to galactic and solar protons. The hard spectra of solar ions at the highest energies (–4 to –5 at rigidities of ≈10 GV) indicate the upcoming very intense solar ion flux with rigidities >50MV, very dangerous for satellite electronics and astronauts. Our calculations demonstrate that with the SEVAN network it will be possible:

- Probe different populations of primary CR from 7GV up to 20–30GV;
- Reconstruct SCR spectra and determine the position of the spectral "knees";
- Classify GLEs in "neutron" or "proton" initiated events.

KIEL-UP • DOI: 10.38072/2748-3150/v1

Measurements of cosmic rays by a mini neutron monitor at Neumeier III from 2014 to 2018

Bernd Heber[1], **Dennis Galsdorf**[1], **Konstantin Herbst**[1], **Patrick Kühl**[1], **Carolin Schwerdt**[2], **Du Toit Strauss**[3], **Michael Walter**[2]

Correspondence

[1] Extraterrestrial Physics,Institute of Experimental and Applied Physics, Kiel University, Germany

[2] Deutsches Elektronen-Synchrotron DESY in Zeuthen, Germany

[3] Center for Space Research, North-West University, Potchefstroom, South Africa

Neutron Monitors (NMs) and Muon Telescopes (MTs) are ground-based devices to measure the flux variation of Galactic Cosmic Rays (GCRs) and Ground Level Enhancements (GLEs). They are reliable devices but difficult to install because of their size and weight. Therefore Moraal et al. (2001) suggested to develop a portable calibration neutron monitor that can be carried to any existing station. Since their measurements are influenced by the variable Earth magnetic field and the atmospheric conditions close to its position a detailed knowledge of the instrument sensitivity with geomagnetic latitude (rigidity), atmospheric pressure but also temporal variations of the environment are essential. One mini NM, constructed by the North West University campus Potchefstroom is measuring the variation of galactic cosmic rays was installed in 2014 and was operational for four years at the German Antarctic Neumeier III station. Here we present the measurements taken by the monitor comparing it with different monitors that have a cutoff rigidity below the atmospheric one.

Session 7:

Data bases and catalogues

Cosmic ray studies with neutron detectors | Volume 1 (2021) 197
KIEL-UP • DOI: 10.38072/2748-3150/p24

Cutoff rigidity and particle trajectories online calculator

Semen M. Belov, Egor Zobnin, Victor G. Yanke

Correspondence
Pushkov Institute of Terrestrial Magnetism, Ionosphere and Radio Wave Propagation (IZMIRAN), Moscow, Russia,
sfrovis@gmail.com, egorizzee@gmail.com, yanke@izmiran.ru

Keywords
magnetospheric effect; cutoff rigidity; particle trajectories; cosmic rays

Abstract
Over the years, many authors have developed unique software packages for calculating the geomagnetic cutoff rigidities and the asymptotic directions of particle arrival. Such programs are used for mass calculations and require some skill. However, it is often necessary to carry out single calculations with the same accuracy. For this purpose, calculator programs have been created on the basis of already developed software packages. One of such programs, a calculator, is described in this work.

1. Introduction

The magnetospheric effect of cosmic rays, i.e. the change in particle flux in response to a change in the state of the magnetosphere or position in the magnetosphere was discovered by Clay in 1927, who revealed the latitudinal effect on the Amsterdam-Sydney route and used the Earth‘s magnetic field as a charged particle spectrometer for the first time. The correct explanation of the Clay effect was given in (Bothe & Kolhorster 1929) in assuming that some of the cosmic rays must be charged particles.

Bruno Rossi (1930) predicted the difference between the intensities of cosmic rays coming from the east and west. It was found that the intensity is higher from the western directions, which indicates that most of the primary particles are positive.

The first who appreciated the extreme importance for space physics of the problem of the motion of charged particles in the Earth‘s magnetic field was Størmer (1930). In the dipole approximation, Størmer obtained an analytical expression for the trajectories of cosmic rays (albeit only in the equatorial plane) and introduced the concept of forbidden trajectories.

Lemaitre and Vallarta (1936a, 1936b), developing Størmer's theory and the concept of a forbidden cone, introduced the concept of a permitted cone when all trajectories are permitted, and the concept of a basic cone, which includes a permitted cone and a penumbra. At the equator, the permitted and main cones coincide, but at mid-latitudes, there are sufficient differences: the region of rigidity between the cones forms penumbra, i.e. many allowed and forbidden trajectories. The relative role of the penumbra increases with increasing geomagnetic latitude and completely disappears at high latitudes. The area of the penumbra was directly discovered by them when calculating the trajectories of particles in a dipole field on analog computers.

Jory (1956) was the first to carry out numerical trajectory calculations of cosmic rays in a dipole magnetic field. McCracken (McCracken et al. 1962) carried out numerical trajectory calculations of cosmic rays already in a real geomagnetic field, represented by six spherical harmonics.

KIEL-UP • DOI: 10.38072/2748-3150/p24

Two key concepts, such as the geomagnetic cutoff rigidity (for describing isotropic variations) and the asymptotic cone of particle acceptance (for describing anisotropic variations), allow us to describe all magnetospheric effects of cosmic rays. When describing long-term variations, it is sufficient to restrict ourselves to the isotropic approximation. At present, the method of numerical integration of the equations of motion of charged particles is generally accepted for determining the cutoff rigidities. With this method, the cutoff rigidity can be calculated with any precision. Moreover, when approximating the geomagnetic field, both internal and external sources of the magnetic field can be taken into account.

The most complete and systematic studies of the magnetospheric effects of cosmic rays, including their long-term changes, were carried out by M. Shea and D. Smart based on the software package (Cutoff Rigidity Program 2020). The global distributions of the vertical rigidity of the geomagnetic cutoff were calculated with a step of 5° × 15° in latitude and longitude for the epochs from 1955 to 2000 (Smart & Shea, 2007a, 2007b). Vertical geomagnetic cutoff rigidities were obtained for all stations of the global network for ten five-year epochs 1955-2000 (Shea & Smart 1965, 1966, 1967; Smart & Shea 1994, 2001, 2003). In Shea & Smart 1975 and Storini et al. 1999, the unevenness of changes in the planetary distribution of geomagnetic cutoff rigidities over 20 years from 1955 to 1975, especially in the southern Atlantic Ocean, is shown. The South Atlantic saw a decrease in rigidity, while the North showed a comparable increase in vertical cutoff rigidity.

In Gvozdevsky et al. 2016, for the vertical directions of particle arrival by the method of trajectory calculations, a planetary distribution of the geomagnetic cutoff rigidities with a step of 5° × 15° in latitude and longitude was obtained for the period 1950–2020 with a forecast up to 2050. For the period 1950-2050, temporal variations of the geomagnetic cutoff rigidities were also obtained for the worldwide network of neutron monitors. From the data of muon telescopes, the geomagnetic cutoff rigidity of inclined directions of particle arrival was also obtained.

The purpose of this work is to create a calculator for obtaining the geomagnetic cutoff rigidity with the most complete graphical presentation of the results. To carry out trajectory calculations, use the developed and debugged software packages.

2. Method of trajectory calculations

The main method for studying the trajectories of charged particles in the geomagnetic field is the numerical integration of the equation of motion. At present, the most widespread use of various modifications of the 4th order Runge-Kutta method, with the use of standard methods of accuracy control, including checking the conservation of the integral of motion - energy (or modulus of velocity). In addition, the reverse integration method is used to check the correctness of the numerical solution. Its essence is that due to the structure of the Lorentz equation, which describes the motion of a charged particle in a stationary magnetic field, with the simultaneous replacement of the sign of the particle charge and its velocity vector with opposite values, the trajectory of motion is completely preserved, but passes in the opposite direction. Having stopped at some point the numerical integration, one can try to return to the starting point (or in its vicinity) by backward integration, thereby estimating the error of the numerical solution. The same method of backward integration is used to determine the initial point at which a cosmic ray particle came from interplanetary space to the boundary of the Earth's magnetosphere. Since the main flux of cosmic rays is made up of protons, the calculations use a proton with the opposite sign.

Integration ends in three cases:

- either after a specified time has elapsed (the particle is considered captured),
- either the particle crossed the magnetopause surface (went beyond the magnetosphere),
- or its radius vector turned out to be less than (R_E + 20) km (the particle returned to the atmosphere).

KIEL-UP • DOI: 10.38072/2748-3150/p24

In the case of the second result, this trajectory is marked as allowed, otherwise, it is prohibited. The described method of trajectory calculations was first formulated and applied in McCracken et al. (1962) and is also described in Smart & Shea (2001). This technique is implemented in works (Gvozdevsky et al. 2015, 2016, 2017, 2018, 2019). Particular attention was paid to the issue of accounting for the penumbra. The results are archived on the server (Mag_Effect 2018).

3. Involved models of the magnetosphere

For the trajectory calculations, the model of the International Geomagnetic Reference Field IGRF-12 (Thebault et al. 2015) was used. This is a model of the main geomagnetic field for the 2015.0 epoch and a linear annual predictive model of the secular variation for 2015.0-2020.0. We have continued this linear approximation of the coefficients of the Gaussian expansion until 2050. The geomagnetic field model is represented by the 13th spherical harmonics, but the predictive model is limited to the 8th harmonics. For trial calculations of the characteristics of the magnetic field at different points of the magnetosphere, one can use a calculator (Magnetic calculator 2019).

The contribution of external magnetic fields was taken into account based on the empirical models of Tsyganenko (Magnetospheric modeling 2020). To describe the contribution of external magnetic fields to quiet or weakly disturbed periods (from Kp = 0 to Kp = 5), the widely used Tsyganenko T89 model was used (Tsyganenko 1989). At higher disturbances, it is necessary to use the T96 model (Tsyganenko 1996), which describes the position of the magnetopause depending on the state of the solar wind. The input parameters in the T96 model are the density and speed of the solar wind, which determine its pressure on the magnetosphere, the By and Bz components of the IMF, and the Dst index of geomagnetic activity. If periods of a very strongly disturbed magnetosphere (Dst≤–65 nT) are considered, then the Ts02 (Tsyganenko 2003) or Ts04 (Tsyganenko 2005, 2013) models should be involved, which differ in different approximations of the same experimental data.

4. Description of the program calculator Cutoff-2050

The Cutoff-2050 Calculator is available at https://tools.izmiran.ru/ (Calculator Cutoff-2050, 2020). The calculator for calculating geomagnetic cutoff rigidities is based on the Cutoff-2050 program, which was used in (Gvozdevsky et al. 2019 and references). Cutoff-2050 program is located at the same address.

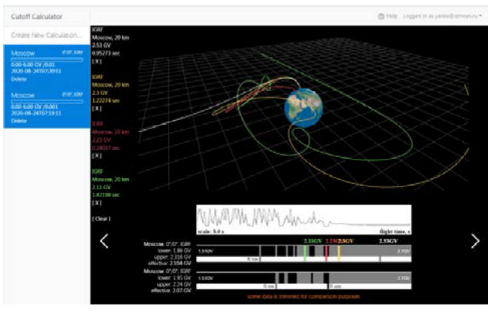

Figure 1: Comparison of the vertical geomagnetic cutoff rigidity at Moscow station obtained with different steps of integration: 0.01 and 0.001 GV.

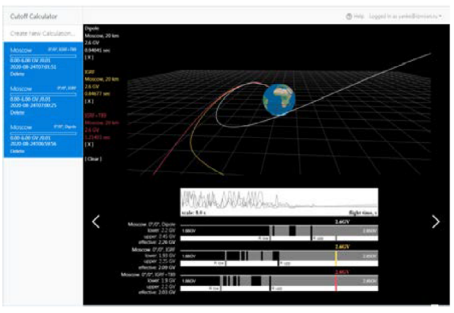

Figure 2: Comparison of the vertical geomagnetic cutoff rigidity at Moscow station obtained with for the models: Dipole, IGRF, IGRF+T89 and integrating step 0.01 GV.

KIEL-UP • DOI: 10.38072/2748-3150/p24

At the first login, any user creates a personal account, in which he can accumulate and compare the results of calculations. When you select Create New Calculation, a dialog box of parameters appears, the values of which are obvious.

So, for example, figure 1 shows the calculations and comparison of the vertical rigidity of the geomagnetic cutoff for the Moscow station for two values of the integration steps. If you select the hardness of a particle on the penumbra scale with the mouse, then the trajectory of this particle in this magnetic field is displayed. Above the penumbra field, there is a graph showing the time of particle motion until it leaves the magnetosphere for each rigidity in the considered range.

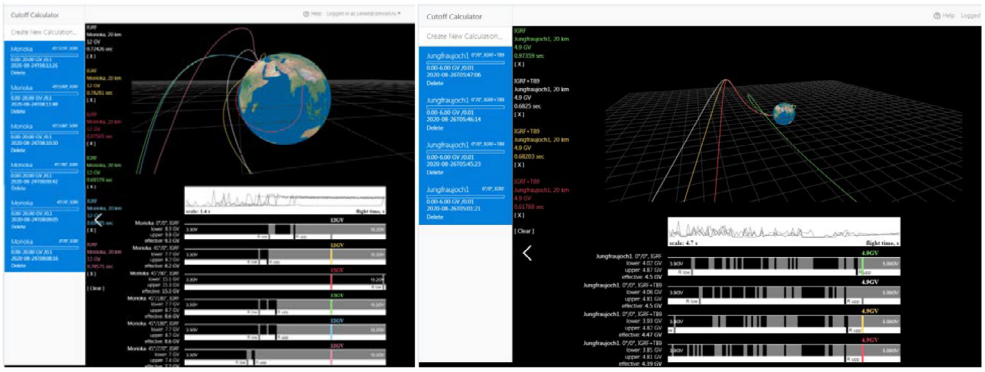

Figure 3: Geomagnetic cutoff rigidity for Morioka under model IGRF+T89 and integrating step 0.1 GV for vertical, zenith angle 45° and azimuth angles 0°, 90°, 180°, 270°.

Figure 4: Geomagnetic cutoff rigidity for Jungfraujoch station at the models IGRF and IGRF+T89 (Kp=0, 2, 4).

Figure 2 shows another example, which compares the results obtained using three magnetic field models: dipole, IGRF, IGRF + T89. Particle trajectories are also displayed after selecting the appropriate stiffness on the penumbra scale. Three trajectories for 2.6 GV particles are compared.

Figure 3 shows an example of vertical and inclined trajectories of particle motion using the Morioka telescope for the IGRF model of the magnetic field. Particle trajectories are also displayed after selecting the appropriate rigidity on the penumbra scale. The trajectories are compared for particles with a rigidity of 12.0 GV.

Figure 4 compares the geomagnetic cutoff rigidities for Jungfraujoch for the IGRF and IGRF + T89 models (Kp = 0, 2, 4).

Table 1 shows the parameters of the test calculations of the calculator for various models. Calculating the geomagnetic cutoff rigidities for the IGRF + T96 model and especially for the IGRF + T02 model requires a lot of computational time and this must be taken into account when planning the calculations.

Model	Parametrs					Result			
						Cutoff rigidities, GV			Calculation time, sec
	Kp	P_{sw}(nPa), Solar wind dynamic pressure	D_{st}-index (nT)	IMF B_y & B_z (nT)	G_1 & G_2	lower	upper	effective	
Dipole						2.337	2.737	2.498	6
IGRF						1.765	2.416	2.185	37
IGRF+T89	4					1.582	2.190	1.922	28
IGRF+T96		2	-50.0	0 and 5		1.518	2.156	1.906	1188
IGRF+Ts02		2	-50.0	0 and 5	6 and 10	1.649	2.234	1.947	3964

rigidity lower and upper limit (GV): 0.0 – 3.0
step 0.001 GV, Maximum time of flight - 180.00 s.

Table 1: For 01.07.2017 00:00:00 and Geographic coordinates (latitude, longitude) (55.00, 40.00), Vertical angle 0.00 and Azimuthal angle 0.00.

KIEL-UP • DOI: 10.38072/2748-3150/p24

5. Available calculators for calculating geomagnetic cutoff rigidities

Several calculators have been developed for calculating geomagnetic cutoff rigidities. A simple online internet project (Cutoff rigidity Calculator 2010) is based on the IGRF model and considers only vertically falling particles. The algorithm described in (Smart & Shea 2001) is applied. Disadvantages: the contribution of the outer magnetosphere is not taken into account, only vertical trajectories are considered, there is no graphical presentation of the results of calculating the penumbra, trajectories.

Another online internet project (Web Calculators 2019) is based on more complex magnetosphere models (Tsyganenko 1996; Tsyganenko et al. 2005) with automatic involving of the input parameters of the interplanetary medium necessary for the magnetosphere model, which is a very convenient and useful option. The program also reconstructs the trajectories of particles inside the magnetosphere. The calculator has a number of other useful features like calculating the Larmor radius inside, R-E converter. Disadvantages: only vertical trajectories are considered, there is no graphical presentation of the results of trajectory calculations - penumbra.

The online calculator (Calculator cutoff 2018) is based on the methodology described in (Gvozdevsky et al. 2019 and references). The result of the calculator's work is the lower, upper and effective values of the geomagnetic cutoff and penumbra stiffness for one of the specified magnetosphere models: dipole, IGRF, Tsyganenko IGRF + T89, IGRF + T96, IGRF + T02 models. Disadvantages: no graphical representation of trajectories.

6. Conclusions

1). The Cutoff-2050 calculator calculates the rigidity of the geomagnetic cutoff and particle trajectory for a given date (1900-2050) and at a given geographic point for magnetosphere models: dipole, IGRF, Tsyganenko model: IGRF + T89 and higher order IGRF + T96 and IGRF + models T02, but the latter require a long calculation time.
2). For regular users, it is possible to organize on the server personal accounts of users to accumulate and store the results obtained.
3). Visualization of all the results obtained: penumbra, time of movement and trajectories of particles.
4). The calculator interface allows you to visually carry out a comparative analysis of trajectories for various models and parameters.
5). The Cutoff-2050 calculator is an effective tool for urgent single calculations.
6). The task has significant educational potential since the capabilities of the online calculator can be used to teach students of the relevant specialties.

Acknowledgments

This work was partially supported by the grant RFBR No. 18-02-00451. Experimentally and methodologically support the project USU „Russian national network of ground stations of cosmic rays". We are grateful to all the staff of the World Network of cosmic ray stations http://cr0.izmiran.ru/ThankYou.

References

Bothe W., Kolhorster W., 1929, Das Wesen der Höhenstrahlung, Ztschr. Phys., Bd. 56, S. 751-777

Cooke, D. J., Humble J. E., Shea M. A., Smart D. F., et al. 1991, "On Cosmic-Ray Cut-Off Terminology" Il Nuovo Cimento C14, 213-234, DOI: https://doi.org/10.1007/BF02509357

Gvozdevsky, B., Dorman L., Abunin, A., Preobrazhensky, M., Gushchina, R., Belov, A., Eroshenko, E.,Yanke, V., 2015, "Variations of the vertical

cut off rigidities for the world wide neutron monitor network over the period of continues monitoring of cosmic rays", Proc. 34th ICRC, Hague, https://pos.sissa.it/236/203/pdf (last accessed April 9, 2021)

Gvozdevsky, B. B., Abunin, A., Kobelev, P. G., Gushchina, R. T., Belov, A. V., Eroshenko. E. A., Yanke, V. G., 2016, Magnetospheric effects of cosmic rays. I. Long-term changes in the geomagnetic cutoff rigidities for the stations of the global network of neutron monitors, Geomagnetism and aeronomy: V. 56, No 4, 381-392, DOI: https://doi.org/10.1134/S0016793216040046

Gvozdevsky, B., Belov, A., Gushchina, R., Eroshenko, E., Preobrazhensky, M., Yanke, V., 2017, "The secular variations of cosmic ray cutoff rigidities, caused by century variations in geomagnetic field, and cosmic ray variations", 35th International Cosmic Ray Conference – ICRC 2017, 10–20 July, 2017, Bexco, Busan, Korea, https://pos.sissa.it, PoS(ICRC2017)067, 12–20, https://pos.sissa.it/301/067/pdf (last accessed April 9, 2021)

Gvozdevsky, B. B., Belov, A. V., Gushchina, R. T., Eroshenko, E. A., Kobelev, P. G., Yanke, V. G., 2017, Long-term changes in the vertical rigidity of the geomagnetic cutoff over the entire period of monitoring of cosmic rays, „Physics of Auroral Phenomena" Proc. XL Annual Seminar, Apatity, 89-93, http://pgia.ru:81/seminar/archive (last accessed April 9, 2021)

Gvozdevsky, B. B., Belov, A. V., Gushchina, R. T., Eroshenko, E. A., Danilova, O. A., Yanke, V. G., 2018a, Peculiarities of long-term changes in the rigidity of geomagnetic cutoff of cosmic rays of inclined directions, „Physics of Auroral Phenomena" Proc. 41st Annual Seminar, Apatity, 80-83, DOI: https://doi.org/10.25702/KSC.2588-0039.2018.41.80-83

Gvozdevsky, B. B., Belov, A.V., Gushchina, R.T., Kobelev, P.G., Eroshenko, E.A., Yanke, V.G., 2018b, "Long-Term Changes in Vertical Geomagnetic Cutoff Rigidities of Cosmic Rays", Physics of Atomic Nuclei, Vol. 81, No. 9, 1382-1389, DOI: https://doi.org/10.1134/S1063778818090132

Gvozdevsky, B. B., Belov, A. V., Gushchina, R.T., Eroshenko, E.A., Yanke, V.G., 2019, "Planetary long term changes of the cosmic ray geomagnetic cut off rigidities" (26th Extended ECRS + 35th RCRC, Barnaul, Russia, 6-10 July 2018. SH34). Journal of Physics: Conference Series, 012008, DOI: https://doi.org/10.1088/1742-6596/1181/1/012008

Jory, F.S., 1956, Selected cosmic-ray orbits in the Earth's magnetic field, Phys. Rev. V.103. № 4., 1068-1075

Lemaitre, G.E., Vallarta, M.S., 1936, On the Geomagnetic Analysis of Cosmic Radiation, Phys. Rev. V. 49, 719-726

Lemaitre, G. E., Vallarta, M.S., 1936a, On the Allowed Cone of Cosmic Radiation, Phys. Rev. V.50, 493-504

McCracken, K.G., Rao, U.R., Shea, M.A., 1962, The Trajectories of Cosmic Rays in a High Degree Simulation of the Geomagnetic Field, M.I.T., Techn. Rep. 77, Lab. for Nucl. Sci. and Eng., Mass. Inst. of Technol., Cambridge

Rossi, B., 1930, "Method of Registrating Multiple Simultaneous Impuls of Several Geigers's Counters", Nature, 125, No. 3156, 636-636, DOI: https://doi.org/10.1038/125636a0

Shea, M.A., Smart, D.F., McCracken K.G., 1965, A study of vertical cutoff rigidities using sixth degree simulations of the geomagnetic field, J.Geophys.Res., V. 70. - N 17. - P.4117-4130

Shea, M.A., Smart, D.F., 1966, "Vertical cutoff rigidities in the South Atlantic", Space Res., 6, 177–187

Shea, M.A., Smart, D.F., 1967, "Worldwide trajectory-derived vertical cutoff rigidities and their application to experimental measurements for 1955", JGR, V72, No7, 2021-2028

Shea, M.A., Smart, D.F., 1975, "A five by fifteen degree world grid of calculated cosmic ray vertical cutoff rigidities for 1965 and 1975", Proc. 14th Int. Cosmic Ray Conf., Munchen, 4, 1298-1303

Smart, D.F., Shea, M.A., 1994, "Geomagnetic cutoffs: A review for space dosimetry applications", Adv. Space Res., 14, 10, 787-796

Smart, D. F., Shea, M. A., 2001, Geomagnetic Cutoff Rigidity Computer Program: Theory, Software Description and Example, NASA Technical Reports Serve, Final Report, 199 pp., 18 January 2001, ID: 20010071975 (last accessed April 9, 2021)

Smart, D.F., Shea, M.A., 2003, "The space developed dynamic vertical cutoff and its applicability to aircraft radiation dose", Adv. Space Res., 32, 1, 103-108

Smart, D.F., Shea, M.A., 2007a, "World Grid of Calculated Cosmic Ray Vertical Cutoff Rigidities for Epoch 1995.0", Proc. 30th ICRC, Mexico, V.1 (SH), 733-736

Smart, D.F., Shea, M.A., 2007b, "World Grid of Calculated Cosmic Ray Vertical Cutoff Rigidities for Epoch 2000.0", Proc. 30th ICRC, Mexico, V.1 (SH), 737-740

Storini, M., Shea, M.A., Smart, D.F., Cordaro, E.G., 1999, "Cuttof variability for Antarctic Laboratory for Cosmic Rays (LARC:1955-1995)", 26th ICR, Salk Lake City, SH3.6.30 (last accessed April 9, 2021), Vol. 7, 402-405,.

Størmer, C., 1930, On the trajectories of electric particles in the field of magnetic dipole with applications to the theory of cosmic radiation, Astrophysics. 1: 237

Thebault, E., Finlay, C. C., Zvereva, T,et al 2015, "International Geomagnetic Reference Field: the 12th generation", Earth, Planets and Space, V 67, No 79, DOI: https://doi.org/10.1186/s40623-015-0228-9

Tsyganenko, N. A., 1989, A magnetospheric magnetic field model with a warped tail current sheet, Planet. Space Sci., 37, No. 1, 5-20, DOI: https://doi.org/10.1016/0032-0633(89)90066-4

Tsyganenko N. A., Stern, D. P., 1996, Modeling the global magnetic field of the large-scale Birkeland current systems, J. Geophys. Res., 101, 27187-27198, DOI: https://doi.org/10.1029/98JA02292

Tsyganenko, N. A., Singer, H. J., Kasper, J. C., 2003, Storm-time distortion of the inner magnetosphere: How severe can it get?, J. Geophys. Res., 108, No. A5, 1209, DOI: https://doi.org/10.1029/2002JA009808

Tsyganenko, N. A., Sitnov, M. I., 2005, Modeling the dynamics of the inner magnetosphere during strong geomagnetic storms, J. Geophys. Res. 110, A03208, DOI: https://doi.org/10.1029/2004JA010798

Tsyganenko, N.A., 2013, Data-based modelling of the Earth's dynamic magnetosphere: a review, Ann. Geophys., 31, 1745-1772, DOI: https://doi.org/10.5194/angeo-31-1745-2013

Online data products

Calculator CutOff-2050, 2020: https://tools.izmiran.ru (last accessed April 9, 2021)

Cutoff rigidity Calculator, 2010, Zreda Marek, COSMOS project University of Arizona, http://cosmos.hwr.arizona.edu/Util/rigidity.php (last accessed April 9, 2021)

Cutoff Rigidity Program, 2020 https://ccmc.gsfc.nasa.gov/modelweb/sun/cutoff.html (last accessed April 9, 2021)

Magnetic calculator, 2019, https://geomag.nrcan.gc.ca/calc/calc-en.php (last accessed April 9, 2021)

KIEL-UP • DOI: 10.38072/2748-3150/p24

Magnetospheric modeling, 2020, http://geo.phys.spbu.ru/magmodel/empiric.html#t13 (last accessed April 9, 2021)

Mag_Effect, 2018, http://cosrays.izmiran.ru/dbs/MagEffect (last accessed May 31, 2021)

Web Calculators, 2019, Boschini M. J., Della T. S., Gervasi M., Grandi D., Rancoita P. G. , Bobik P., Kudela K., http://www.geomagsphere.org (last accessed April 9, 2021)

Questions and answers

Monica Laurenza: Is it possible for the user to change all model parameters?
Answer: Yes, it is possible. But it should be remembered that the computation time for IGRF + T96 model, for example, and higher models can be quite long.

Alexander Mishev: What is the rigidity resolution for the computations 0.01, 0.001 Gv or less?
Answer: The integration step is especially important in the penumbra area. An integration step of 0.01 results in a rigidity error of ~ 0.1 GV, an integration step of ~ 0.001 leads to a rigidity error of ~ 0.05 GV.

Question: Is it possible to use the program on a PC?
Answer: Yes, it is possible.

Christian T. Steigies: IGRF has been updated recently (2019?), are you using the latest model?
Answer: No, this version was not involved. The IGRF-2015 model was used with a forecast up to IGRF-2020. But there are no problems with the inclusion of IGRF-2019.

James Ryan: Can this be adapted to low Earth orbiting spacecraft, like PAMELA?
Answer: Yes, the calculations are applicable across the entire magnetosphere.

Marc Duldig: Historically please remember the first paper to comprehensively discuss the CR penumbra: Cooke D. J., Humble J. E., Shea M. A., Smart D. F., et al. "On Cosmic-Ray Cut-Off Terminology" Il Nuovo Cimento C14, 213-234 1991, DOI: https://doi.org/10.1007/BF02509357
Answer: Yes, thank you, the historical overview and helpful discussion of terminology should be preserved in our work.

Rolf Bütikofer: Do you plan to offer the determination of cutoff rigidities for a network with a selected mesh size in a single run?
Answer: No, we did not plan, but we shall plan, if necessary. The server http://tools.izmiran.ru contains tables (5 ° × 15 ° grid) of planetary distributions of geomagnetic cutoff rigidities from 1900 to 2050 with a step of 5 years. But for a list of stations, such calculations can be organized.

Marc Duldig: Will you optimize using parallel processing with PC GPU?
Answer: No, until not.

Cosmic ray studies with neutron detectors | Volume 1 (2021)
KIEL-UP • DOI: 10.38072/2748-3150/p25

Data management at the Oulu cosmic ray station

Stepan Poluianov[1,2], **Ilya Usoskin**[1,2], **Askar Ibragimov**[3]

Correspondence
[1] Sodankylä Geophysical Observatory, University of Oulu, Finland, stepan.poluianov@oulu.fi, ilya.usoskin@oulu.fi
[2] Space Physics and Astronomy Research Unit, University of Oulu, Finland
[3] Independent researcher, Helsinki, Finland, askar.ibragimov@gmail.com

Keywords
cosmic rays; neutron monitor; data management

Abstract
With the recent electronics upgrade of Antarctic neutron monitors (NMs) DOMC and DOMB in 2019, the Oulu cosmic ray station (Sodankylä Geophysical Observatory, Finland) receives a significantly larger amount of data than before. This has led to a need for an important upgrade of the configuration of servers working at the station. The new configuration has three types of servers: a web-server, a datamaster server and data acquisition machines. The web-server provides a user interface for services of the station: the main website, the GLE database and other services. The datamaster is the main server, which stores all data in raw files and a database. Data acquisition machines are computers that directly receive data from the instruments and send the files farther to the datamaster server. This work describes technical details of the cosmic ray station setup providing reliable and secure data acquisition, handling and publication.

1. Introduction

With new NM DOMC/DOMB, and particularly with much higher data flow caused by their new electronics (see Poluianov, Usoskin and Strauss, this issue), the Oulu cosmic ray station needed an upgrade of its data management system. The changes were aimed to increase the reliability of the system and to raise its capability for new instruments and data.

2. What is new?

Briefly, the new improvements in the data management system are:

- Data storage and web-services split into different machines,
- additional acquisition computer for tests at OULU NM,
- new backups to remote storages SGO Jako and CSC Allas,
- new alerting system,
- new code repository and its deployment,
- new wiki-like documentation.

Most of them are described in detail in the following sub-sections.

KIEL-UP • DOI: 10.38072/2748-3150/p25

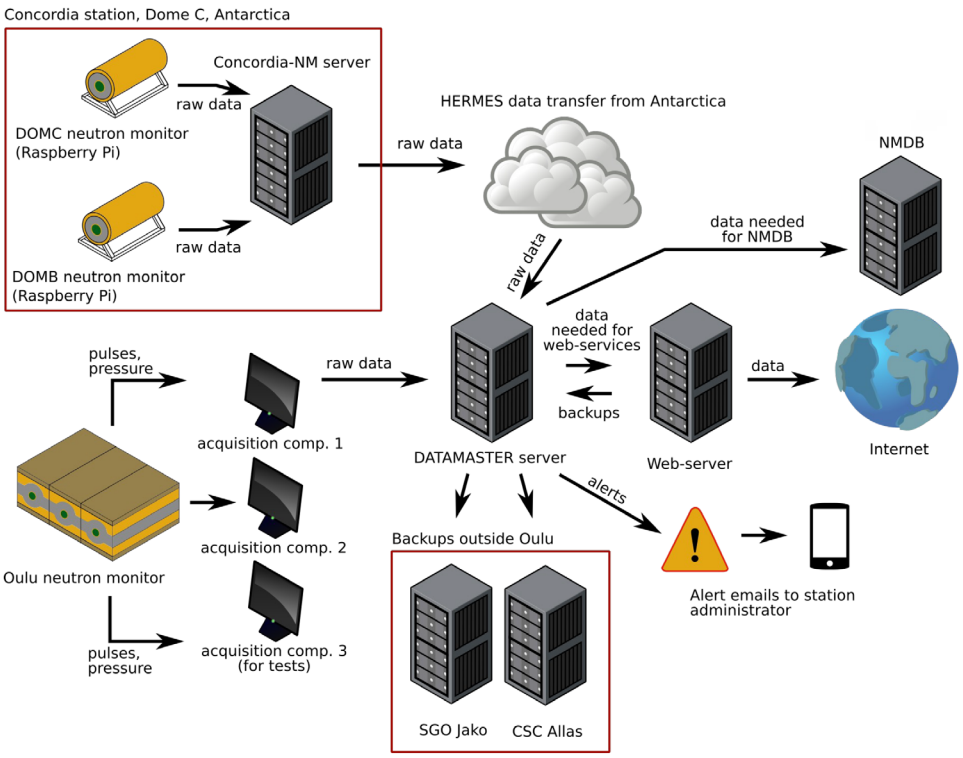

Figure 1: Data flow of the Oulu cosmic ray station.

2.1 Split data acquisition, storage and web services

OULU NM has two independent data acquisition chains (TTL-converters, counters, barometers, GPS-receivers, watchdogs, computers) for reliability. It also has an additional acquisition chain for the development of software and tests. Raw data from OULU, as well as from DOMC/DOMB go to a dedicated data-server. That machine has the only purpose to keep original raw files from instruments and a database. It was designed and set up for that particular purpose. For safety reasons, the data-server and acquisition computers are protected by a firewall and are not available from the internet. Access of users to the cosmic ray data is provided via the web-server, which hosts also various station services, e.g., websites http://cosmicrays.oulu.fi, http://gle.oulu.fi (last accessed April 12, 2021).

2.2 Backup

All important parts of the system are backed up daily. We follow and even exceed the so-called 3-2-1 rule (actually, we have more than 3 copies, 2 types of backups, with all copies stored in different locations in Finland). For that purpose, we use software Restic (https://restic.net, last accessed April 12, 2021). We back up not only data but also the code repository, configuration playbooks, documentation and websites.

2.3 Alerts

To react fast to possible non-nominal situations with measurements, there are set up alert emails, which go to station administrators. We use the service SendGrid (https://sendgrid.com, last accessed April 12, 2021) for that purpose.

KIEL-UP • DOI: 10.38072/2748-3150/p25

2.4 Code repository and deployment

New instruments and services led to an increase of the amount of written code (more programs, scripts, configuration files, documentation, etc.), which should be also stored properly (safely, with version control and backups). We use Git (https://git-scm.com, last accessed April 12, 2021) with our own repository hosted at the web-server. Handling the code stored in Git adds more convenience and reliability in the development of station services. With more servers at work, automatic configuration and code deployment were established. This also makes the station much less dependent on the experience level of a single person. This function is realized with software Ansible (https://www.ansible.com, last accessed April 12, 2021).

2.5 Documentation

All documentation (logbooks, descriptions and configurations of instruments and servers, instructions) are regularly updated and are available at a protected wiki-like website hosted at the web-server. This website is run with Confluence (https://www.atlassian.com/software/confluence, last accessed April 12, 2021). The documentation is a "reference book" for the team describing how to work with instruments, servers and data, how to share, update files and so on. This is also an important component of making the station less dependent on a single person.

3. Data revision policy

The station has the rule "No modification of raw data" applied to all acquired data. All changes are stored in copies of raw data files labeled as "corrected" and/or in the database (pressure, efficiency, temperature correction coefficients). The original raw files serve as the only "source of truth".

4. Summary

The instrumental basis and computer infrastructure of the Oulu cosmic-ray station have been significantly upgraded and expanded during recent years. The list of changes includes separation of data storage and web-services to different machines, a new backup system, new email alerts, Git version control of the code and configurations, comprehensive documentation. The described changes at the Oulu cosmic ray station have significantly increased its reliability of operation and capacity to new data and instruments if they come.

Acknowledgments

The work was partly supported by FINNARP and Academy of Finland (projects 264378 CRIPA, 304435 CRIPA-X, ReSoLVE and 321882 ESPERA).

References

Ansible, https://www.ansible.com (last accessed November 23, 2020)
Atlassian, https://www.atlassian.com/software/confluence, (last accessed November 23, 2020)
Git community, https://git-scm.com (last accessed November 23, 2020)
Restic community, https://restic.net (last accessed November 23, 2020)
Twilio SendGrid, https://sendgrid.com (last accessed November 23, 2020)

Cosmic ray studies with neutron detectors | Volume 1 (2021)
KIEL-UP • DOI: 10.38072/2748-3150/v1

Session 7: Abstracts

Major update of the International GLE database: detrended GLE profiles

Ilya Usoskin, Sergey Koldobskiy, Agnieszka Gil, Gennady A. Kovaltsov, Inna Usoskina, Askar Ibragimov, Teemu Willamo

Correspondence
University of Oulu, Finland

High-energy and high-intensity events of solar energetic particles, called ground-level enhancements (GLEs), form a special class of solar eruptive events with the highly efficient acceleration of charged particles. These events are studied using continuous measurements performed by the global network of ground-based neutron monitors (NMs). All available NM data related to GLE events since 1956 are collected in the International GLE Database (IGLED, http://gle.oulu.fi/, last accessed April 9, 2021). The data are presented in the form of relative NM count rate increases with respect to the constant pre-increase background count rate level due to galactic cosmic rays (GCR). However, the implicit assumption of the constancy of the GCR background level throughout GLE events is often not valid, since the GCR background may vary essentially even during relatively short GLE events. Here we revisited all the GLE NM records and de-trended GLE count rate increases considering the actual variable GCR background. The detrended count-rates have been added to the IGLED database for all GLE events since 1956. This forms a basis for more precise studies of parameters of SEP events and, thus, for solar and space physics.

Status of the NMDB

Christian T. Steigies

Correspondence
Extraterrestrial Physics,Institute of Experimental and Applied Physics, Kiel University, Germany

Since 2008 the EU FP7 funded Neutron Monitor Database (NMDB) is providing access to 1-minute neutron monitor data in real-time as well as different neutron monitor data products for the public. Several space weather services routinely rely on the availability of the neutron monitor data from the worldwide network, and NMDB is continuing to provide real-time data even ten years after the official end of the project. To ensure the availability of this data in the future, a major upgrade to the database infrastructure of NMDB was performed in the fall of 2019. An overview of the new setup, usage statistics, the status of the data quality, software tools and the (new) website will be given.

Program of the meeting

July 13, 2020

Opening of NMDB@Home, obituaries

Chairperson: Ludwig Klein
Session manager: Christian T. Steigies

Time [UTC]	Presenter	Title
1200–1210	Ludwig Klein	Welcome and AOB
1210–1220	Paul Evenson	Roger Pyle - a short obituary talk
1220–1230	Agnieszka Gil	Michael Alania - a short obituary talk

Cosmic rays in the heliosphere: spatial and time variability I

Chairperson: Ludwig Klein
Session manager: Christian T. Steigies

1230–1245	Sergey Koldobskiy	Use of AMS-02 and PAMELA experiments data for calibration of NM network and verification of NM yield functions
1245–1300	Anatoly Belov	Comparison of longterm changes in the flux of cosmic rays according to ground-based detectors, Pamela and AMS-02
1300–1315	Eugenia A. Eroshenko	Experimental spectrum of cosmic ray variations in the rigidity range 1-20 GV in the Earth's orbit by AMS-02 data

Cosmic rays in the heliosphere: spatial and time variability II

Chairperson: Ludwig Klein
Session manager: Christian T. Steigies

1330–1345	Athanasios Papaioannou	Interplanetary coronal mass ejections as the driver of non-recurrent forbush decreases
1345–1400	Simone Benella	A new method to model magnetic cloud-driven Forbush decreases
1400–1415	Dimitra Lingri	Precursory signals of Forbush decreases with and without shock wave
1415–1430	Christopher Light	Interplanetary coronal mass ejection associated forbush decreases in neutron monitors

Short poster presentations

1430–	Mohanad Mahdi Salih	Cosmic ray data and explanation: energetic and raw material
	Victor Yanke	About long term modulation of cosmic rays in the 23-24 solar activity cycles
	Maria Abunina	Ring of stations method in cosmic rays variations research
	Petr Gololobov	Dynamics of energetic spectrum of solar-diurnal variations of cosmic rays in 19-24 solar activity cycles
	Suyeon Oh	Seasonal variation of cosmic ray intensity observed by ground neutron monitor
	Anna Lukovnikova	Analysis of the rigid spectrums of variations of cosmic rays during Forbush effect on October 8, 2012
–1500	Fraser Baird	Wavelet analysis of long-term variations in NM, sunspot, and solar wind data

July 14, 2020

Cosmic rays in the heliosphere: spatial and time variability III

Chairperson: Olga Kryakunova
Session manager: Rolf Bütikofer

Time [UTC]	Presenter	Title
1200–1215	Liudmila Trefilova	Unusual decrease of the cosmic ray intensity in May 2019 on the background of the minima solar activity
1215–1230	Renata Modzelewska	Recurrence of galactic cosmic rays anisotropy and intensity during solar cycle 24
1230–1245	David Ruffolo	Tracking cosmic-ray spectral variation during 2007-2018 Using neutron monitor time-delay measurements
1245–1300	Gonzalo Tancredi	Using cosmic rays detected by HST as geophysical markers
1300–1315		General discussion: cosmic rays in the heliosphere

GLE analysis and Space Weather research and services I

Chairperson: Maria Abunina
Session manager: Danislav Sapundjiev

1330–1345	Alexander Mishev	Application of the updated NM yield function and GLE database for an improved GLE analysis
1345–1400	Sergey Koldobskiy	Reconstruction of SEP fluences during GLE events: description of the new method and its application to the data
1400–1415	Rolf Bütikofer	SEP spectra derived from neutron monitor data and from EPHIN space detector data during recent GLEs and sub- GLEs
1415–1430	Karl-Ludwig Klein	Relativistic solar particle events, pion decay gamma rays, and magnetic connectivity
1430–1445	Alexander Mishev	Extension of the global NM network - optimization for space weather purposes
1445–1500	General discussion:	GLE analysis and space weather research and services I

July 15, 2020

Cosmic rays and the atmosphere

Chairperson: Danislav Sapundjiev
Session manager: Ludwig Klein

1200–1215	Ashot Chilingarian	Measuring atmospheric electric field by the European network of SEVAN detectors
1215–1230	Alejandro López-Comazzi	Short-term periodicities observed in neutron monitor counting Rates
1230–1245	Martin Schrön	Monitoring environmental water with ground albedo neutrons from Cosmic Rays

Short poster presentations

1245-	Anastasia Tezari	Cosmic radiation exposure of aviators for solar cycles 23 and 24
	Jongil Jung	Comparison between Daejeon neutron monitor data and clouds data during 2012-2018
-1315	General discussion:	Cosmic rays and the atmosphere

Space weather research and services II

Chairperson: Rolf Bütikofer
Session manager: Ludwig Klein

Time [UTC]	Presenter	Title
1330–1345	Petr Gololobov	NMDB database and global survey method
1345–1400	Olga Kryakunova	High-energy magnetospheric electron enhancements in 22-24 solar activity cycles and Forbusheffects
1400–1415	Chihiro Kato	A new cosmic ray observation at Syowa station in the Antarctic
1415–1430	Agnieszka Gil	Signs of geoeffective space weather events in cosmic rays during the first half of the solar cycle 24

Short poster presentations

1430–	Wataru Kihara	A particular ICME event in August 2018 observed with the ground based muon detectors and neutron monitors
	Tigran Karapetyan	Status of a European network of SEVAN detectors
	Sindulfo Ayuso	A new directional muon telescope for space weather application
	Alexander MacKinnon	Local intermittency measure analysis of neutron monitor data
	Maria Papailiou	Relationship of the characteristics of large Forbush decreases and the heliolongitude of their sources
	Nicolas Fuller	Kerguelen and Terre Adelie neutron monitors - a status report
	Noelia Santos	First results from the operative cosmic ray detector at Marambio Base, Antarctic Peninsula.N.A.
–1500	General discussion:	Space weather research and services II

July 16, 2020

Neutron detector instrumentation I

Chairperson: David Ruffolo
Session manager: Monica Laurenza

1200–1215	Warit Mitthumsiri	Measuring single and multiple atmospheric secondary particles from cosmic rays using cross-counter neutron time delay distributions from the Princess Sirindhorn Neutron Monitor
1215–1230	Alejandro Sáiz	Recent upgrade of the neutron monitor at Mawson, Antarctica
1230–1245	Du Toit Strauss	Refurbishment of the SANAE neutron monitor
1245–1300	Juanjo Blanco	A new neutron monitor at Livingston Island (Antarctic Peninsula)
1300–1315	Stephan I. Böttcher	Novel registration system for neutron monitors

Neutron detector instrumentation II

Chairperson: Ilya Usoskin
Session manager: Maria Abunina

Short poster presentations

1330–	Stepan Poluianov	Data management of the Oulu cosmic ray station
	Victor Yanke	Reformatting of neutron monitor to increase its effectivity
	Jongil Jung	Installation of Jang Bogo neutron monitor in Antarctica
– 1345	Stepan Poluianov	Upgrade of electronics of neutron monitors DOMC and DOMB

Neutron detector response functions

Chairperson: Ilya Usoskin
Session manager: Maria Abunina

Time [UTC]	Presenter	Title
1345–1400	Waraporn Nuntiyakul	Responses of bare neutron counters to cosmic rays during 1995 and 2009 latitude surveys
1400–1415	Lev Dorman	Variability of effective cutoff rigidities for neutron monitors during 1950 – 2050
1415–1430	Danislav Sapundjiev	Comparison between the observed and the computer mode led neutron monitor count rates

Short poster presentations

1430–	Waraporn Nuntiyakul	FLUKA simulation of neutron detector responses in latitude surveys to vertical secondary particles from cosmic rays
	Mary Zazyan	Calculations of the sensitivity of the SEVAN network to galactic and solar cosmicrays
	Markus Similä	Study of multiplicity at the Antarctic high-altitude double neutron monitor DOMC and DOMB: atmospheric vs. instrumental cascades
	Lev Dorman	Snow effect in neutron monitors
–1500	General discussion:	Instrumentation, response functions

July 17, 2020

Long-term stability of neutron detectors

Chairperson: Monica Laurenza
Session manager: Danislav Sapundjiev

1200–1215	Du Toit Strauss	Measurements of cosmic rays by a mini neutron monitor at Neumeier III from 2014 to 2018
1215–1230	Anna Lukovnikova	Cosmic ray stations of ISTP SB RAS

Data bases and catalogues I

1230–1245	Ilya Usoskin	Major update of the International GLE database: detrended GLE profiles
1245–1300	Christian T. Steigies	Status of the NMDB
1300–1315	Semen Belov	Cutoff rigidity and particle trajectories online Calculator

Data bases and catalogues II

Chairperson: Monica Laurenza
Session manager: Danislav Sapundjiev

Short poster presentations

1330–	Pauli Väisänen	Global neutron monitor network data for the period of 1953-2019: survey for quality control
–1335	Grigori Karapetyan	The database of directivity functions of neutron monitors
1335–1350	Paul Evenson	PHA analysis - telemetry and data acquisition
1350 –	General discussion:	Neutron detector instrumentation, Neutron detector response functions, long-term stability of neutron detectors, databases and catalogues


Universitätsverlag Kiel
Kiel University Publishing

Universitätsbibliothek Kiel
Leibnizstr. 9, 24118 Kiel, Deutschland
verlag@ub.uni-kiel.de, www.ub.uni-kiel.de